THERMOVISCOELASTIC CHARACTERIZATION AND PREDICTIONS OF KEVLAR/EPOXY COMPOSITE LAMINATES

by

Kurt C. Gramoll

Dissertation submitted to the Graduate Faculty of the
Virginia Polytechnic Institute and State University
in partial fulfillment of the requirements for the degree of

DOCTOR OF PHILOSOPHY
in
Engineering Mechanics

APPROVED

H.F. Brinson, Co-Chairman

D.A. Dillard, Co-Chairman

S.L. Hendricks

K.L. Reifsnider

C.E. Knight, Jr.

May, 1988

Blacksburg, Virginia

THERMOVISCOELASTIC CHARACTERIZATION AND PREDICTIONS OF KEVLAR/EPOXY COMPOSITE LAMINATES

by

Kurt C. Gramoll

Committee Co-Chairman: H.F. Brinson and D.A. Dillard
Engineering Science and Mechanics

(ABSTRACT)

This study consisted of two main parts, the thermoviscoelastic characterization of Kevlar 49/Fiberite 7714A epoxy composite lamina and the development of a numerical procedure to predict the viscoelastic response of any general laminate constructed from the same material. The four orthotropic material properties, S_{11}, S_{12}, S_{22}, and S_{66}, were characterized by 20 minute static creep tests on unidirectional ($[0]_8$, $[10]_8$, and $[90]_{16}$) lamina specimens. The Time-Temperature-Superposition-Principle (TTSP) was used successfully to accelerate the characterization process. A nonlinear constitutive model was developed to describe the stress dependent viscoelastic response for each of the material properties.

A new numerical procedure to predict long term laminate properties from lamina properties (obtained experimentally) was developed. Numerical instabilities and time constraints associated with viscoelastic numerical techniques were discussed and solved. The numerical procedure was incorporated into a user friendly microcomputer program called Viscoelastic Composite Analysis Program

(VCAP), which is available for IBM 'PC' type computers. The program was designed for ease of use and includes graphics, menus, help messages, etc.

The final phase of the study involved testing actual laminates constructed from the characterized material, Kevlar/epoxy, at various temperature and load levels for 4 to 5 weeks. These results were then compared with the VCAP program predictions to verify the testing procedure (i.e., the applicability of TTSP in characterizing composite materials) and to check the numerical procedure used in the program. The actual tests and predictions agreed, within experimental error and scatter, for all test cases which included 1, 2, 3, and 4 fiber direction laminates.

The end result of the study was the development and validation of a user friendly microcomputer program that can be used by design engineers in industry to predict thermoviscoelastic properties of orthotropic composite materials.

ACKNOWLEDGEMENTS

The author wishes to express acknowledgement and appreciation for the financial support of NASA-Ames under contract NASA-NCC 2-71, monitored by . He is also deeply indebted to both of his advisors, Dr. Brinson and Dr. Dillard, for their guidance and support throughout the course of this study. Furthermore, work performed by other investigators previously at VPI&SU is gratefully acknowledged. Also, the Kevlar/epoxy composite specimens supplied by the I.E. DuPont de Nemours & Co., Inc. were appreciated.

Above all, the author wishes to acknowledge the unwavering support and understanding given him by his wife and children

TABLE OF CONTENTS

Chapter 1

INTRODUCTION

The use of laminated fiber reinforced plastic (FRP) composites in today's world is increasing due to their light weight and high strength. One dramatic example of their usefulness recently was the Voyager aircraft, whose structure was composed of more than 90% composite materials and was able to circle the globe without refueling. However, one problem with polymer based composite materials is that they exhibit time dependent structural properties, such as creep. These time dependent or viscoelastic properties are also adversely affected by elevated temperatures, high humidity and long time spans. For the continued use of composite materials, and for safety reasons, these properties must be better understood and a reliable method to predict long term laminate creep needs to be developed.

There are two major difficulties in understanding and predicting long term properties of FRP composite materials. The first and most obvious problem in characterizing and modeling long term material behavior is the length of time necessary to perform the tests. This problem is magnified for FRP composites since they are generally anisotropic requiring the determination of more material constants than the usual two for isotropic materials. In order to minimize the test time length, acceleration techniques have been developed, such as

the Time-Temperature-Superposition-Principle which relates time and temperature but such procedures are not without problems and difficulties.

The second problem relates to the infinite number of possible laminates that can be constructed from the same basic unidirectional lamina since the individual plies are free to be stacked and oriented in any manner. As a result, each particular laminate will have an unique set of viscoelastic properties, even though the fiber and matrix materials are the same. Therefore, some method of predicting properties, without actually physically testing each possible laminate, is needed to aid the designer of composite materials and reduce testing complexity.

While progress has been made in the last ten years in understanding the viscoelasticity of FRP composites, there are still many unanswered questions that this study addresses. First, this study fully characterized the thermoviscoelastic properties of a FRP composite material composed of Kevlar 49 fibers and Fiberite 7714A epoxy with a cure temperature of 121° C (250° F). One reason for examining a Kevlar based composite system is that the fibers as well as the epoxy are viscoelastic as opposed to the graphite/epoxy systems where the fibers are time-independent or non-viscoelastic. The characterization tests were performed at various temperature levels in order to accelerate the characterization process and to better understand the thermal effects. Nonlinear stress effects were also included in the characterization. This portion of the study also

included the development of constitutive models that describe the viscoelastic response so that they could be used in a numerical procedure.

The second major portion of this study involved the development of a numerical procedure to predict the laminate response once the lamina is thermoviscoelastically characterized. This new procedure overcomes the stability and time of calculation problems present in the current numerical methods. An important aspect of this study was the development of a self-contained microcomputer-based program that encompasses this numerical procedure. This was done to facilitate the use of the by program design engineers in industry who require computer programs to be transportable, inexpensive to operate, support graphics and user friendly, all of which can only be accomplished with a microcomputer based program.

The three step process of characterizing the lamina, developing long term compliance models, and using a numerical procedure to predict the laminate response is diagrammed in Fig. 1.1. The final part of this study was the validation of this characterization process and numerical procedures by testing actual laminates and comparing them with the program prediction. The prediction and tests agreed well for all laminate types and temperature levels tested.

Previous Efforts

Even though the elastic properties of FRP composite laminates are fairly well understood, the viscoelastic properties are still unknown

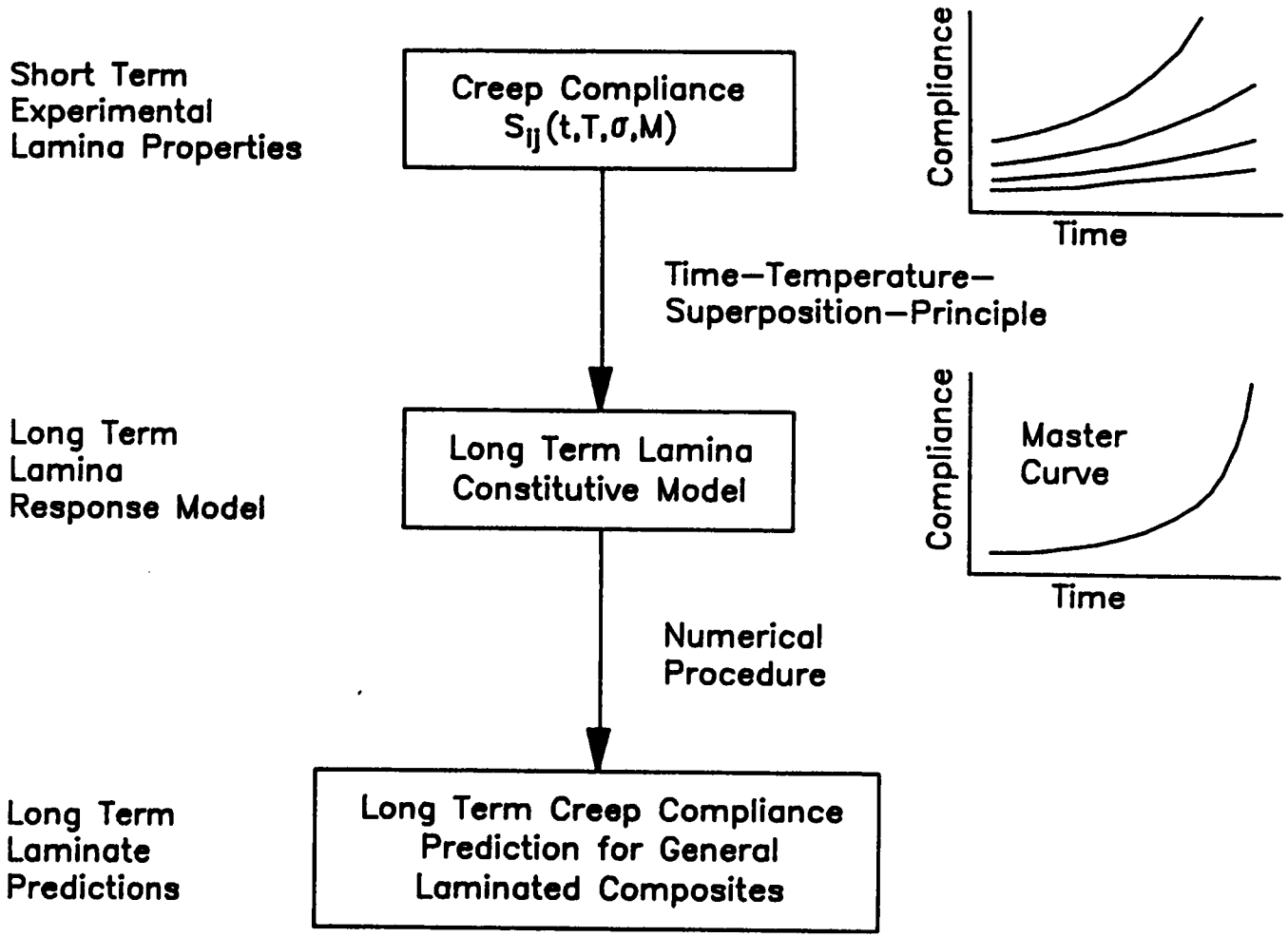

Fig. 1.1 Long Term Characterization of Viscoelastic Composite Materials.

for most composite systems. Only in the last ten to twenty years has any major effort been expended to understand the viscoelasticity of polymeric based composite materials. Early research in this area drew heavily on the work done on polymer materials [1-8,14,15]. Since FRP composite materials are organic polymeric materials, many of the polymer viscoelasticity concepts are applicable, however, the theories had to be generalized and modified to account for the anisotropic and nonhomogeneous nature of composites. New testing techniques were also needed for characterizing FRP composites to reduce the testing time and to account for their anisotropic nature.

There are various methods to characterize a material for viscoelastic properties such as creep tests, stress relaxation tests, dynamic mechanical testing, etc. [9-18]. Through these tests, an understanding about the time dependent compliance and modulus can be obtained for the material property desired. For example, the time dependent compliance can be determined from a creep test since the load, which is constant, is known and the strain can be recorded at various times. For an isotropic material only two independent variables are needed, such as Young's modulus and the shear modulus, but an orthotropic material has nine independent variables [19-22]. These nine variables can be reduced to four if one considers only a two dimensional plane and assumes a plane state of stress. This is acceptable since most FRP composites are made from thin lamina sheets and the loading is generally in-plane loads. However, for a complete characterization of an orthotropic composite, all nine variables

should be determined. From a practical standpoint, this may be quite difficult.

One problem with viscoelasticity for any type of material is how to represent the compliance or modulus functions. A great deal of work has been spent to derive models that will accurately describe the viscoelastic response. One of the simplest and still the most widely used models is the power law for the compliance function. For linear viscoelasticity, this model requires only three parameters to be determined from test data (five for nonlinear viscoelasticity), which makes it easy to implement and use. The power law was used by Findley [23-28] to successfully describe compliance of various laminated materials, such as asbestos, rayon, canvas, polyethylene, polystyrene, for both linear and nonlinear viscoelasticity. He used hyperbolic sine functions to represent two of the three parameters to describe the nonlinear stress aspects of creep.

Another commonly used model is an integral equation method which was developed by Schapery [33,34]. This model is based on thermodynamics and has been shown to describe the viscoelastic response of composite materials very accurately [29-32,35,36]. One draw back with this model is the seven parameters that need to be determined from experimental data, dictating a large number of tests. In addition to the integral model, Schapery has contributed to the understanding of the experimental as well as the theoretical aspects of composite viscoelasticity. He has generated a tremendous amount of test data on various composite systems. Along with the data he has

given insights on test methods and techniques, plus an understanding of the data and how to fit it to various viscoelastic models.

Other models include fractional exponents and a general power law [12,37-39]. Both of these hold promise since they can describe a secondary plateau, or rubbery region, which polymeric materials exhibit. Free volume based theories have also been used and have great future promise, especially for polymeric composites [40-43].

Adams, et al, [44-46] has also done extensive experimental and theoretical work in composite viscoelasticity. They showed that one could characterize the resin and fiber separately and then predict unidirectional lamina properties through the use of a finite element computer program [47]. However the results where limited to only predicting lamina properties and no effort was made to predict laminate properties.

Other noteworthy contributions to the understanding of FRP composite viscoelasticity are Crossman, et al, and Weisman, et al. They both have done experimental as well as analytical work. Crossman [48-51] has done a large amount of work in characterizing linear viscoelastic properties of composites in adverse temperature and humidity environments. He has shown that humidity can be used to accelerate the testing process of some FRP composites. Humidity shift factors can be calculated and master curves developed similar to temperature derived master curve. Weisman [52-56] has extensively investigated the thermoviscoelastic response of FM-73 adhesive and also has examined humidity and damage aspects of composite

viscoelasticity. There has been and still is a large effort in Europe [38-39,57-58] and in Russia [12,59-71] to understand composite viscoelasticity.

At Virginia Polytechnic Institute and State University a large effort has also been expended in characterizing viscoelastic properties of composite materials under the guidance of Brinson [72-82]. The work started with Yeow [72] who looked at the T300/934 graphite/epoxy fiber reinforced composite system. He used temperature to accelerate the testing and then used the Time-Temperature-Superposition-Principle (TTSP) to obtain master curves for unidirectional material. By this method he was able to obtain creep compliance curves for over 25 decades of time from short term (16 minute) creep tests. His shifted curves correlated fairly well with 25 hour creep tests that were performed to verify the master curves. The master curves were for the transverse (S_{22}) and shear (S_{66}) compliance terms. The fiber direction (S_{11}) and the coupling term (S_{12}) compliance were found to be only elastic or time-independent. He also formulated a method to predict rupture times for laminated composites and developed a numerical method to predict the stress-strain response of composites.

Griffith [73] later continued pursuing this idea of predicting the viscoelastic properties of fiber reinforced plastic laminate by using the TTSP. He showed that the stress and temperature could both be used as shifting parameters to generate master curves. He proceeded to generate the transverse (S_{22}) and shear (S_{66}) compliance

master curves for the same composite system, T300/934. These master curves were used to predict the compliance of various off-axis lamina samples and then were compared to actual long term tests on those samples. The agreement was fairly good for unidirectional cases but no work was done for predicting laminate compliances. Time-to-failure predictions were also performed using a modified kinetic rate theory.

Continuing this work at VPI&SU was Dillard [74,77,78,81] who also studied the T300/934 graphite/epoxy system. Using the creep test data obtained by Griffith, he characterized and modeled the nonlinear time-dependent properties for the S_{22} and S_{66} terms. He used the Findley Power Law model to describe the S_{22} and S_{66} terms. The S_{11} and S_{12} terms were assumed time-independent. Based on the previous work of Yeow [72], he developed a numerical procedure that would predict the creep, stresses, strains and time-to-failure of a general laminate constructed from T300/934 material at 160° C (320° F). In some cases the agreement was good but in others (most noticeably for laminates constructed with three or more layers at different fiber angles) the predicted compliance would deviate from the actual test results. Creep rupture predictions were also made for various laminates with limited success. Although the TTSP was not used, it was shown that laminate viscoelastic properties can be predicted at a particular temperature if the lamina properties are well characterized at that temperature.

Later work by Tuttle [75,79] showed that the T300/5208 graphite/epoxy system could also be characterized at a certain

temperature and then by a numerical procedure the laminate viscoelastic properties could be predicted. This showed that the characterization and prediction method for laminate properties developed previously can be used for different composite systems. One notable difference in his characterization process was the use of the Schapery integral to describe the nonlinear compliance of the S_{22} and S_{66} terms (the S_{11} and S_{12} terms were once again assumed time-independent). He also showed that the power law exponent used in most creep models is very sensitive and long term predictions could contain large errors since the error grows exponentially in time.

Heil [76], while working at VPI&SU continued this investigation into the understanding of viscoelasticity of composite materials. He examined T300/934 graphite/epoxy and generated long term creep characteristics as a function of stress and temperature levels. He also looked in detail at the resin system and tried to infer certain characteristics of the unidirectional lamina properties. He used the Schapery integral approach to model the S_{22} and S_{66} compliance terms. He also compared laminate predictions to actual tests.

Overview of Current Study

The first phase of the current research was the characterization of the Kevlar 49/Fiberite 7714A epoxy composite system for thermoviscoelastic properties. This particular composite system was examined since the fibers and epoxy are both viscoelastic and therefore all material properties are time dependent, and also because

of its increased use in industry. Three basic specimen types, unidirectional 0^0 10^0 and 90^0 coupons, were used to determine the four orthotropic compliance matrix terms (S_{11}, S_{12}, S_{22}, and S_{66}) by means of static creep tests. All terms were found to be both temperature and stress dependent [58,83-84], which required that each material property be tested at various temperature levels and stress levels. Due to the vast number of possible tests needed to completely characterize each compliance term, specimens were reused where possible. The TTSP was used to develop master curves for each of the compliance terms in order to obtain long term results.

Constitutive models were then developed from the test data for each of the four compliance matrix terms (S_{11}, S_{12}, S_{22}, and S_{66}) that describes both linear and nonlinear temperature and stress effects. While various established models such as the Findley power law, Schapery integral equation, partial fraction equation, or the generalized power law, were examined a new model called the quadratic nonlinear power law was developed and used in this study. Various nonlinear stress parameters, such as the octahedral shear stress, were also examined for use in the constitutive model.

One of the principle objectives of the research performed in this study was the development of a computer aided engineering (CAE) program for use by design engineers in industry for designing composites structures with viscoelastic response. The experiments performed were aimed at developing and testing this program. The models developed for the compliance matrix terms from the experimental

data, were integrated into a new computer program to predict laminate properties. This program overcomes the problems and restrictions, such as numerical instabilities, restrictions on time step size, difficulty in user operation, temperature range, that plagued the VISLAP program developed by Dillard [85-91].

The new program, Viscoelastic Composite Analysis Program (VCAP), was designed to run on a 'PC' or compatible microcomputer to facilitate ease of use, to reduce operation costs and to increase the portability of the program from computer to computer. The program was written in the PASCAL programming language for its graphics ability, ease of programming, portability to many computers, and modular programming style which aids maintenance and later addition of more options. Extensive use of user interface aids such as menu screens, graphics, and error help messages were included to make the program user friendly. The program allows the operator to use models and material systems other than the Kevlar/epoxy system characterized in this study. In addition to the VCAP program, data reduction, curve fitting and curve shifting programs were also developed to aid others in analyzing creep and creep recovery tests to characterize their own material systems.

The final phase of the study involved testing actual laminates constructed from the characterized material, Kevlar/epoxy, at various temperature and load levels. These results were then compared with the VCAP program predictions to verify the testing procedure (i.e., the applicability of TTSP in characterizing composite materials) and

to check the numerical procedure used in the program. The actual tests and predictions agreed well for all test cases which included 1, 2, 3, and 4 fiber direction laminates.

Other subjects associated with viscoelastic characterization and testing procedures were also investigated. These include examining the 'fiber truss' effect, mechanical conditioning, and temperature conditioning.

Summary

In summary the purpose of this research was to obtain a better understanding of the viscoelastic response of Kevlar/epoxy laminates under various temperature and loading conditions. The end result is a microcomputer based computer program to predict the time-dependent stresses and strains of any polymeric composite laminate. Other benefits of this research is a comprehensive test method of nonlinear characterization of composites for various stress and temperature levels.

The basic procedure followed in this research was first, unidirectional specimens were tested at various temperature and load levels. Second, nonlinear constitutive models were developed for an orthotropic material that included both temperature and stress effects. Third, a microcomputer program was developed to predict laminate viscoelastic properties. And fourth, the testing procedure and program was validated with actual creep tests on laminates.

Chapter 2

BACKGROUND INFORMATION

Various basic subjects regarding composites and viscoelasticity are reviewed and special terminology used in this study are defined. The subjects covered are the analysis and terminology of orthotropic materials, experimental methods to determine the compliance matrix of orthotropic materials, linear and nonlinear viscoelasticity viscoelastic constitutive models, and the Time-Temperature-Superposition-Principle (TTSP).

Composite Orthotropic Materials

Fiber reinforced plastic (FRP) composite materials are constructed from two different materials, long or short fibers and resin. The particular composite system of interest in this study is made with long continuous fiber that are relatively stiff and strong when compared to the resin. When these fibers are oriented in a single direction within a resin matrix, they are referred to as an 'unidirectional lamina'. Although the thickness of a lamina can be any size, it is generally only 0.1 - 0.2 mm thick due to processing constraints. The real benefit of FRP composite materials is the ability to combine unidirectional lamina layers together in any direction to form a laminate structure. If all the layers are oriented in a single direction then it is generally referred to as an

unidirectional laminate, or just an unidirectional composite. The unidirectional laminates used in this study to characterize the material system were constructed with 8 or 16 unidirectional plies (1.0 mm and 2.0 mm thick, respectively).

The most general material type classification for a unidirectional composite is transversely isotropic which has five independent material properties. However, since the thickness of FRP composites is generally thin in comparison to the width and length they are more conveniently classified as a two dimensional orthotropic material with only four material properties. In general, for an anisotropic material the elastic stress strain constitutive equations can be written in tensor form as

$$\varepsilon_{ij} = S_{ijkl}\,\sigma_{kl} \qquad i,j,k,l = 1,2,3 \tag{2.1}$$

ε_{ij} = strain tensor

σ_{kl} = stress tensor

S_{ijkl} = 81 term compliance tensor (only 21 independent constants)

but for a two dimensional orthotropic unidirectional lamina with no out-of-plane loads ($\sigma_{33} = \tau_{23} = \tau_{31} = 0$) this will reduce to [19]

$$\begin{Bmatrix} \varepsilon_1 \\ \varepsilon_2 \\ \gamma_{12} \end{Bmatrix} = \begin{bmatrix} S_{11} & S_{12} & 0 \\ S_{21} & S_{22} & 0 \\ 0 & 0 & S_{66} \end{bmatrix} \begin{Bmatrix} \sigma_1 \\ \sigma_2 \\ \tau_{12} \end{Bmatrix} \tag{2.2}$$

or

$$\{\varepsilon\} = [S]\,\{\sigma\}$$

where

ε_1, ε_2 = in-plane strains

$\gamma_{12} = 2\varepsilon_{12}$ = in-plane engineering shear strain

σ_1, σ_2 = in-plane normal stresses

τ_{12} = in-plane shear stress

S = reduced compliance matrix

The reduced compliance matrix can be written in terms of the engineering properties as

$$S_{11} = 1/E_{11} \tag{2.3a}$$

$$S_{12} = S_{21} = -\nu_{12}/E_{11} = -\nu_{21}/E_{22} \tag{2.3b}$$

$$S_{22} = 1/E_{22} \tag{2.3c}$$

$$S_{66} = 1/G_{12} \tag{2.3d}$$

where E_{11} and E_{22} are the stiffness or modulus in the fiber and transverse direction, respectively, ν_{12} and ν_{21} are the Poisson's ratios, and G_{12} is the shear modulus. Similarly, the S_{11} is commonly referred to as the fiber direction compliance, S_{12} as the fiber/transverse coupling compliance, S_{22} as the transverse direction compliance, and S_{66} as the shear compliance.

The subscript numbers 1 and 2 used with the stresses and strains refer to the local coordinates or the principal direction of the lamina with the 1 direction parallel with the fibers as illustrated in Fig. 2.1. The global coordinate system uses the subscript letters x and y for the laminate (or global) stresses and strains. This

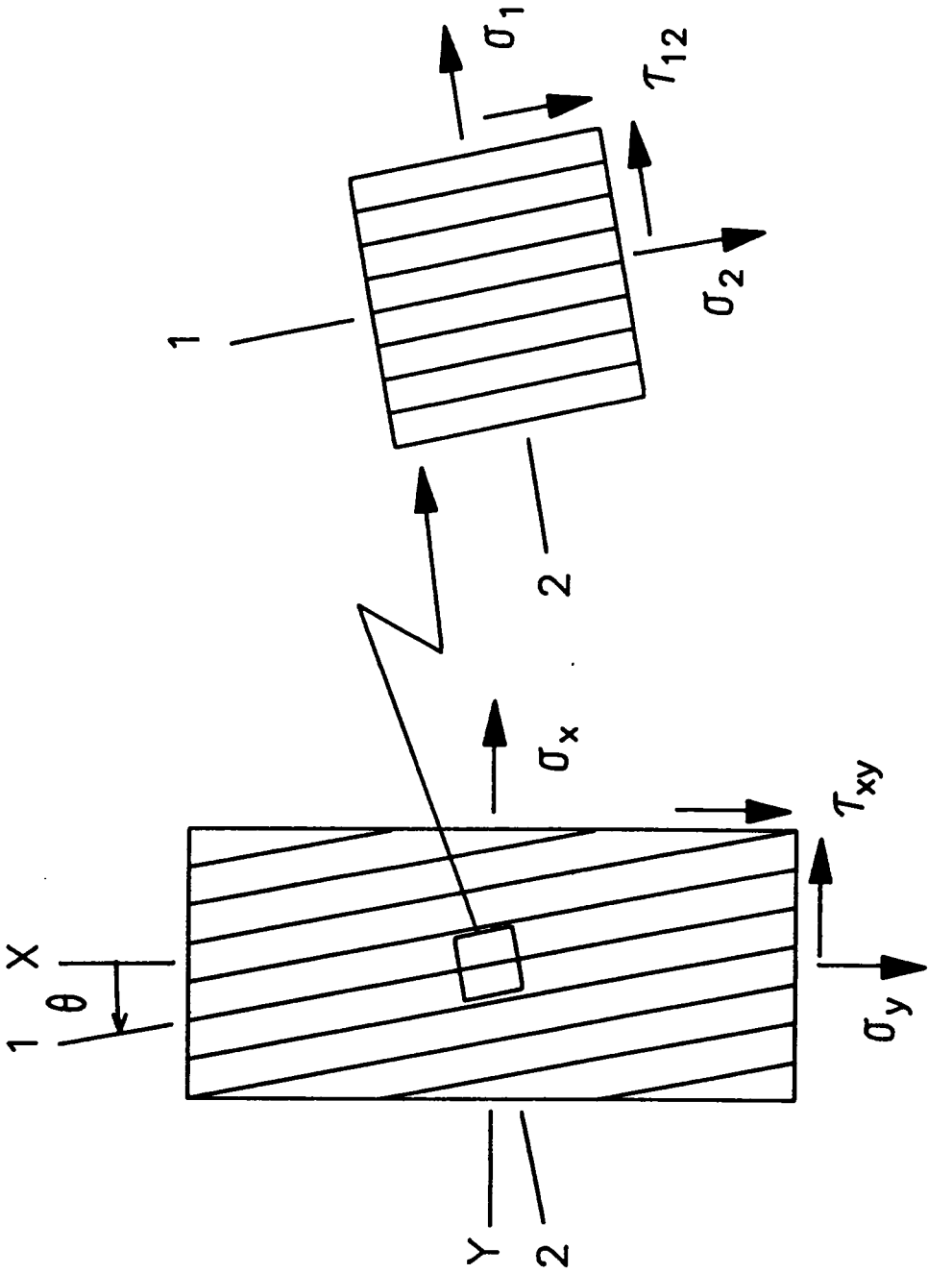

Fig. 2.1 Coordinate Systems Used to Describe Local (1–2) and Global (x–y) Stresses and Strains.

convention is well established in the composite literature (although not the only one) and will be used in this study.

Since laminates are constructed from plies at arbitrary orientations it is necessary to relate the local and global coordinate systems through transformation matrices. These relationships for stress and strain are

$$\{\sigma\}_{12} = [T_1]\{\sigma\}_{xy} \quad \text{or} \quad \{\sigma\}_{xy} = [T_1]^{-1}\{\sigma\}_{12} \tag{2.4}$$

$$\{\varepsilon\}_{12} = [T_2]\{\varepsilon\}_{xy} \quad \text{or} \quad \{\varepsilon\}_{xy} = [T_2]^{-1}\{\varepsilon\}_{12} \tag{2.5}$$

where the transformation matrices are defined as

$$[T_1] = \begin{bmatrix} m^2 & n^2 & 2mn \\ n^2 & m^2 & -2mn \\ -mn & mn & m^2-n^2 \end{bmatrix} \qquad [T_2] = \begin{bmatrix} m^2 & n^2 & mn \\ n^2 & m^2 & -mn \\ -2mn & 2mn & m^2-n^2 \end{bmatrix} \tag{2.6}$$

where $m = \cos(\theta)$ and $n = \sin(\theta)$. Using Eqs. 2.2, 2.4 and 2.5, the unrotated or local compliance matrix [S] can be transformed to the rotated or global coordinates as

$$\{\varepsilon\}_{xy} = [T_2]^{-1}\{\varepsilon\}_{12} = [T_2]^{-1}[S][T_1]\{\sigma\}_{xy} \tag{2.7}$$

$$\text{where } [\bar{S}] = [T_2]^{-1}[S][T_1]$$

The bar above the S now signifies the global coordinate with the subscript numbers 1,2 and 6 now representing the global coordinate system. Written out in full, the rotated $\bar{S}_{ij}$ is

$$\bar{S}_{11} = S_{11}m^4 + (2S_{12} + S_{66})m^2n^2 + S_{22}m^4 \tag{2.8a}$$

$$\bar{S}_{22} = S_{11}n^4 + (2S_{12} + S_{66})m^2n^2 + S_{22}n^4 \qquad (2.8b)$$

$$\bar{S}_{12} = \bar{S}_{21} = S_{12}(m^4 + n^4) + (S_{11} + S_{22} - S_{66})m^2n^2 \qquad (2.8c)$$

$$\bar{S}_{16} = \bar{S}_{61} = (2S_{11} - 2S_{12} - S_{66})m^3n + (2S_{12} - 2S_{22} + S_{66})mn^3 \qquad (2.8d)$$

$$\bar{S}_{26} = \bar{S}_{62} = (2S_{11} - 2S_{12} - S_{66})n^3m + (2S_{12} - 2S_{22} + S_{66})nm^3 \qquad (2.8e)$$

$$\bar{S}_{66} = 2(2S_{11} + 2S_{22} - 4S_{12} - S_{66})m^2n^2 + S_{66}(m^4 + n^4) \qquad (2.8f)$$

These rotated compliance terms will be used extensively in chapter 4 for developing the numerical procedure to predict the creep of any general laminate.

The stress, strain or stiffness analysis of a laminate is more conveniently done using the constitutive relations written in terms of the reduced stiffness matrix

$$\{\sigma\}_{12} = [Q]\{\varepsilon\}_{12} \qquad (2.9)$$

where $[Q] = [S]^{-1}$ and $[\bar{Q}] = [\bar{S}]^{-1}$

The advantage of using the stiffness matrices is that they can be algebraically added, which cannot be done with the individual ply compliance matrices, to produce the laminate stiffness, [A],

$$[A] = \sum_{k=1}^{N} [\bar{Q}]^k t_k \qquad (2.10)$$

where N is the total number of plies

$[\bar{Q}]^k$ is the laminate stiffness of the k^{th} ply in global coordinates

t_k is the thickness of the k^{th} ply

The laminate stiffness matrix allows the laminate load or elastic strains to be calculated, depending on which is initially known, by

$$\{N\}_{xy} = [A]\{\varepsilon\}^{e}_{xy} \tag{2.11}$$

or

$$\{\varepsilon\}^{e}_{xy} = [A]^{-1}\{\sigma\}^{e}_{xy} \tag{2.12}$$

Once the laminate strains are known then the individual ply strains can also be calculated by

$$\{\sigma\}^{k}_{12} = [Q]^{k}\left\{ \{\varepsilon\}^{t}_{12} - \{e\}^{r}_{12} \right\} = [Q]^{k}\{\varepsilon\}^{e}_{12} \tag{2.13}$$

where $\{\varepsilon\}^{t}_{12}$ is the total laminate strain and $\{\varepsilon\}^{r}_{12}$ is the residual laminate strain in the local coordinate system of k^{th} ply. The residual strain can be regarded as any non-elastic strain such as thermal, hygroscopic, or viscoelastic creep strains. The process described above is commonly referred to as Classical Lamination Theory (CLT) which is more fully examined in Refs. 19-21.

One major disadvantage in dealing with the reduced stiffness matrix [Q] is viscoelastic creep is generally expressed in terms of compliance. Therefore the compliance terms, S_{11}, S_{12}, S_{22}, and S_{66}, are functions of time which inhibits the direct inversion of the compliance matrix to get the stiffness matrix which is used in Eq. 2.10 since they are not direct inverses of one another ($[Q] \neq [S]^{-1}$). There are numerical methods available to convert from

the time-dependent compliance to stiffness for linear systems but the process is difficult to implement.

Numerical methods have been developed to solve the inversion problem for composite materials by solving for the creep strains and then treating them similar to thermal loads [74-75]. Chapter 3 will examine these numerical procedures in more detail. The final solution method to be used for this study will only rely on the reduced compliance matrices.

Regardless of whether the stiffness or compliance form of the material properties is used, there are certain assumptions inherent in the CLT that should be noted. First, a given straight line normal to the laminate surface will remain normal and straight after deformation. This is referred to as the Kirchoff hypothesis. Second, no out-of-plane loads are accounted for so that only in-plane or bending loads are permitted. Lastly, CLT is a solution method for point stresses and strains and does not account for free edge effects which have been documented for the elastic case [19,20]. This study examines the free edge effect for viscoelastic response in chapter 4.

Experimental Methods to Determine Creep Compliance

There are four compliance terms to be determined experimentally to fully characterize a FRP composite, S_{11}, S_{12}, S_{22}, and S_{66}. The most common method in determining the compliance is through the use of resistance foil strain gages mounted on test specimens loaded under a known stress. By knowing the strain and stress fields it is possible

to calculate the compliance. Although other methods are available to measure strain, such as extensometers and Moire interferometry, strain gages still remain the most widely used method. Further details on the actual strain measuring devices used in this study are discussed in chapter 4.

The S_{11} is typically determined by loading unidirectional laminate, $[0]_x$, in the fiber direction and measuring the axial strain and obtaining $S_{11} = \sigma_1/\varepsilon_1$. Likewise, S_{22} can be calculated by measuring the strain transverse to the fibers in a $[90]_x$ specimen when the specimen is loaded in the transverse direction, $S_{22} = \sigma_2/\varepsilon_2$. The S_{12} ($=S_{21}$) is best determined by loading a $[0]_x$ specimen in the fiber direction and measuring the strains transverse to the fibers, giving $S_{12} = \sigma_1/\varepsilon_2$. However, S_{12} could also be determined by loading a $[90]_x$ specimen in the transverse direction and recording the strains in the fiber direction, giving $S_{12} = S_{21} = \sigma_2/\varepsilon_1$. The second method however is impractical since the transverse direction is not strong enough to withstand the stress levels, σ_2, necessary to produce measurable ε_1 strains due to the stiff fibers relative to the matrix.

The determination of S_{66} is more difficult and susceptible to error than the other compliance terms. There have been numerous studies, Yeow, et al [72], Brouwer [39], Pindera and Herakovich [93], Pipes and Cole [92] to name a few, conducted on methods to determine shear compliance of composite materials. One method that has received wide use and acceptance is the 10° off-axis test proposed by Chamis and Sinclair [94]. For most composite materials where S_{11} is a order

of magnitude greater than the S_{22} and S_{66}, the shear strain, γ_{12}, when normalized to the axial strain, ε_x, is close to a maximum at 10° which facilities accurate strain measurements. For Kevlar/epoxy, the maximum is at approximately 9.0° as shown in Fig. 2.2. However the 10° off-axis test is sensitive to misalignment of the strain gages or load direction. To verify the reliability of the test for the Kevlar/epoxy composite system used in this study, tests were performed on 10° and 30° off-axis specimens. The results for both tests, shown in Fig. 2.3, are nearly identical and confirms the usefulness of off-axis tests for shear compliance.

The shear strain, γ_{12}, is measured by use of a three gage rosette such as a rectangular or delta rosette strain gage. By knowing the strains in three directions, the transformation matrices can be used to back calculate γ_{12} and ultimately the shear compliance. This study used the rectangular rosette type strain gage mounted in the 0° direction as shown in Fig. 2.4. Using Eq. 2.4 the shear strain in the local coordinate system can be written in terms of the global strains

$$\gamma_{12} = (\varepsilon_y - \varepsilon_x)\sin(2\theta) + \gamma_{xy}\cos(2\theta) \qquad (2.14)$$

Similarly, the actual gage strains can be expressed in terms of the global coordinate system giving

$$\varepsilon_x = \varepsilon_{g2} \qquad (2.15a)$$

$$\varepsilon_y = \varepsilon_{g1} - \varepsilon_{g2} + \varepsilon_{g3} \qquad (2.15b)$$

$$\gamma_{xy} = \varepsilon_{g1} - \varepsilon_{g3} \qquad (2.15c)$$

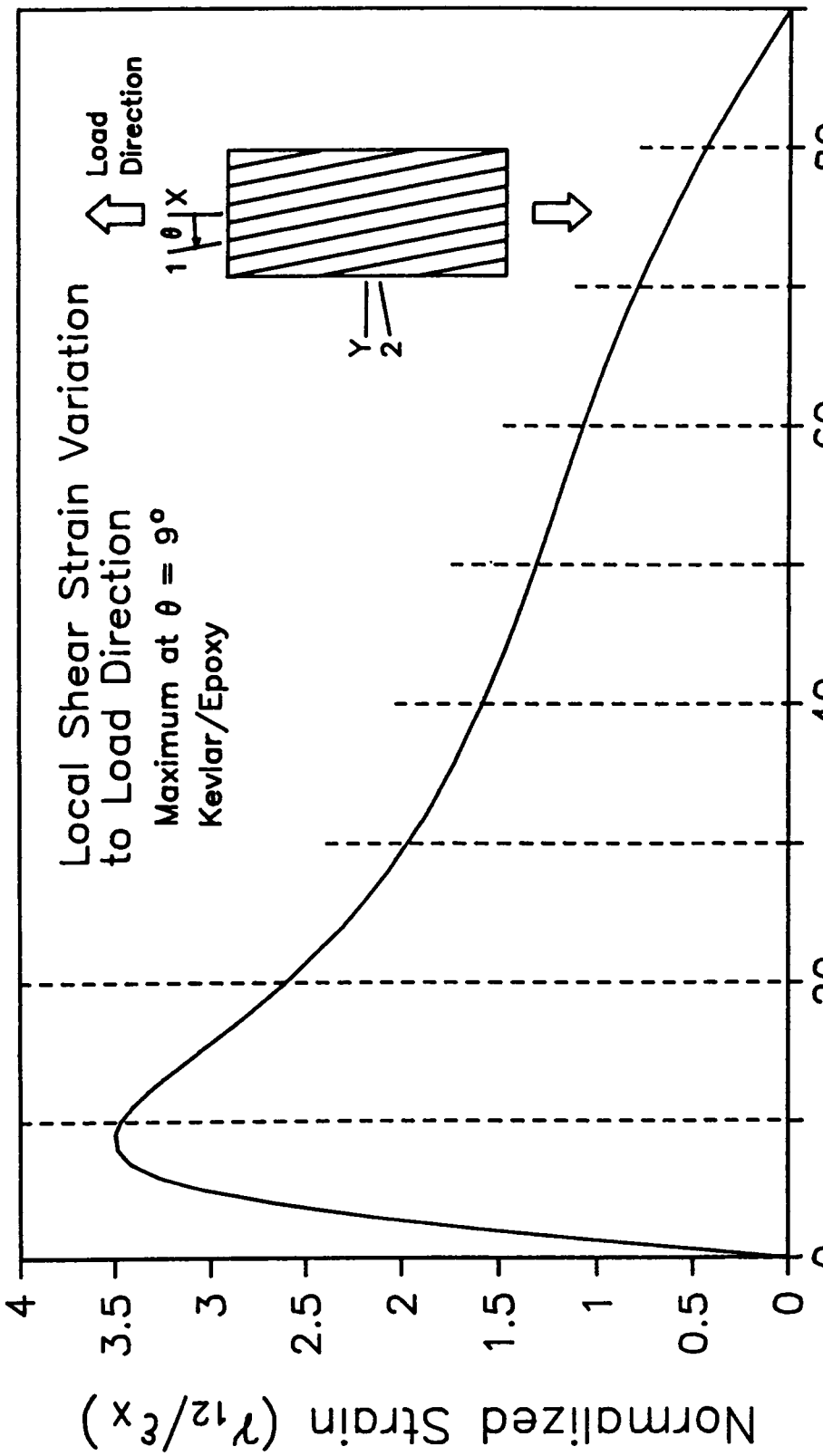

Fig. 2.2 Variation of Local Shear Strain in a Unidirectional Kevlar/Epoxy Composite.

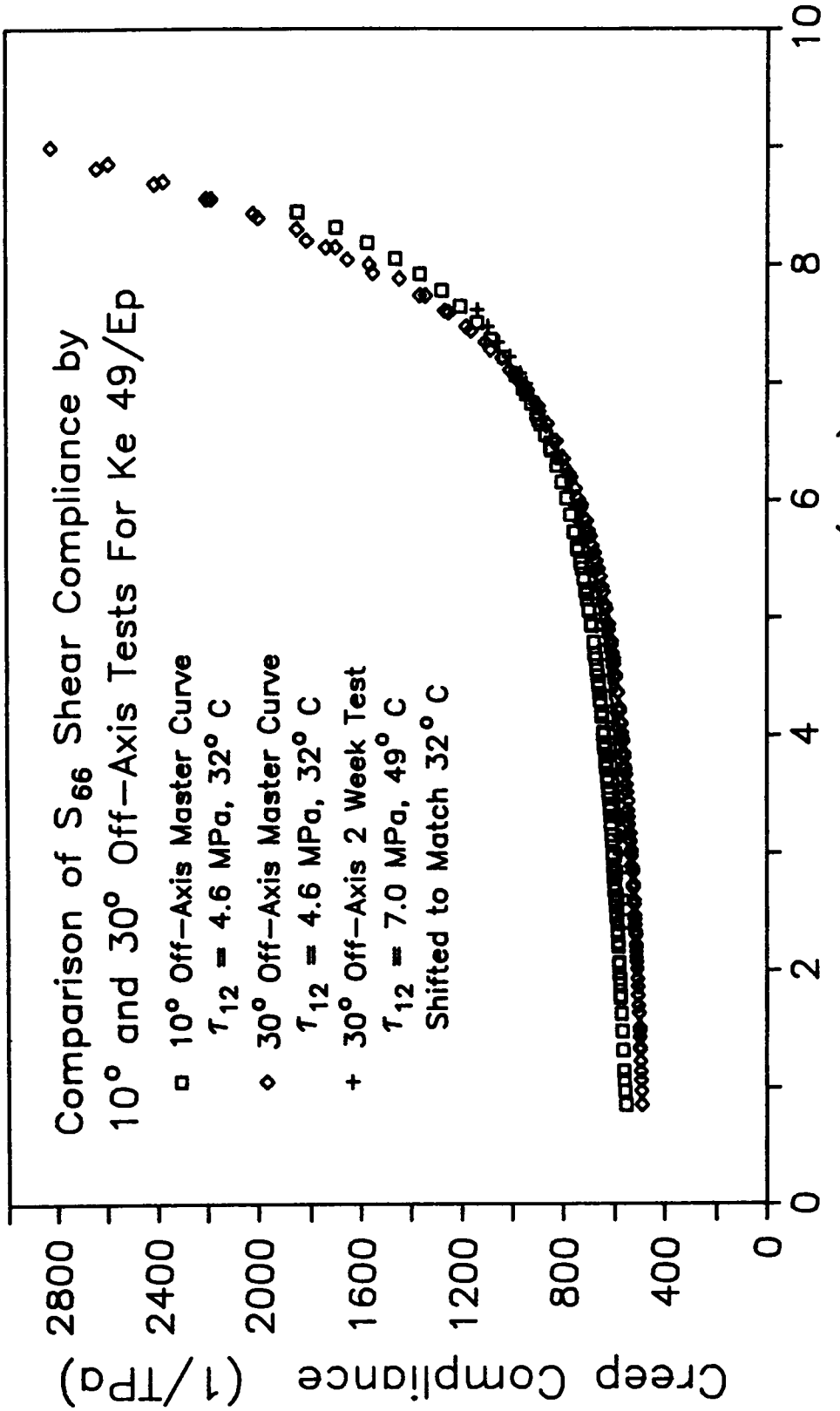

Fig. 2.3 Comparison of Shear Creep Compliance from 10° and 30° Off-Axis Tests on Kevlar 49/7714A Epoxy.

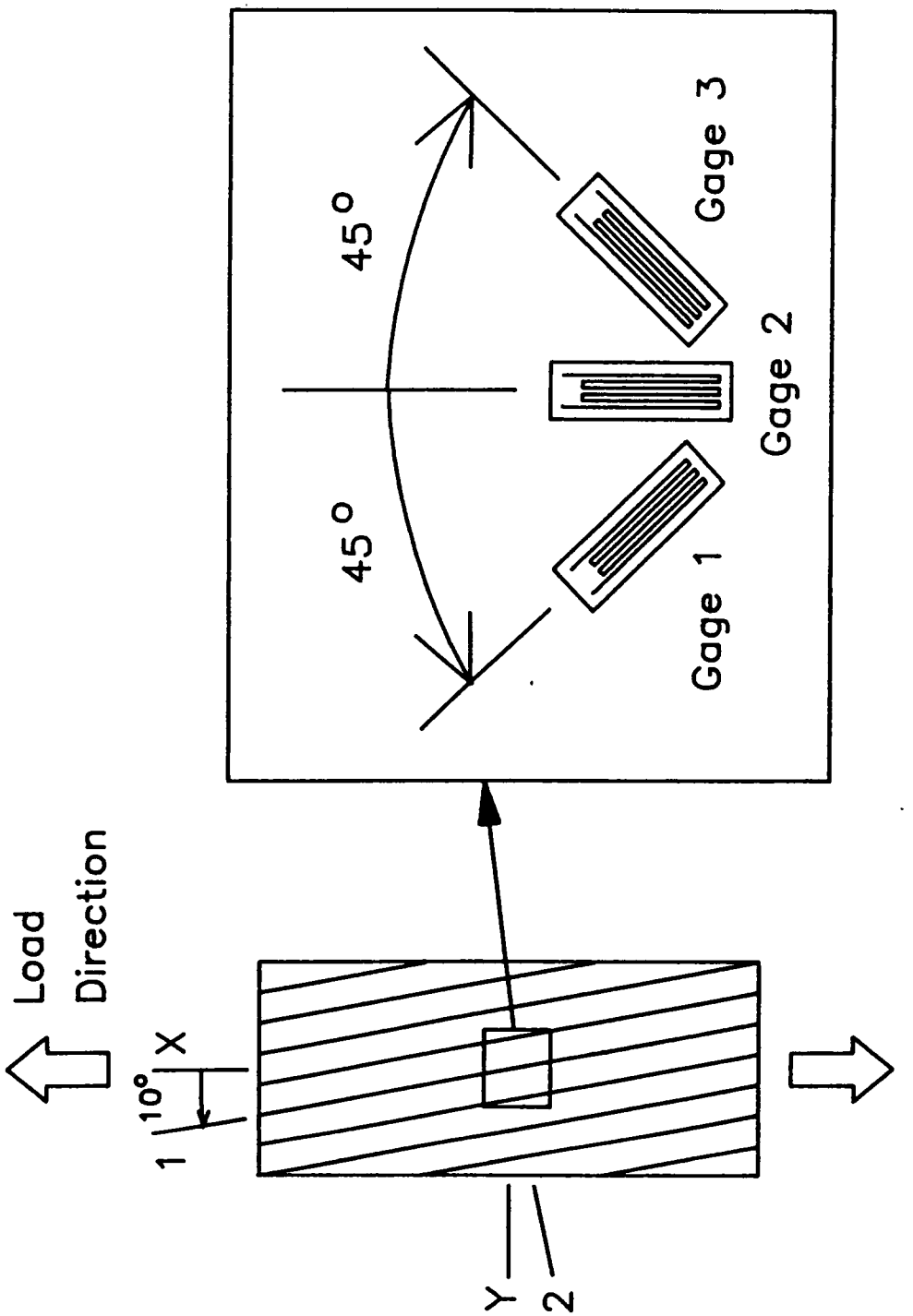

Fig. 2.4 Rectangular Strain Gage Rosette Configuration on 10° Off-Axis Test Specimen.

where ε_{g1} ε_{g2} and ε_{g3} are the strains in gages 1, 2 and 3, respectively.

Substituting Eqs. 2.15a-c into Eq. 2.14 and setting θ to 10° gives the shear strain in terms of only the gage strains

$$\gamma_{12} = 1.282\ \varepsilon_{g1} - 0.684\ \varepsilon_{g2} - 0.598\ \varepsilon_{g3} \qquad (2.16)$$

The shear compliance can then be easily be calculated for a load in the 0° direction (σ_x) by recalling

$$S_{66}\ \sigma_{12} = \gamma_{12} \qquad (2.17)$$

Since $\sigma_2 = \sigma_{12} = 0$,

$$S_{66}\ \sin(2\theta)\ \sigma_x = 2\gamma_{12} \qquad (2.18)$$

or

$$S_{66} = \frac{1}{\sigma_x}\left\{7.495\ \varepsilon_{g1} - 4.000\ \varepsilon_{g2} - 3.495\ \varepsilon_{g3}\right\} \qquad (2.19)$$

Therefore, since σ_x, ε_{g1}, ε_{g2}, and ε_{g3} are known, S_{66} can be easily calculated.

Viscoelasticity

Viscoelasticity, the study of time dependent response of materials with memory, is the central topic of this study. While there are many aspects of viscoelasticity, the discussion herein will focus on the constitutive relationships and viscoelastic models currently used to describe and understand creep. The reader is directed to the many good books on viscoelasticity [1,9,10,12,13] for

a broader and more complete understanding of the subject.

Viscoelasticity is commonly associated with the process of creep where the material undergoes a change in deformation even under constant load. Similarly, creep recovery refers to a material slowly returning to its original configuration after a load has been removed. Viscoelasticity is also commonly associated with stress relaxation where the stress of a deformed body changes with time but the displacement or strain is fixed. As with creep, the material may return to its natural state after the deformation is released. Another name for viscoelasticity is hereditary solid mechanics since the materials exhibit a memory like behavior. While most materials have little or no detectable viscoelastic behavior, polymeric materials, such as the Kevlar/epoxy composite examined in this study, exhibit strong viscoelastic behavior which needs to be understood.

The end result of any study of the viscoelastic response of a material is to develop a mathematical relationship to describe the observed stress-strain relationship. For a material under creep loading, the generalized constitutive equation for linear viscoelasticity can be stated as

$$\varepsilon_{ij}(t) = S_{ijkl}(t)\,\sigma_{kl_o} \qquad i,j,k,l = 1,2,3 \qquad (2.20)$$

where $S_{ijkl}(t)$ is the time dependent compliance matrix and σ_{kl_o} is the input or known stress function which is defined as

$$\sigma_{kl}(t) = \sigma_{kl_o} H(t) \tag{2.21}$$

where H(t) is the Heavyside function. Similarly, for stress relaxation, the constitutive equation is defined as

$$\sigma_{ij}(t) = C_{ijkl}(t)\, \varepsilon_{kl_o} \qquad i,j,k,l = 1,2,3 \tag{2.22}$$

where $C_{ijkl}(t)$ is the time dependent stiffness matrix and ε_{kl_o} is defined as

$$\varepsilon_{kl}(t) = \varepsilon_{kl_o} H(t) \tag{2.23}$$

The creep compliance can easily be obtained by subjecting a material to a static load and observing the deformation. However, the relaxation stiffness is much harder to obtain since a constant strain field must be maintained while the stress is monitored. Since it was not necessary to know the stiffness matrix for the present study and due to the difficulties in performing stress relaxation tests, only creep and creep recovery tests were performed. The stiffness can be calculated from the compliance [29-31] but it is not a trivial task since they are not the simple inverse of one another as with elastic materials.

For linear viscoelasticity, Eq. 2.20 can be generalized for various loading states as

$$\varepsilon_{ij}(t) = S_{ijkl}(t)\, \sigma_{kl_o} H(t) + S_{ijkl}(t-t_1)\, (\sigma_{kl_1} - \sigma_{kl_o})\, H(t-t_1) +$$

$$.. + ..\ S_{ijkl}(t-t_n)\, (\sigma_{kl_n} - \sigma_{kl_{n-1}})\, H(t-t_n) \tag{2.24}$$

where n is the total number of different stress levels and σ_{kl_n} is the stress level at time n. This equation can be further generalized to give the Boltzman Superposition Principle.

$$\varepsilon_{ij}(t) = \int_{-\infty}^{t} S_{ijkl}(t-\tau) \frac{d\sigma_{kl}(\tau)}{d\tau} d\tau \qquad (2.25)$$

where $-\infty$ is generally taken as 0 assuming that the material has experienced no previous stress or strain histories. This integral form, also commonly referred to as a Duhammel integral, is only valid for linear viscoelastic materials [9,13].

The compliance matrix has been shown analytically [31] to be a symmetric tensor. This also has been shown experimentally by Morris, et al., [55]. Thus for an orthotropic material in plane stress, the constitutive equation for constant stress can be written as

$$\begin{Bmatrix} \varepsilon_1(t) \\ \varepsilon_2(t) \\ \gamma_{12}(t) \end{Bmatrix} = \begin{bmatrix} S_{11}(t,T,\sigma) & S_{12}(t,T,\sigma) & 0 \\ S_{12}(t,T,\sigma) & S_{22}(t,T,\sigma) & 0 \\ 0 & 0 & S_{66}(t,T,\sigma) \end{bmatrix} \begin{Bmatrix} \sigma_{1_o} \\ \sigma_{2_o} \\ \tau_{12_o} \end{Bmatrix} \qquad (2.26)$$

where T represents temperature and σ is the nonlinear stress parameter which can be best defined as a function of various components of the stress tensor σ_{ij}. For the one dimensional case, the nonlinear stress parameter would be only the stress in that one dimension. The nonlinear stress parameter will be discussed in detail in the 'Nonlinear Stress Parameter' section of this chapter. The four terms

shown are the four independent material properties of an orthotropic composite lamina. Note also, that the compliance terms are no longer just functions of time but of temperature and stress level. As with the nonlinear stress effects, the temperature, and other accelerating factors such as moisture, will be presented later in this chapter. The models described in the following section will present various nonlinear compliance models that use a nonlinear stress parameter.

Viscoelastic Constitutive Models

This section will examine briefly some the more popular viscoelastic compliance models used in both linear and nonlinear viscoelasticity. They will only be presented here from a one dimensional point of view, i.e. $\varepsilon(t) = S(t,\sigma)\cdot\sigma$, but all four compliance terms of an orthotropic material under plane stress can be modeled similarly.

The mechanical analogy model of springs and dashpots is one of the most basic and easiest to understand models for viscoelasticity. By placing a sufficient number of springs and dashpots in series and/or parallel, any linear material property can be accurately modeled. The most commonly used configuration to model creep compliance is a series of Kelvin elements (a single spring and dashpot in parallel) with a single free spring as shown in Fig. 2.5. For linear springs and dashpots the compliance function becomes

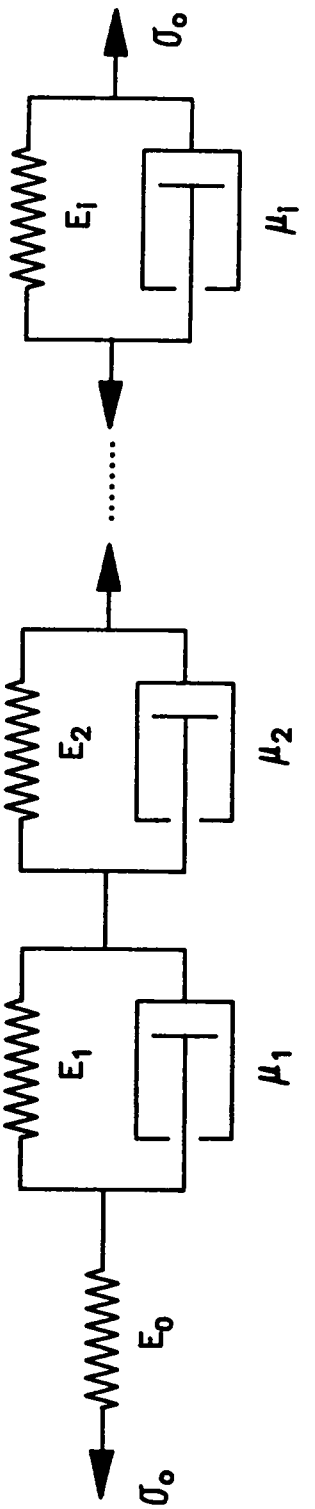

Fig. 2.5 Kelvin Elements and Single Spring in Series (Prony Series).

$$S(t) = \frac{1}{E_o} + \sum_{i=1}^{n} \frac{1}{E_i} \left[1 - e^{-E_i t/\mu_i} \right] \qquad (2.27)$$

Where E is the spring stiffness and μ is the dashpot viscosity. The model shown in Fig. 2.5 is considered a viscoelastic solid since there is no permanent flow. If a single dashpot is added in series, thereby allowing permanent deformation to occur, the resulting model would be considered a viscoelastic fluid [10]. These linear mechanical models can be extended to include nonlinear stress effects by simply allowing the springs and/or dashpots to be nonlinear. This idea is more fully developed in chapter 3 when the numerical procedure to solve nonlinear viscoelastic problems is presented. The major drawback of using mechanical analogy models is the large number of parameters that must be defined or determined.

One of the first models to consider the nonlinear stress effect was the multiple integral by Green and Rivlin [95] which is based on the Volterra-Frechet integral. For general loading this model is expressed as

$$\varepsilon(t) = \int_{-\infty}^{t} S_1(t-\tau) \frac{d\sigma(\tau)}{d\tau} d\tau + \int_{-\infty}^{t}\int_{-\infty}^{t}\int_{-\infty}^{t} S_3(t-\tau_1, t-\tau_2, t-\tau_3) \cdot$$

$$\frac{d\sigma(\tau_1)}{d\tau_1} \frac{d\sigma(\tau_2)}{d\tau_2} \frac{d\sigma(\tau_3)}{d\tau_3} d\tau_1 d\tau_2 d\tau_3 + \ldots\ldots \qquad (2.28)$$

This model is similar to the Boltzman integral for the first integral

term. The additional terms, while complex, simply allow the nonlinear effects to be modeled. While this model can accurately model most viscoelastic materials, the complexity of the model limits its usefulness. Even if the expression is limited to only triple integrals, there are still 12 kernels to be determined experimentally which is beyond the ability of most testing methods and patience of many investigators.

Another method to account for the stress nonlinearities is through the use of a superposition principle similar to the Time-Temperature-Superposition-Principle, TTSP, (see the TTSP section). Given the basic equation

$$S(t,\sigma) = S_o + b_\sigma \Delta S(\xi) \qquad (2.29)$$

where b_σ = vertical shift factor

ξ = reduced time given by $\xi = t/a_\sigma$ and a_σ is the horizontal shift factor due to the stress level

one can see how the various stress effects could be shifted to generate a master curve based on short term testing. This expression has been used for nonlinear stress effects in graphite/epoxy composites by Griffith [73] with some success. However, this scheme does not lend itself to a numerical procedure and thus was not pursued as a viable model.

Power Law Based Viscoelastic Constitutive Models (Both Linear and Nonlinear)

The simple power law

$$S(t) = S_o + mt^n \tag{2.30}$$

where S_o is the instantaneous compliance, and m and n are constants, is a common method used to describe the linear viscoelastic response of a material . This model has been shown to work well for a large variety of both metallic and polymeric materials. The power law can be modified to include nonlinear stress effects by assuming both S_o and m are functions of stress. Findley [23-28] proposed that the stress function should be in the form of a hyperbolic sine function, such that

$$S_o = S_o' \sinh(\sigma/\sigma_s) \tag{2.31a}$$

$$m = m' \sinh(\sigma/\sigma_m) \tag{2.31b}$$

$$n = \text{constant (assumed independent of stress level)}$$

where S_o', σ_s, m', and σ_m are material constants. Even though this model (often referred to as the Findley power law) is basically an empirical model, it has been applied to various material systems with success [27,27,78]. The advantage of the power law is in its simplicity and relatively few constants which need to be determined from experimental data.

This study used the power law but instead of the hyperbolic sine function to model the nonlinear stress effects, a simple quadratic

function was used, giving

$$S(t,\sigma) = (1 + g\sigma^2)S_o + (1 + f\sigma^2)mt^n \qquad (2.32)$$

where S_o and m are the linear constants and g and f are the nonlinear stress constants. The reason for this modification was two fold. First, the hyperbolic sine function can cause numerical difficulties at high stress levels since the sinh function increases rapidly for values larger than 1. Second, by simply allowing f and g to be zero, the linear form is regained, whereas with the sinh function, f needs to go to infinity, which is conceptually and numerically more difficult. Furthermore, the general idea of the nonlinear effect being a higher order effect of the linear case is also easily understood. This model will be referred to as the 'quadratic power law' in this study.

The equation parameters for both the Findley and quadratic power law models, 5 total, (S_o, m, n, f, and g for the quadratic power law), can be obtained solely from creep tests. The linear terms, S_o, m, and n, are first determined by using a least-squares fitting routine. The nonlinear terms, f and g, are obtained by fitting the quadratic function to a series of S_o and m values that were determined from a series of creep tests at different stress levels. A least-squares routine is also used in this model fitting. An interactive computer program was written to do the model fitting on a microcomputer, which is described in Appendix A. While some investigators [31,76] have argued that creep recovery tests should be exclusively used to

determine the exponent n, this study on Kevlar/epoxy composite showed that both creep and creep recovery tests will give the same n value as is graphically shown in Fig. 2.6. Other tests that were conducted in this study showed similar results. Furthermore, the accuracy of fit for the creep data was substantially better than for the creep recovery data, based on the coefficient of variation (Fig. 2.7) for all tests. Therefore, this study used only the creep test data in determining the viscoelastic parameters.

Another insight obtained from Fig. 2.6 is the exponent 'n' of the power law is dependent on the temperature of the test. Since the time and temperature are related through the TTSP, this temperature dependence can also be viewed as a time dependency. The low temperature tests are representative of the relatively flat initial portion of a power law curve whereas the higher temperature tests reflect the curve at longer times where it is changing rapidly (Fig. 2.8). Thus, it is not surprising for the low temperature to have a low 'n' value since they are trying to model the flat initial region of the power law. The 'n' value does tend to become constant for the higher temperature tests since they are in the upper portion of the curve where it is changing rapidly. Similarly, Heil [76] showed that the 'n' value increases as the length of the creep tests increases but will become constant at some point, presumably when the creep tests enters into the upper portions of the power law. In view of this effect, short term tests should not be used to model long term effects but master curves or actual long length tests where both the

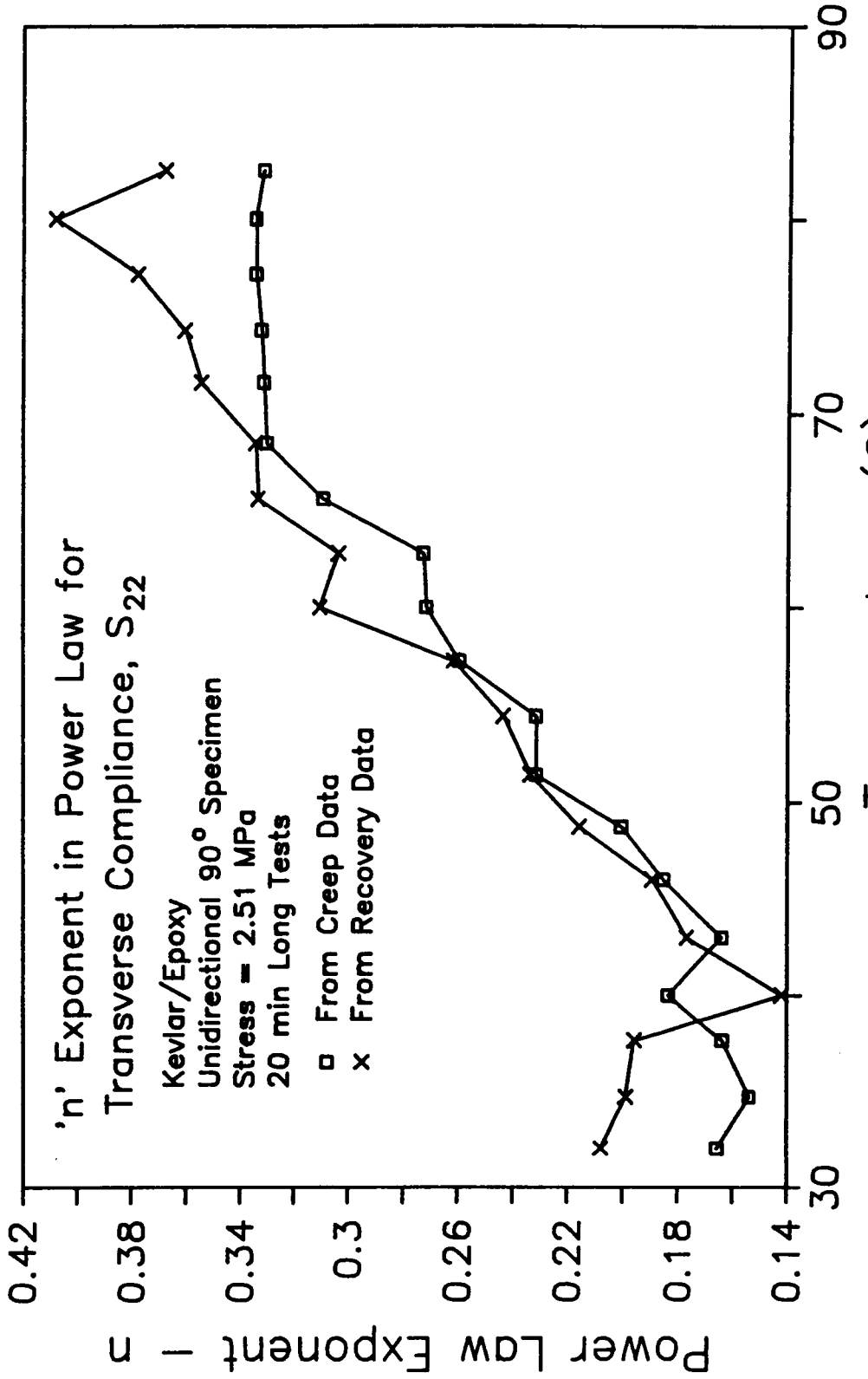

Fig. 2.6 Comparison of 'n' Values in Power Law from Creep and Creep Recovery Data.

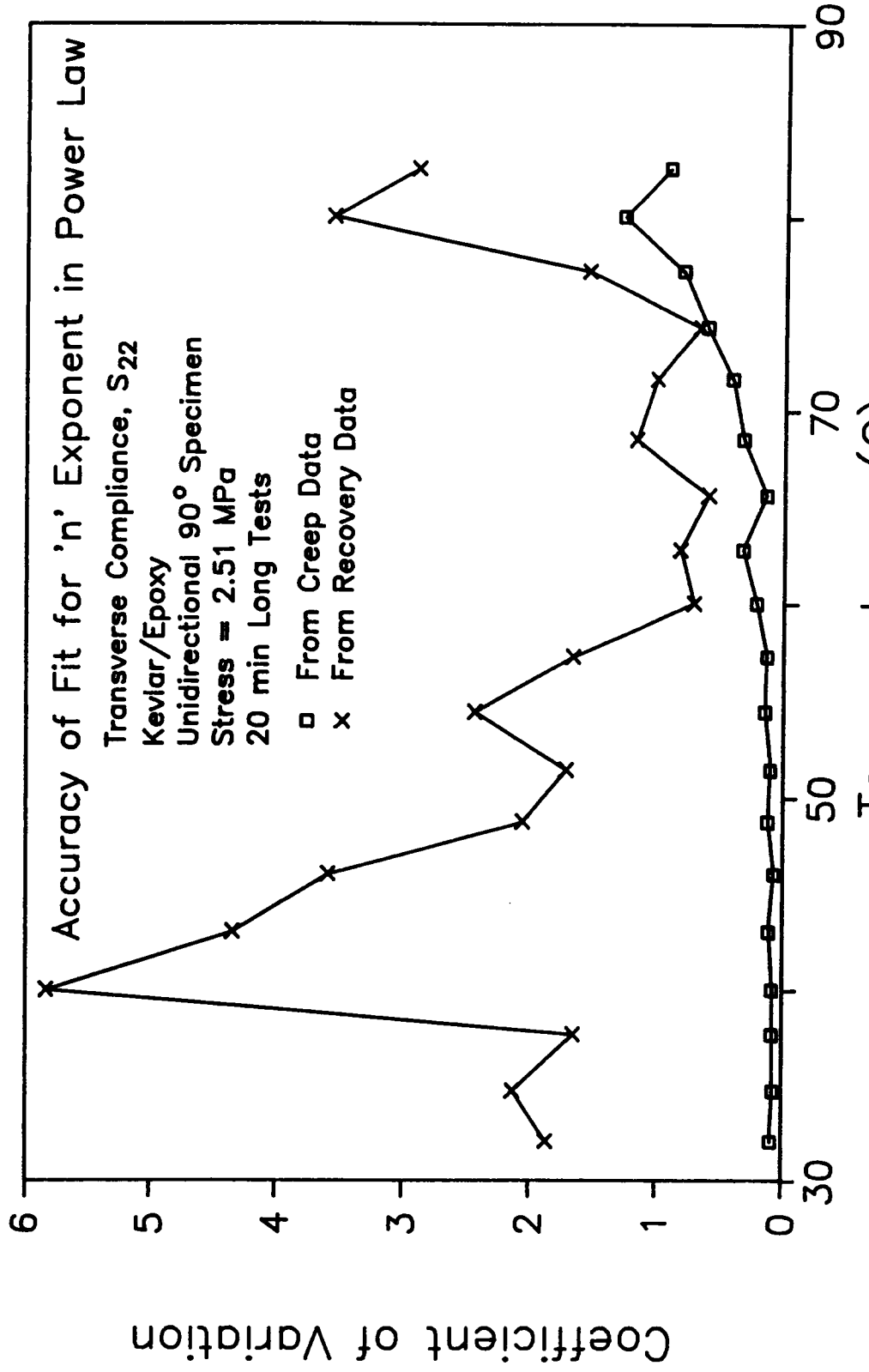

Fig. 2.7 Comparison of Fit Accuracy for Power Law 'n' Exponent from Creep and Creep Recovery Data.

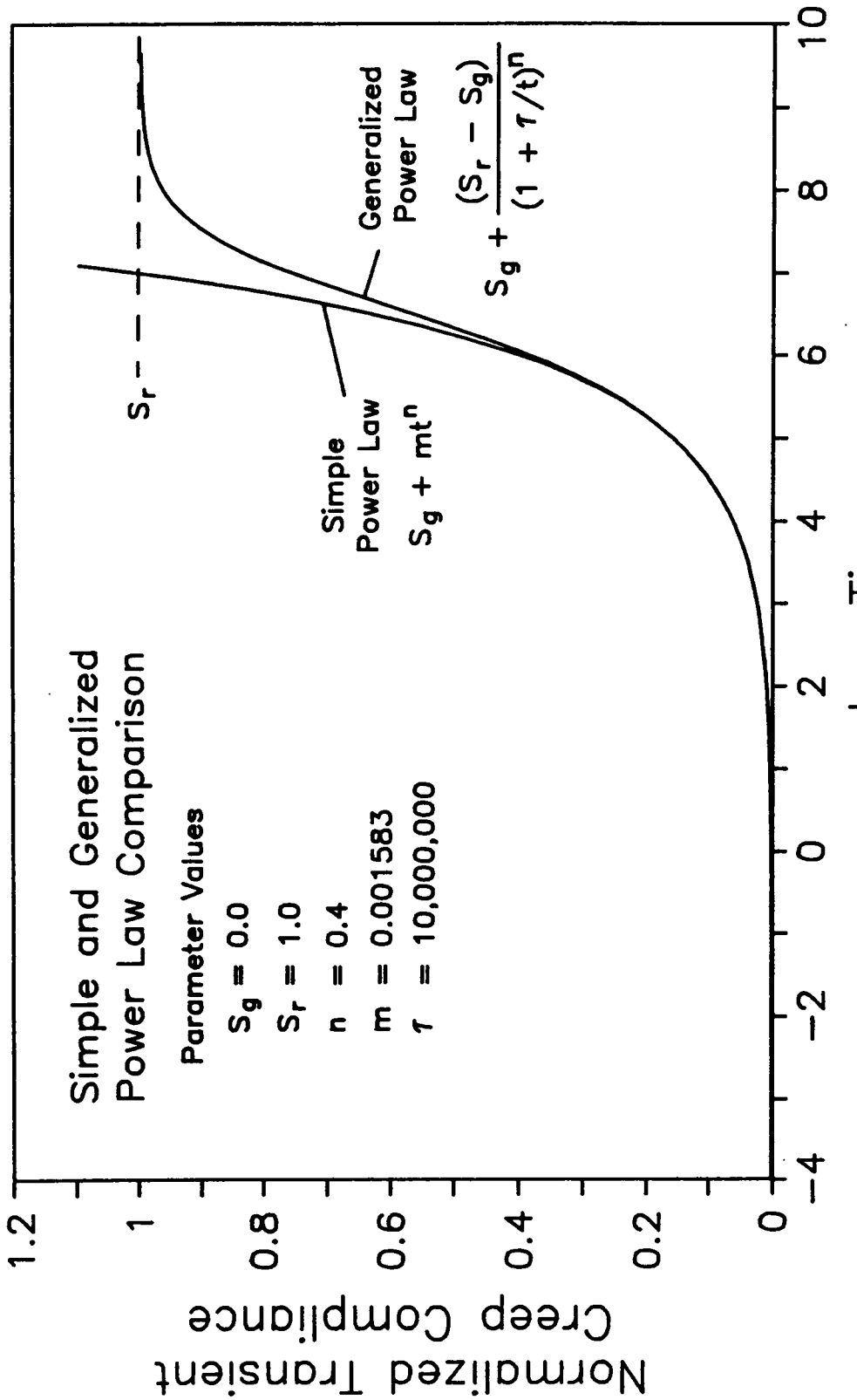

Fig. 2.8 Simple and Generalized Power Law Compliance Comparison.

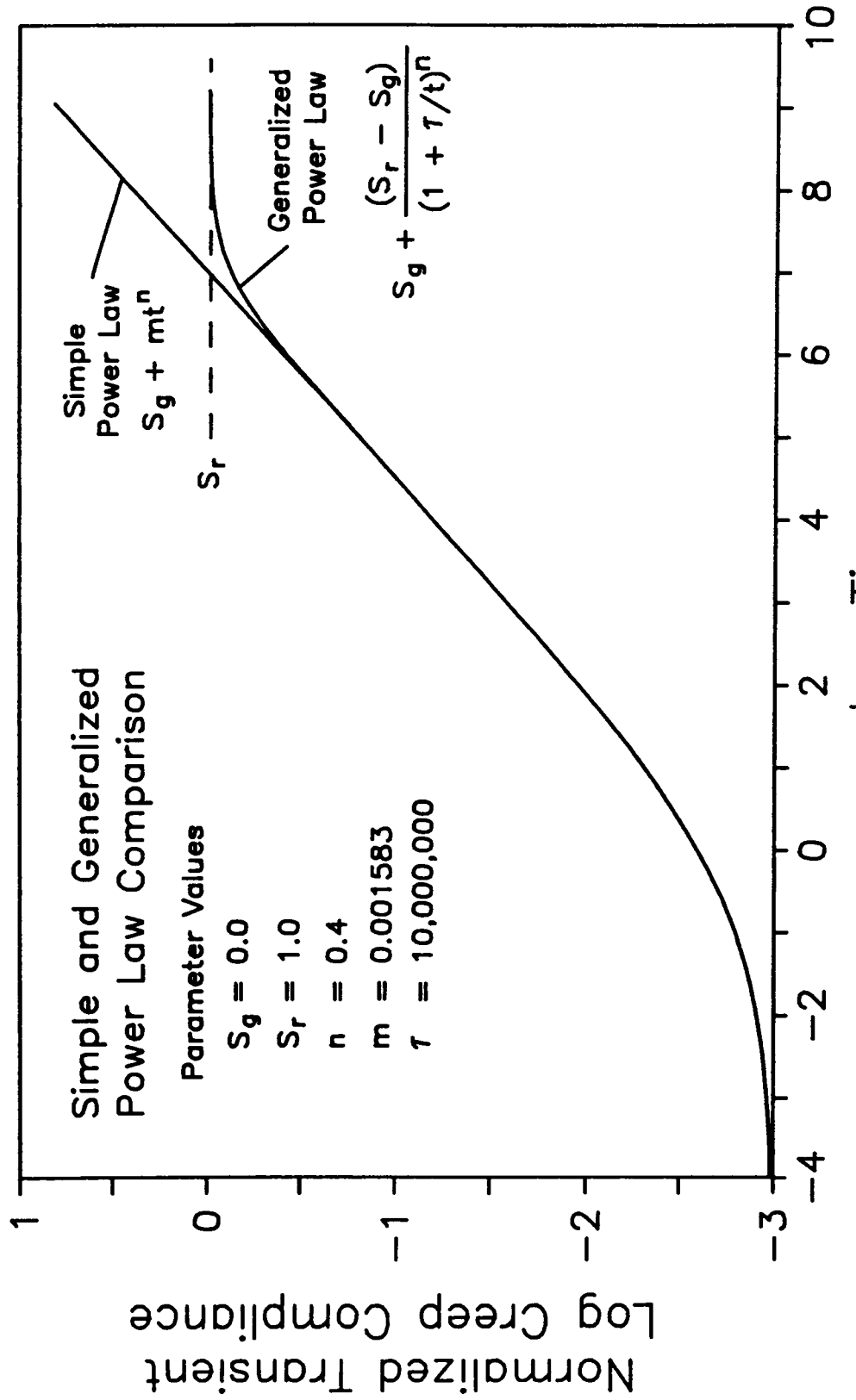

Fig. 2.9 Simple and Generalized Power Law Log Compliance Comparison.

initial and upper portion of the power law curve are evident should be used. This study uses master curves, constructed using the TTSP, which enables 'n' to be obtained for the entire curve at one time.

In recent years the general power law has increased in popularity. The linear model can be written as

$$S(t) = S_g + \frac{(S_r - S_g)}{(1 + \tau/t)^n} \qquad (2.33)$$

where S_g is the initial (or glassy) compliance, S_r is the long term or rubbery compliance, τ is the characteristic time of the power law and n is the power law exponent. This model has four parameters, which is one more than the simple power law. This allows the rubbery plateau region of the compliance, which is common in polymeric materials to be modeled. Figures 2.8 and 2.9 show how the simple and general power laws compare in both normal compliance and log compliance scales.

Schapery Integral (Nonlinear Viscoelastic Constitutive Model)

Another widely used nonlinear viscoelastic model is the Schapery integral model which is derived from the fundamental principles of irreversible thermodynamics [29-34]. This model has been used successfully on graphite/epoxy composites [76]. For uniaxial stress the final form for strain is written

$$\varepsilon(t) = g_o S_o \sigma + g_1 \int_{-\infty}^{t} \Delta S(\psi - \psi') \frac{d(g_2\sigma)}{d\tau} d\tau \qquad (2.34)$$

where

S_o, $\Delta S(\psi)$ = initial and transient compliance for the linear viscoelastic response

$$\psi = \psi(t) = \int_o^t \frac{dt'}{a_\sigma}$$

$$\psi' = \psi'(\tau) = \int_o^\tau \frac{dt'}{a_\sigma}$$

g_o, g_1, g_2, a_σ = nonlinearizing stress functions

It should be noted that both S_o and ΔS compliances are independent of stress and the nonlinear stress effects are introduced through the g_o, g_1, g_2, and a_σ terms. The a_σ can be considered as a 'stress shift factor' similar to the temperature shift factor a_T (to be discussed in a subsequent section). While the ΔS function is not restricted to any particular form, the power law, $\Delta S(\psi) = m\psi^n$, is generally used for convenience. Equation 2.34 then becomes

$$\varepsilon(t) = g_o S_o \sigma + g_1 m \int_{-\infty}^{t} (\psi - \psi')^n \frac{d(g_2\sigma)}{d\tau} d\tau \qquad (2.35)$$

If the nonlinear parameters are equal to 1 ($g_o=g_1=g_2=a_\sigma=1$) then the linear Boltzman Superposition Principle equation is obtained (Eq 2.25). For a simple static creep test, with the load equal to σ_o, Eq. 2.35 can be further simplified to

$$\varepsilon(t) = \left[g_o S_o + \frac{g_1 g_2 m t^n}{a_\sigma^n} \right] \sigma_o \qquad (2.36)$$

This form is similar to the nonlinear power law type models previously reviewed, except for the form of the nonlinear stress functions, which are compared in Table 2.1.

Table 2.1. Comparison of Functions for Compliance.

Schapery Integral	Findley Power Law	Quadratic Power Law	Basic Power Law
$g_o(\sigma)$	$\sinh(\sigma/\sigma_s)$	$(1 + g\sigma^2)$	S_o
$\frac{g_1(\sigma)\ g_2(\sigma)}{a_\sigma(\sigma)^n}$	$\sinh(\sigma/\sigma_m)$	$(1 + f\sigma^2)$	m

Since the form of the stress functions can be chosen arbitrarily for the Schapery model, the difference between the three models is only minor. For a more detailed derivation and understanding of the Schapery integral as applied to composite materials, refer to Tuttle [75] or Heil [76].

The Schapery integral equations in the form of Eq. 2.35 require 7 constants to be determined from the experimental data as opposed to 5 for the nonlinear Findley or quadratic power law model. The additional parameters allow more flexibility in modeling the nonlinear

stress effects but have the disadvantage of requiring additional experimental tests to obtain those parameters. To determine all seven parameters, creep and creep recovery data must be used in a four step curve fitting procedure. The first two steps determine the linear parameters, S_o, m and n, from creep and creep recovery data in the linear stress range. The remaining nonlinear parameters, g_o, g_1, g_2, and a_σ, are determined from the creep and creep recovery data in the nonlinear stress range. Two difficulties in using this procedure are: first, the linear and nonlinear stress range must be determined before the fitting process and second, recovery data must be used. While the first objection can be overcome by repeated fittings until the best linear and nonlinear ranges are found the second poses more serious drawbacks. The strain in a creep/creep recovery test should theoretically return to zero for a true viscoelastic solid, which is the assumption of the Schapery integral model. However, actual tests have shown that the recovery many times does not return to zero and the concept of permanent deformation must be introduced [75,76]. This permanent deformation is generally subtracted from the creep recovery data before calculating the 7 parameters by curve fitting. Furthermore when repeated tests are performed on the same specimen, which is necessary when using the Time-Temperature-Superposition-Principle (see later section), the creep recovery data becomes very sensitive to long term recovery of previous tests. This is especially true at high test temperature. Also the weight of the grips, which must remain attached to the specimens in the ovens during the creep

recovery portion of the test, can have a significant effect on the S_{22} and S_{66} compliance terms due to the low stiffness and strength of those compliances.

This study will use the quadratic power law model due to its ease of use and understanding, and the ability to get all parameters from the creep curves. Also, the difference between the Schapery integrals, quadratic and Findley power law models in the final form differ only in the stress function form which is totally arbitrary (see Table 2.1).

Nonlinear Stress Parameter

The expressions for the nonlinear power law type models and Schapery integral model presented previously were simplified for a one dimensional type material in a uniaxial stress state. In those cases the nonlinear stress parameter was simply the applied stress level, the only stress component. However, for materials in a state of plane stress, such as composite laminate, there can be three stresses, σ_1, σ_2, and τ_{12}, all of which could affect the viscoelastic response. Furthermore, this stress state can be broken down into the matrix and fiber stresses giving a total of six stresses that could possibly influence the nonlinear stress effect. The most general form of the nonlinear viscoelastic compliance term would be

$$S_{ij} = S_{ij}(T, t, \sigma_1^f, \sigma_2^f, \tau_{12}^f, \sigma_1^m, \sigma_2^m, \tau_{12}^m) = S_{ij}(T, t, \sigma) \qquad (2.37)$$

where f and m superscript refers to the fiber and matrix stresses,

respectively and σ is some combination of the stresses referred to as the nonlinear stress parameter. In matrix form the equation would be

$$\begin{Bmatrix} \varepsilon_1(t) \\ \varepsilon_2(t) \\ \gamma_{12}(t) \end{Bmatrix} = \begin{bmatrix} S_{11}(t,T,\sigma) & S_{12}(t,T,\sigma) & 0 \\ S_{12}(t,T,\sigma) & S_{22}(t,T,\sigma) & 0 \\ 0 & 0 & S_{66}(t,T,\sigma) \end{bmatrix} \begin{Bmatrix} \sigma_{1_o} \\ \sigma_{2_o} \\ \tau_{12_o} \end{Bmatrix} \quad (2.38)$$

In order to account for the stress interaction, the matrix octahedral shear stress, τ^m_{oct}, was introduced by Schapery [31], and has been used successfully by others [74-76] for use with composite materials. The general form for τ^m_{oct} is

$$\tau^m_{oct} = \frac{1}{3}\left[(\sigma^m_1 - \sigma^m_2)^2 + (\sigma^m_1)^2 + (\sigma^m_2)^2 + 6(\tau^m_{12})^2\right]^{\frac{1}{2}} \quad (2.39)$$

where the matrix stresses are given by

$$\begin{Bmatrix} \sigma^m_1 \\ \sigma^m_2 \\ \tau^m_{12} \end{Bmatrix} = \begin{bmatrix} \left(\frac{E_m}{E_{11}}\right) & \left(1 - \frac{E_m}{E_{11}}\nu_{12}\right) & 0 \\ 0 & 1 & 0 \\ 0 & 0 & 1 \end{bmatrix} \begin{Bmatrix} \sigma_1 \\ \sigma_2 \\ \tau_{12} \end{Bmatrix} \quad (2.40)$$

However, τ^m_{oct} is only applicable for those compliance terms, mainly S_{22} and S_{66}, where the fiber direction stress, σ_1, does not influence the nonlinear creep. For graphite/epoxy composites, τ^m_{oct} has worked well [74-76] since the fibers are non-viscoelastic and thus only the S_{22} and S_{66} compliance terms need to be modeled. For Kevlar/epoxy composites, the S_{11} and S_{12} compliance terms are viscoelastic and

require some sort of nonlinear stress parameter. Because, the stresses in the matrix will have little effect on the creep in the fiber direction, τ^{m}_{oct} cannot be used for the nonlinear stress parameter in the S_{11} and S_{12} terms.

Griffith [73] in his study of viscoelastic effects of Graphite/epoxy composites used a simple but seemly effective nonlinear parameter of σ_2 ($=\sigma^{m}_{2}$) for S_{22}, and τ_{12} ($=\tau^{m}_{12}$) for S_{66} which will be referred to as the 'direct stress method' in this study. He thus neglected the stress interaction between the different stresses but still had reasonable results. This was used in the present study with the added nonlinear parameter of σ_1 for S_{11} and S_{12} since this is the dominant stress for both of those compliances. Various numerical creep predictions were performed on the Kevlar/epoxy laminates to identify the difference between using the τ^{m}_{oct} or direct stress method. The results of these tests showed no difference (<0.1%) for all test cases. The final constitutive relationship used in this study to describe the nonlinear stress effects are

$$\begin{Bmatrix} \varepsilon_1(t) \\ \varepsilon_2(t) \\ \gamma_{12}(t) \end{Bmatrix} = \begin{bmatrix} S_{11}(t,T,\sigma_1) & S_{12}(t,T,\sigma_1) & 0 \\ S_{12}(t,T,\sigma_1) & S_{22}(t,T,\sigma_2) & 0 \\ 0 & 0 & S_{66}(t,T,\tau_{12}) \end{bmatrix} \begin{Bmatrix} \sigma_{1_o} \\ \sigma_{2_o} \\ \tau_{12_o} \end{Bmatrix} \quad (2.41)$$

where $S_{ij}(t,T,\sigma) = S_{ij}\ (1 + g_{ij}\sigma^2) + m_{ij}\ (1 + f_{ij}\sigma^2)t^{n_{ij}}$.

Time-Temperature-Superposition-Principle

The Time-Temperature-Superposition-Principle (TTSP) in viscoelasticity, simply stated, relates time and temperature effects on the behavior of polymers. This principle, also known as the Time Translation Equivalence, Method of Reduced Variables, or Time Temperature Analogy, is important in characterizing the time dependent response of polymer based viscoelastic materials because the temperature parameter can be used to accelerate the time dependent processes, such as creep. Even though the TTSP is generally considered an empirical process and relies heavily on experimental data to formulate the time temperature relationship, it has been used extensively in characterizing polymer based materials with good results. One of the main objectives of this study is to characterize Kevlar/epoxy, where both the fibers and resin are polymers, for long periods of time using only short term tests. This requires an accelerated test method such as the TTSP. Basic background information concerning the TTSP will be presented in this section along with simple examples demonstrating its usefulness and methodology of application.

Leaderman was first to explicitly state that time and temperature are related, forming the basis of the TTSP [96]. He noted that the creep compliance curve at an elevated temperature is the same shape as a creep compliance curve at a lower temperature but displaced in time. This effect, which is also referred to as contraction of the time scale or reduced time, is best understood with a graphical example

such as Fig 2.10. In principle, any part or section of a creep compliance curve can be obtained quickly by simply changing the temperature and shifting the curve horizontally by the shift factor a_T (a_T is defined in detail in the following paragraph). By extending this concept to multiple compliance creep curves at various temperature levels, one can readily see how a long term master curve can be constructed by horizontal shifting the short term individual curves together as graphically shown in Fig. 2.11. The TTSP also works equally well on creep recovery, modulus, and vibration type tests. Also there has been some effort to extend the TTSP concept to yielding and delayed failure.

The relationship between time and temperature is generally referred to as the shift factor, a_T, which identifies the amount of horizontal shifting one curve must under go to match another curve at a different temperature, as shown in Fig 2.10. This shift factor could be thought of as a scaling time factor which relates the time, t, at the reference temperature with the reduced time, t′, at a different temperature. This relationship is generally written as

$$t' = \int_o^t \frac{dt}{a_T} \tag{2.42}$$

which can be simplified to

$$t' = \frac{t}{a_T} \tag{2.43}$$

if a_T does not change with time. This requires the temperature to be

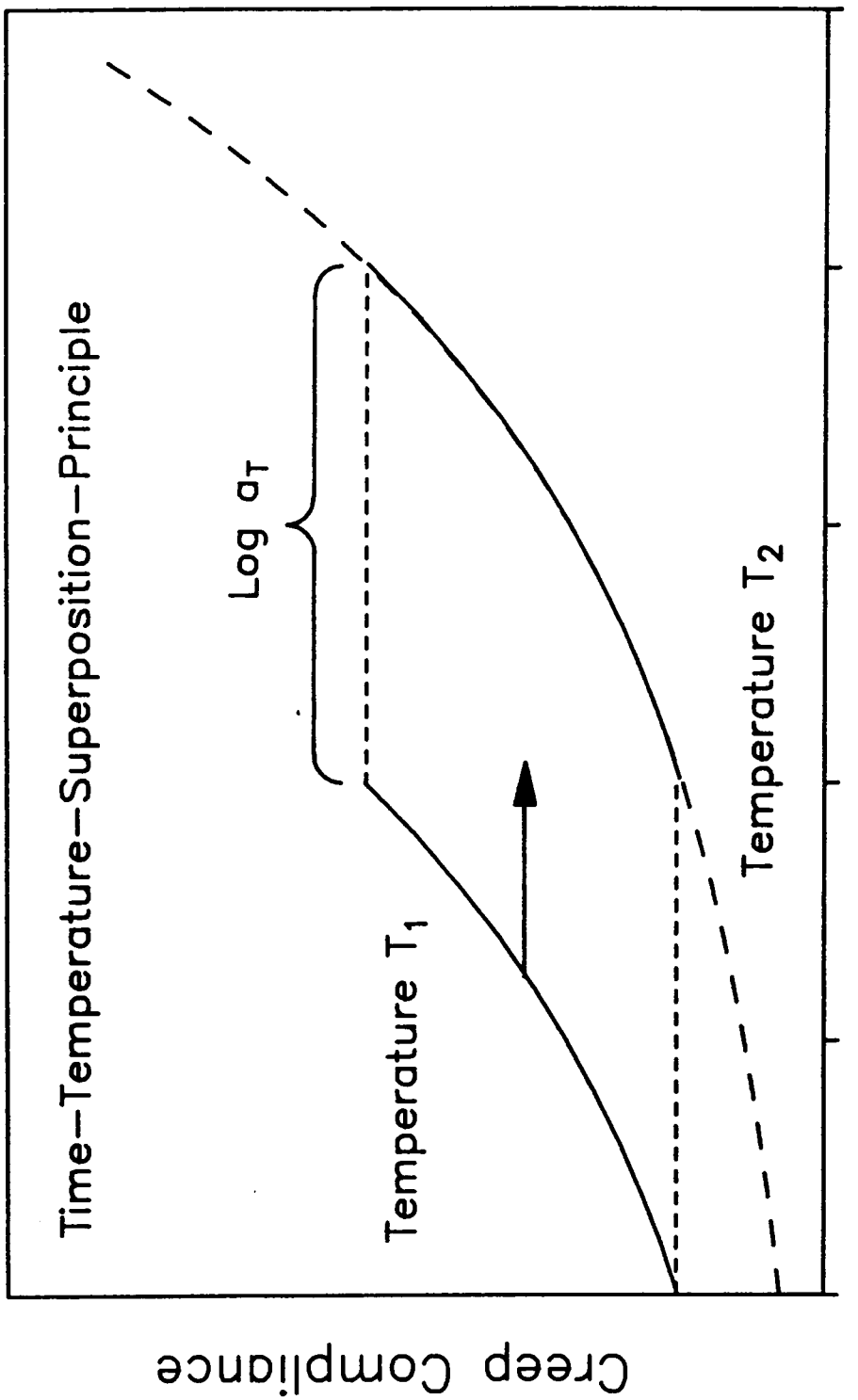

Fig. 2.10 Similar Curves at Different Temperatures.

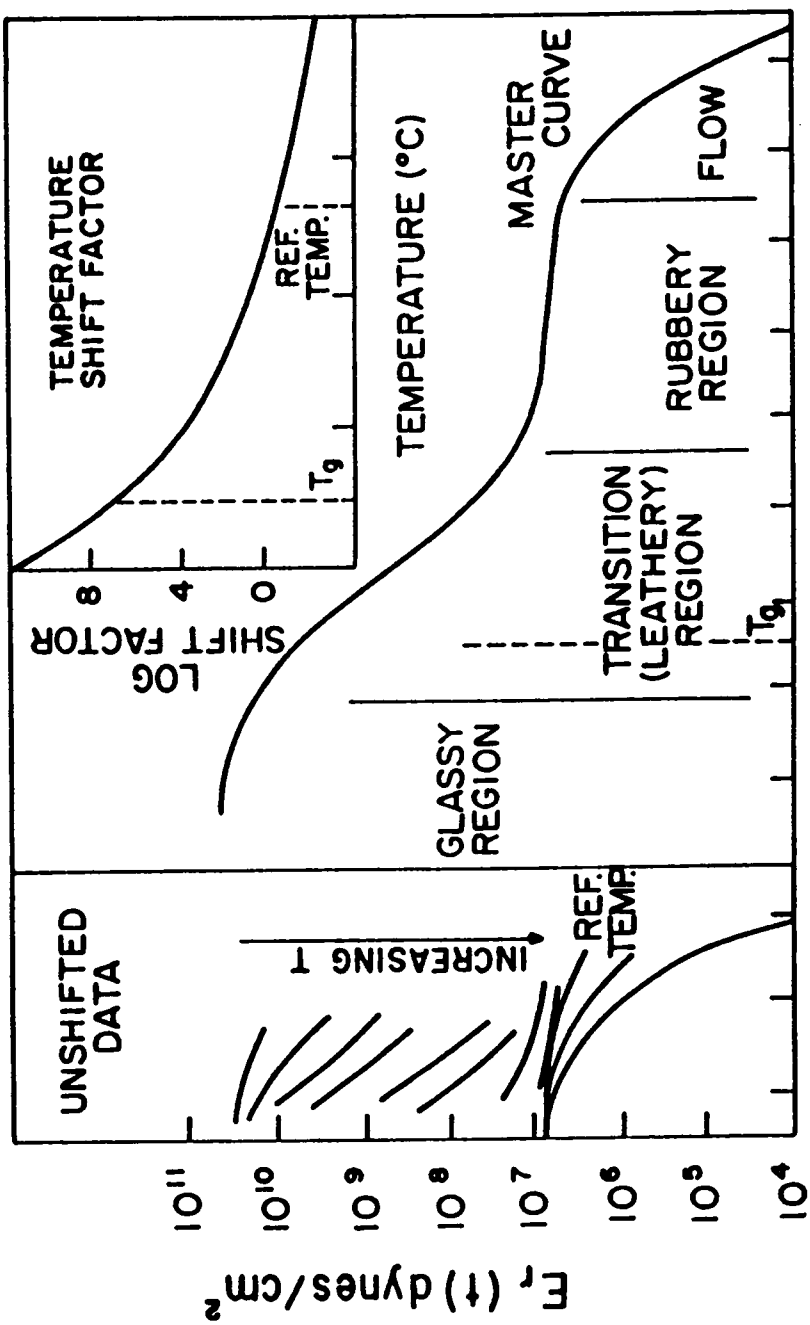

Fig. 2.11 Example of the TTSP Formation Process (Rosen [8]).

constant, which is generally true for most experimental tests. Therefore, given a creep compliance function at a reference temperature T_o,

$$S(T_o,t) = S_o + S_c(T_o,t) \tag{2.44}$$

the creep compliance at another temperature, T, becomes

$$S(T,t) = S_o + S_c(T_o,t') \tag{2.45}$$

or

$$S(T,t) = S_o + S_c(T_o,t/a_T) \tag{2.46}$$

where the shift factor, a_T, is known at the reference temperature. This shifting process is more obvious if the log of Eq. (2.43) is taken

$$\text{Log } t' = \text{Log } t - \text{Log } a_T \tag{2.47}$$

The creep curve at the new temperature can now be viewed as a simple shifting of curves in log time by the amount of Log a_T. The shifting will be left if Log a_T is positive (the new temperature is below the reference temperature) and right if Log a_T is negative. Although this is the accepted convention in the western world there are other conventions.

Every temperature will have a different a_T and the function that relates a_T and temperature is called the shift factor function. An example of such a function is shown in the upper right hand corner of Fig. 2.11. A tremendous amount of effort has gone into using the TTSP

on a wide variety of materials with the hopes of finding a single shift factor function for all materials. However, the shift factor function is still generally determined experimentally by performing various creep, creep recovery, or dynamic loading tests at various temperatures and time periods.

There are, however, two well known and well used equations developed for shift factor function that work for a wide variety of materials. The most famous is the WLF (Williams-Landel-Ferry) [4] equation given as

$$\text{Log } a_T = \frac{-C_1(T - T_o)}{C_2 + T - T_o} \tag{2.48}$$

where T_o is the reference temperature (C) which is generally the glass transition temperature T_g, T is the actual temperature (C), and C_1 and C_2 are constants. This equation has been found to fit experimental data for many polymeric based material when C_1 and C_2 are equal to 17.44 and 51.6, respectively for the temperatures between T_g, and 100° C above the T_g. For a further understanding of the WLF equation see Ferry [1].

A second equation that has been generally used for temperatures below the T_g is based on the Arrhenius equation

$$a_T = B \exp\left\{\frac{\Delta H}{RT}\right\} \tag{2.49}$$

where B is a constant, ΔH is the activation energy, R is the universal

gas constant, 1.985 cal/mole-K, and T is temperature. By taking the log of both sides and integrating between the reference temperature T_o, and the desired temperature T, gives the better known form of

$$\text{Log } a_T = \frac{\Delta H}{2.303\ R}\left[\frac{1}{T} - \frac{1}{T_o}\right] \tag{2.50}$$

where T and T_o are in degrees Kelvin.

Even though both the WLF and Arrhenius equations have been shown to work well with many material systems, experimental data still should be used to determine the shift factor function of any new material. Therefore, it can be said that all shift factor functions are empirical and any function could be used to describe the shift factors. Along these lines, this study will use a simple linear function for the shift factor function due to its simplicity and ease of use in the numerical scheme which will be employed.

Although this study will not examine humidity or moisture effects, others have shown that these also behave similar to temperature in that the superposition principle can be used [51,65,66]. The Time-Temperature-Moisture-Principle (TMSP) would then include a moisture shift factor into the reduced time parameter, t′, as

$$t' = \frac{t}{a_T\, a_M} = \frac{t}{a_{TM}} \tag{2.51}$$

where a_M is the moisture shift factor and a_{TM} is the combined shift factor. Crossman and Flaggs [48] were able to successfully obtain a

two dimensional plot showing the combined shift factor as a function of temperature and moisture for ±45° cross ply laminates made from graphite/epoxy. Others have also proposed that stress be used as a shift factor similar to temperature and moisture, which has been termed as the Time-Stress-Superposition-Principle (TSSP) [40,73].

The TTSP discussed so far has been theoretically applicable only to 'thermorheologically simple material' (TSM). This class of material generally includes only isotropic and homogeneous materials with only one viscoelastic component. On the other hand 'thermorheologically complex materials' (TCM), includes two part materials such as composite materials, where it is possible for both the fibers and resin to have different viscoelastic components. For TCM vertical shifting of creep compliance curves may become necessary for all temperature ranges, whereas vertical shifting is only necessary above the T_g for TSM. There are a number of methods to perform the vertical shifting but most rely on visual inspection of the shifted curves. Griffith [73] gives a review of the many vertical shifting methods and the difficulties encountered in trying to include vertical shifting.

This study will not use vertical shifting in the construction of master curves even though both materials in the composite system tested are viscoelastic which would classify the composite TCM. There was three main reasons for this; first, the fibers will dominant the fiber direction compliance, S_{11}, and the fiber/transverse coupling compliance, S_{12}, and likewise the resin will dominant the transverse

direction compliance, S_{22}, and shear compliance, S_{66}. This domination in the respective directions will cause the results for each direction to behave like a TSM. The second reason is the vertical shifting involves a visual or subjective decision on the shifting amount. In addition, the many different methods available for vertical shifting in itself casts doubt on its reliability. Recall, one of the end results of this study is a self contained test procedure for accelerated testing of time dependent properties of composite materials and a computer program for the design engineer in industry and thus simplicity is of prime importance. Third, Ferry [1] stated that there should be no vertical shifting in the glassy region for most polymer materials. The temperature ranges that the Kevlar/epoxy system used in this study were within the glassy region. A further justification is the good and repeatable results obtained in using only horizontal shifting on the Kevlar/epoxy composite system tested in this study which will be presented in later chapters.

As mentioned in the previous paragraphs, the shifting process needs to be automated to insure consistency and ease of use. For this purpose an automated curve shifting procedure was developed and incorporated into a computer program. The program requires the individual short term curves, up to 30 at one time, and then it will calculate the best fit to form a master curve at the reference temperature of the first curve. For a complete understanding of the theory used and operating procedures, refer to Appendix D.

Chapter 3

NUMERICAL SOLUTION METHODS FOR VISCOELASTIC ORTHOTROPIC MATERIALS

Solving time dependent or viscoelastic problems for a homogeneous isotropic material can be involved and tedious. Extending this to nonhomogeneous and anisotropic materials such as layered fiber reinforced composite materials can be nearly impossible for closed form solutions. However, with numerical methods, the designer or engineer of these materials can predict, with reasonable accuracy, the viscoelastic response without doing actual creep tests on each possible laminate.

The overall criterion for an acceptable viscoelastic numerical method is one that will be stable for large time steps, converge to the correct answer, and minimize the necessary computer memory and time requirements. In addition to these conditions, this study requires the numerical method to operate on a microcomputer, which further restricts the computer memory and time. However, there are many benefits to using a microcomputer, such as ease of use, transportability, and ease of access to the program. Also, design engineers are able to make the design process, with its many 'what if' conditions and numerous rerunning, preceed easier and faster.

This chapter will examine various numerical methods that have been used in solving numerical viscoelastic methods. A new method,

called the Nonlinear Differential Equation Method (NDEM), which is based on the prony series, will be introduced and compared with the currently available methods. The latter part of this report will deal with the actual implementation and verification of the NDEM method.

Previous Numerical Work at VPI&SU

The concept of predicting the viscoelastic response in any general laminate has been previously investigated by others at Virginia Polytechnic Institute and State University. Yeow [72] and later Dillard, et al,[74,77] proposed using known unidirectional material properties (obtained experimentally) of a composite lamina to predict the nonlinear viscoelastic response of any general laminate constructed from the same material by numerical methods. They examined the graphite/epoxy T300/934 composite system and closely predicted the response of various general laminate composites. Others, Tuttle [75] and Heil [76], have also used this basic concept to predict the response of other graphite/epoxy systems.

The numerical solution method used by Dillard was based on classical lamination theory, with time incremented in a step fashion. The solution scheme first calculates the static stress and then begins the time step increments. The strain state is determined at $t+\Delta t$, using the stress state at time t and the viscoelastic constitutive equation for that particular material. The stress state is assumed to be constant throughout the time step from t to $t+\Delta t$. The new ply stresses are then determined at $t+\Delta t$ based on the current creep

strains and the applied mechanical load. This cycle is repeated, with the new stresses substituted back into the nonlinear compliance functions, until the stresses converge. A new time step is then taken and the process is repeated. The algorithm for calculating creep strains is similar to the classical lamination theory method of calculating the strains due to thermal loads. This procedure was implemented on an IBM mainframe computer and was called VISLAP (VIScoelastic LAmination Program) by Dillard [77].

There were three major difficulties with VISLAP and its numerical method. One, the basic algorithm of substituting old stresses back into the nonlinear compliance functions, and repeating the solution process until all stresses converge can have stability problems. This algorithm of successively substituting an unknown variable into a set of equations until convergence is achieved is called the Gauss-Seidel or successive substitution method, and is not unconditionally stable. For example, if the coefficient matrix, [C], in the following set of equations, represented in matrix form,

$$[C]\{x\} = [B] \tag{3.1}$$

is not positive definite then it will not converge [97]. In some laminate cases, predominantly two fiber angle laminates, VISLAP was unstable for this reason.

The second difficulty with VISLAP concerns the large time step size necessary to reach a solution for problems covering long time spans. If the time step is sufficiently large, stability problems

will arise. VISLAP basically uses a first order forward integrating method, called the Euler Method [98], to solve for the creep strains at each step, which will have a maximum step size to remain stable.

In conjunction with the time step size problem is the third difficulty with VISLAP; the actual computer time and computer memory space needed for a solution grows exponentially with each additional time step. Since the solution method is based on solving a convolution integral, the creep strain must be recalculated over the entire time span back to the initial start time for each time step. This requires that all stresses at each time step must be stored and used for calculations at the next time step. This recalculation of the creep strain integral at each time step becomes more time consuming with each additional step. In order to minimize the computer solution time and memory, VISLAP increases time step sizes in a logarithmic manner as the solution progresses. However, as stated earlier, this can cause numerical instabilities.

In order to overcome some of the problems in VISLAP but still retain its ability to calculate the complex, time dependent stress and strain state of an orthotropic composite laminate, various common numerical solution techniques will be investigated in the following sections. Also, a new method will be presented which resolves all the problems dealing with stability and solution time length.

Direct Iteration of the Volterra Integral

Viscoelastic problems naturally fall into the broad class of

mathematical problems called convolution integral equations, of which the Volterra integral equation of the second kind is the most common. The general form of the Volterra equation is

$$u(x) = f(x) + \lambda \int_a^x k(x,t)\, u(t)\, dt \tag{3.2}$$

where u(x) is the unknown function and f(x), k(x,t), and λ are known functions or constants. By simply changing the variable and function names and forms, the well known hereditary integral in viscoelasticity [10] becomes evident.

$$\varepsilon(t) = \sigma_o\, S(t) + \int_0^t S(t-\tau)\, \frac{\partial \sigma(\tau)}{\partial \tau}\, d\tau \tag{3.3}$$

where $\varepsilon(t)$ is the total strain, S(t) is the compliance function, and $\sigma(\tau)$ is the stress function. This form is for a single homogeneous material. For a material made from multiple homogeneous layers, i.e., composite laminates, the total strain $\varepsilon(t)$ will be a function of the stresses in each of the plies and Eq. (3.3) becomes

$$\varepsilon(\sigma(t),t) = \sigma(o)S(t) + \int_0^t S(t-\tau)\, \frac{\partial \sigma(\tau)}{\partial \tau}\, d\tau \tag{3.4}$$

which is a Volterra integral of the second kind.

A simple example of such a system would be a one dimensional laminate material that is constructed from two parallel materials as illustrated in Fig. 3.1. The two materials have different compliance

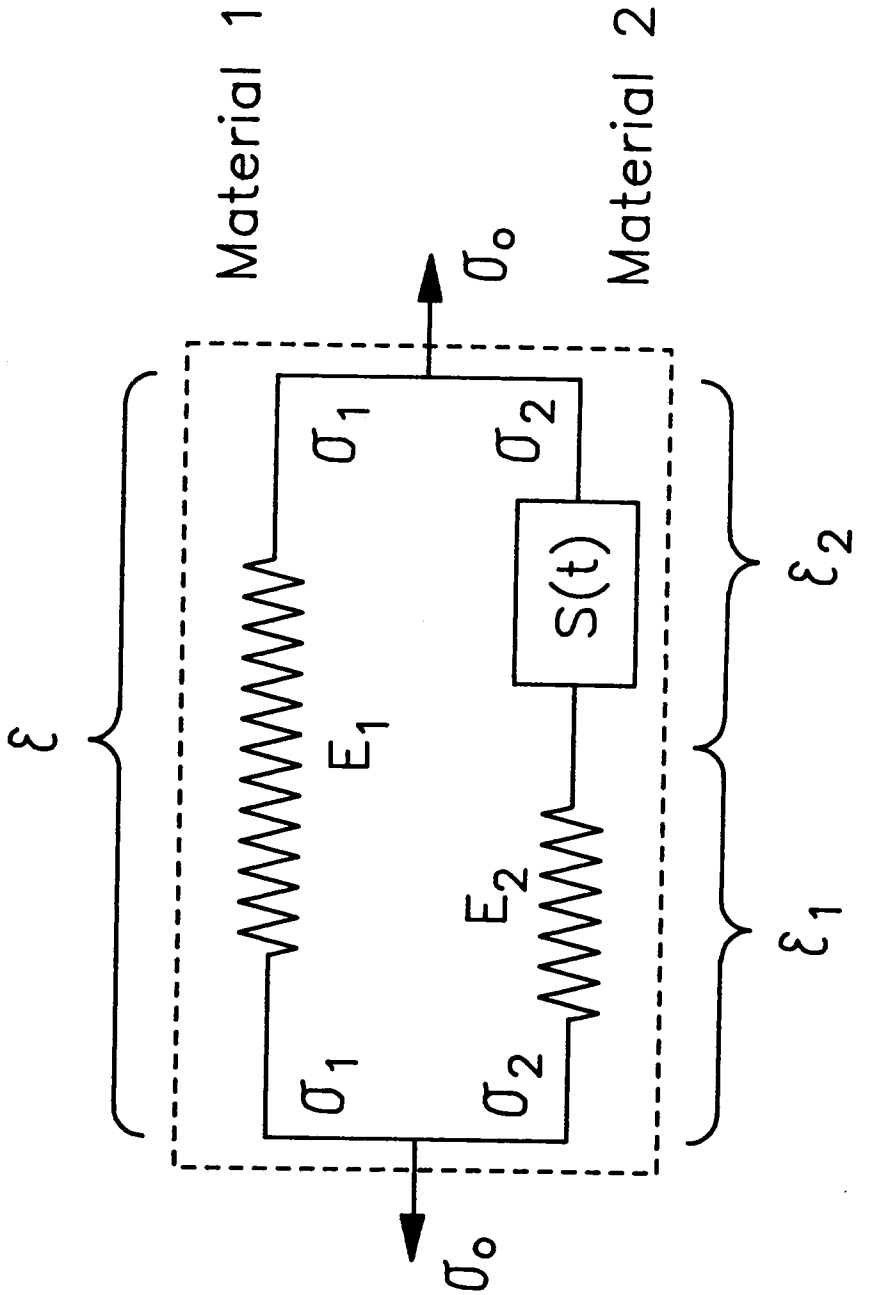

Fig. 3.1. Two Part Viscoelastic Material Model.

functions and the complete laminate is under a constant load. In this example one material will be elastic and the other viscoelastic with σ_1 and σ_2 as the stresses in material 1 and 2, respectively and σ_o as the total applied stress. If S(t) represents any time dependent compliance function then

$$\varepsilon_2(t) = \sigma_2(o)S(t) + \int_0^t S(t-\tau) \frac{\partial \sigma_2(\tau)}{\partial \tau} d\tau \qquad (3.5)$$

By using the relationships

$$\varepsilon_1(t) + \varepsilon_2(t) = \varepsilon(t) \qquad (3.6a)$$

$$\sigma_1(t) + \sigma_2(t) = \sigma_o(t) = \sigma_o \qquad (3.6b)$$

$$E_1\varepsilon(t) = \sigma_1(t) \qquad (3.6c)$$

$$E_2\varepsilon(t) = \sigma_2(t) \qquad (3.6d)$$

it can be shown that

$$\frac{\sigma_1(t)}{E_1} - \frac{\sigma_2(t)}{E_2} = \int_0^t S(t-\tau) \frac{\partial \sigma_2(\tau)}{\partial \tau} d\tau + \sigma_2(o)\, S(\tau) \qquad (3.7)$$

or

$$\sigma_2(t)\left[E_1+E_2\right] = \sigma_o E_2 - E_1E_2\int_0^t S(t-\tau) \frac{\partial \sigma_2(\tau)}{\partial \tau} d\tau - E_1E_2\sigma_2(o)S(t) \qquad (3.8)$$

This can be further simplified by integrating by parts to give

$$\sigma_2(t) = \frac{\sigma_o E_1}{E_1+E_2} + \frac{E_1 E_2}{E_1+E_2} \int_0^t \frac{\partial S(t-\tau)}{\partial \tau} \sigma_2(\tau)\, d\tau \qquad (3.9)$$

This form can be more easily evaluated since S(t) is usually given and its derivative can be calculated directly, whereas $\sigma_2(t)$ is not known and its derivative is difficult to find. Eq. 3.9 is in the standard convolution Volterra integral form which has been studied in detail by others [99-101] from a mathematical point of view. Once $\sigma_2(t)$ is known, the total strain $\varepsilon(t)$ can easily be calculated from Eq. 3.6a-d. It should be noted that the one dimensional example presented a very simplified case and for a more natural multidimensional material the equation would not only be more complex, but there would be several coupled equations and not just one. However, to understand the basic principles and difficulties in solving the Volterra by numerical methods, the given example will be examined.

A closed form solution of Eq. 3.9 is possible for certain compliance functions, S(t), such as a linear dashpot model where $S(t) = t/\mu$, or a Kelvin element model where $S(t) = 1-\exp(-tE/\mu)$. However, compliance functions with solutions are scarce and are found for only simple functions. One important function that is widely used in linear viscoelastic analysis, and does not have a closed form solution, is the viscoelastic portion of the power law equation (see Fig. 3.1)

$$S(t) = mt^n \tag{3.10}$$

where m and n are constants. Since closed form solutions are difficult to obtain and limited to certain compliance functions, numerical methods need to be applied to obtain most solutions.

Four concepts to be considered when employing numerical methods are convergence, error, stability, and solution time. The solution time length becomes especially critical when dealing with convolution Volterra integrals, due in part because $\sigma(t)$ and $\partial S(t-\tau)/\partial\tau$ continually change with each new time step. This requires the complete integral to be recalculated for each new time step. Unlike standard integrals, past results cannot be used to calculate future points, but the total integral, from t_o (t=0) to the current time, t, must be recalculated. At long times, i.e. large number of time steps, this method can require a tremendous amount of time and computer memory storage. If, however, the time steps can be varied, such as short steps at the start where the function is changing rapidly and long steps towards the end where the function is changing slowly, then this method can be economical.

Convergence is generally not a problem for a non-singular kernel or compliance function, S(t). However it does become a concern if the kernel is not well behaved or is singular. The power law (Eq. 3.10), which is used extensively in viscoelasticity, is classified as weakly singular, meaning the derivative at some point is singular or undefined (at zero for the power law). The solution of the integral

can converge with weakly singular functions if the time steps around the weakly singular point are sufficiently small. Convergence of the power law and its associated problems will be demonstrated with an example later in this section.

Stability or numerical oscillations can occur in the solution of numerical problems. Even if the problem seems to converge and the error is small, it could diverge after a certain time step or step size. Two common causes of stability problems are: 1) the numerical precision of the computer or code, which leads to round off errors and truncation, and 2) the time step size. Generally the precision of the computer is not a problem or can be solved by upgrading to a better computer or programming language. On the other hand, most numerical solution techniques have a limit on the time step size before stability becomes a concern. All forward or explicit numerical integration techniques, which are generally used for the convolution integral, are not absolutely stable for all time step sizes [98,99]. This is a serious concern with viscoelastic analysis since increasing time steps are necessary to reduce the computer calculation time and memory size, as explained in the preceding paragraphs.

Error is associated with the accuracy of the computer and the algorithm used to solve the problem. Various algorithms have been developed [99,100] for the solution of convolution integral equations which include, in ascending order of accuracy, Euler, Modified Euler or trapezoidal, Simpson rule with trapezoidal end, Simpson rule with $\frac{3}{8}$ rule, and Runge-Kutta. The higher order methods take more time for

each time step but the accuracy is generally higher and larger time step sizes are possible. The trapezoidal algorithm will be presented in detail to demonstrate how the Volterra Integral can be solved numerically. Other methods are similar and will not be presented. However, the solution of the example problem presented earlier by all methods mentioned above will be compared at the end of this section.

An approximation for the convolution integral can be written

$$\int_0^{t_i} K(t_i-\tau)\ \sigma(\tau)\ d\tau \cong h \sum_{j=0}^{i} w_{ij}\ K(t_i-\tau_j)\ \sigma(\tau_j) = h \sum_{j=0}^{i} w_{ij}\ K_{ij}\ \sigma(\tau_j)$$

$$i = 0,1,2,..N \qquad (3.11)$$

where h is the step size, $K_{ij} = \partial S(t_i-\tau_j)/\partial\tau$, and w_{ij} are the weights for the appropriate integration rule. For example, the weights for the trapezoidal method are $w_{i0} = w_{ii} = \frac{1}{2}$, and $w_{ij} = 1$. All of the preceding weights assume equal step sizes. In this manner the first few steps of Eq. 3.9 for the trapezoidal method are

$$\sigma_2(t_0=0) = \frac{\sigma_o E_1}{E_1 + E_2} \qquad (3.11a.d)$$

$$\sigma_2(t_1) = \frac{\sigma_o E_1}{E_1 + E_2} + \frac{E_1 E_2 h}{E_1 + E_2}\left[w_{10}K_{10}\sigma_2(t_0) + w_{11}K_{11}\sigma_2(t_1)\right]$$

$$= \frac{\sigma_o E_1}{E_1 + E_2} + \frac{E_1 E_2 h}{E_1 + E_2}\left[\frac{1}{2}K_{11}\sigma_2(t_0) + \frac{1}{2}K_{11}\sigma_2(t_1)\right]$$

$$\sigma_2(t_2) = \frac{\sigma_o E_1}{E_1 + E_2} + \frac{E_1 E_2 h}{E_1 + E_2}\left[\frac{1}{2}K_{20}\sigma_2(t_0) + K_{21}\sigma_2(t_1) + \frac{1}{2}E_{22}\sigma_2(t_2)\right]$$

$$\sigma_2(t_i) = \frac{\sigma_o E_1}{E_1 + E_2} + \frac{E_1 E_2}{E_1 + E_2} \frac{h}{2}\left[K_{i0}\sigma_2(t_0) + K_{ii}\sigma_2(t_i)\right] + \sum_{j=1}^{i-1} K_{ij}\sigma_2(t_j)$$

In each of these steps the unknown stress, $\sigma_2(t_i)$, can be factored out and solved for by manipulating the equation algebraically. However, if the kernel K(t) is nonlinear in terms of stress, then all i nonlinear equations would need to be solved simultaneously. This quickly becomes prohibitive since there will be thousands of time steps in a typical problem, which translates to solving thousands of nonlinear equations simultaneously. Similar relationships to Eq. 3.12 can be constructed for other integrating schemes. For higher order methods such as the Simpson rule or Runge-Kutta, a starting procedure [100-104] needs to be used which should be of the same order of magnitude in accuracy.

To evaluate the use of the Volterra integral for viscoelastic materials, the one dimensional example described at the beginning of this section (Fig 3.1) will be used. Two different but common compliance functions, S(t), were chosen to be examined, a dashpot, $S(t) = t/\mu$, where μ is the viscosity constant of the dashpot and a power law, $S(t) = mt^n$, where m and n are assumed given.

The dashpot function has an exact solution to Eq. 3.9, which will be used to verify the numerical results,

$$\sigma_2 = \sigma_o \frac{E_2}{E_1 + E_2} e^{-\lambda t} \qquad (3.13)$$

where $\lambda = E_1E_2/\mu(E_1 + E_2)$ and σ_o is constant. Five different integrating techniques were used to solve the example problem: Euler, trapezoidal, trapezoidal with 3-point starting technique, Simpson with 3-point starting technique and trapezoidal rule for even last data point, and Simpson with 3-point starting technique and 3/8 rule for the even last data point. The results are shown on Fig. 3.2. Even though the time step, h, was large, all but the Euler method are within acceptable accuracy limits.

The second compliance function to be examined, the power law, has no closed form solution to compare with the numerical results. However, by examining the results of various integrating techniques the solution can be deduced. The same five integrating techniques used for the dashpot test case were also used for the power law (constants m = 5 and n = 0.2) and the results are shown in Fig. 3.3. The time step was h = 0.1, two magnitudes smaller than for the dashpot example, but unlike the dashpot results the power law results vary and even oscillate. If the step size is reduced, the solution tends to converge to smaller values (Fig. 3.4) and it becomes evident that the time step size affects the solution convergence. The solution does seem to slowly approach a limiting value as $h \Rightarrow 0.0$.

The solution of the power law function is inaccurate because it is a weakly singular function at zero. The derivative of the power law at zero is infinity and the derivative changes rapidly for small values of time. This requires very small time steps, ($\cong 10^{-6}$) near the origin for any of the numerical integration techniques to converge.

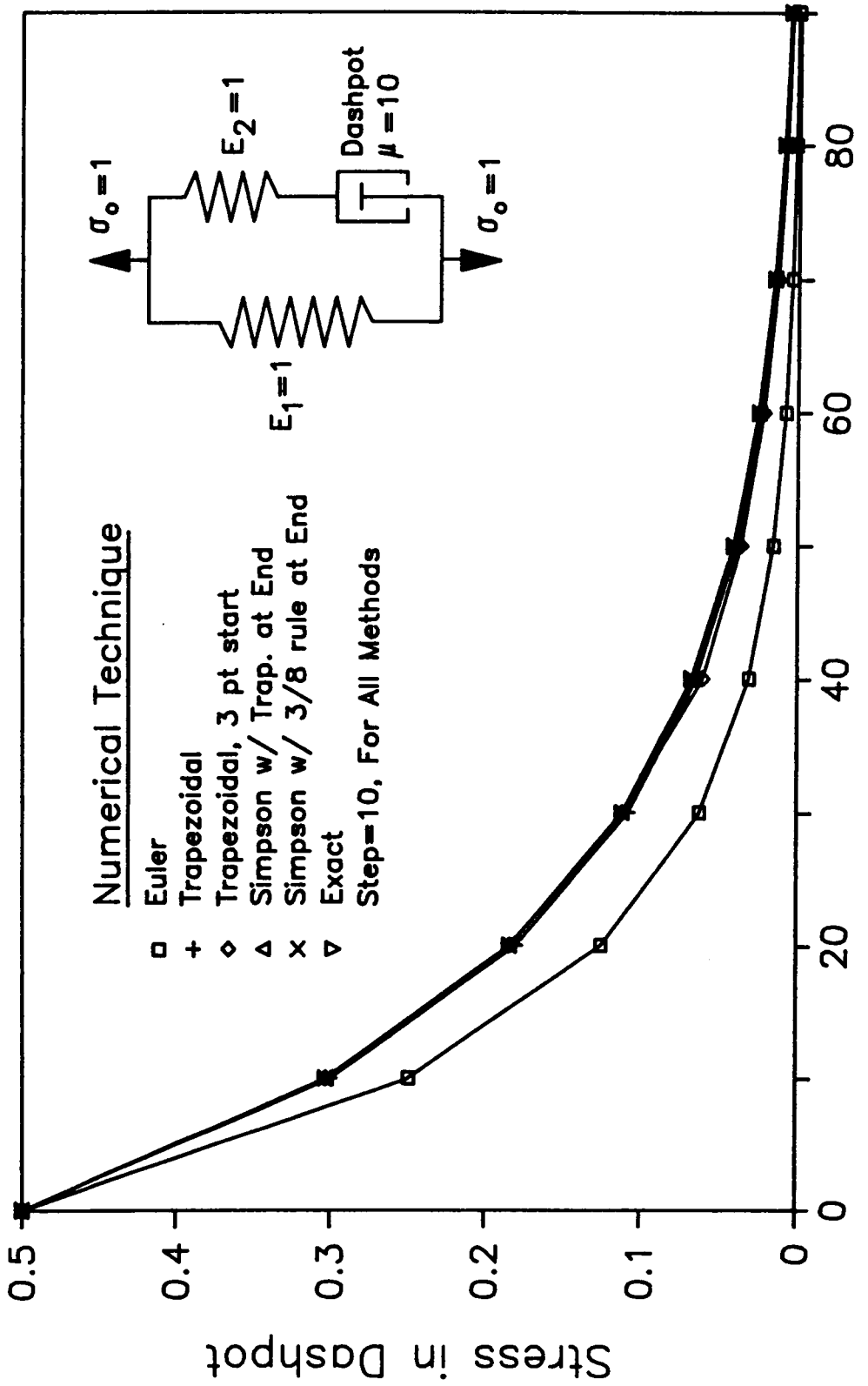

Fig. 3.2 Numerical Solutions of a 3 Parameter Dashpot Model Using the Volterra Integral.

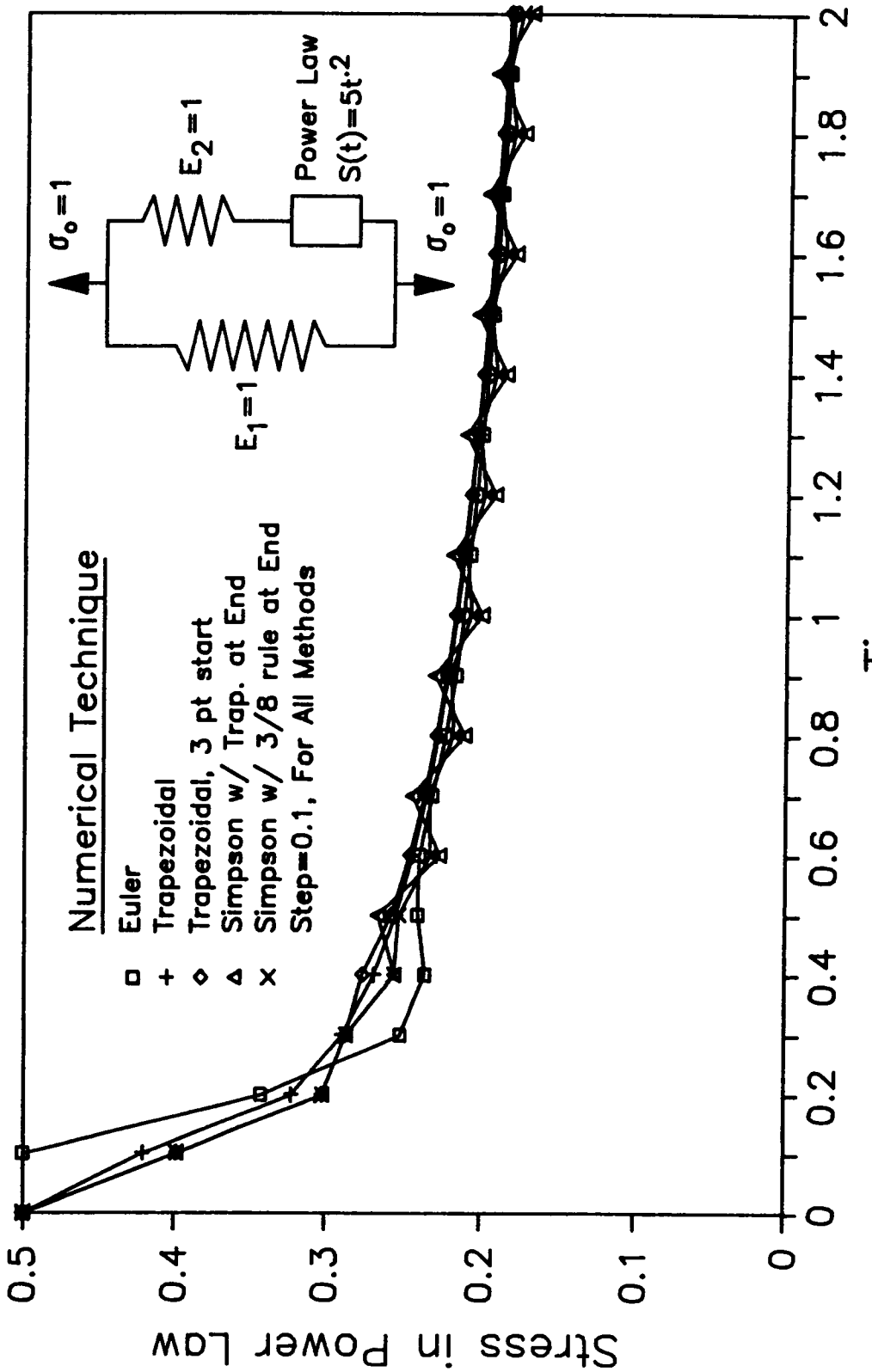

Fig. 3.3 Numerical Solutions of a 3 Parameter Power Law Model Using the Volterra Integral.

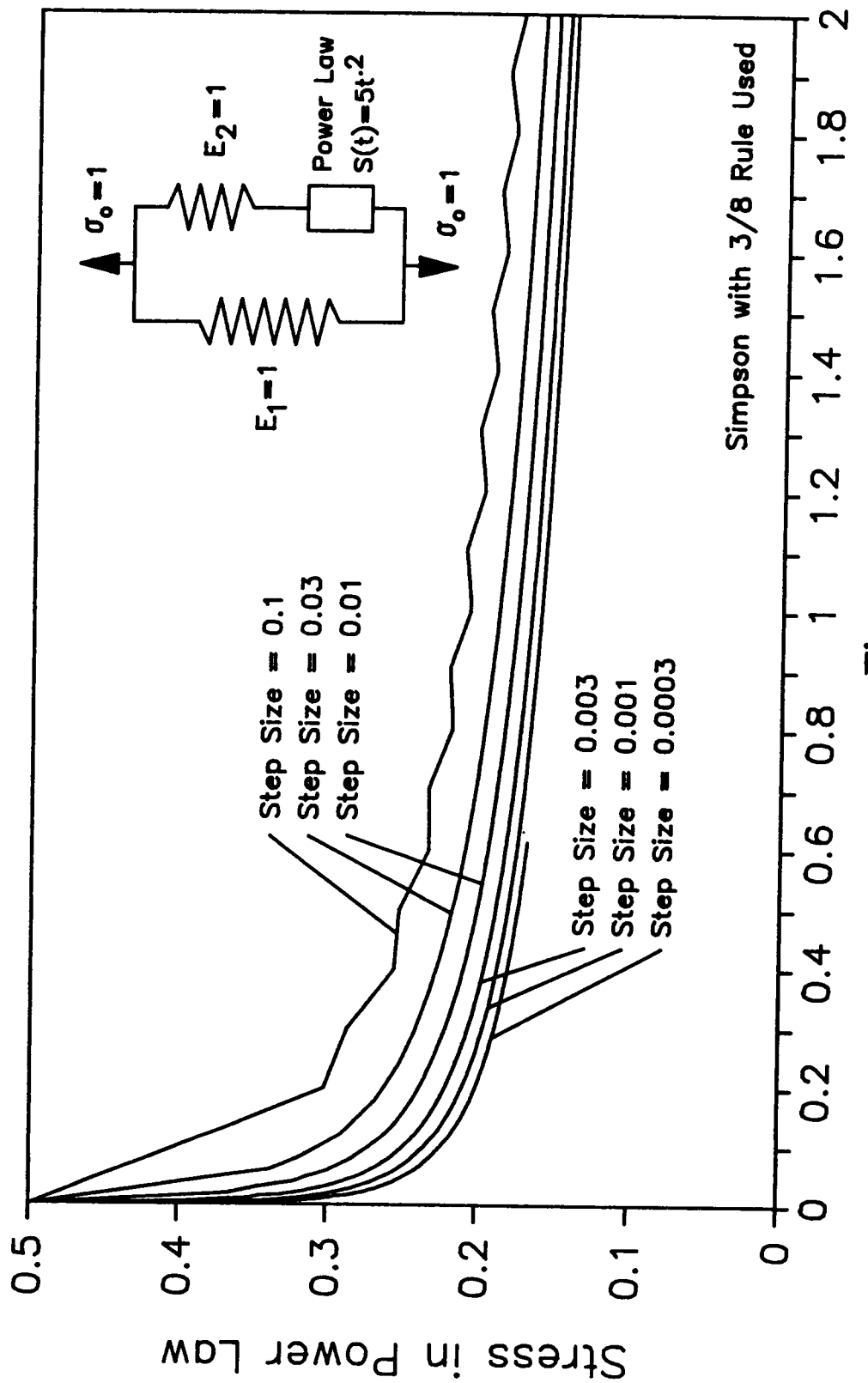

Fig. 3.4 Numerical Solutions of the Volterra Integral Using the Simpson Rule with the 3/8 Rule.

However, with small time steps, the time required to solve the problem increases tremendously which then limits the time span. The time step size can be increased as the time becomes larger but there will be an upper limit on step size before stability difficulties develop.

In conclusion, the direct numerical integration of the Volterra integral for linear viscoelastic problems is not recommended. The biggest difficulty was the long run times necessary for any numerical solution to converge when using the power law compliance function. This was caused by the weakly singular nature of the power law. Other difficulties would be the inclusion of nonlinear stress effects, thus creating a large number (on the order of hundreds) nonlinear equation that would need to be solved simultaneously. It should also be noted that the above difficulties would be magnified for multidimensional materials such as orthotropic composite materials.

Prony Series in Modeling Linear Viscoelastic Response

The Prony series is a method to model viscoelastic response that is derived from a series of Kelvin elements. This series can best be understood by first looking at a single Kelvin element, which has a spring and dashpot in parallel as shown in Fig. 3.5. The Kelvin element needs two parameters to describe its response to a given load or displacement, the spring constant, E ,and the dashpot viscosity, μ. The load or stress, σ_o, and the strain, ε, can be related by summing the stress in both the spring and dashpot.

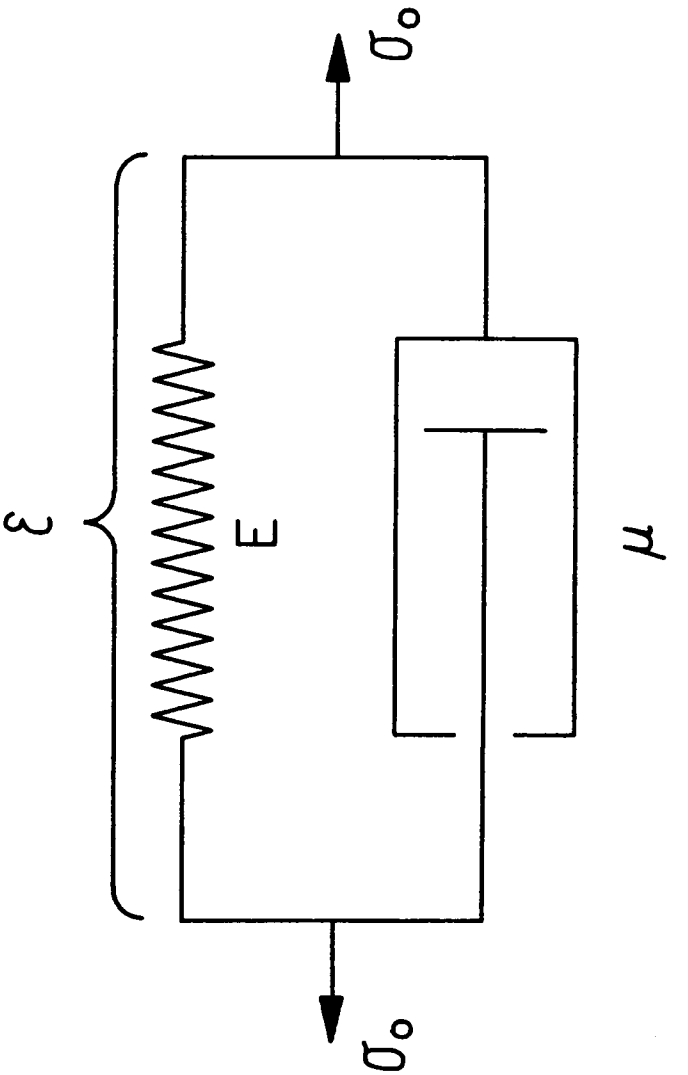

Fig. 3.5 A Single Kelvin Element.

$$\sigma_s + \sigma_d = \sigma_s \tag{3.15}$$

Substituting the constitutive equations for a spring and dashpot gives

$$\varepsilon E + \dot{\varepsilon}\mu = \sigma_o \tag{3.16}$$

Solving for ε, and assuming σ_o is constant will give

$$\varepsilon(t) = \frac{\sigma_o}{E}\left[1 - e^{-Et/\mu}\right] \tag{3.17}$$

This can be generalized with a series of Kelvin elements as

$$\varepsilon(t) = \sigma_o \sum_{i=1}^{n} \frac{1}{E_i}\left[1 - e^{-E_i t/\mu_i}\right] \tag{3.18}$$

where n is the total number of Kelvin elements in the series. As a further generalization, a single spring can be placed in series with the Kelvin elements such that

$$\varepsilon(t) = \frac{\sigma_o}{E_s} + \sigma_o \sum_{i=1}^{n} \frac{1}{E_i}\left[1 - e^{-E_i t/\mu_i}\right] \tag{3.18}$$

where E_s is the spring constant in the single spring. Eq. 3.18 is often referred to as a Prony series which can model the creep of a viscoelastic material accurately if the retardation times ($\tau = \mu/E$) of the individual Kelvin elements are properly spaced. Since one Kelvin element influences the strain over about $1\frac{1}{2}$ decades of time, the retardation times should be spaced about one per decade of time that is being modeled.

One advantage of the Prony series is its ability to accurately represent any data over any time span if enough elements are used. This is especially useful if that data is not uniform or does not conform to any general curve shape. Of course, this is also a disadvantage since a large number of material properties, two for every element, are required. In a contrast, the linear power law only has 3 parameters, $\varepsilon = \varepsilon_o + mt^n$, to describe the linear viscoelastic strain response. Another major difference between the Prony series and the power law is the extrapolation of creep response outside the actual collected data range. The Prony series is derived or fitted only to actual data and after the last data point the series stops. The power law is also derived from actual data but after the last data point the equation still indicates or predicts a change in creep over time. Although prudent engineering prohibits the use or extrapolation of results past actual collected data, it is still useful to understand the expected creep response or trend.

One of the most important advantages of the Prony series is that each Kelvin element can be solved independently as a differential equation (see Eq. 3.15) and then the solutions can be summed together. A differential equation in the form of Eq. 3.15, allows the use of common and well understood numerical methods for solving differential equations. Since the problem has been transformed to solving differential equations and not a convolution integral (i.e., the Volterra Integral) the solution techniques are simpler and easier to implement on a computer. The results of each time step no longer need

to be stored and reused to calculate future creep steps like the convolution method requires. All information needed to take another time step is available in the current solution of each differential equation.

The concept of using Kelvin elements and their respective differential equations to solve viscoelastic problems was presented by Zienkiewicz, et al [87,105]. They used the differential equation formulation in conjunction with the finite element method to successfully solve geometrically complex problems. The constant stress solution, Eq. 3.16, was used to develop a solution technique. By taking a small time step, Eq. 3.16 can be written as

$$\left[\varepsilon_c\right]_{t+\Delta t} = \frac{\sigma_o}{E}\left[1 - e^{-\frac{E}{\mu}(t+\Delta t)}\right]$$

$$= \frac{\sigma_o}{E}\left[e^{-\frac{E}{\mu}\Delta t} - e^{-\frac{E}{\mu}\Delta t}\right] + \frac{\sigma_o}{E}\left[1 - e^{-\frac{E}{\mu}(t+\Delta t)}\right]$$

$$= e^{-\frac{E}{\mu}\Delta t}\left[\frac{\sigma_o}{E}\right]\left[1 - e^{-\frac{E}{\mu}t}\right] + \frac{\sigma_o}{E}\left[1 - e^{-\frac{E}{\mu}\Delta t}\right]$$

$$= e^{-\frac{E}{\mu}\Delta t}\left[\varepsilon_c\right]_t + \frac{\sigma_o}{E}\left[1 - e^{-\frac{E}{\mu}\Delta t}\right] \qquad (3.19)$$

where $(\varepsilon_c)_t$ is the strain from the previous time step solution and Δt is the current time step size. If the stress is constant for all time steps, Eq. 3.19 will give an exact answer to Eq. 3.15. However, in most practical problems, the stress is constantly changing due to

relaxation, temperature changes, load changes, etc. If the time step is small and the stress changes gradually, then Eq. 3.19 gives accurate results as shown by Zienkiewicz.

In order to describe the viscoelastic response over long periods of time, Kelvin elements with different relaxation times may be combined in series as shown in Fig. 3.6. Each Kelvin element is described by a differential equation and the solution can be written in the form of Eq. 3.19. These solutions can then be summed together to give the total strain

$$ {}^{T}\varepsilon = \sum_{i=0}^{l} \left[\varepsilon_c^i\right]_{t+\Delta t} = \sum_{i=0}^{l} \left\{ e^{-E_i \Delta t/\mu_i} \left[\varepsilon_c^i\right]_t + \frac{\sigma_o^i}{E_i} \left[1 - e^{-E_i \Delta t/\mu_i}\right] \right\} \quad (3.20) $$

where l is the total number of Kelvin elements in the series.

Solution techniques based on Eq. 3.20 have been widely used for stress analysis of linear isotropic materials for limited time spans [88,89,105]. There are three main deficiencies with the Eq. 3.20 formulation. First, only linear viscoelastic materials can be analyzed, whereas many of today's materials, specifically plastics, are nonlinear. A nonlinear viscoelastic material will have a different compliance and rate of change of compliance at different stress levels. Since Eq. 3.20 does not account for these nonlinearities, the numerical results will possibly not agree with actual experimental results. Hendriksen [89] and Roy [107] have extended the Zienkiewicz method to include nonlinear stress effects by reformulating Eq. 3.20 as part of the Schapery integral model.

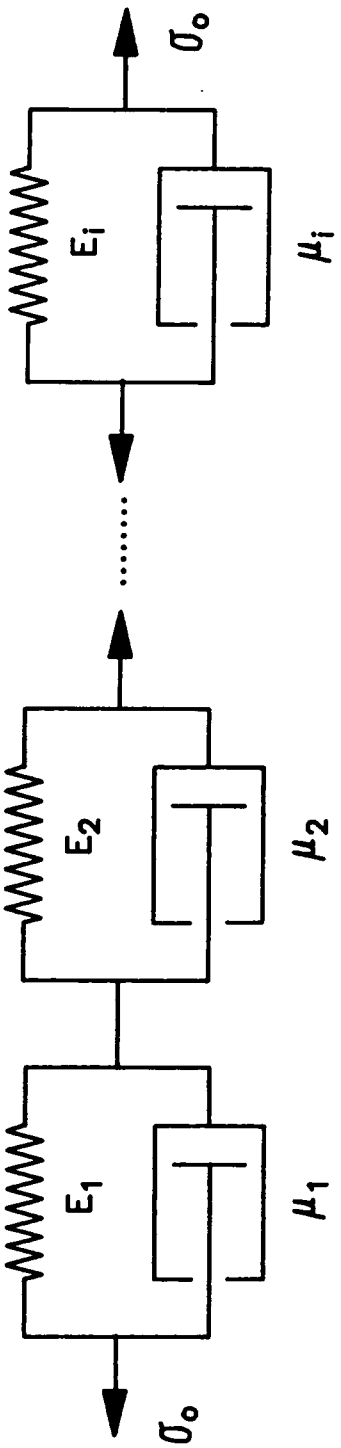

Fig. 3.6 Kelvin Elements in Series (Prony Series).

However, both used a forward explicit solution method which limits the time step size before instabilities develop as is discussed in the next paragraph.

The second drawback of Eq. 3.20 is that the time step size has an upper limit at which the numerical solution technique will become unstable since the equation is a forward difference or an explicit method. Only an implicit numerical method can be 'unconditionally stable' for all time step sizes [98]. Limiting the time step size in a viscoelastic problem, which can span many decades of time, is a concern since large time steps become necessary toward the end of the problem. The large but unstable time step problem can been overcome by returning to the original differential equation, Eq. 3.16, and formulating a higher order solution technique that is stable, such as the Modified Backward Euler method [98]. Both Snyder and Bathe [106], and Booker and Small [88] have successfully used this for isotropic materials.

Third, Eq. 3.20 is only a first order numerical solution technique, commonly referred to as the 'Euler Method', for differential equations. To increase the accuracy and/or decrease the number of steps necessary, a higher order solution technique should be employed. Again by using Eq. 3.16 directly, a solution method can be used to increase the accuracy.

Other general problems with Eq. 3.20 are the constant stress assumption at each time step and the difficulties of using it with orthotropic materials. However, the two advantages of not having to

store all past results and not having to recalculate strain at previous time steps for every new time step taken overshadows the disadvantages. The following section will present a method to extend the Prony series method to solve orthotropic, nonlinear viscoelastic problems for long time spans.

Nonlinear Differential Equation Method with the Prony Series

The basic concepts of Kelvin elements and Prony series presented in the previous section will be utilized and extended to include nonlinear effects, viscoelastic orthotropic materials, and unconditionally stable time steps. It was these three difficulties that limited the use of the Zienkiewicz differential equation method for viscoelastic analysis.

The basic differential equation for a single Kelvin element can be written as (see Eq. 3.15 and Fig. 3.5)

$$\dot{\varepsilon} = \frac{D}{\lambda}\sigma - \frac{1}{\lambda}\varepsilon \qquad (3.21)$$

Where D is the compliance of the spring (1/E) and λ is the retardation time (μ/E). Both the compliance and retardation time are considered known and can be obtained from the Prony series used to describe the viscoelastic response (see Eqs. 3.17 and 3.18). A single differential equation of the form Eq. 3.21 can be used for each term in a given Prony series.

Up to this point only one material property has been dealt with at a time. However, all materials are defined, as a minimum, by at

least two material properties which need to be considered simultaneously. Isotropic materials are generally described by Youngs' Modulus and Poisson's ratio, whereas orthotropic materials have four independent material in-plane properties which are commonly referred to as the fiber direction stiffness (E_{11}), the transverse direction stiffness (E_{22}), the shear modulus (E_{66} or G_{12}), and Poisson's ratio of the fiber direction to transverse direction (υ_{12}). In condensed matrix form, these properties relate stress and strain as

$$\begin{Bmatrix} \varepsilon_1 \\ \varepsilon_2 \\ \gamma_{12} \end{Bmatrix} = \begin{bmatrix} 1/E_{11} & -\upsilon_{12}/E_{11} & 0 \\ -\upsilon_{12}/E_{11} & 1/E_{22} & 0 \\ 0 & 0 & 1/G_{12} \end{bmatrix} \begin{Bmatrix} \sigma_1 \\ \sigma_2 \\ \sigma_{12} \end{Bmatrix} \qquad (3.22)$$

where ε_1 and σ_1 are strain and stress, respectively, in the fiber direction, $\varepsilon_2$and σ_2 are strain and stress in the transverse direction, respectively, and γ_{12} and σ_{12} are shear strain and stress, respectively. The matrix containing E_{11}, E_{22}, υ_{12}, and G_{12} is referred to as the compliance matrix [S] which can be written as

$$\begin{Bmatrix} \varepsilon_1 \\ \varepsilon_2 \\ \gamma_{12} \end{Bmatrix} = \begin{bmatrix} S_{11} & S_{12} & 0 \\ S_{12} & S_{22} & 0 \\ 0 & 0 & S_{66} \end{bmatrix} \begin{Bmatrix} \sigma_1 \\ \sigma_2 \\ \sigma_{12} \end{Bmatrix} \qquad (3.23)$$

where S_{11}, S_{12}, S_{22}, and S_{66} are the four independent properties needed to characterize an orthotropic material. These four terms will be referred to as S_q where q goes from 1 to 4, such that $S_{11} = S_1$,

$S_{12} = S_2$, $S_{22} = S_3$, and $S_{66} = S_4$. This numbering convention becomes necessary, as will be seen later, to differentiate these orthotropic compliance terms from the rotated compliance matrix terms, which will use the double subscripts (S_{ij}).

The viscoelastic portion of each of the unrotated, S_q terms can be described by a Prony series. The general form is

$$S_q = \sum_{l=1}^{n} {}_lD_q \left[1 - e^{-t/\lambda_l}\right] \qquad l = 1,2,3..n \qquad (3.24)$$

where ${}_lD_q$ is the compliance coefficient variable for the l^{th} Kelvin unit in the q^{th} direction and λ_l is the retardation time. Both ${}_lD_q$ and λ_l are unknowns that need to be determined from experimental data. However, the retardation time, λ_l can be forced to be the same for each l^{th} Kelvin element in each of the four material directions. This is reasonable since λ_l is predetermined or fixed when fitting a Prony series to experimental data with only ${}_lD_q$ allowed to vary.

Furthermore, each layer in a composite laminate will have a set of four S_q terms describing its compliance matrix. If all the layers are of the same type of material and not rotated, i.e. all 0° direction, then ${}_kS_q = S_q$ where k is the ply layer in the laminate and Eq. 5.3 becomes

$$\begin{Bmatrix} \varepsilon_x \\ \varepsilon_y \\ \gamma_{xy} \end{Bmatrix}^k = \begin{bmatrix} \sum_{l=1}^{n} {}_{kl}S_1 & \sum_{l=1}^{n} {}_{kl}S_2 & 0 \\ \sum_{l=1}^{n} {}_{kl}S_2 & \sum_{l=1}^{n} {}_{kl}S_3 & 0 \\ 0 & 0 & \sum_{l=1}^{n} {}_{kl}S_4 \end{bmatrix} \begin{Bmatrix} \sigma_x \\ \sigma_y \\ \sigma_{xy} \end{Bmatrix}^k \qquad (3.25)$$

However, if ply k is rotated, then the compliance matrix becomes fully populated,

$$\begin{Bmatrix} \varepsilon_x \\ \varepsilon_y \\ \gamma_{xy} \end{Bmatrix}^k = \begin{bmatrix} \sum_{q=1}^{4} \sum_{l=1}^{n} {}_{kl}S_{q11} & \sum_{q=1}^{4} \sum_{l=1}^{n} {}_{kl}S_{q12} & \sum_{q=1}^{4} \sum_{l=1}^{n} {}_{kl}S_{q16} \\ \sum_{q=1}^{4} \sum_{l=1}^{n} {}_{kl}S_{q12} & \sum_{q=1}^{4} \sum_{l=1}^{n} {}_{kl}S_{q22} & \sum_{q=1}^{4} \sum_{l=1}^{n} {}_{kl}S_{q26} \\ \sum_{q=1}^{4} \sum_{l=1}^{n} {}_{kl}S_{q16} & \sum_{q=1}^{4} \sum_{l=1}^{n} {}_{kl}S_{q26} & \sum_{q=1}^{4} \sum_{l=1}^{n} {}_{kl}S_{q66} \end{bmatrix} \begin{Bmatrix} \sigma_x \\ \sigma_y \\ \sigma_{xy} \end{Bmatrix}^k \qquad (3.26)$$

Where each of the ${}_{kl}S_{q1j}$ terms can be calculated from the transformation matrices [19,20]. Similarly, the compliance coefficients, ${}_{l}D_{q}$, which will be used exclusively from this point on, can also be written in matrix form and rotated giving

$$\begin{Bmatrix} \varepsilon_x \\ \varepsilon_y \\ \gamma_{xy} \end{Bmatrix}^k = \begin{bmatrix} \sum_{q=1}^{4} \sum_{l=1}^{n} {}_{kl}D_{q11} & \sum_{q=1}^{4} \sum_{l=1}^{n} {}_{kl}D_{q12} & \sum_{q=1}^{4} \sum_{l=1}^{n} {}_{kl}D_{q16} \\ \sum_{q=1}^{4} \sum_{l=1}^{n} {}_{kl}D_{q12} & \sum_{q=1}^{4} \sum_{l=1}^{n} {}_{kl}D_{q22} & \sum_{q=1}^{4} \sum_{l=1}^{n} {}_{kl}D_{q26} \\ \sum_{q=1}^{4} \sum_{l=1}^{n} {}_{kl}D_{q16} & \sum_{q=1}^{4} \sum_{l=1}^{n} {}_{kl}D_{q26} & \sum_{q=1}^{4} \sum_{l=1}^{n} {}_{kl}D_{q66} \end{bmatrix} \begin{Bmatrix} \sigma_x \\ \sigma_y \\ \sigma_{xy} \end{Bmatrix}^k \qquad (3.26a)$$

where for fiber direction term, q = 1;

$$
\begin{aligned}
{}_{kl}D_{111} &= m_k^4 \, {}_{kl}D_1 \\
{}_{kl}D_{112} &= m_k^2 \, n_k^2 \, {}_{kl}D_1 \\
{}_{kl}D_{116} &= 2 \, n_k \, m_k^3 \, {}_{kl}D_1 \\
{}_{kl}D_{122} &= n_k^4 \, {}_{kl}D_1 \\
{}_{kl}D_{126} &= 2 \, m_k \, n_k^3 \, {}_{kl}D_1 \\
{}_{kl}D_{166} &= 4 \, m_k^2 \, n_k^2 \, {}_{kl}D_1
\end{aligned}
\qquad (3.27a\text{-}f)
$$

for fiber/transverse coupling term, q = 2;

$$
\begin{aligned}
{}_{kl}D_{211} &= 2 \, m_k^2 \, n_k^2 \, {}_{kl}D_2 \\
{}_{kl}D_{212} &= (m_k^4 + n_k^4) \, {}_{kl}D_2 \\
{}_{kl}D_{216} &= 2 \, m_k \, n_k \, (n_k^2 - m_k^2) \, {}_{kl}D_2 \\
{}_{kl}D_{222} &= 2 \, n_k^2 \, m_k^2 \, {}_{kl}D_2 \\
{}_{kl}D_{226} &= 2 \, m_k \, n_k \, (m_k^2 - n_k^2) \, {}_{kl}D_2 \\
{}_{kl}D_{266} &= -8 \, m_k^2 \, n_k^2 \, {}_{kl}D_2
\end{aligned}
\qquad (3.27g\text{-}l)
$$

for transverse direction term, q = 3;

$$
\begin{aligned}
{}_{kl}D_{311} &= n_k^4 \, {}_{kl}D_3 \\
{}_{kl}D_{312} &= m_k^2 \, n_k^2 \, {}_{kl}D_3 \\
{}_{kl}D_{316} &= -2 \, m_k \, n_k^3 \, {}_{kl}D_3 \\
{}_{kl}D_{322} &= m_k^4 \, {}_{kl}D_3 \\
{}_{kl}D_{326} &= -2 \, n_k \, m_k^3 \, {}_{kl}D_3 \\
{}_{kl}D_{366} &= 4 \, m_k^2 \, n_k^2 \, {}_{kl}D_3
\end{aligned}
\qquad (3.27m\text{-}r)
$$

for shear term, q = 4;

$$
\begin{aligned}
{}_{kl}D_{411} &= m_k^2\, n_k^2\, {}_{kl}D_4 \\
{}_{kl}D_{412} &= (n_k^4 - m_k^4)\, {}_{kl}D_4 \\
{}_{kl}D_{416} &= m_k\, n_k\, (n_k^2 - m_k^2)\, {}_{kl}D_4 \\
{}_{kl}D_{422} &= n_k^2\, m_k^2\, {}_{kl}D_4 \\
{}_{kl}D_{426} &= 2\, m_k\, n_k\, (m_k^2 - n_k^2)\, {}_{kl}D_4 \\
{}_{kl}D_{466} &= (m_k^2 - n_k^2)^2\, {}_{kl}D_4
\end{aligned}
\qquad (3.27s\text{-}x)
$$

where $m_k = \cos(\theta_k)$, $n_k = \sin(\theta_k)$, ${}_{kl}D_q$ is the unrotated and ${}_{kl}D_{qij}$ the rotated compliance terms (θ is the angle of rotation). Although it seems unnecessary and overly complex to split ${}_{kl}D_{qij}$ into four parts, one for each material property direction, this allows different stress nonlinear effects to be modeled in each of the four direction, which will be developed later.

Unlike the compliance terms, ${}_{kl}D_q$, the relaxation times, λ_l, are constrained to be the same in each of the four directions which eliminates the need to rotate them. All layers or plies are also assumed to be made of the same material which alleviates the need to keep track of the ply number when dealing with λ_l. There are, however, some limitations on λ_l. There should be at least one Kelvin element for every $1\frac{1}{2}$ decades of time that is being examined since the effect of the Kelvin element is only felt over that time period. The common practice is one Kelvin element, thus one relaxation time, λ_l, for every decade of time. For orthotropic materials it is further convenient to set λ_l the same in all material property directions. A

typical Prony series might have $\lambda_1 = 1$, $\lambda_2 = 10$, $\lambda_3 = 100$, etc., for each ply and direction.

If all the stresses in each layer and direction were constant, then the time dependent strain could be easily calculated at this point by substituting the Prony series (Eq. 3.24) for each direction into the constitutive equations relating stress and strain (Eq. 3.26) and solve for the desired time. However the stresses in each ply can in fact change with time which means stress is a function of the current strain rate as well as the current strain. Even though the restriction of constant stress was used to get the original Prony series in characterizing the material, that restriction is not necessarily true in the actual numerical solution process. The matrix Eqs. 3.23, 3.25, and 3.26 are still needed to show how the compliance terms can be manipulated and rotated to obtain the ${}_{kl}D_{qij}$ terms but they are not used to obtain the strain. Instead the strain and stress equilibrium equation can be employed to calculate the strain. However an expression for the strain without the strain rate must first be developed.

The original differential equation, Eq. 3.21, can be rewritten as

$$ {}_{kl}\dot{\varepsilon}_{ij} = \sum_{q=1}^{4} \left[\frac{{}_{kl}D_{qij}}{\lambda_l} \right] {}_{kl}\sigma_{ij} - \frac{{}_{kl}\varepsilon_{ij}}{\lambda_l} \qquad (3.28) $$

where ${}_{kl}\dot{\varepsilon}_{ij}$ and ${}_{kl}\varepsilon_{ij}$ are the strain rate and strain, respectively, and ${}_{kl}\sigma_{ij}$ is the stress in each Kelvin element, l, ply, k, compliance direction, q, and rotated position, (i,j). This equation can be

approximated by

$$\frac{{}_{kl}\varepsilon_{ij}^{t+1} - {}_{kl}\varepsilon_{ij}^{t}}{\Delta t} = \sum_{q=1}^{4} \left[\frac{{}_{kl}D_{qij}}{\lambda_1} \right] {}_{kl}\sigma_{ij}^{t+1} - \frac{{}_{kl}\varepsilon_{ij}^{t+1}}{\lambda_1} \qquad (3.29)$$

where Δt is the time step size, t+1 is the new time and t is the old time. This particular approximation is called a Backward Euler Method (BEM) and is classified as a first order implicit method. By using an implicit method, the solution, ${}_{kl}\varepsilon_{ij}^{t+1}$, will be unconditionally stable regardless of the time step size. This is not to say that it will converge to the correct answer but it will not diverge or oscillate. This 'unconditionally stable' characteristic only holds true for the first and second order implicit numerical approximations [98]. Higher order implicit methods and all explicit methods are only conditionally stable, i.e. has a maximum time step before it might diverge.

The BEM, a first order implicit method, will be examined in detail in the remainder of this section. The second order implicit method, call the Backward Trapezoidal Method (BTM) is developed in Appendix B. Equation 3.29 can be rearranged to give

$${}_{kl}\varepsilon_{ij}^{t+1} \left[1 + \frac{h}{\lambda_1} \right] = h \sum_{q=1}^{4} \left[\frac{{}_{kl}D_{qij}}{\lambda_1} \right] {}_{kl}\sigma_{ij}^{t+1} + {}_{kl}\varepsilon_{ij}^{t}$$

or

$${}_{kl}\varepsilon_{ij}^{t+1} = \frac{h}{(\lambda_1 + h)} \sum_{q=1}^{4} \left[{}_{kl}D_{qij} \right] {}_{kl}\sigma_{ij}^{t+1} + \frac{{}_{kl}\varepsilon_{ij}^{t} \lambda_1}{(\lambda_1 + h)} \qquad (3.30)$$

where $\Delta t = h$. The unknowns are ${}_{kl}\varepsilon_{ij}^{t+1}$ and ${}_{kl}\sigma_{ij}^{t+1}$ while h, λ_l, and ${}_{kl}D_{qij}$ are given and ${}_{kl}\varepsilon_{ij}^{t}$ is known from the previous time step. The total creep strain, ${}_{k}^{c}\varepsilon_{i}$, for a particular direction, i, and layer, k, is simply the sum of all the creep strains in that direction

$$ {}_{k}^{c}\varepsilon_{i} = \sum_{j=1}^{3} \sum_{l=1}^{n} \left\{ {}_{kl}\varepsilon_{ij}^{t+1} \right\} \tag{3.31} $$

It should be noted that Eq. 3.30 is only for linear viscoelastic materials. In order to include nonlinear stress effects, ${}_{kl}D_{qij}$ needs to be modified to become a function of stress. This is easily done by multiplying ${}_{kl}D_{qij}$ by a dimensionless stress function which would account for any nonlinear stress effects such as

$$ {}_{kl}D_{qij}\, f_q({}_{k}\sigma) \tag{3.32} $$

where $f(\sigma)$ is a stress dependent function. This type of formulation allows the nonlinear compliance at any stress level to be scaled up or down from the linear compliance. As an example, consider the linear compliance S represented by a single Kelvin element

$$ S(t) = D\left[1-e^{-t/\lambda}\right] \tag{3.33} $$

If the nonlinear stress function is assumed to be $f(\sigma) = (1+a\sigma^2)$ then the nonlinear compliance would be

$$ D^{*} = S(t)\cdot(1+a\sigma^2) = D\left[1-e^{-t/\lambda}\right]\cdot(1+a\sigma^2) \tag{3.34} $$

where a is a constant and σ is the current stress. If the linear and nonlinear compliance curves are graphed, the scaling factor, $(1+a\sigma^2)$, is quickly identified (see Fig. 3.7). This formulation only works if the nonlinear stress can be described by a vertical multiplication of the compliance curves.

Vertical shifting of the basic compliance curve to account for nonlinear stress effects is a common method of modeling nonlinear viscoelastic response [11,31]. Most nonlinear viscoelastic models such as the Schapery, Findley, and other power law based models employee this concept by using nonlinear stress functions. Figure 3.8 shows a simple nonlinear power law with a nonlinear stress function, $f(\sigma)$, and how it is scalable. Since this vertical shifting concept works well for power law based models it should also work for a Prony series since, for many cases, the Prony series will just be a fitted equation to a power law model. The Prony series can be scaled by just scaling the compliance coefficients, D, for a particular material direction by the same amount that the power law would be scaled. Thus all Kelvin elements, $\imath$, will be have the same nonlinear scale factor, $f_q({}_k\sigma)$. However, since the stresses are different in each ply, k, there will be a different scale factor for each ply.

The nonlinear stress parameter, ${}_k\sigma$, used in the nonlinear stress function can be any function of the matrix or fiber stress states. A common parameter for the transverse and shear nonlinear compliance is the octahedral shear stress in the matrix which is a function of matrix transverse stress, σ_2^m, and matrix shear stress, τ_{12}^m. A more

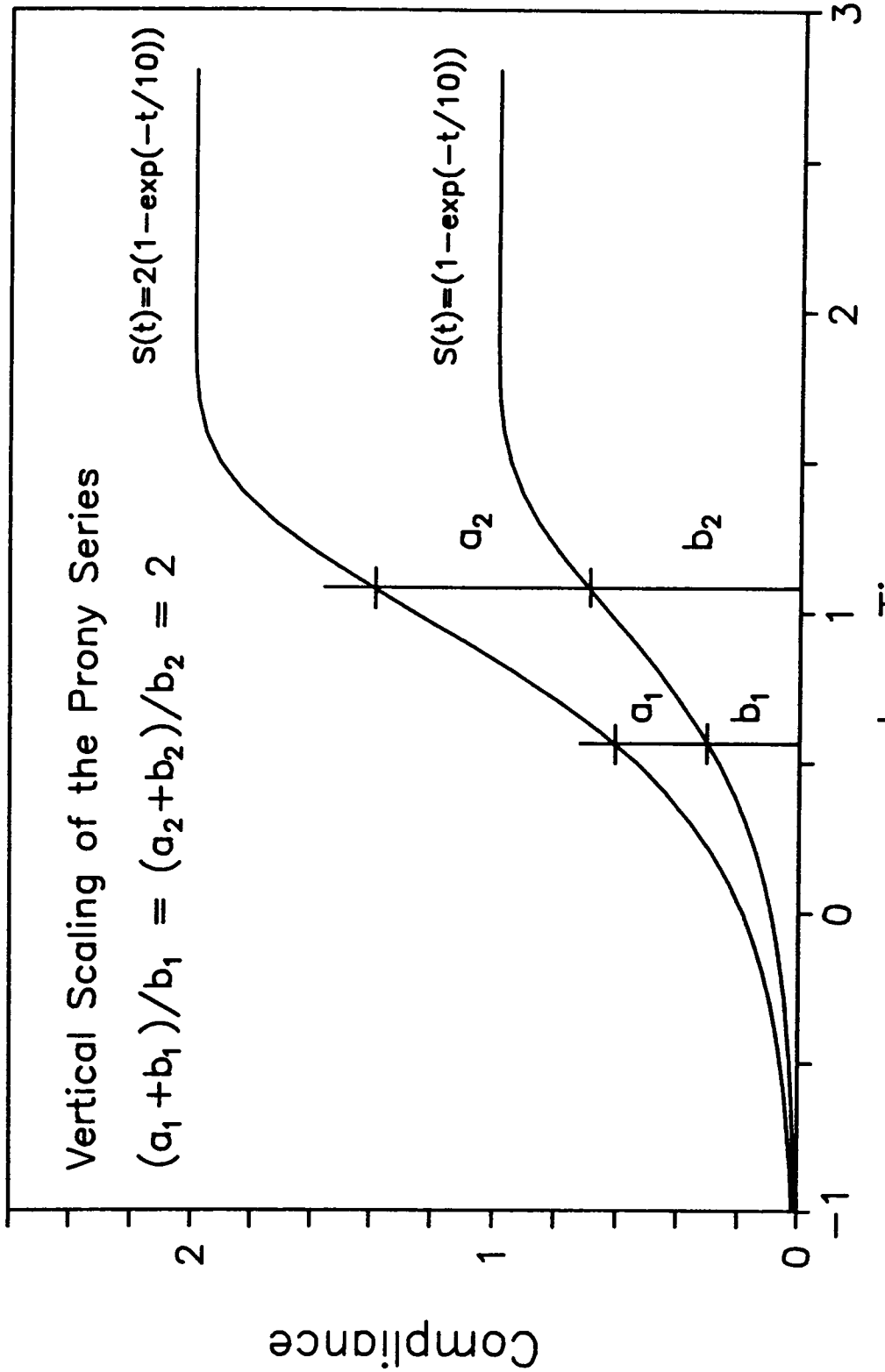

Fig. 3.7 Vertical Scaling of a Single Kelvin Element.

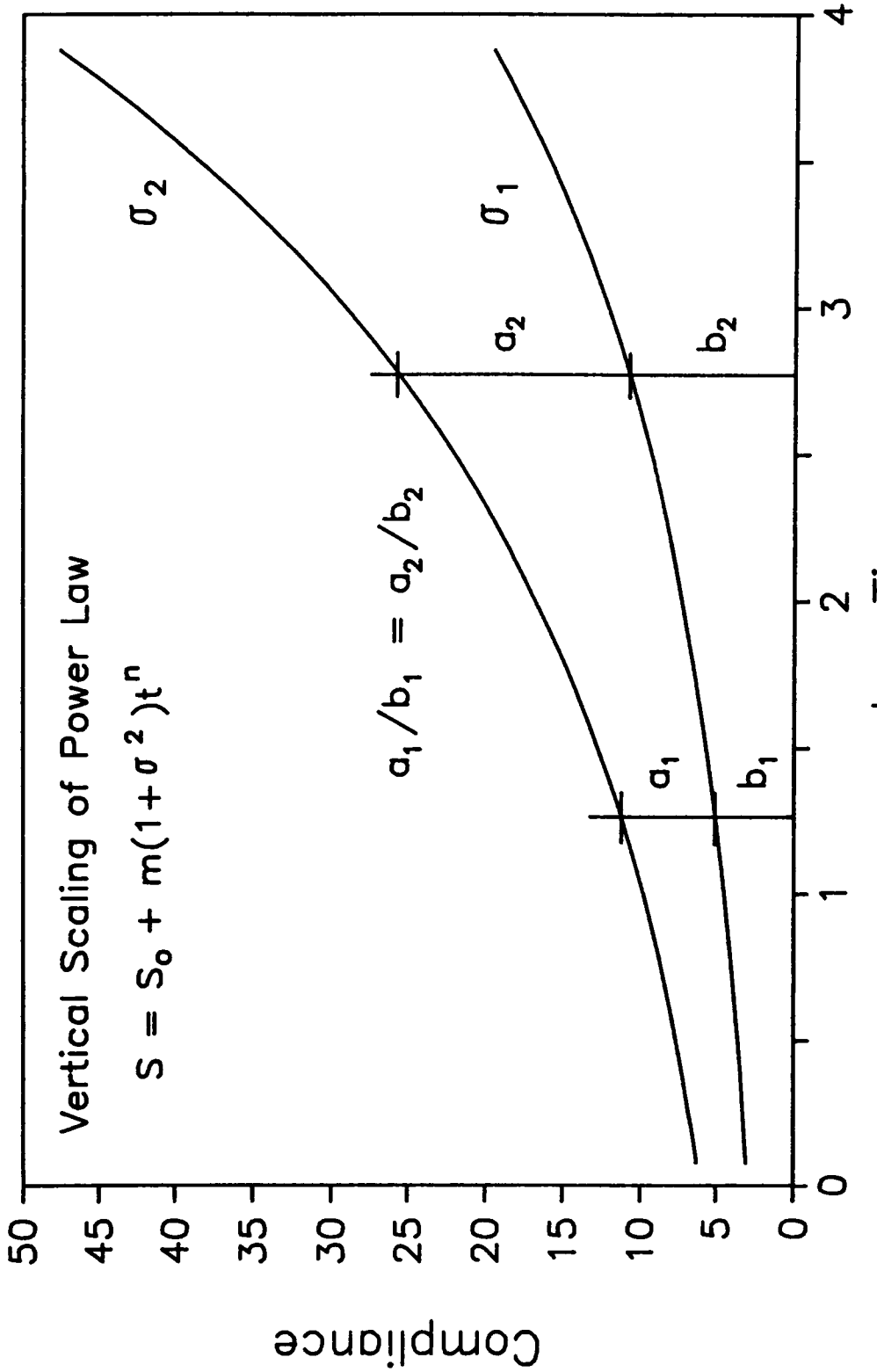

Fig. 3.8 Vertical Scaling of a Power Law Compliance Function.

detailed explanation of the octahedral shear stress parameter can be found in chapter 2. It is sufficient to say at this point that ${}_k\sigma$ will be a function of the ply's stress state, ${}_k\sigma_1$, ${}_k\sigma_2$, and ${}_k\sigma_3$ $(={}_k\sigma_{12})$, regardless of the complexity.

To introduce the nonlinear compliance function into the general formulation, substitute Eq. 3.32 into Eq. 3.30 to give

$$ {}_{kl}\varepsilon_{ij}^{t+1} = \frac{h}{(\lambda_1+h)}\sum_{q=1}^{4}\left[{}_{kl}D_{qij}\cdot f_q({}_k\sigma^{t+1})\right]{}_{kl}\sigma_{ij}^{t+1} + \frac{{}_{kl}\varepsilon_{ij}^{t}\cdot\lambda_1}{(\lambda_1+h)} \qquad (3.35) $$

Where $f(\sigma)$ is evaluated at t+1. Note that $f(\sigma^{t+1})$ is a function of the future ply stress state, ${}_k\sigma_1^{t+1}$, ${}_k\sigma_2^{t+1}$, and ${}_k\sigma_3^{t+1}$, all of which are unknown. Thus Eq. 3.35 can be a complex nonlinear function of σ_j^{t+1} which necessitates the need for a numerical solution method. Equation 3.35 can be rewritten as

$$ {}_{kl}\varepsilon_i^{t+1} = \sum_{q=1}^{4}\left[{}_{kl}C_{qij}\cdot f_q({}_k\sigma^{t+1})\right]{}_k\sigma_j^{t+1} + {}_{kl}E_{ij}^{t} \qquad (3.36) $$

where $$ {}_{kl}C_{qij} = \frac{h}{(\lambda_1+h)}\cdot {}_{kl}D_{qij} $$

$$ {}_{kl}E_{ij}^{t} = \frac{{}_{kl}\varepsilon_{ij}^{t}\cdot\lambda_1}{(\lambda_1+h)} $$

$$ {}_k\sigma_j^{t+1} = {}_{kl}\sigma_{ij}^{t+1} $$

The subscript 1 has been dropped from σ because the stress is the same

for all Kelvin elements in a particular material direction since they are all in series. The subscript i was also dropped since stress is a vector and not a tensor quantity. Similarly, the subscript j was dropped from the strain. The dropping of subscripts i and j for the stress and strain quantities, respectively, can be understood by reviewing the matrix equations Eq. 3.22 and 3.23.

Substituting equation 3.35 into 3.31 will give the total creep strain for ply, k, and direction, i,

$$ {}^{c}_{k}\varepsilon_{i}^{t+1} = \sum_{j=1}^{3}\sum_{l=1}^{n}\left\{\sum_{q=1}^{4}\left[{}_{kl}C_{qij}\cdot f_{q}({}_{k}\sigma^{t+1})\right]{}_{k}\sigma_{j}^{t+1} + {}_{kl}E_{ij}^{t}\right\} \qquad (3.37) $$

For the total strain, the elastic strain also needs to be added to Eq. 3.34. The elastic strain can be modeled as a nonlinear spring in series with the Prony series for each direction.

$$ {}^{e}_{kl}\varepsilon_{i}^{t+1} = {}^{e}_{k0}\varepsilon_{i}^{t+1} = \sum_{q=1}^{4}\left[{}_{k0}D_{qij}\cdot g_{q}({}_{k}\sigma^{t+1})\right]{}_{k}\sigma_{j}^{t+1} \qquad (3.38) $$

where ${}_{k0}D_{qij}$ is the linear compliance of the spring (l=0), $g_{q}({}_{k}\sigma^{t+1})$ is the nonlinear function of stress for each direction (similar to $f(\sigma)$), and ${}^{e}_{k0}\varepsilon_{i}^{t+1}$ is the elastic nonlinear strain. Adding Eq. 3.37 and 3.38 gives

$$ {}^{T}_{k}\varepsilon_{i}^{t+1} = \sum_{j=1}^{3}\sum_{l=1}^{n}\left[\left\{\sum_{q=1}^{4}\left[{}_{kl}C_{qij}\cdot f_{q}({}_{k}\sigma^{t+1})\right]{}_{k}\sigma_{j}^{t+1} + {}_{kl}E_{ij}^{t}\right\}\right. $$

$$+ \sum_{q=1}^{4} \left[{}_{k0}D_{qij} \cdot g_q({}_k\sigma^{t+1}) \right] {}_k\sigma_j^{t+1} \Bigg]$$

or

$${}^T\varepsilon_i^{t+1} = \sum_{j=1}^{3} \sum_{l=1}^{n} \sum_{q=1}^{4} \left[{}_{kl}C_{qij} \cdot f_q({}_k\sigma^{t+1}) \cdot {}_k\sigma_j^{t+1} \right]$$

$$+ \sum_{j=1}^{3} \sum_{q=1}^{4} \left[{}_{k0}D_{qij} \cdot g_q({}_k\sigma^{t+1}) \cdot {}_k\sigma_j^{t+1} \right] + \sum_{j=1}^{3} \sum_{l=1}^{n} \left[{}_{kl}E_{ij}^{t} \right] \qquad (3.39)$$

where T denotes total strain and ${}_k^T\varepsilon_i^{t+1} = {}^T\varepsilon_i^{t+1}$ since it is assumed that layers deform equally without debonding or damage. There are a total of 3k+3 unknowns, ${}^T\varepsilon_i^{t+1}$ and ${}_k\sigma_j^{t+1}$, but there are only 3k equations from Eq. 3.39. The additional 3 equations come from imposing stress equilibrium in each of the 3 stress directions

$${}^{\circ}N_j = \sum_{k=1}^{m} N_j \qquad (3.40)$$

where ${}^{\circ}N_j$ is the input load on the laminate and N_j is the actual load in each layer, k, when loaded. Equation 3.40 can be rewritten in terms of stress to give

$${}^{\circ}\sigma_j = \frac{\sum_{k=1}^{3} \left[{}_k\sigma_j^{t+1} \cdot {}_kt \right]}{\sum_{k=1}^{3} {}_kt} \qquad (3.41)$$

where ${}^{\circ}\sigma_j$ is the input stress and ${}_kt$ is the thickness of each ply.

This equation gives the 3 additional equations necessary to solve for the stress and strain unknowns at t+1 time.

The Eqs. 3.39 and 3.41 are nonlinear in terms of stress and are ill-conditioned. They can be solved by an iteration technique called the Newton-Raphson Method. Simpler direct methods such as Gauss-Seidel can't be used since the coefficient matrix is not guaranteed to be diagonally positive for orthotropic materials. However, for isotropic material this is not a concern since their compliance matrices are positive semi-definite [88]. The Newton-Raphson takes longer to solve the nonlinear set of equations for each iteration, since the Jacobian matrix must be calculated, but it converges much more rapidly than the other direct iteration methods.

The complete solution process can best be understood by a flowchart as shown is Fig. 3.9. The first three steps consist of defining the laminate layup, load, temperature, material properties, and calculating the rotated Prony Series parameters. For each time step, including t=0, the basic strain and stress equations (Eqs. 3.39 and 3.41) are developed and solved, using the Jacobian matrix. After the the global stresses and strains are known, then the local stresses and strains can be calculated to be used in the next time step. Time is then incremented, the next time step is taken and the loop is started again. While simple in theory, there are still hundreds of constants and differential equations that must be kept track of throughout the solution process dictating the need to use a computer. The above solution method has been programed for use on a

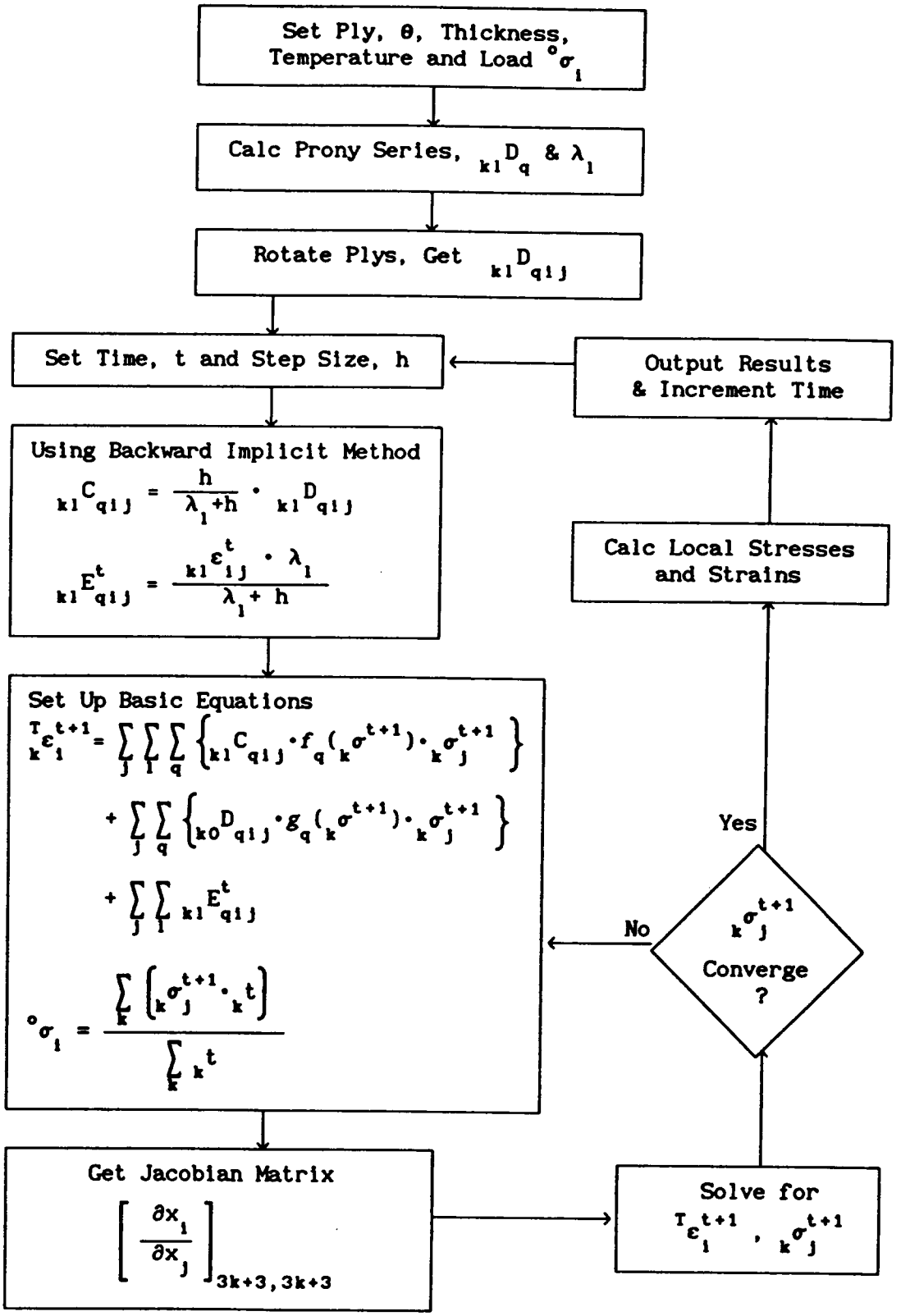

Fig. 3.9 Flow Chart for NDEM Solution Method.

microcomputer. The program is called Viscoelastic Composite Analysis Program, or 'VCAP' and a complete explanation of its operation and abilities can be found in Appendix C.

In summary then, the three major problems with the current composite nonlinear viscoelastic analysis programs, nonlinear effects, stability, and orthotropic material, have been solved by using a differential equation formulation based on a series of nonlinear Kelvin elements. Implementation and results of this solutions technique are discussed in the next section.

Verification of the Nonlinear Differential Equation Method

The method of solution presented in preceding section, the nonlinear differential equation method (NDEM), to calculate the nonlinear viscoelastic for orthotropic composite materials needs to be verified by comparing it to exact solutions and other solution techniques. This section will present two simple examples, one based on the Kelvin element and the other on the power law, of a multilayered viscoelastic material for both linear and nonlinear cases. The solution will be compared to the exact solution, if obtainable, and other numerical solutions.

The first example is a simple one-dimensional two part material; one part is viscoelastic and the other elastic. The elastic material is modeled by a single spring and the viscoelastic material by a spring and a Kelvin element in series, as shown in Fig. 3.10. Since this example is relatively simple and one-dimensional, it is possible

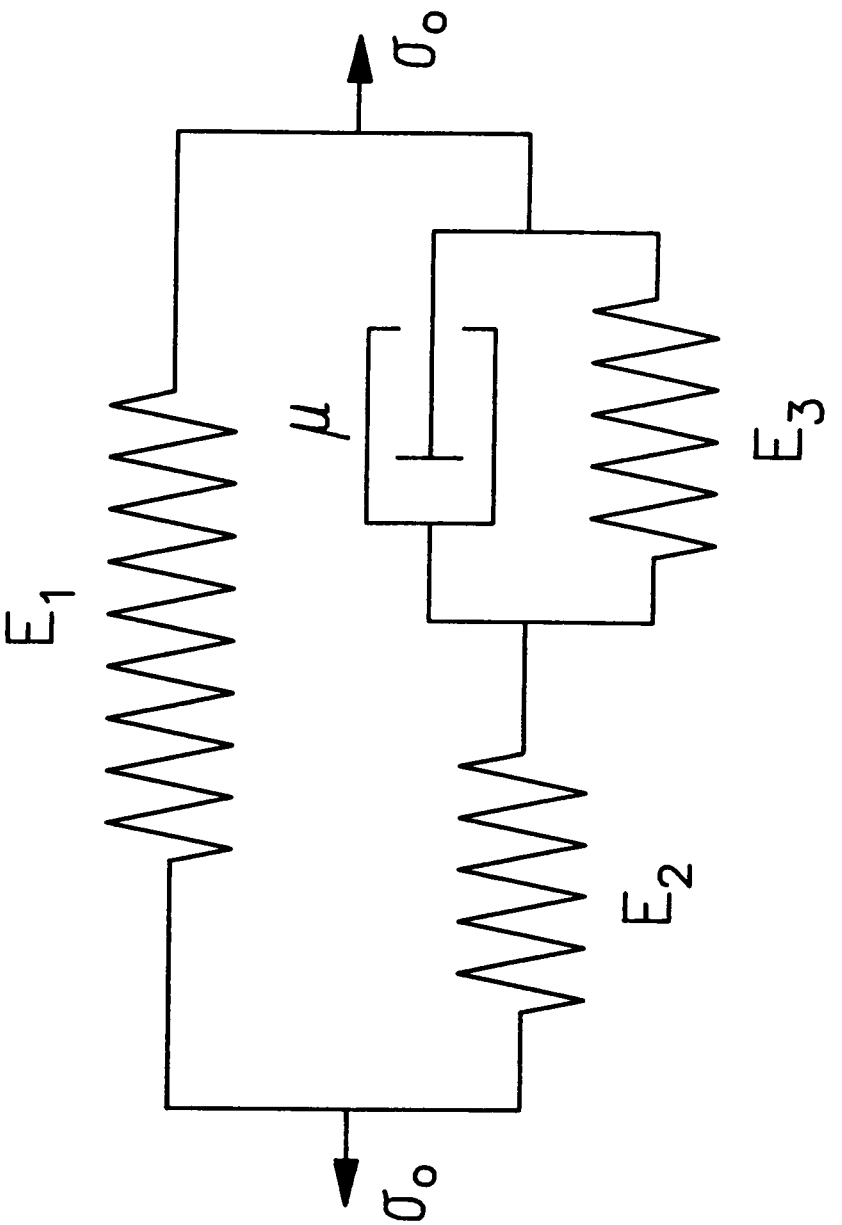

Fig. 3.10 Four Parameter Kelvin Element Test Model.

to find a closed form solution for the linear case. For the nonlinear case, however, a Runge-Kutta method was employed to solve the resulting nonlinear first order differential equation.

The linear case, assuming the applied stress, σ_o, is constant has a closed form solution of

$$\varepsilon = \left\{ \frac{1}{E_1+E_2} - \frac{K_2}{K_1} \right\} \sigma_o e^{-K_1 t} + \sigma_o \frac{K_2}{K_1} \qquad (3.42)$$

Where $$K_1 = \frac{E_1E_2 + E_2E_3 + E_1E_3}{\mu(E_1 + E_2)}$$

$$K_2 = \frac{E_2 + E_3}{\mu(E_1 + E_2)}$$

The numerical results of the NDEM technique, both by the Backward Euler Method (BEM) and Backward Trapezoidal Method (BTM), are shown in Fig. 3.11 along with the exact solution and the VISLAP program technique solution. The spring and dashpot constants were assumed to be $E_1 = E_2 = 1$, $E_3 = 0.11$, $\mu = 1$, and σ_o is constant, equal to 1, for all solution methods. The second order BTM solution matches the exact results closely whereas the first order VISLAP and BEM solutions are high and low, respectively. This deviation can be accounted for by being only a first order solution technique. It is interesting to point out that the VISLAP solution begins to oscillate and become unstable, as would be expected since it is an explicit solution method whereas the NDEM, for both BEM and BTM, is an implicit method. Also

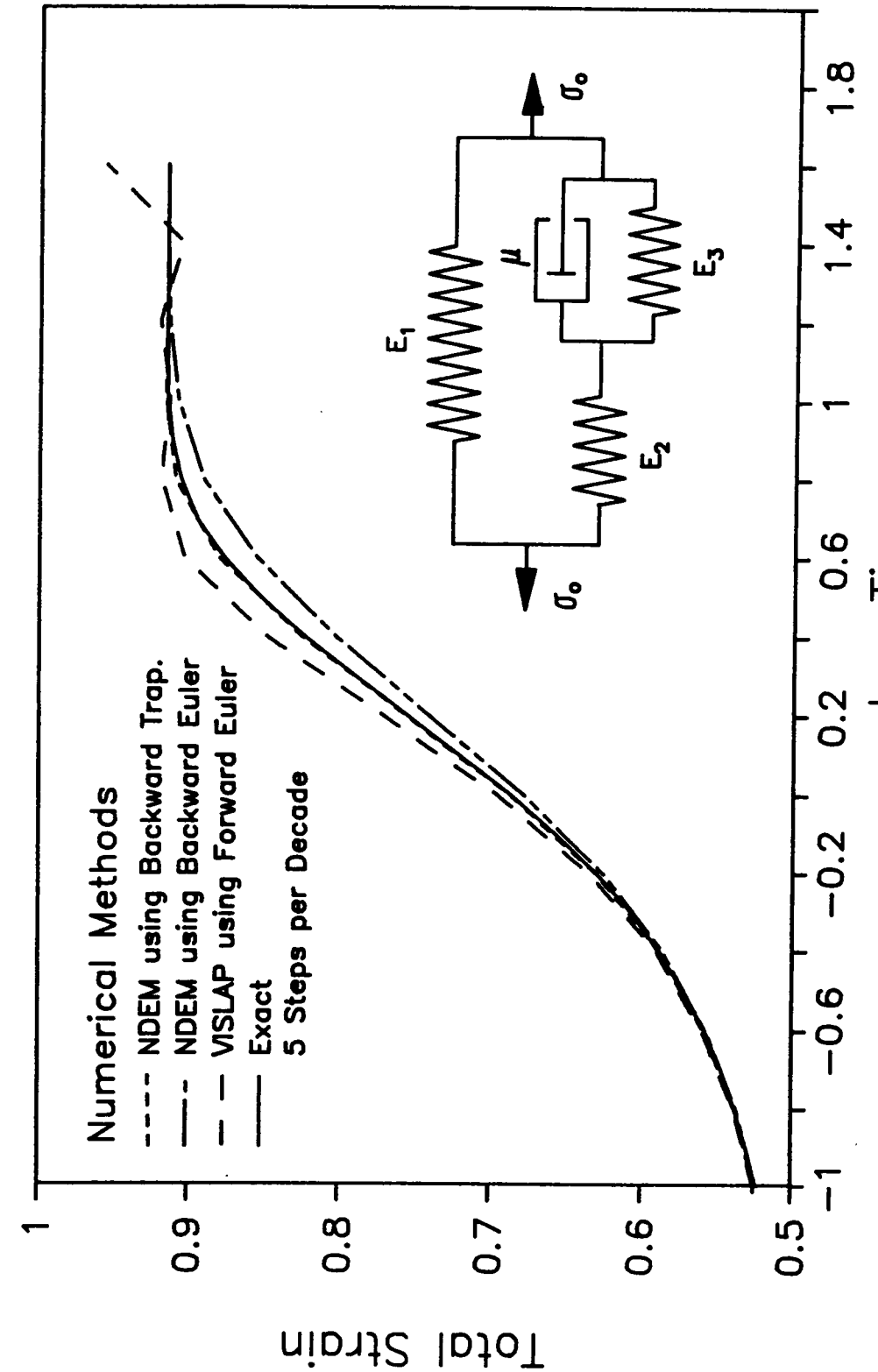

Fig. 3.11 Results of Various Numerical Techniques for the Four Parameter Linear Kelvin Element Test Case.

notice that the step size is large, 5 steps per decade, which would be considered the maximum step size but yet the second order NDEM is very accurate.

The same basic model can be used for a nonlinear viscoelastic material by simply changing E_3 and μ to include nonlinear stress effects. For the current nonlinear example, E_3 and μ are as follows

$$E_3 = 0.1 \frac{\sigma_o}{\sigma_2} + 0.1 \tag{3.43}$$

$$\mu = 10 \left\{ 0.1 \frac{\sigma_o}{\sigma_2} + 0.1 \right\} = 10\ E_3 \tag{3.44}$$

where σ_2 is the stress in material 2 (Fig. 3.10). This type of nonlinearity will cause the material to become stiffer as time progresses since the stress, σ_2, is decreasing in the nonlinear dashpot. As the stress decreases in the Kelvin element, the spring becomes stiffer and can ultimately carry more of the total load. Likewise, the nonlinear dashpot will become more viscous and the viscoelastic response will be retarded. The other parameters are similar to the linear case, $E_1 = E_2 = 1$ and $\sigma_o = 1$. The results of both the NDEM and VISLAP techniques are shown in Fig. 3.12 for the nonlinear Kelvin element. To obtain the exact solution, one must solve a nonlinear equation of the form

$$\dot{\varepsilon} + K_1\varepsilon + K_2\varepsilon^2 + K_3 = 0 \tag{3.45}$$

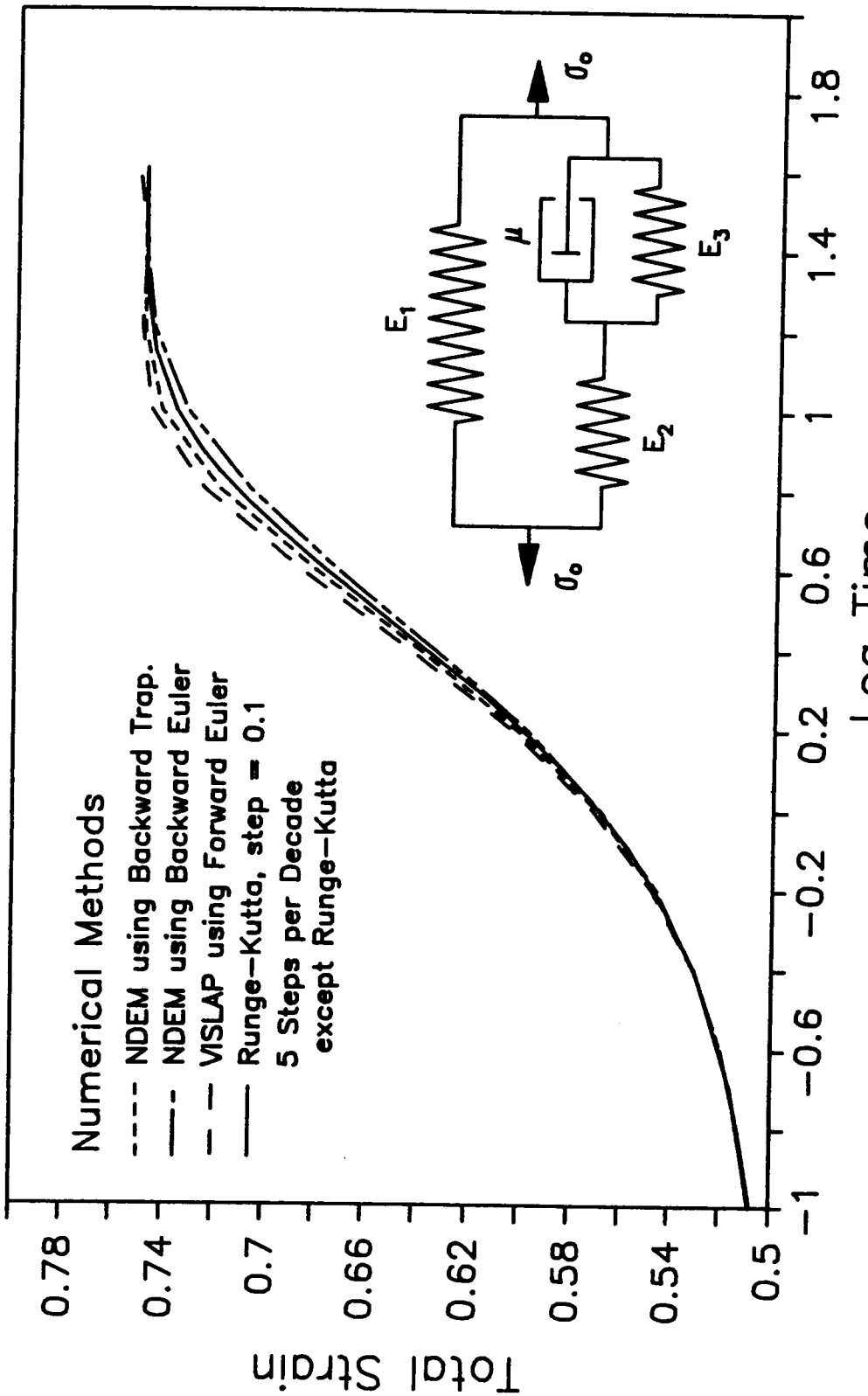

Fig. 3.12 Results of Various Numerical Techniques for the Four Parameter Nonlinear Kelvin Element Test Case.

with $\varepsilon(o) = c$

This equation is difficult to solve for a closed form solution but good results can be obtained by using a Runge-Kutta numerical method with small time steps. The results from a Runge-Kutta solution are also plotted on Fig. 3.12. For a simple nonlinear example model, like the one being examined, it is possible to use a Runge-Kutta solution, a well proven and reliable numerical method, as a check. However, for the general orthotropic problem, the Runge-Kutta method cannot be used, as discussed in the proceeding sections.

Similar to the linear case, the first order solution methods, VISLAP and NDEM using BEM, are not as accurate as the second order NDEM using BTM. Also the explicit method, VISLAP, becomes unstable at long time steps.

The second example case is again a two part one- dimensional material with one part viscoelastic and the other elastic. This viscoelastic material is modeled as a power law and a spring in series, and the elastic material as a spring. Figure 3.13 shows the mechanical model describing this test case.

The power law parameters used are m = 0.1 and n = 0.25 for the linear case and

$$m = 0.1 \frac{\sigma_o}{\sigma_2} + 0.1 \qquad (3.46)$$

and n = 0.25 for the nonlinear case. For both the linear and nonlinear case $E_1 = E_2 = 1.0$. The results comparing just the VISLAP and

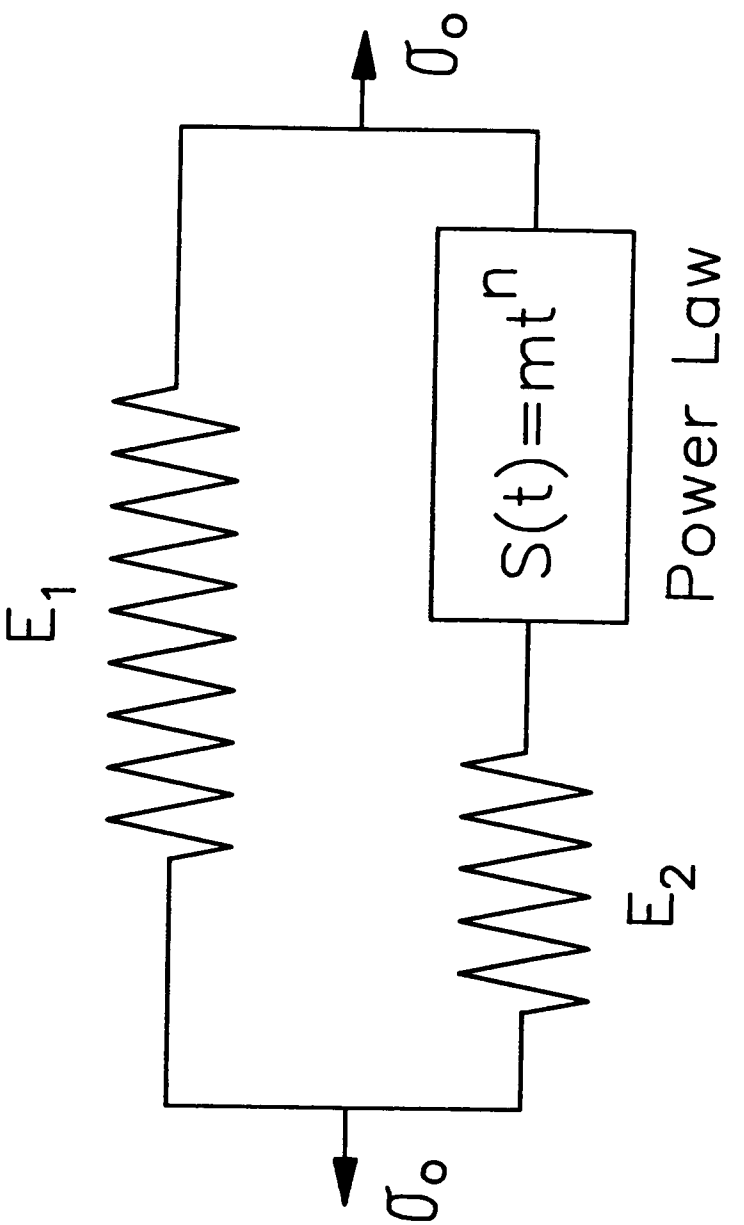

Fig. 3.13 Power Law Test Model.

NDEM (BEM and BTM) methods are shown in Figs. 3.14 and 3.15. Both the linear and nonlinear cases show the results for all methods very close, with the BTM between the other two methods. This is similar to the results of the linear and nonlinear Kelvin cases discussed earlier. There is no exact solution available to compare results and the resulting equation can't be solved by the Runge-Kutta in a convenient manner. However the results of both the VISLAP and NDEM techniques are similar, giving some reassurance that the answer is correct.

In summary, the nonlinear differential equation method (NDEM) of solving nonlinear viscoelastic problems that involve multiple material layers has been shown to be an accurate method and does converge to the correct answer. The two test cases examined, Kelvin and power law models, showed the NDEM results match the exact solution and/or other numerical methods. The second order BTM technique proved to be the most accurate and was stable for all time steps.

Numerical Conclusions

This chapter has looked at various methods to solve nonlinear viscoelastic problems that deal with orthotropic materials such as fiber reinforced composites. Earlier methods, such as the VISLAP computer program algorithm, was examined and some of the deficiencies discussed. The main three problems of these methods were 1), stability of the solution technique, 2), time step size stability, and 3), solution time length and computer memory storage. Two other

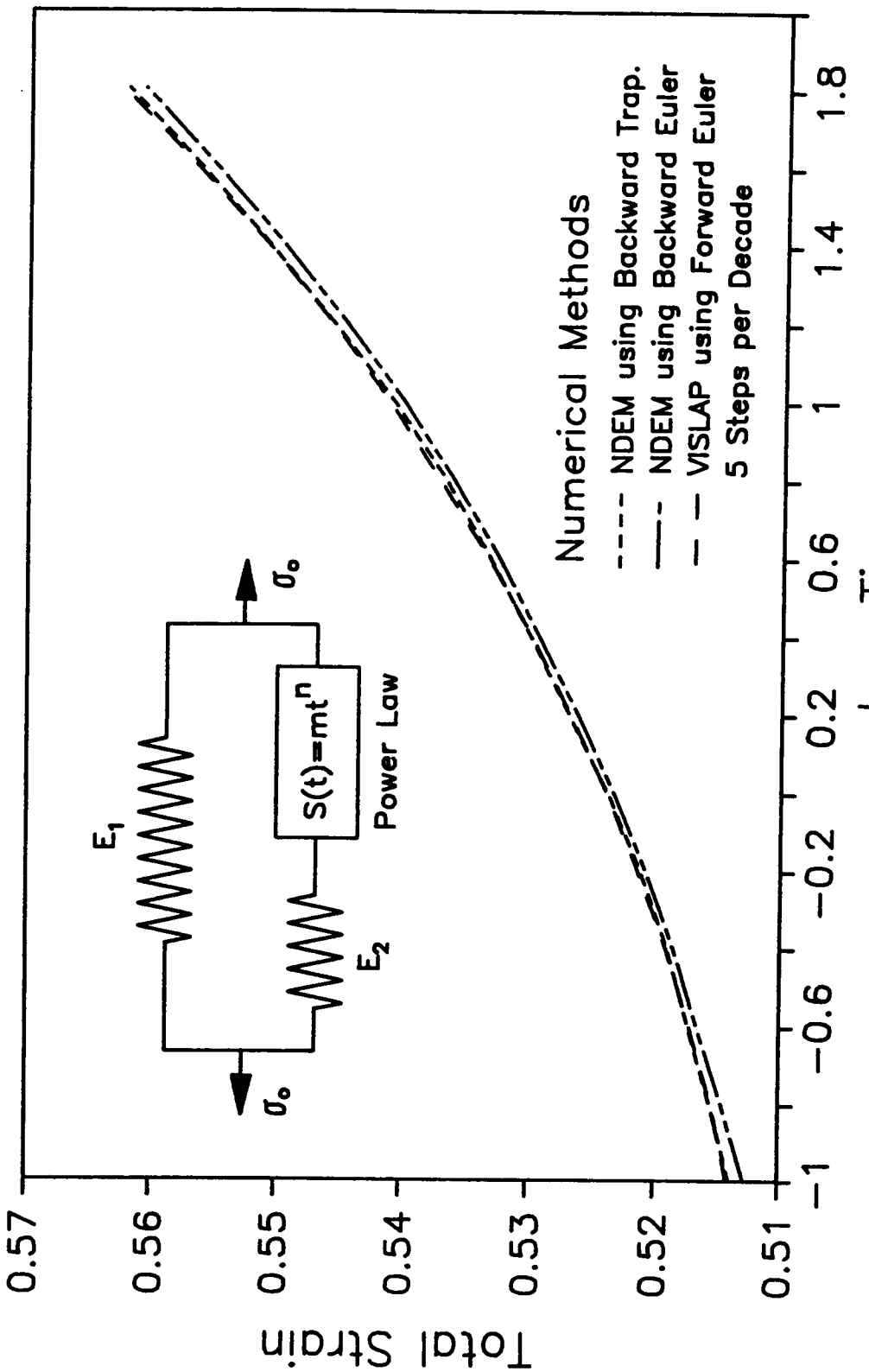

Fig. 3.14 Results of Various Numerical Techniques for the Linear Power Law Test Case.

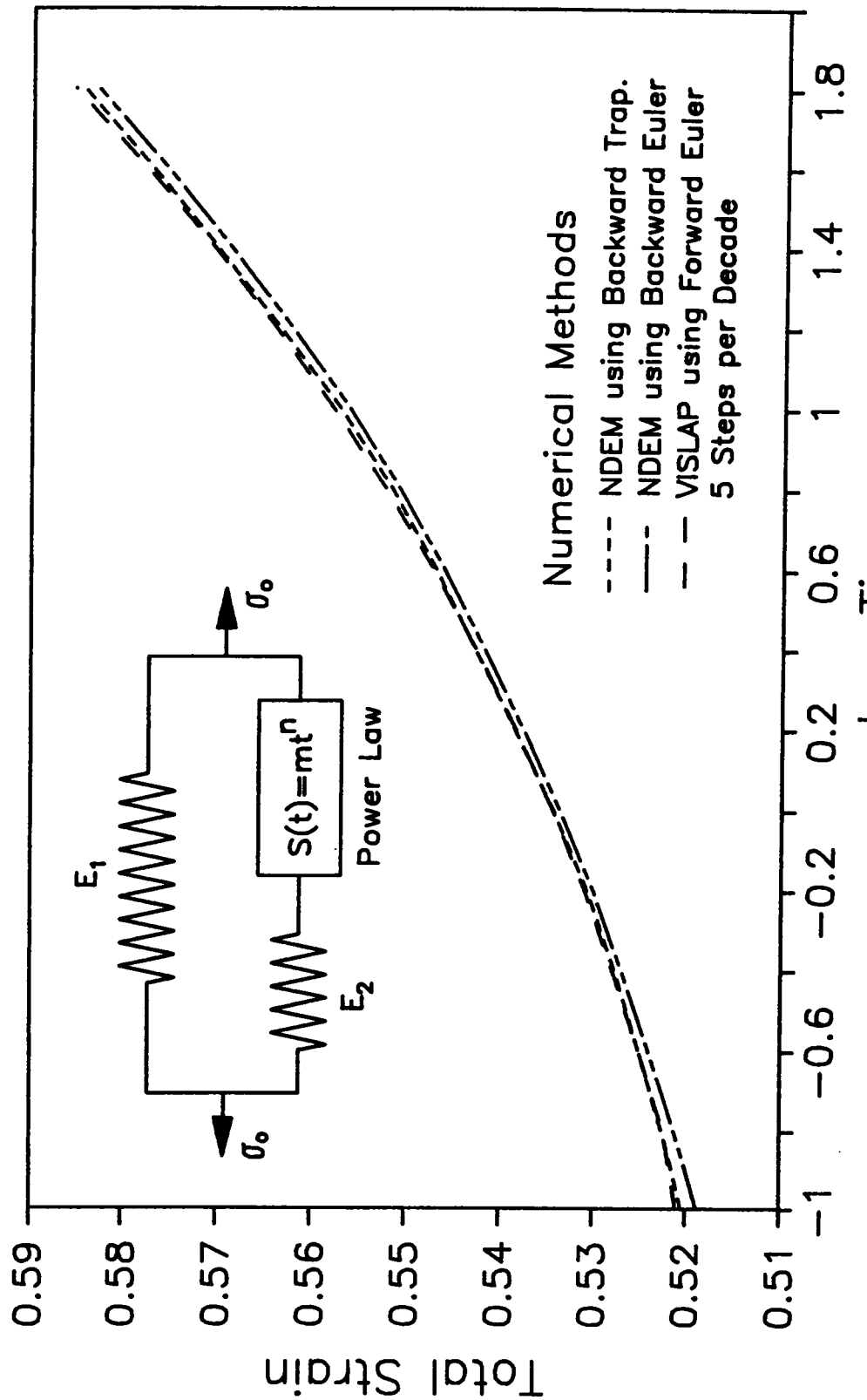

Fig. 3.15 Results of Various Numerical Techniques for the Nonlinear Power Law Test Case.

methods were examined in detail, Volterra Integral and the Zienkiewicz method, plus a new method, the Nonlinear Differential Equation Method (NDEM) was developed to try to overcome some of the deficiencies.

The Volterra Integral allowed the implementation of higher order solution techniques but it had difficulties solving singular and weakly singular compliance functions. The power law compliance function, which is weakly singular, was solvable only with very small time steps. This method also needs an ever increasing amount of computer time as the solution process goes further out in time, similar to the VISLAP method. This was due to the hereditary type integral solution process which must recalculate the total integral for each additional time step. This method was found to be unacceptable for reasons of computer time needed and accuracy.

The second method examined was the Zienkiewicz solution technique which requires the viscoelastic response to be modeled by a Prony series. This method works well for linear viscoelastic isotropic materials and small time steps. The biggest advantage of this technique is that the solution algorithm can be written in a recursive fashion which does not require the recalculation of the past results like the VISLAP and Volterra Integral methods. This allows the solution at long times to be done efficiently and quickly. One disadvantage of the original formulation is the limit on time step size since the method uses an explicit solution technique. Thus the solution can become unstable and diverge from the correct answer. Others, Booker and Snyder, have extended Zienkiewicz formulation to be

stable for large time steps.

To overcome the above deficiencies a new method, NDEM, was developed. This method requires the viscoelastic response be described by a modified Prony series which allows nonlinear stress effects to be included. The differential equations that model each of the Kelvin elements in the Prony series, are then solved simultaneously. By using the basic differential equations, an implicit solution method can be used. This causes the solution process to be unconditionally stable for any time step. While others [88,106] have also formulated stable algorithms for viscoelastic problems, they were only for linear isotropic materials whereas the NDEM is for nonlinear layered orthotropic materials. The general method of solving the nonlinear simultaneous equation used was the Newton-Raphson method which assures convergence even if the coefficient matrix of the equations is not positive definite, which is generally the case for orthotropic composite materials.

The NDEM technique was shown to be accurate and stable on two test cases, Kelvin and Power law based, for both linear and nonlinear conditions. The advantages of NDEM is that it is stable for all time step sizes, the solution algorithm is stable and converges to the correct solution, and the computer time is minimized.

Chapter 4

TESTING METHODS

One of the main objectives of this study is the characterization of unidirectional Kevlar/epoxy composite laminae. This information then becomes the foundation or database for use in the numerical procedure to predict the viscoelastic response of a general laminate. Since the experimental data will be used to make further predictions, the testing methods must be reliable and well understood to enhance the accuracy of the initial data which will ultimately affect the prediction accuracy. The testing methods that are to be discussed in this chapter are: testing equipment, specimen preparation, specimen size, strain measuring device (strain gages), mechanical conditioning and thermal conditioning.

Testing Equipment

The creep testing method used in this study was static tensile tests. The equipment used for this purpose were two different dead-weight creep frames which used a lever arm loading mechanism.

The majority of the tests, both long and short term, were done on a five station creep frame that was designed and built in-house [75]. The frame was constructed from channel and I-beam weldment and used hardened tool steel (R_c 58-60) for all knife edges and mating surfaces. All five of the lever arm loading mechanisms had a 10:1

ratio with a design maximum applied load of 13,340 N (3000 lb_f). However, during the testing process, the maximum load applied was only 4450 N (1000 Lb_f). At higher loads, the knife edges tended to twist or rotate during loading. There was an individually controlled oven for each of the five frames with an accuracy of ±1° C which used resistance heating elements.

For Creep tests needing high loads, such as unidirectional 0° specimens, an Applied Test Systems (ATS) creep machine was used. This creep machine has a maximum capacity of 88,960 N (20,000 lb_f) and has an automatic loading system and load re-leveler. The lever arm for this frame is adjustable to either 3:1 or 20:1 ratio. There is an ATS series 2912 oven attached and temperatures were maintainable to ±1.1° C.

Both frames use friction type grips to load the specimens. However, the five station creep frame has double pivot, tuning fork-type grips which allowed the specimen to rotate at ends and placed the pivot points at the specimen/grip junction. The double pivot system minimizes any bending moments that might be induced by the gripping mechanism and is especially convenient for nonsymmetric laminates and off-axis unidirectional lamina. The ATS creep frame used the conventional pin-thru-the-grip mechanism to load the specimen.

Creep and creep recovery strains and test temperature were measured using a computerized data acquisition system. The computer was a Hewlett-Parkard (HP) series 9000 model 300 computer system which

used a HP 3497A Data Acquisition Control Unit, HP 3457A Multimeter, and HP 6214B Power Supply Unit. A program to monitor five creep frames simultaneously was written for this study which allows the user to stop and start any single test without affecting other tests. Besides strain gage readings, the program monitors the temperature level of the test specimen in the oven by using thermocouples.

The data acquisition system takes five readings for each strain or temperature measurement, disregards the first and last reading, and then averages the remaining three together to give the final recorded strain or temperature. The sampling rate is variable and can be specified by the user with a minimum rate of 1/sec and a maximum of 1/day. The data is stored in memory and printed on paper for each strain and temperature reading along with the current time of day, current creep or recovery time, frame number, and current power supply voltage. After or during a test the complete printout of test results can be obtained. By using a computerized data acquisition system, quick and systematic compilation of creep data was possible. especially at the beginning of the tests where creep rates are highest and most critical.

Strain Measuring Devices

There are two common methods of measuring creep strain of composite materials, resistance strain gages and extensometers, each with their own advantages and disadvantages. There are important points that need to be considered in deciding which method to use are

the cost, accuracy, and usability. The initial purchase price of extensometers is higher but they can be reused indefinitely whereas strain gages are relatively inexpensive to purchase, but they cannot be reused and gage installation can be costly an time consuming. Aside from the initial purchase cost, extensometers are easier to use and attach to the specimen which further reduces its operating cost. Therefore, from the point of view of cost, extensometers are generally cheaper per test if a large number of tests are performed.

The second and more important consideration between the extensometers and strain gages is accuracy. Extensometers are generally only accurate to the ±10 μ-in/in where as strain gages are in the ±1 μ-in/in range. Since creep needs to be monitored very closely for longs periods of time the increased accuracy is necessary for reliable results. An additional problem with extensometers is the bending moment induced in the specimen from the extensometer's own weight. If the material is stiff and a high load is applied then the bending moment is insignificant, but for the Kevlar/epoxy at moderately high temperatures, tests revealed that the bending moment can be significant. For example, at 90° C, the extensometers physically twisted an unidirectional 90° specimens when tested. On the other hand, strain gages tend to reinforce the gage section of the test specimen with its epoxy backing and metal grid work [107-108]. This reinforcement, although generally small can be important for soft material.

The third aspect in selecting a strain measuring device is the

usability or, in other words, can it measure the strain in the direction needed. Strain gages are very versatile and can be used to measure strains in almost any direction whereas extensometers are generally restricted to axial and transverse strain measurements. This is a problem when measuring shear strains from the 10° off-axis test since the strains must be measured in three directions which is not possible with extensometers.

Due to the accuracy limitation and usability problems with extensometers, strain gages where chosen to be used in this study. Furthermore, test equipment for multiple extensometer monitoring, which was necessary to complete the large number of creeps planned, was not available at the time of this study. As a comparison of the extensometers and strain gages, creep and creep recovery tests were carried out on four different laminates using both methods. Agreement was good between methods for all samples except at high temperature and near failure which should be expect.

During preliminary creep tests, the type of strain gages, adhesive system, and adhesive cure temperature were found to affect the strain readings. These preliminary creep tests revealed that in some cases the strain would increase, as expected, but then later decrease without any load changes. This phenomenon, termed reverse creep, was identified as an strain gage adhesive creep problem. The adhesive system used on the specimens that experienced reverse creep was M-Bond 200 (Sold by Micro-Measurements) cured at room temperature. Even though the specification published by the manufacture indicate an

operating temperature range of up to 65° C, if the adhesive is used above the cure temperature for creep tests, one can experience inaccurate strain readings. To eliminate reverse creep, the adhesive should be a high temperature adhesive and cured at least 20° C above the maximum expected test temperature [109].

For this study all gages used where M/M EA-06-xxxxx-350 type gages where xxxxx is the size and style which varied for each of the different types of specimens tested, i.e. unidirectional 0°, 90°, and 10° or laminates. 350-Ohm resistance gages were used verses the 120-Ohm gages to reduce localized heating of the specimen around the gage area [79].

Specimen Preparations

All specimens used in this study were supplied by E.I. DuPont De Nemours & Company, Inc. (DuPont) in two batches. The first batch of specimens (received October 1985) were fabricated and cut by DuPont and the second batch (received November 1986) were fabricated by Dupont in 24" by 12" sheets and subsequently cut by the author at VPI with a slow speed diamond saw. The specimens were stored in sealed plastic bags until used.

The unidirectional specimens used for the lamina characterization (0°, 10°, and 90°) were 1/2 inch wide and 7-9 inches long. The laminate specimens were generally 1 inch wide and 7-9 inches long. The laminates, especially three or more fiber directions, were wider to minimize the free edge effect which will be further discussed later

in this chapter.

In preparation for strain gage application, the specimens were lightly roughed with 400 grit sand paper to insure a good bonding surface. Normal strain gage bonding techniques were then followed in the application of the gages. Both Micro-Measurements M-Bond 600 and AE-15 high temperature adhesives were used to adhere the gages. Strain gage clamps and pressure pads were used to apply the required pressure while curing took place.

The specimens were cured in an conventional type oven at 121° C for 150 minutes. The oven temperature was increased and decreased at approximately 3° C per minute. The cure temperature could not be higher than 121° C since that was the temperature at which the composite epoxy was cured. Some early specimens, which were cured at higher temperatures (up to 150° C), had debonding and bubbles visible and were not used. To insure the largest possible temperature range for the thermoviscoelastic characterization of the composite, the adhesive was cured at 121° C.

Strain gages were mounted on both sides of all specimens to average out any bending effects that might occur due to eccentrically loaded specimen. After the gages were mounted the specimens were placed inside a desiccator until actually used in a creep test, generally 3 to 5 days later.

Mechanical Conditioning of Test Specimens

A major concern in any test program with composites is the repeatability of the results. This is especially true for viscoelastic characterization tests where time is involved. Ideally, one should be able to conduct two tests on the same specimen and obtain the same creep and creep recovery curve, assuming the test parameters such as temperature, stress level, humidity, etc., remain the same. Even with the above parameters constant, two composite creep tests are rarely the same since the first test will change the composite slightly, thus affecting the second test. This difference between tests has been associated with straightening slightly crooked or irregular fibers, plastic yielding and permanent deformation of the matrix, isolated debonding of matrix and fibers, etc., that are caused during the first or second loading cycle. This raises the need for mechanically conditioning test specimens to insure repeatable and reliable tests.

Many principal investigators have used mechanical conditioning [30,35,39,82] in order to produce consistent creep results. Others argue that mechanical conditioning permanently changes the material by matrix yielding and local geometry modifications [76]. This is a special concern for those applications that will receive only one loading, and the virgin material needs to be characterized. Another argument against mechanical conditioning is the difficulty encountered when performing long term creep tests. For even a moderate length test of one week would require two to three tests of the same length

to properly condition the sample and with the accompanying recovery time the total test could easily take three to five months.

Regardless of the above arguments for or against mechanical conditioning, one overriding factor is the finite number of test specimens and the need to perform multiple tests on the same specimen. For example, to effectively use the TTSP to obtain master curves the same sample should be used for all temperature levels. If different specimens are used at different temperatures, the experimental error or scatter between samples for composite material are great enough, in most cases, to effectively make shifting of the individual compliance curves impossible. Also the same sample needs to be used when determining nonlinear stress effects for the same reason. Besides, if a different specimen is used for each test, the total number of specimens required would be unwieldy and too costly to prepare each one with strain gages. One could argue that when the temperature or stress level is increased from a previous test, then the material is virgin again since the material has not experienced that higher stress or temperature level. However, generally most mechanical conditioning of the material takes place on the first loading, regardless of stress level (if at least 10% of ultimate) or temperature. Thus when testing for stress dependency of temperature effects and the same specimen is used for the whole series or set of tests, then the specimen is receiving mechanical conditioning as the tests are performed.

It was concluded that some type of mechanical conditioning should be employed since, 1) the TTSP would be used extensively to

characterize the material and thus multiple tests would have to be performed on the same specimen, and 2) it would be too costly to use a new virgin specimen for each of the thousands of tests necessary. The most common method of conditioning is to run multiple tests for the same length of time as the real test [30]. As mentioned earlier this can take a considerable amount of time. Jerina, at el. [110] modified the conditioning tests to vary in length as, shown in Fig. 4.1b, until the last conditioning test is equal in time length as the actual test. Although this reduces the total test time, it still can be rather lengthy. A third conditioning method would be to simply load and unload the specimen to the expected stress level without holding the stress load for any amount of time. This has the advantage of being performed in a reasonable amount of time but the disadvantage of not conditioning the specimens in a viscoelastic manner. This method was used successfully by Brouwer [39] in testing graphite/epoxy specimens and is shown in Fig. 4.1a.

The method proposed by Brouwer was thought to be acceptable as a mechanical conditioning method for this study. To better understand that method for Kevlar/epoxy laminates, which are used in this study, testing was carried out on two types of laminates, $[\pm 45]_{2s}$ and $[90_2/45/-45]_s$, both 8 plies thick. Two sets of specimens of each laminate type were used, one set had mechanical conditioning, as per Fig 4.1b, and the other did not. The mechanical conditioning consisted of 5 short (30 seconds) loading and unloading cycles. It was believed that if there is any fiber realignment, fiber crack, or

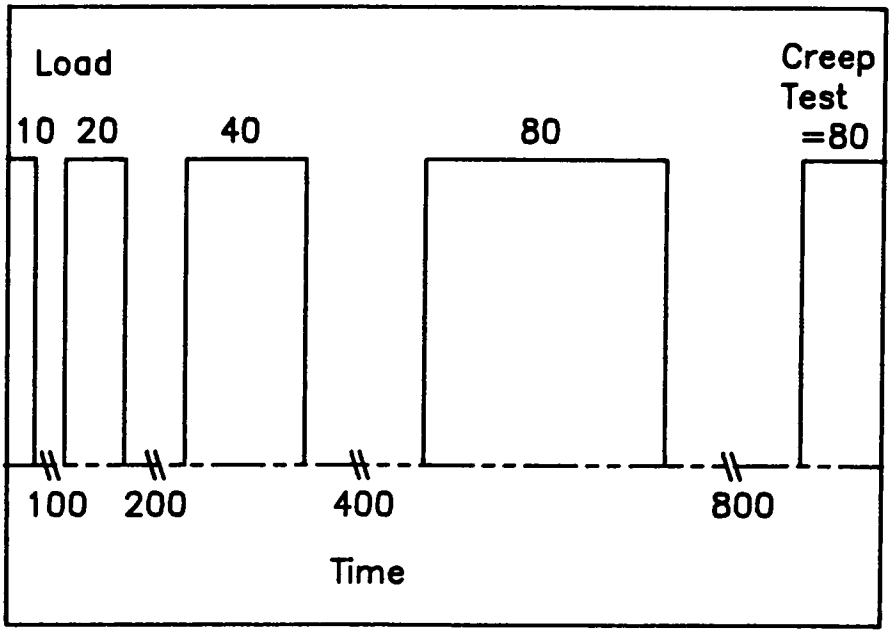

Fig. 4.1b Conditioning Cycle as Proposed by Jerina [110].

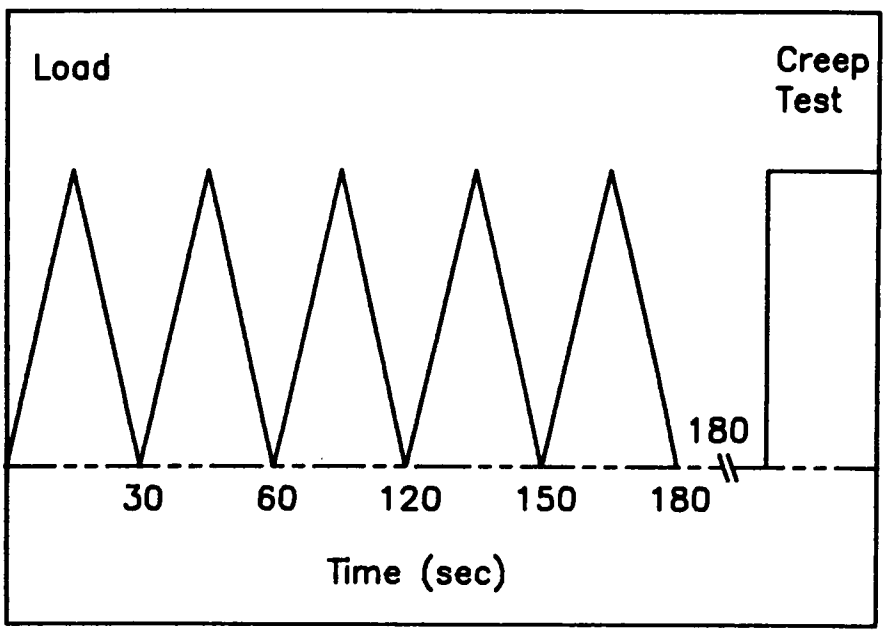

Fig. 4.1a Conditioning Cycle as Used on Prelimanary Conditioning Tests and Similar to Method Proposed by Brouwer [39].

micro-debonding, it would take place with short test as well as long tests.

The results of the mechanical conditioning tests were surprising. First, the $[90_2/45/-45]_s$ seemed not to be affected by mechanical conditioning, as shown in Fig. 4.2. Other stress and temperature levels showed the same results for the same laminate type. However, the $[\pm 45]_{2s}$ laminates, at the lower temperature of 38° C, showed mechanical conditioning stabilizes the creep (Fig. 4.3) whereas at the higher temperature of 51° C the short loading method of conditioning seems to have had no effect (Fig. 4.4). This temperature effect could be explained partially by thinking of mechanical conditioning having two parts, elastic and viscoelastic. At the lower temperatures (the glassy region), the specimens need mechanical conditioning primarily for stabilization of the elastic response, but for higher temperatures (transition or rubber region), specimen must be both viscoelastically as well as elastically conditioned. Mechanical conditioning of unidirectional laminates, mainly 0°, 10° and 90° specimens, were also examined and found to be insensitive to mechanical tests.

Possible conclusions that could be reached by the mechanical conditioning tests are 1) only certain laminates need conditioning, mainly two fiber direction laminates, and 2) the simple loading and unloading does not work for all cases, especially high temperature tests. Therefore, this study performed mechanical conditioning on all specimens for the same length of time that the actual creep test would be loaded. However, the number of conditioning tests was allowed to

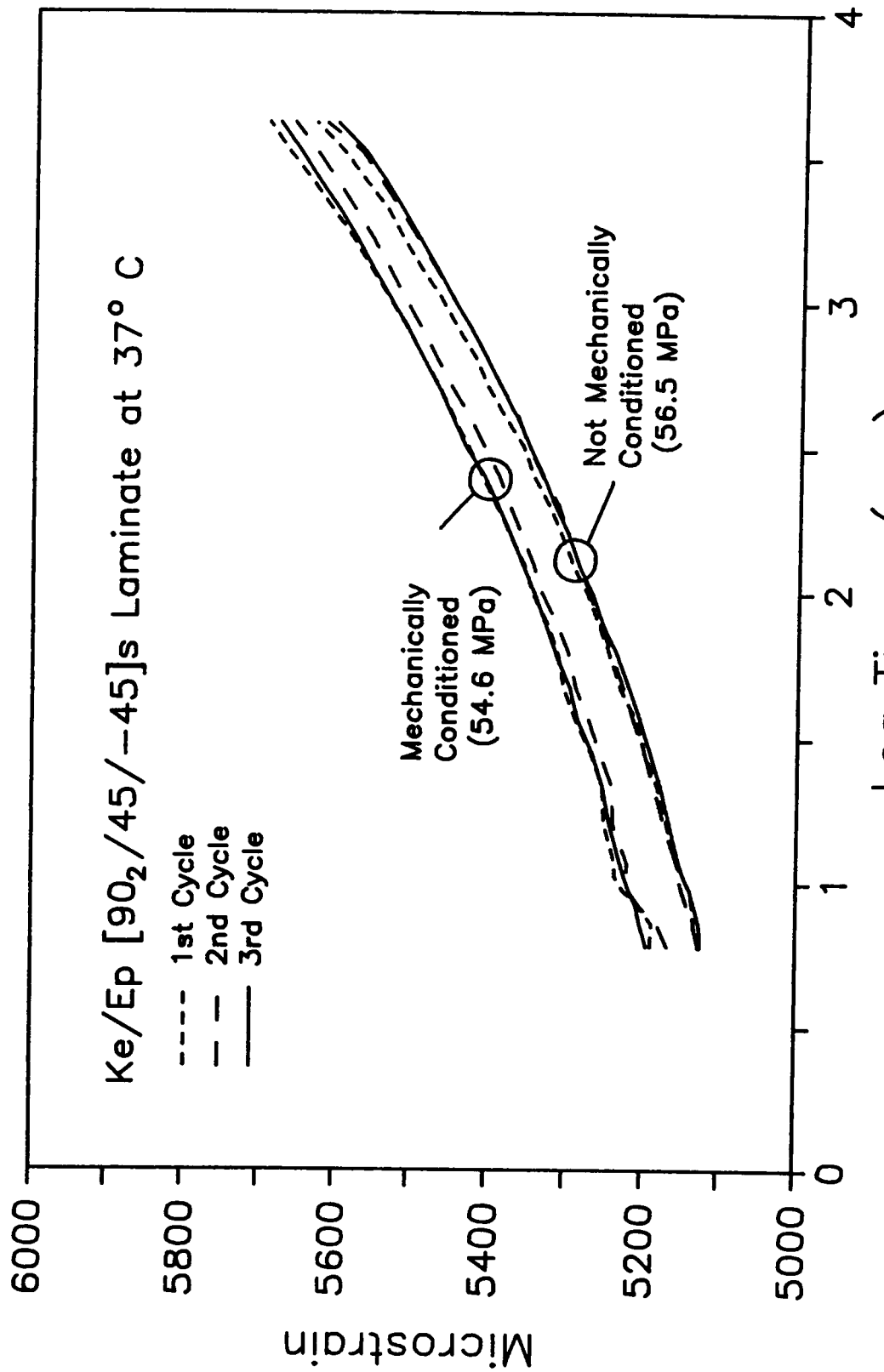

Fig. 4.2 Comparison of $[90_2/45/-45]_s$ Specimens for Mechanical Conditioning at 37° C.

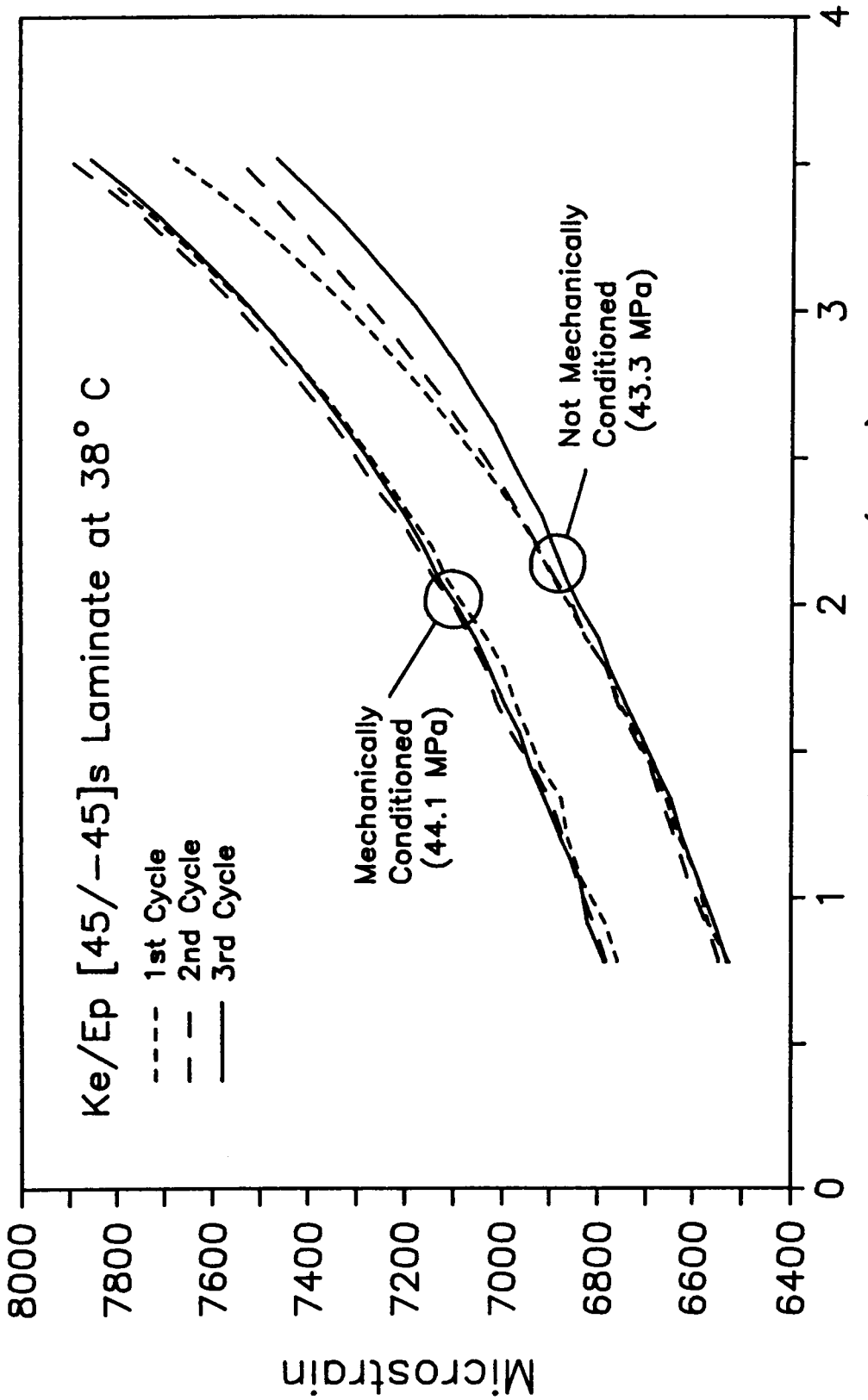

Fig. 4.3 Comparison of [45/−45]s Specimens for Mechanical Conditioning at 38° C.

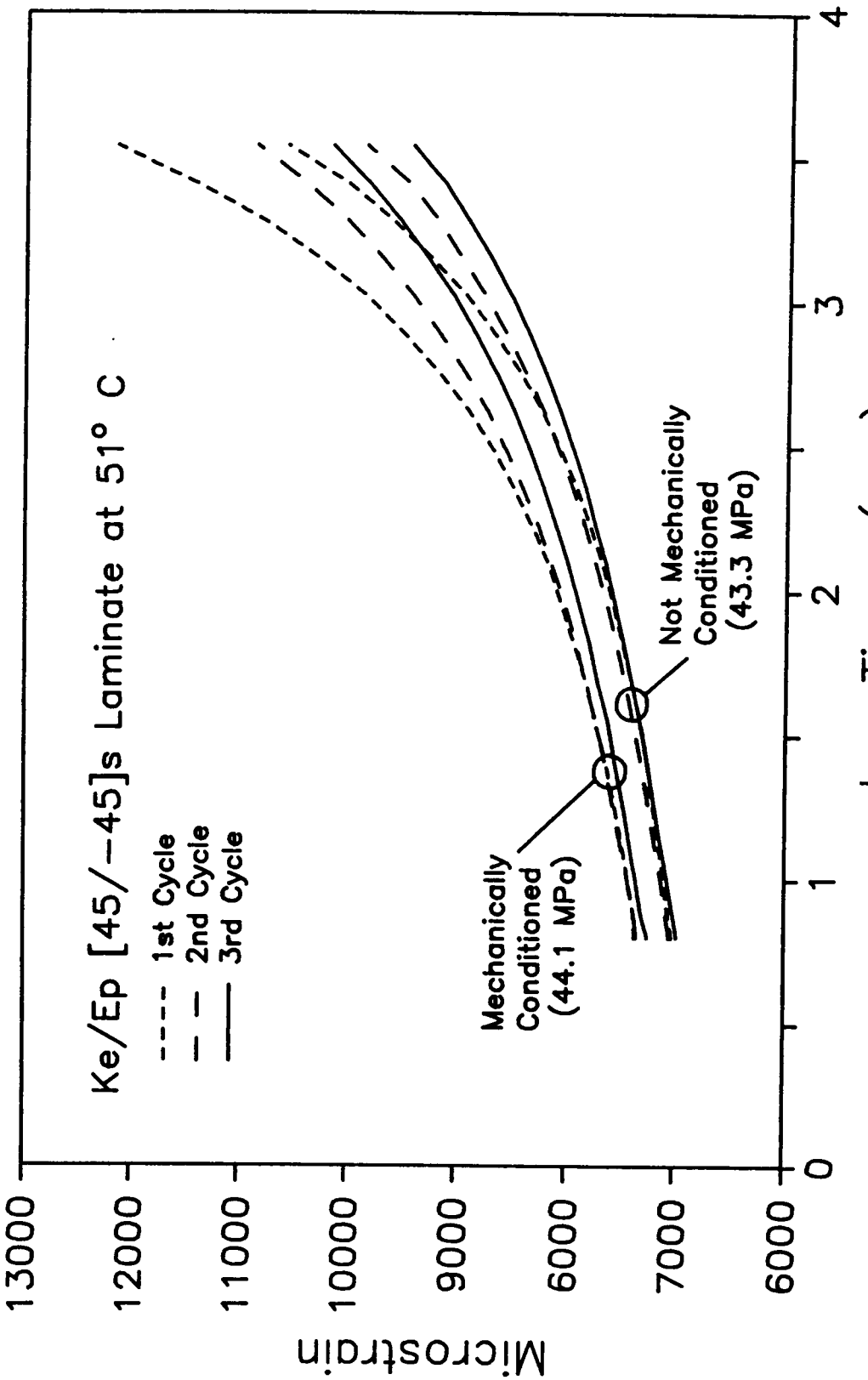

Fig. 4.4 Comparison of [45/−45]s Specimens for Mechanical Conditioning at 51° C.

vary. Conditioning tests were performed on a specimen until the creep was approximately the same (±2%) as the preceding test.

Generally, the creep and creep recovery strain for the first conditioning test and the actual test were the same for unidirectional laminates, and laminates with three or four fiber directions. Again, the two fiber directions needed three to four conditioning tests, which is thought to be due to the scissoring effect the two direction ply material exhibit when loaded. One exception to the above conditioning plan is for the long term (2 to 4 weeks) tests which experience only multiple short term conditioning tests since long term conditioning tests were impractical due to time considerations.

Thermal Conditioning

Similar to mechanical conditioning, thermal conditioning is performed to insure reproducible results on any one specimen by exposing the specimen to the test temperature several times before the actual mechanical test. This could be a particular problem for this study, since the same specimen is tested at various increasing temperatures in order to use the TTSP and construct a master curve. If the tests are affected by past thermal exposure, then the TTSP can be not be employed without thermal conditioning.

Since all specimens were exposed to 121° C for 150 minutes in order to cure the strain gage adhesive and post cure the specimen it was felt that this would suffice for thermal conditioning. Actual thermal conditioning tests were not performed because of the

difficultly in separating the mechanical conditioning from the thermal conditioning in any type of test procedure. However, before all tests, the specimens were exposed to the test temperature for approximately the length of the test, except for long term tests. It was felt that thermal conditioning is not a problem except at temperatures near the cure temperature (121° C) of the laminate.

A more severe problem that is associated with thermal conditioning is aging. The physical material properties of polymer based material systems have been shown to exhibit aging effects [1,111]. Since both the fibers and resin are polymeric based, they should be affected by time. Other investigators of viscoelastic response of composites have mentioned aging as a possible mechanism for the long term predictions not matching the actual test results [73,75]. Since the purpose of this study to investigate only the time-temperature effects on Kevlar/epoxy laminates, aging was not examined. Furthermore, long term tests agreed well with predictions (chapter 7) which minimizes the concern. The aging phenomenon should be investigated in more detail, particularly how it effects viscoelastic response.

Sample Width and Fiber Truss Effect

The width of the test specimen can be an important factor in measuring and predicting viscoelastic response of reinforced fiber composite laminates. If the test specimen is narrow, the edges effects can significantly affect the viscoelastic response. This is

especially true of three or more fiber direction laminates such as $[90_n/45/-45]_s$ which can form a fiber truss network of stiff fibers. This causes prediction problems since the numerical procedure (chapter 3) assumes all normals to the laminate remain normal after the load is applied as per classical lamination theory [19].

Predictions for laminates with more than two fiber orientations have been accurate at short times, but have fallen well below the experimental results obtained on narrow (12 mm.) specimens with three fiber directions. Further testing in this study has helped establish that relaxation of the fiber trusses along the free edges of narrow specimens is much more significant for time-dependent behavior than under short term conditions. Insights into the design of laminated composites for long term loading and certain precautions for experimental evaluation of time-dependent properties are also given in this section. By using wide specimens the effect of the edges can be reduced greatly. The section will present test results confirming the specimen width effect.

The compliance predictions of the numerical procedure (chapter 3) have been quite good for laminates which consist of only two fiber directions. Figure 4.5 illustrates the degree of fit which has been obtained for these types of layups for a graphite epoxy T300/934 composite laminate where the fibers are assumed to be non-viscoelastic [74]. This plot is for a T300/934 Gr/Ep cross ply laminate which is loaded with a uniaxial load applied 15° off axis from the 0° direction. The degree of fit is quite good and one should note that

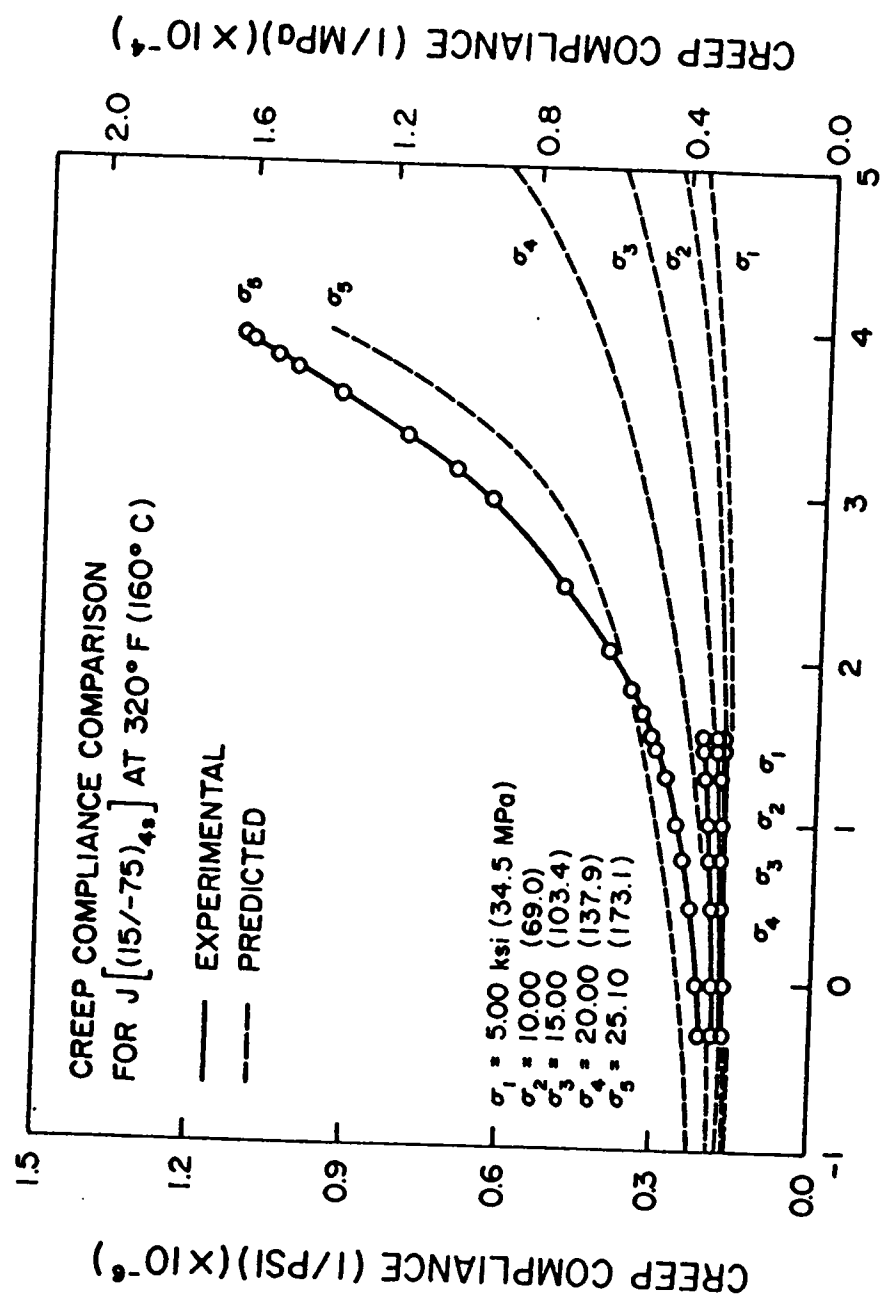

Fig. 4.5 Comparison of Numerical and Actaul Creep Compliance of $[15/-75]_{3s}$ Gr/Ep T300/934 Laminate at 160 °C [74].

the predictions for the compliance at the longer times indicate a very strong dependence on the applied stress level although this effect is quite small at the short times. This serves to caution against the use of static results to estimate the long term behavior unless the viscoelastic processes are adequately recognized. One should further note that the creep is quite large -- more than 4 times the static strain after only one week of loading (at an elevated temperature). These large strains are typical of laminates consisting of only two fiber directions because the fibers tend to scissor and result in very large deformations. Because these laminates are highly susceptible to large viscoelastic deformations, they should be avoided for applications where it is possible for the load directions to deviate from the predominant fiber direction. A typical application of such two fiber orientation systems has been for piping and various pressure vessels. Such designs may be adequate where the stress state is well behaved, but mounting brackets, fittings, and bending or twisting can introduce long term loads which cannot be adequately carried indefinitely.

The numerical predictions obtained for the graphite epoxy laminates consisting of three (or more) fiber directions have been less satisfactory [74]. Because of the assumptions of classical lamination theory, the program assumes that normals through the laminate remain straight and normal. When the fibers are present in at least three directions, the CLT assumptions imply that the fibers act as pinned trusses which form a vast network of triangular truss

elements. Because triangular trusses are rigid, the program predictions tend to asymptotically approach an upper limit which we have referred to as the fiber truss limit. This theoretical limit can be obtained by assuming that the matrix properties totally relax, thereby forcing the elastic fibers to carry all of the load. Actual experimental results and predictions are shown in Fig. 4.6 for a T300/934 laminate with three fiber directions [74].

The matrix stress relaxation and load shifting to fibers will generally take place over a long period of time. As an example, the relaxation of the matrix octahedral shear stress, which is a function of the lamina transverse stress, σ_{22}, and shear stress, σ_{12}, for the laminate used in Fig. 4.6 takes place over 18 to 19 decades of time (see Fig. 4.7). It should not be assumed that the individual lamina stresses, σ_1, σ_2 and σ_{12}, monotonically approach zero stress. Figures 4.8 and 4.9 show the transverse and shear stresses in each ply. Notice that the transverse stresses in the individual plies can actually change from tension to compression, as the stress approaches zero. This fluctuation of stresses can be attributed to the different relaxation rates that each of the directions (transverse, shear, and fiber) and ply orientation exhibit. The shear will shed its stress faster than the transverse direction, thus causing the transverse stress to actually pick up load in the first few decades and then shed this load later after the shear has totally relaxed.

While the numerical procedure predicts the fiber truss effect, narrow (13mm) specimens with three fiber directions may exhibit creep

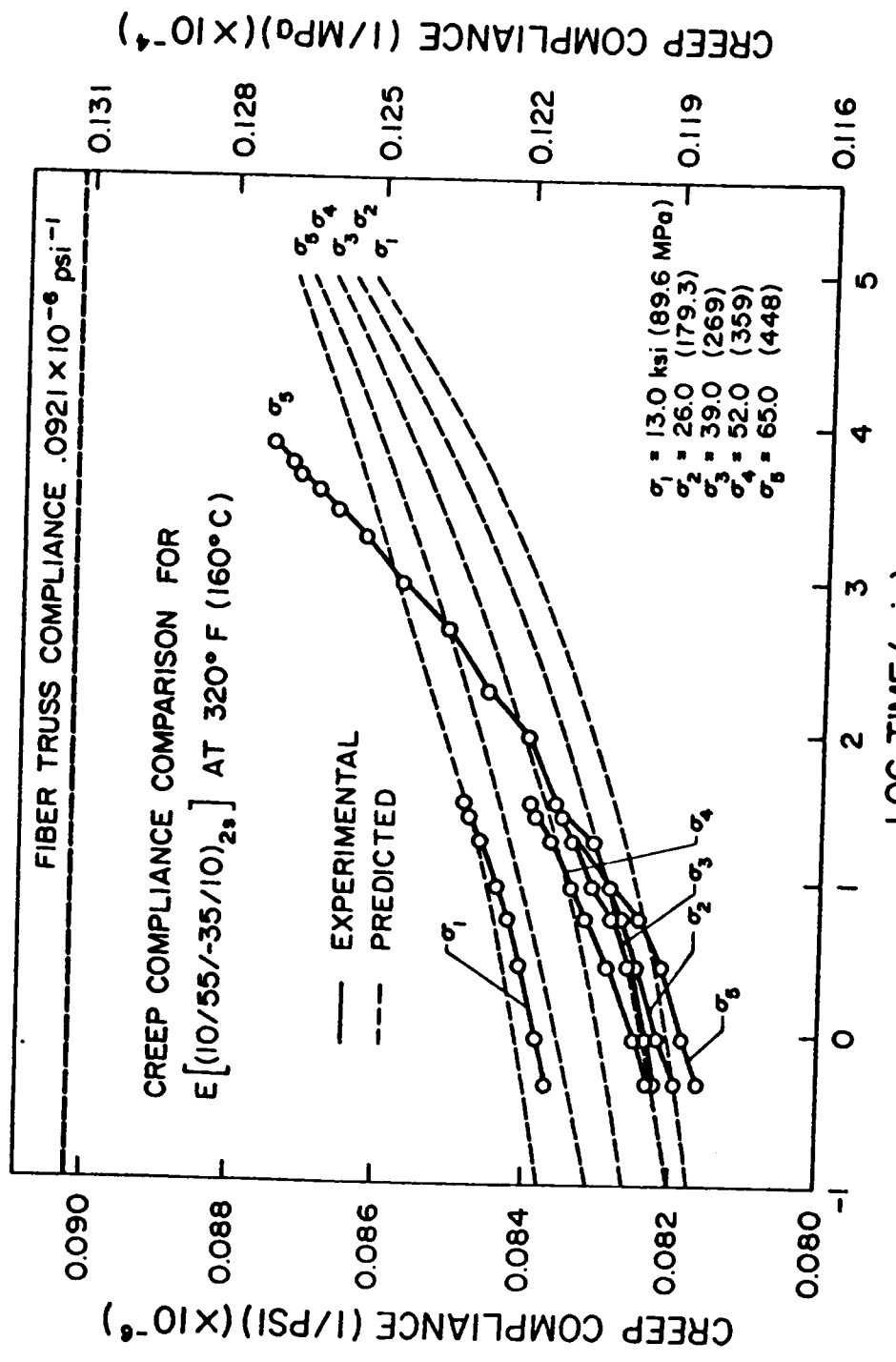

Fig. 4.6 Comparison of Numerical and Actaul Creep Compliance of $[10/55/-35/10]_s$ Gr/Ep T300/934 Laminate at 160 °C [74].

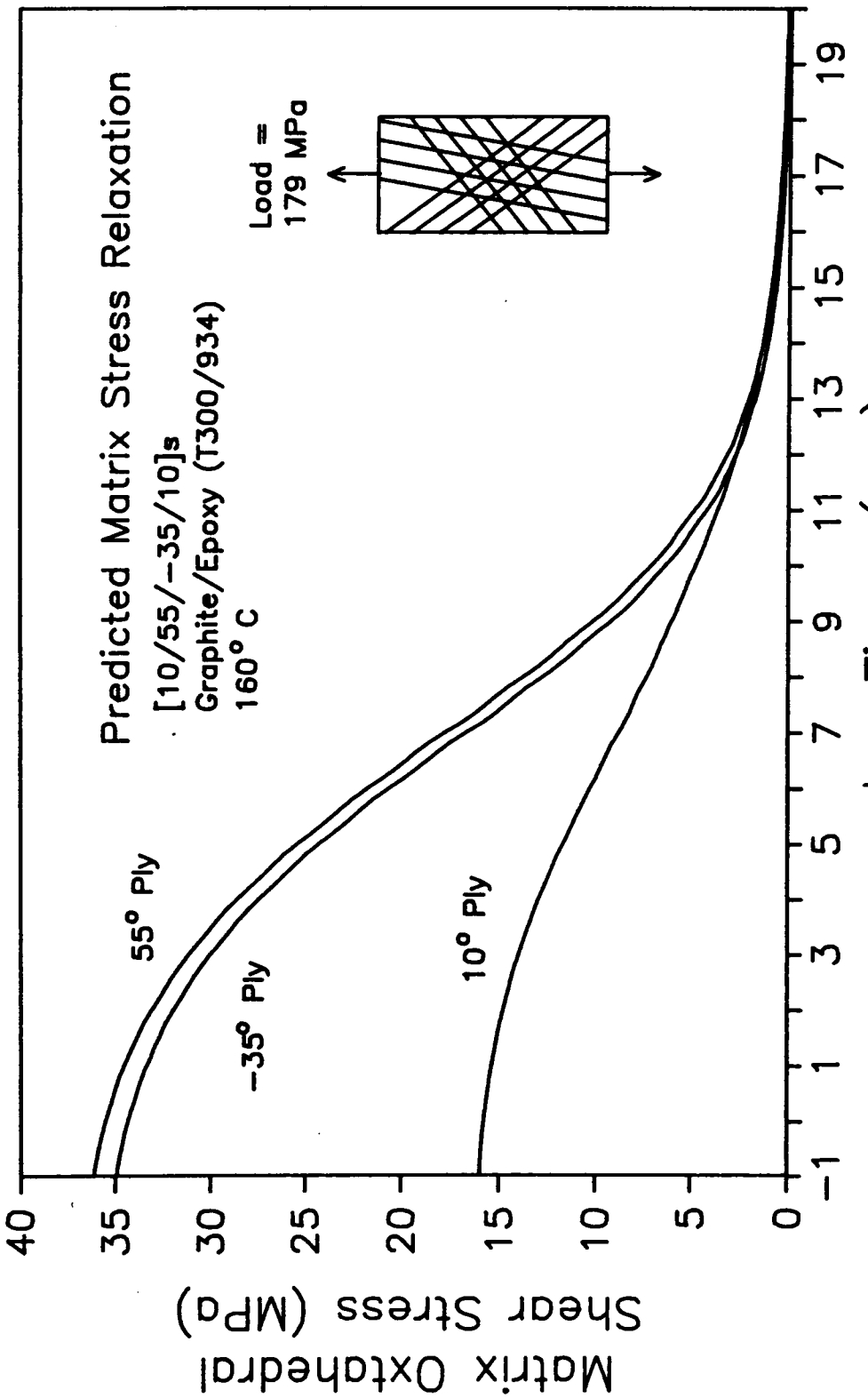

Fig. 4.7 Numerical Prediction of Stress Relaxation in Matrix for Graphite/Epoxy Laminate.

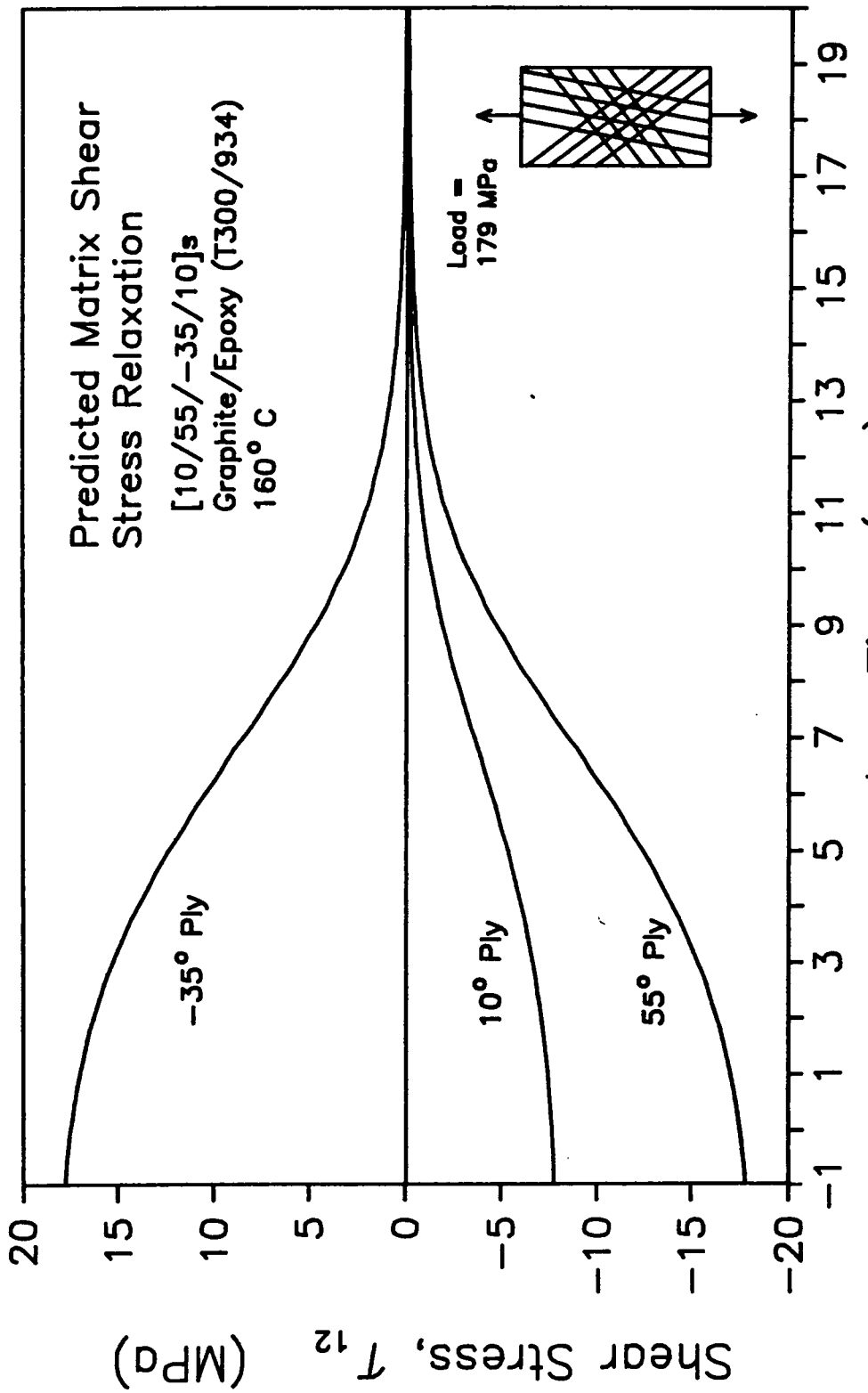

Fig. 4.8 Numerical Prediction of Shear Stress Relaxation in Matrix for Graphite/Epoxy Laminate.

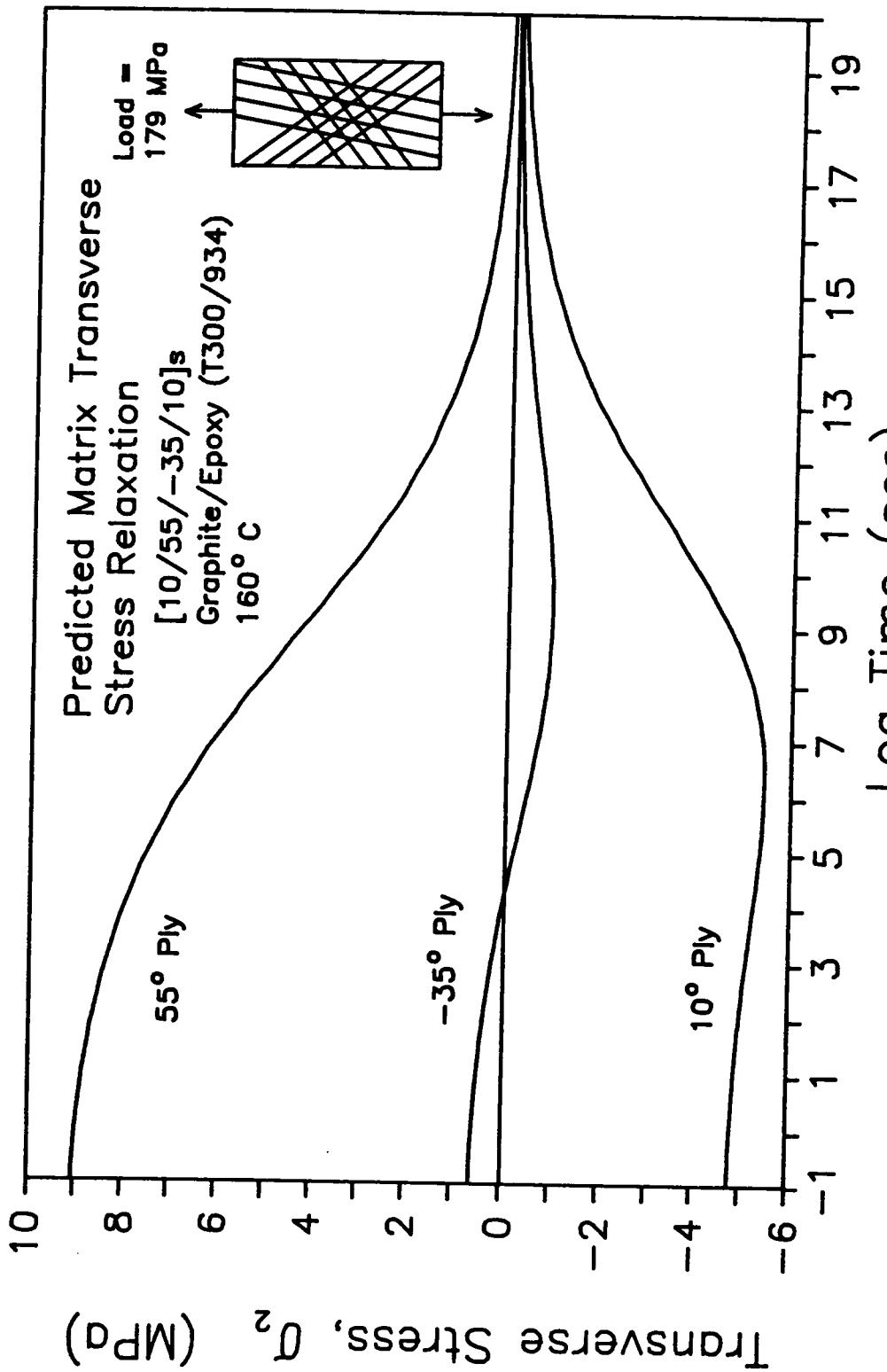

Fig. 4.9 Numerical Prediction of Transverse Stress Relaxation in Matrix for Graphite/Epoxy Laminate.

which is considerably greater than that predicted. This concept is illustrated schematically in Fig. 4.10 for a composite system with non-viscoelastic fibers. Much of the discrepancy apparently arises because the assumptions of lamination theory are not valid near the free edges of these specimens. CLT does slightly over-predict the static modulus of narrow specimens, but the time dependent deviation can be much larger. Since the interlaminar shear strains are controlled by the viscoelastic resin, this edge effect can increase significantly at longer times. Experimental data for Kevlar/epoxy composites was collected to illustrate the effect of specimen width on the measured viscoelastic response of laminated composites which will be presented later in this section. As specimen width is increased, the ratio of area in proximity to the free edge with that at the specimen interior decreases, and one approaches the predictions obtained from the numerical procedure. The implications are twofold: 1) the program predictions appear to be valid for wider specimens and structural components, and 2) care must be used in selecting specimen size for creep measurements in the laboratory.

This fiber truss effect has several consequences for the design of composite structures for long term durability. Specifically, the model can provide insights for designing laminates to provide better resistance to long term deformations. It is well known that the stiffness and strength estimates predicted by classical lamination theory and measured experimentally can be significantly higher than the corresponding predictions from a rule of mixtures or netting

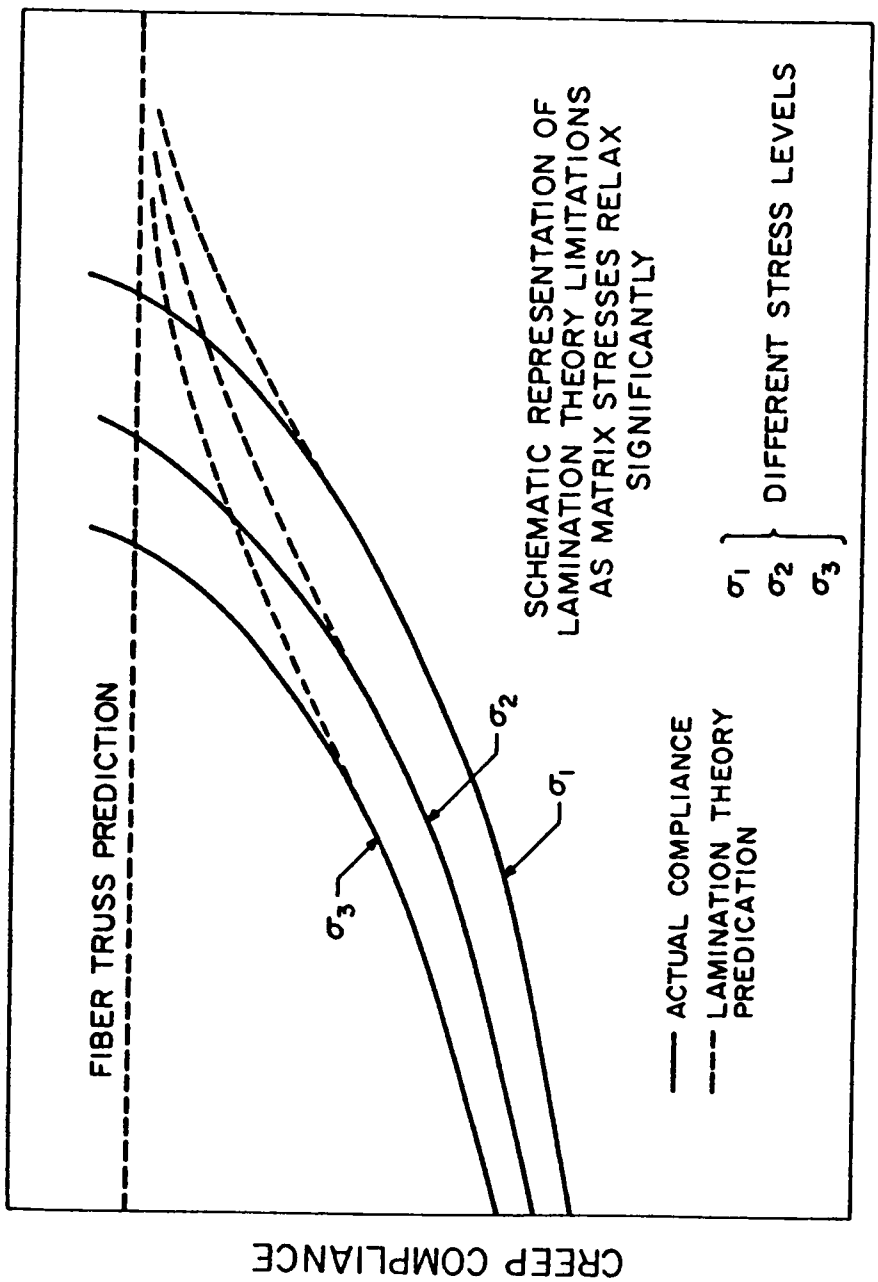

Fig. 4.10 Schematic Representation of the Fiber Truss Limitation of Creep Compliance for FRP Composites with Non-Viscoelastic Fibers [74].

analysis because of the constraint imposed by the plies on one another. From a viscoelastic standpoint, much of this increased stiffness and strength can be attributed to the presence of the fiber trusses imposed by three or more fibers and the assumptions of CLT. These assumptions that normals remain straight and normal can be rigorously demonstrated for regions away from free edges and where the applied stress field is relatively uniform and the individual plies have uniform properties in plan form. At the free edges, these assumptions are not valid, and yet for many practical structures, the region affected by the free edges is relatively small. Obvious examples are aircraft wing skins which are bolted at the edges, and tubular structures. This ignores the localized behavior around holes and cut-outs, but addresses the overall properties of the structure. Obviously the localized effects are very important for failure analysis, but they have less relevance for compliance of the structure as a whole.

Because the matrix properties are often much more viscoelastic than the fibers, one would expect that the laminates will be much more time dependent in directions which are not dominated by fibers. Figure 4.11 illustrates the predicted response of a $[45/-45/90_x]_s$ laminate (T300/934) as x is varied from 0% to 30% of the total laminate ply content. These predictions are based on the properties obtained for the load applied in the 0° direction. The compliance at short times is 40% greater for the laminate with no 90° plies than for the case where x = 30%. While this difference is not small, one notes

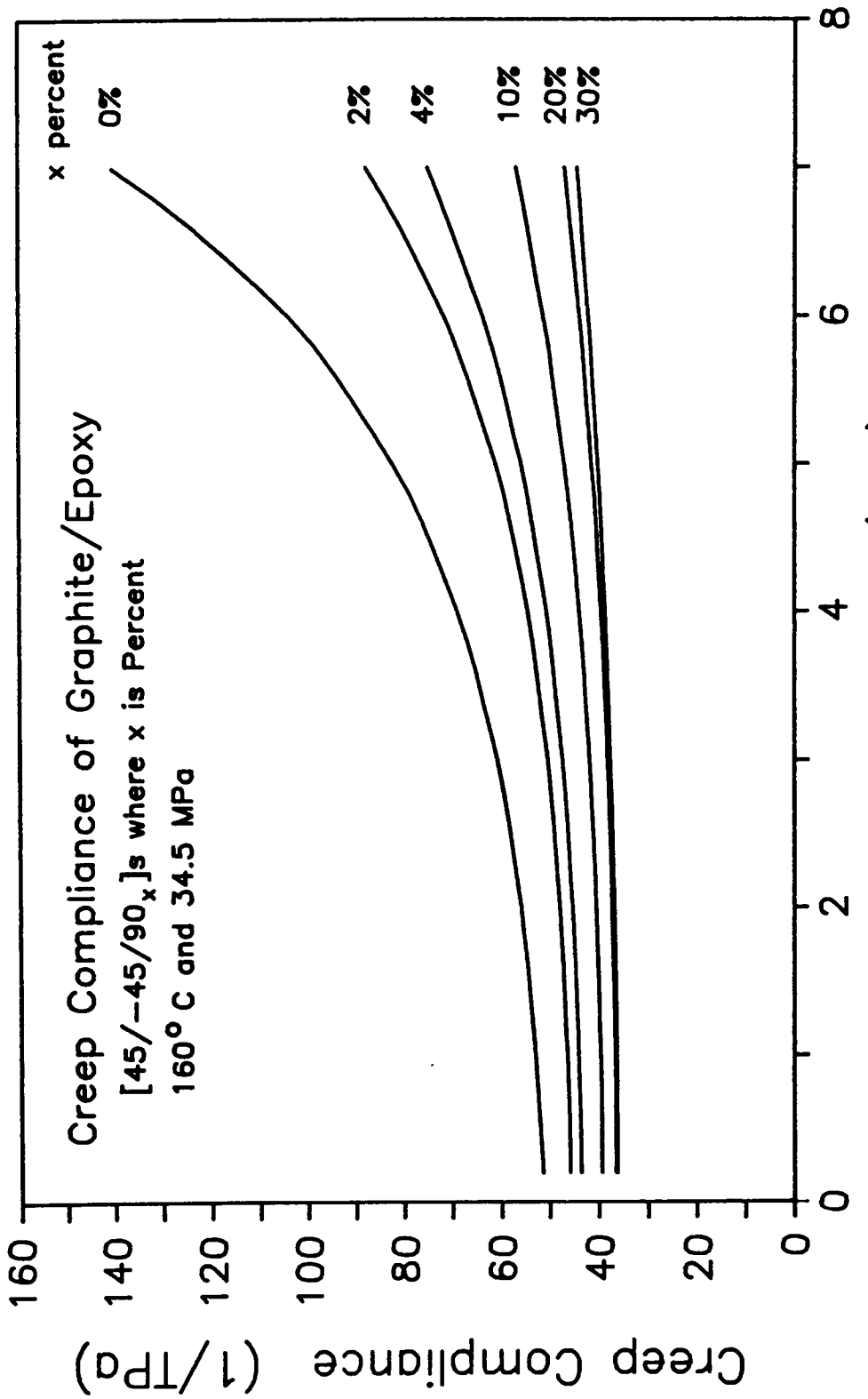

Fig. 4.11 Numerical Example of Creep Compliance for $[45/-45/90_x]_s$ With Percent of 90° Ply Varing.

that the response after ten weeks is estimated to be more than 200% greater than the laminate with 30% 90° plies. One should also note that only 3% 90° plies is sufficient to reduce this difference by a factor of two. The ability of a few 90° plies to significantly increase stiffness in the 0° direction is even more pronounced for time-dependent behavior than for the static case. Again these predictions caution the designer about using short term behavior to infer long-term properties. The wide divergence appears quite slowly, but results in long term behavior which is grossly different than initial observations would imply.

Another example is illustrated in Fig. 4.12 for a more fiber dominated type of laminate. The $[0/90]_{ns}$ laminate may be typical of certain laminates which have been used widely for pressure vessel applications and is similar to many of the minimum thickness skins for aircraft which are fabricated from woven material. Consider the case where a uniaxial load is applied at small angles away from the principal material directions. Although the actual loading is often biaxial, this loading situation will illustrate the point. Figure 4.13 shows that the addition of only 4% (45/-45) plies can significantly reduce the time dependence of the laminate. Figure 4.14 suggests that the time dependence is minimal when the percentage of (45/-45) plies is increased to 10%. Again one should note that the observations at short times could lead to grossly non-conservative estimates of long term behavior.

To illustrate the general validity of these predictions, tests

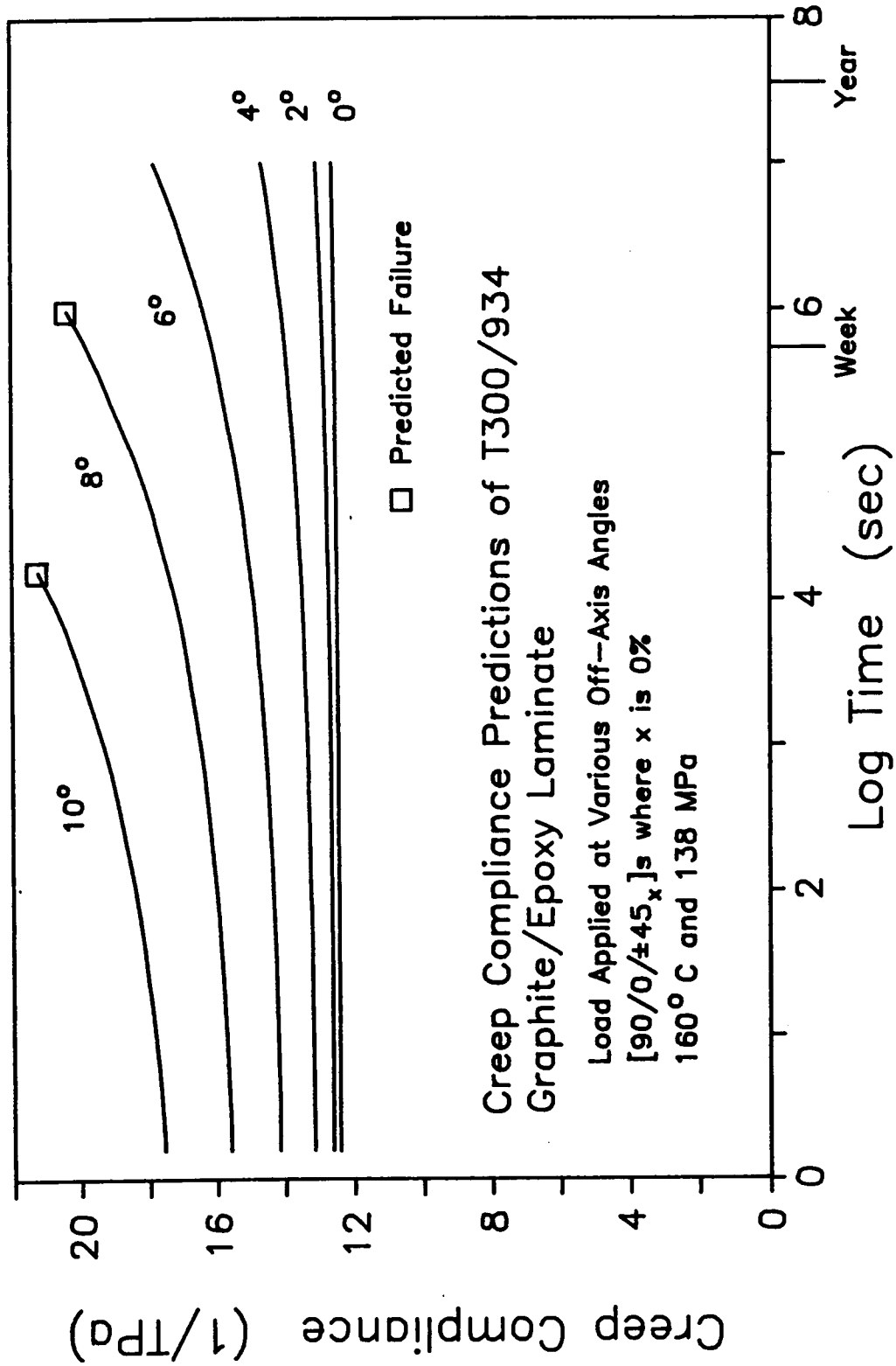

Fig. 4.12 Numerical Example of Predicted Creep Compliance for [90/0]s with Load Applied at Various Angles.

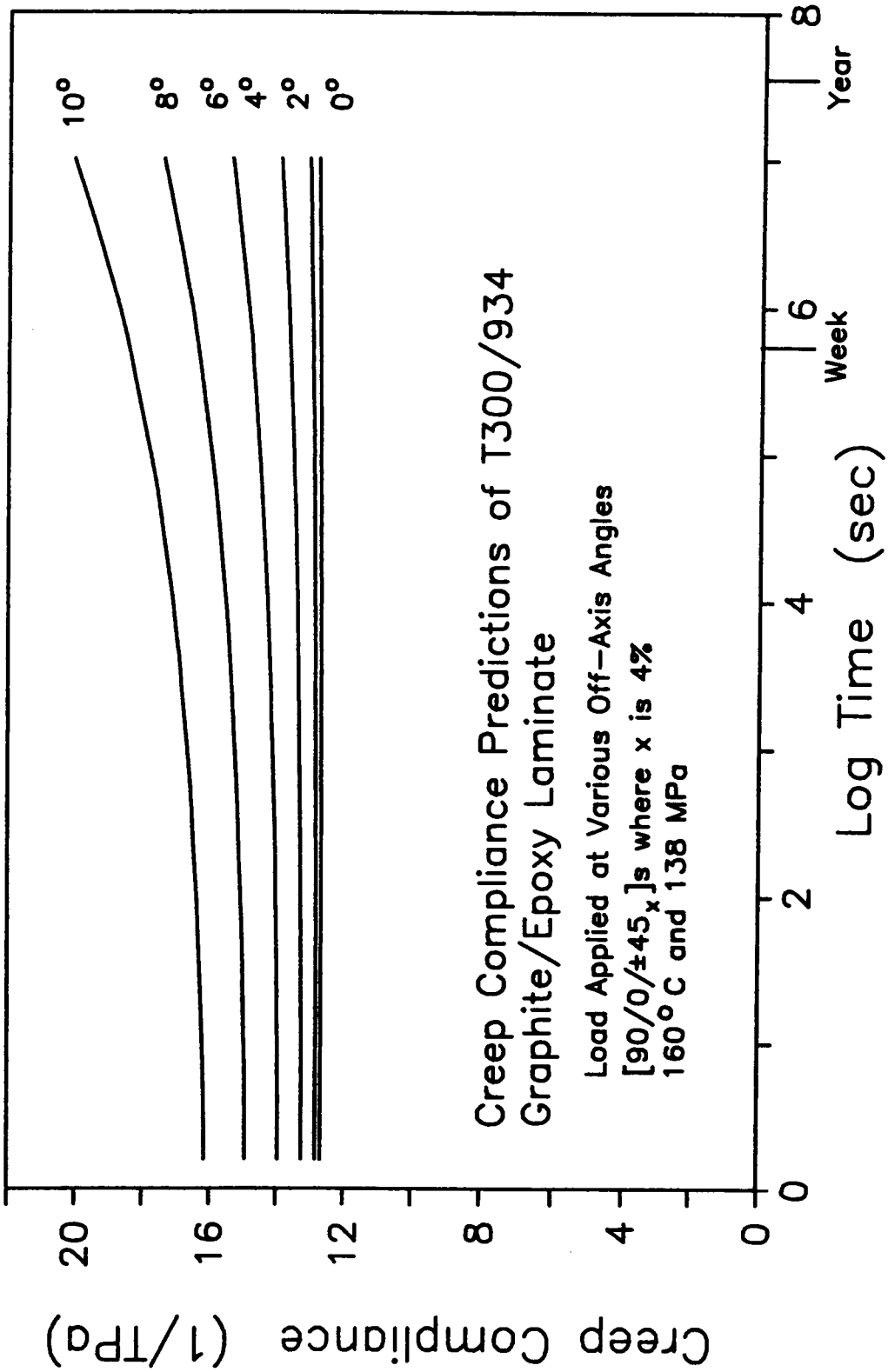

Fig. 4.13 Numerical Example of Predicted Creep Compliance for [90/0/−45/45]s with Load Applied at Various Angles.

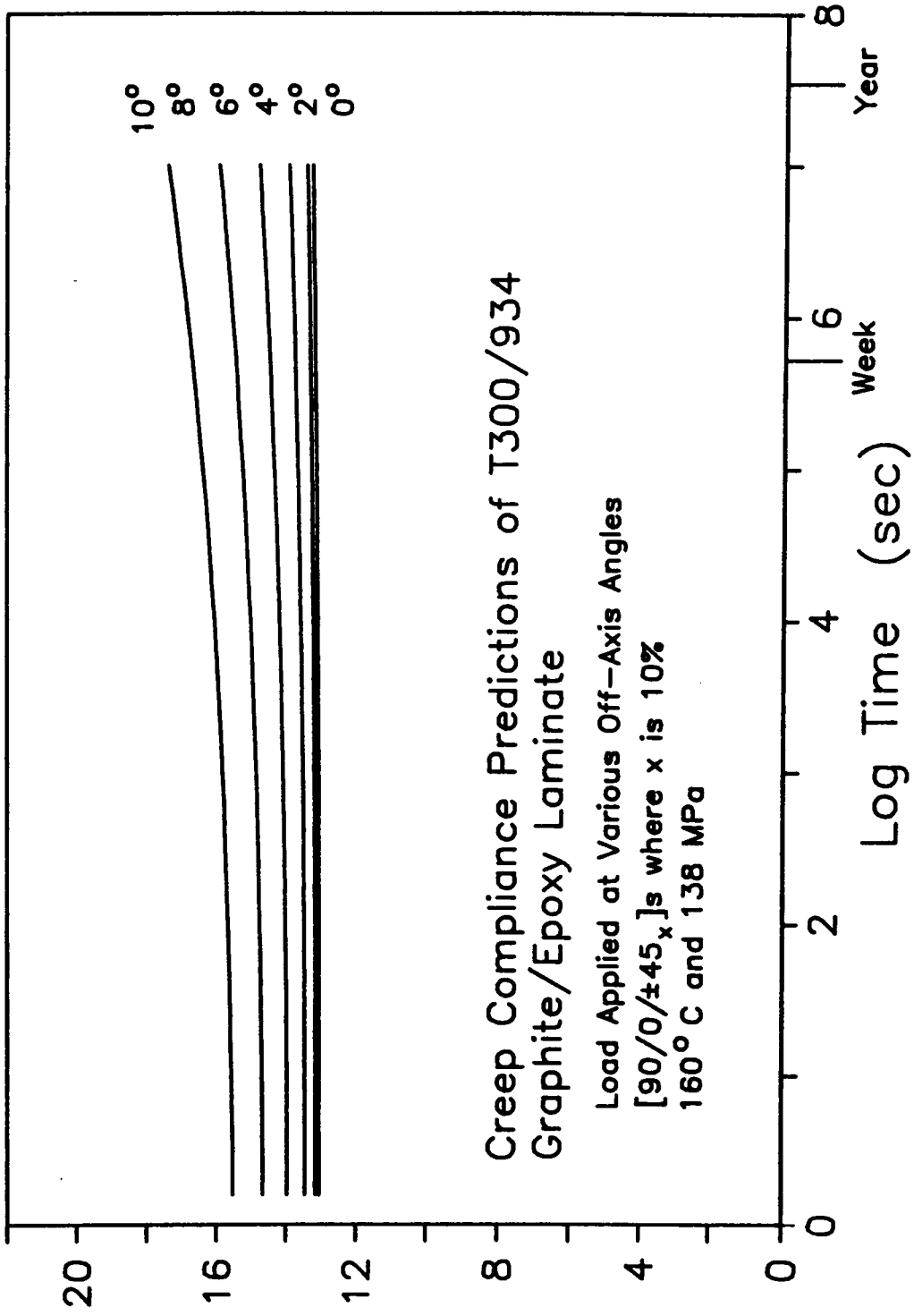

Fig. 4.14 Numerical Example of Predicted Creep Compliance for [90/0/−45/45]s with Load Applied at Various Angles.

have been run on several specimens made of Kevlar/epoxy. Figure 4.15 shows the significant effect of the third fiber direction on 25 mm wide specimens of Kevlar/epoxy at 82° C. The specimens were loaded to produce the same initial strain in each. The load on the $[\pm 45]_{2s}$ specimen was 3.0 MPa, and the load on the $[45/-45/90_2]_s$ specimen was 20.0 MPa. Note the extreme divergence of the laminate with only two fiber directions. The initial compliances were different by a factor of nearly seven. This occurred because at the higher temperature, the short time response was shifted far to the right on a figure such as Fig. 4.12.

In an evaluation of the width effect, data was collected for specimens of different widths with layups of $[\pm 45]_{2s}$ and $[45/-45/90_2]_s$, the results of the latter being given in Fig. 4.16 and 4.17. There is a trend for the compliance of both laminates to be somewhat larger for narrow specimens than for wider specimens. This width effect is more pronounced for the laminate with three fiber directions as would be predicted by an understanding of the interaction of the free edges and the fiber truss effect. While this effect was fairly small for these laminates, the width effect should be greater as the laminate compliance reaches the fiber truss limit. Also, Fig. 4.18 confirms the fiber truss concept by demonstrating almost no width effect for only two fibers direction laminates, as would be expected.

The effect of the free edge has been shown to be more significant for long term compliance of laminates than might be predicted by short

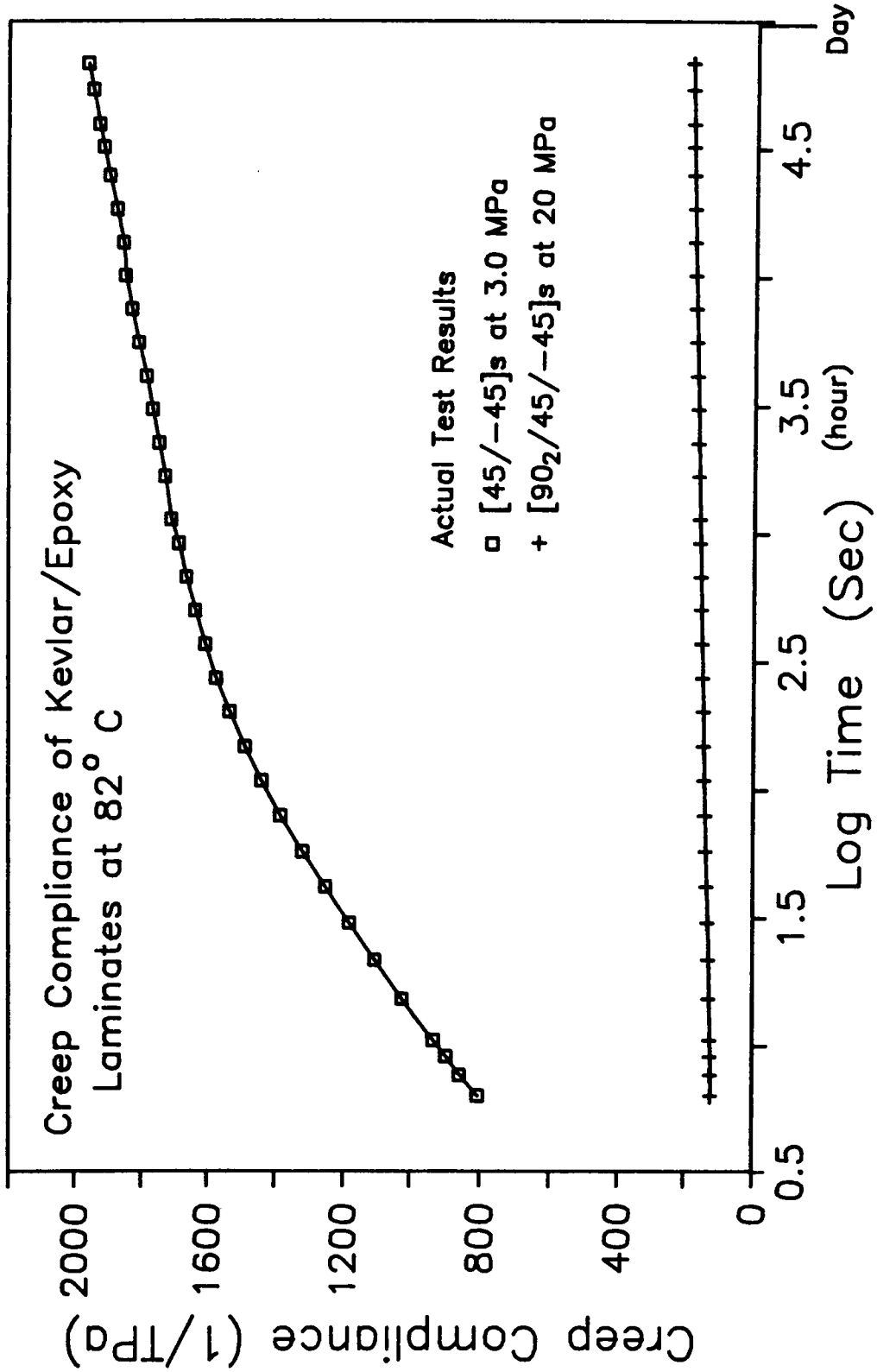

Fig. 4.15 Comparison of Actual Creep Test Results of [45/−45]s and [90_2/45/−45]s Kevlar/Epoxy Laminates.

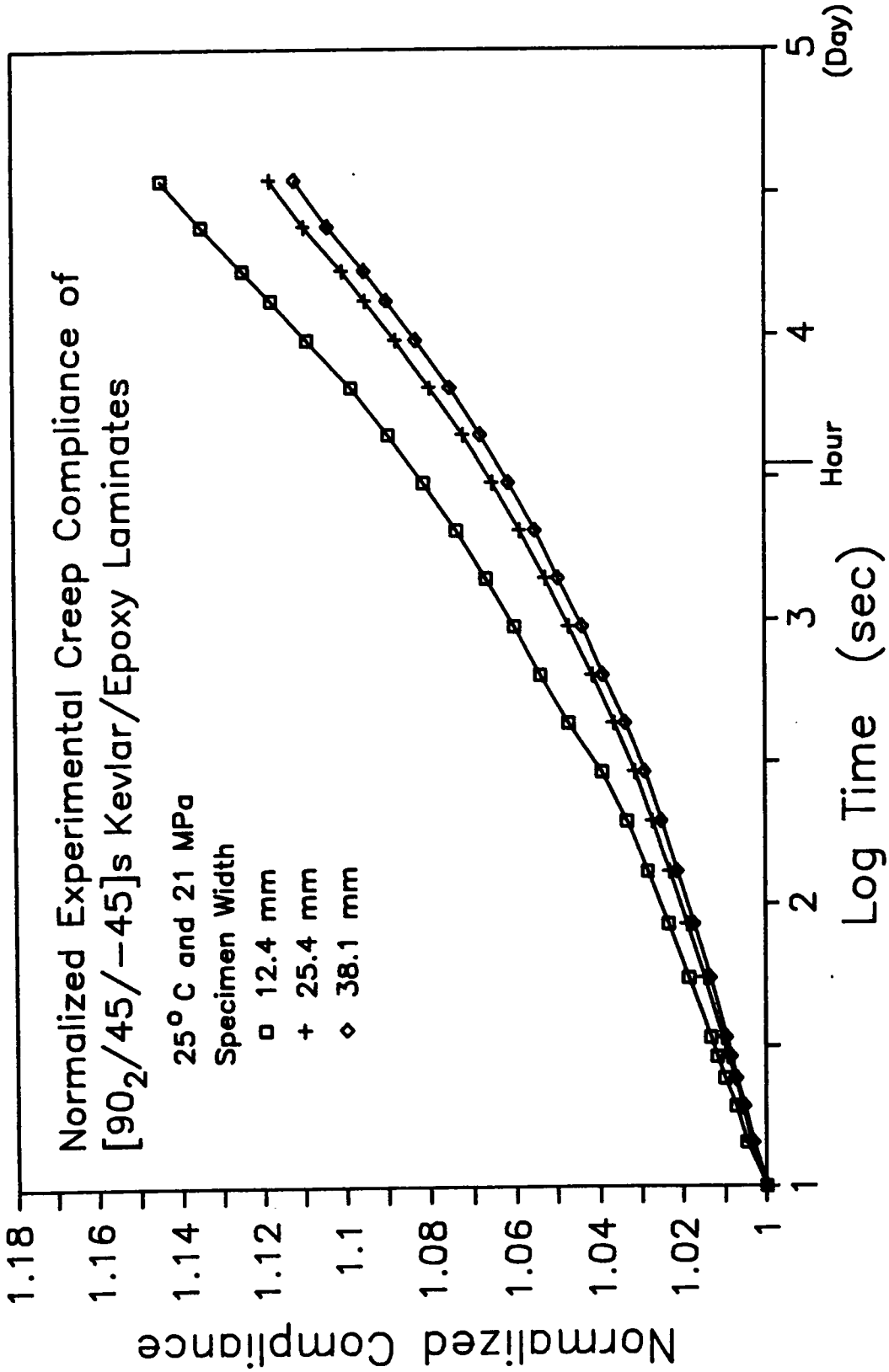

Fig. 4.16 Truss Effect on $[90_2/45/-45]_s$ Kevlar/Epoxy Laminates.

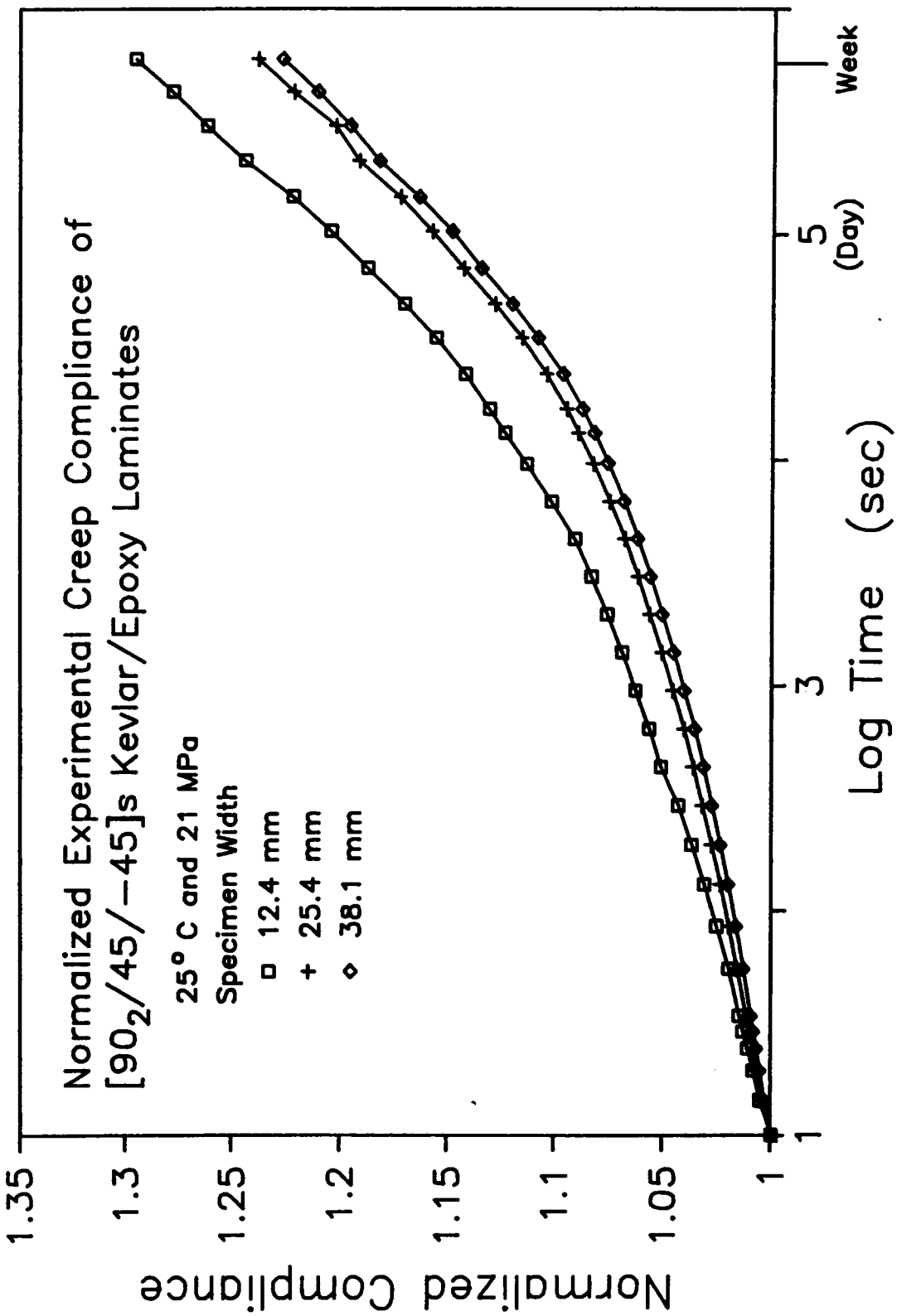

Fig. 4.17 Truss Effect on $[90_2/45/-45]_s$ Kevlar/Epoxy Laminates.

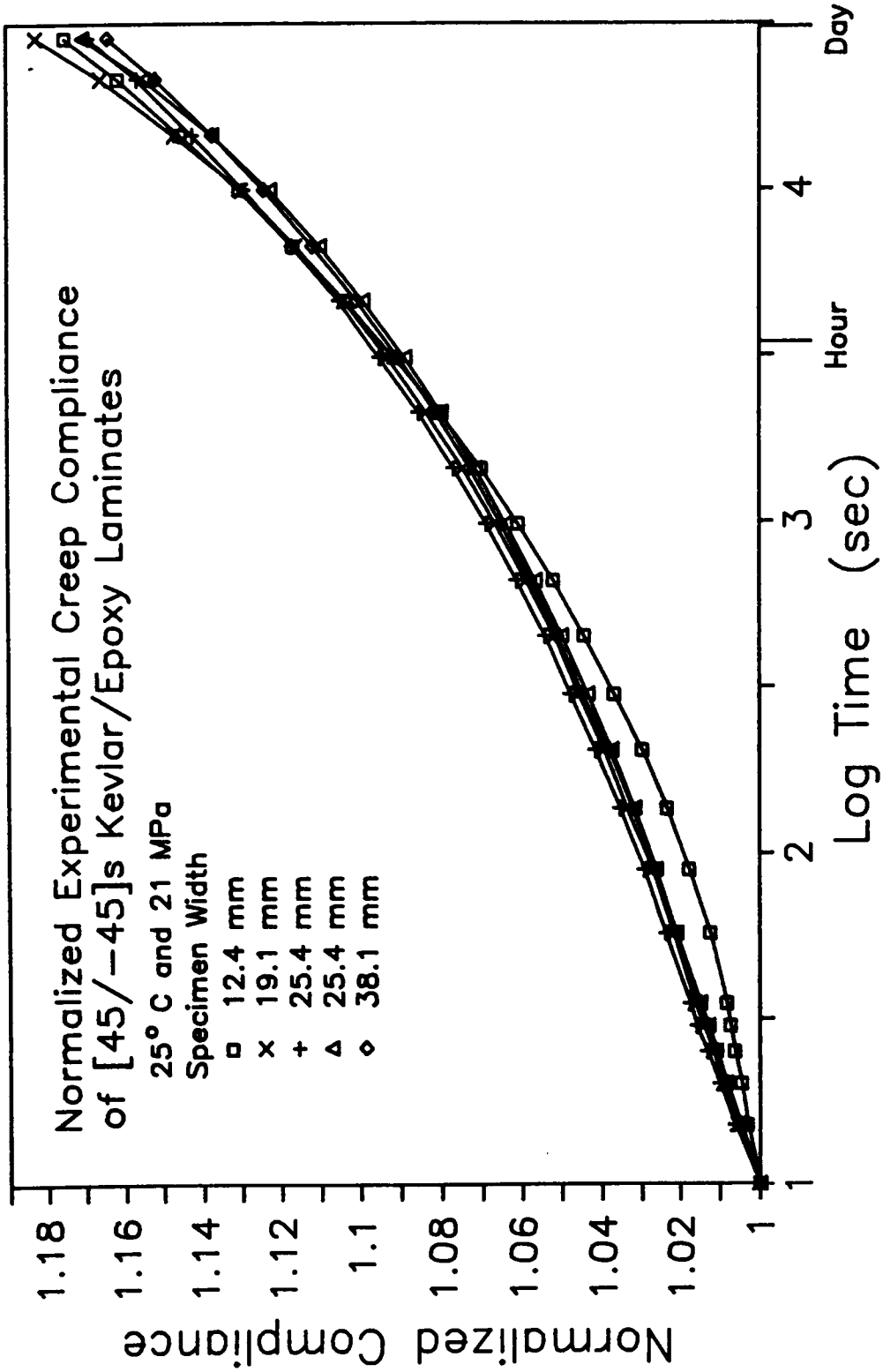

Fig. 4.18 Creep Compliance of [45/−45]s Kevlar/Epoxy Laminates (Note Lack of Fiber Truss Effect).

term observations. This free edge effect can cause narrow specimens to be significantly more compliant than CLT would predict. Therefore in this study all laminate specimens of three or more fiber angles were 1 inch wide to minimize the viscoelastic edge effect. For long term durability, it has been demonstrated that specimens with three or more fiber directions have dramatically less creep than laminates consisting of only two fiber directions, even though the difference for short term loading is much smaller.

Chapter 5

THERMOVISCOELASTIC CHARACTERIZATION OF KEVLAR/EPOXY COMPOSITE

There are several obstacles in characterizing and predicting the long term viscoelastic properties of a FRP composite laminate. First, it is not practical to perform long term tests of the same duration that the product might experience in service. Although the product might be in service for 20 years, tests of more than a few weeks are difficult and expensive to perform. Furthermore, FRP composites are orthotropic at the lamina level, thus requiring the determination of four material parameters instead of the usual two for an isotropic material which adds to the total number of tests necessary. These problems can be reduced to manageable levels by using the Time-Temperature-Superposition-Principle (TTSP), which was presented in chapter 2, to characterize the long term response of the unidirectional lamina for all four material properties.

This chapter will show how the TTSP has been successfully applied to an orthotropic composite material to obtain long term lamina viscoelastic property data from short term tests. The material system tested was made from Kevlar 49 fibers and Fiberite 7714A epoxy. This composite system was chosen since Kevlar fiber are viscoelastic in the longitudinal direction. By having viscoelastic fiber in a viscoelastic matrix all four material properties will be viscoelastic and this insures a viscoelastic orthotropic material. A second reason

for examining Kevlar/epoxy is due to its increasing use in industry and the current lack of understanding of viscoelastic properties of composite made from Kevlar.

The results obtained in this experimental phase of the study will be used in the numerical model developed in chapter 3 to predict long term response of any general laminate constructed from the Kevlar/epoxy composite system. Three basic results will be generated in this chapter for each of the four material property direction. One, a master curve for general linear viscoelastic response will obtained. Two, a shift factor function will be generated. And, three, the nonlinear viscoelastic response will be presented.

General Stress-Strain Response

Before extensive viscoelastic testing was performed, sample unidirectional specimens were tested for ultimate strength and stress-strain behavior at a high loading rate. This information was basically used to determine the stress levels for the viscoelastic tests and to verify the basic material properties as published by the DuPont, the supplier of the specimens. The results of these tests for the fiber direction, S_{11} and transverse direction, S_{22} are shown in Fig. 5.1.

The ultimate stress for the fiber direction, $_{u}\sigma_{1}$, and transverse direction, $_{u}\sigma_{2}$, are 1300 MPa (188.6 KSI) and 12.3 MPa (1.88 KSI), respectively. The $_{u}\sigma_{1}$ is comparable with the published ultimate tensile strength of Kevlar/epoxy [112] of 1379 MPa. The slight

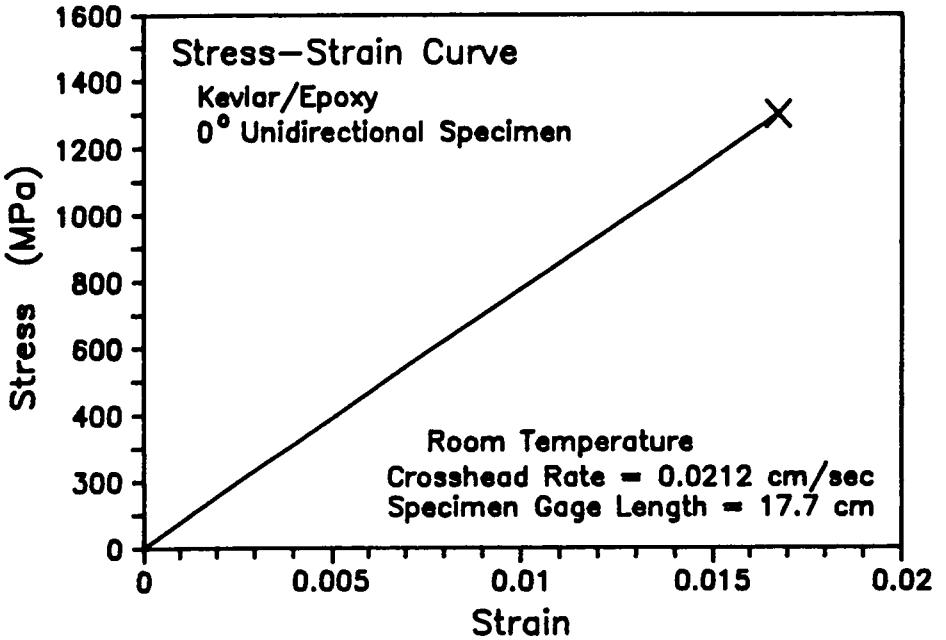

Fig. 5.1a Stress–Strain Curve in Fiber Direction.

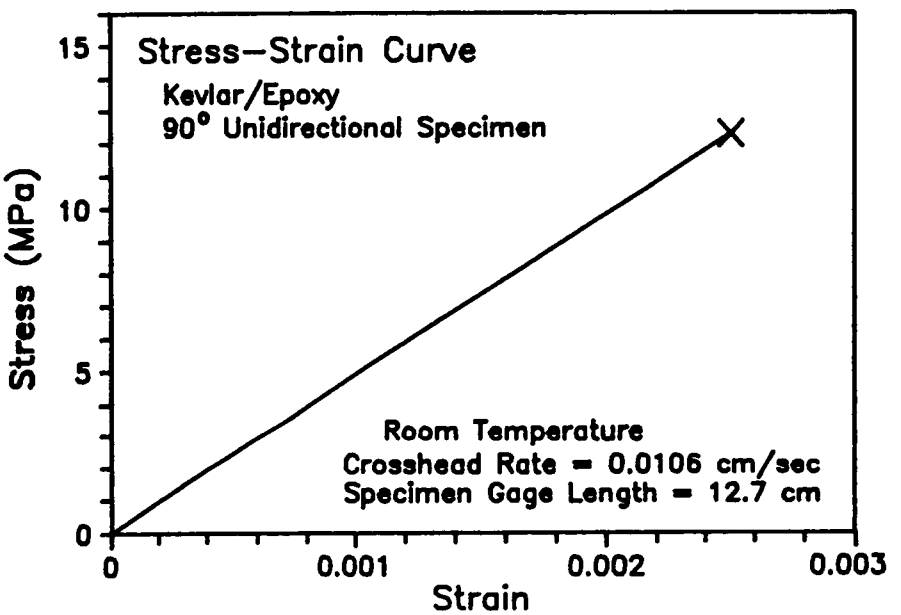

Fig. 5.1b Stress–Strain Curve in Transverse Direction.

decrease is could be due to the gripping mechanism not being the optimum type, possible slight misalignment, and experimental error. The $_{u}\sigma_{2}$ is considerably less then the normal transverse strength of 28 MPa reported by DuPont [112,113] but the same for the results reported by Tsai of 12 MPa [114]. The same results of low $_{u}\sigma_{2}$ strength were experienced in the viscoelastic creep testing done in this study where σ_{2} of 10 MPa or more would fail the specimen in a delayed rupture mode. While the shear strength was not tested directly, unidirectional 10° off-axis specimens were tested for ultimate stress since these type specimens were used in the viscoelastic test. The ultimate specimen stress, $_{u}\sigma_{x}$, was 164 MPa (23.8 KSI) which is lower then the predicted strength of 210 MPa for a 10° unidirectional specimen load at 0° using ultimates given by Tsai [114]. If the specimen was slightly misaligned, say 12° instead of 10°off-axis, then the predicted ultimate would be only 162 MPa. Thus the lower strength could be due to slight load misalignment. In summary, the ultimate stress loads for the 0°, 10°, and 90° specimens were found to be 1.30 GPa, 164 MPa, and 12.3 MPa, respectively. These ultimates were used only as guidelines to base the stress level selection for the viscoelastic creep tests.

Accelerated Testing Using TTSP

The validity of the TTSP has been well established for polymeric materials as a means to accelerate time dependent testing [1]. Since many fiber reinforced composites have a polymeric based resin for the

matrix material, it is reasonable to expect these composites will also be viscoelastic and that the TTSP could be used for accelerated testing. Furthermore, Kevlar fibers are also viscoelastic which increases the overall composite viscoelastic response and at the same time complicates the application of TTSP to composites.

Brinson, et al. [72] originally proposed an accelerated characterization procedure for laminated materials. It was suggested that a minimal amount of short-term tests could be performed on the unidirectional material at different temperatures, stress and moisture levels and then horizontally shifted to construct master curves using theories such as TTSP, TSSP (Time-Stress-Superposition-Principle) and TMSP (Time-Moisture-Superposition-Principle). They showed that graphite/934 epoxy composite lamina can be characterized for long times from short term tests by using temperature and/or stress as the accelerating factor [73,76]. Results for other laminated composites under various load and temperature levels can be found in Refs. 67 and 115.

Because the individual lamina of FRP composites can be considered to be orthotropic, four independent material constants that relate stress and strain (assuming a state of plane stress) need to be determined. These constants can be functions of time, stress level, temperature, moisture, aging, and other environmental factors [30]. The stress-strain relationship or constitutive equations can be written as

$$\begin{Bmatrix} \varepsilon_1 \\ \varepsilon_2 \\ \gamma_{12} \end{Bmatrix} = \begin{bmatrix} S_{11}(t,T,\sigma,M) & S_{12}(t,T,\sigma,M) & 0 \\ S_{12}(t,T,\sigma,M) & S_{22}(t,T,\sigma,M) & 0 \\ 0 & 0 & S_{66}(t,T,\sigma,M) \end{bmatrix} \begin{Bmatrix} \sigma_1 \\ \sigma_2 \\ \tau_{12} \end{Bmatrix} \quad (5.1)$$

where S_{11}, S_{12}, S_{22}, and S_{66} are the compliances in the fiber direction, transverse/fiber coupling direction, transverse direction, and in shear, respectively. Each of these terms can be determined from a unidirectional lamina through experimental testing. For some FRP composites, such as graphite/epoxy, the fibers are essentially elastic and thus S_{11} and S_{12} terms are time independent. However, for Kevlar/epoxy which was used in this study, all four terms are time dependent and must be determined. The method used to determine these compliance terms were static creep and creep recovery tests on 0°, 90°, and 10° unidirectional lamina specimens as described in chapter 4. The master curves were constructed from short term tests, and then a viscoelastic model was fitted to the master curves.

Linear Viscoelastic Characterization of Kevlar/Epoxy

To construct the master curves by using TTSP, short term tests, 15-20 minutes, were first conducted at various temperature levels but at the same, constant stress level. The same test specimen was used at all temperature levels for each set of short term tests in order to assure consistent and shiftable results. Three to four different samples, each at a different stress level, were tested in this manner for each direction, i.e., S_{11}, S_{12}, etc.

The four stress levels tested on the 0° specimens for the S_{11} compliance were 83.7, 193, 298, 443 MPa (6.4%, 15%, 23%, and 34% of ultimate, respectively). The individual creep curves for all temperature levels are shown in Figs. 5.2-5.5. All four stress levels showed an constant creep rate at every temperature levels.

The short term curves were then shifted to construct master curves and to determine the shift factor function (see following section). The shifting was done by use of a microcomputer based program called 'ACS' (Automated Curve Shifting) written for this study that employs both numerical and graphically shifting methods (see Appendix D). The constant creep and consistency between tests for the S_{11} compliance facilitated the curve shifting.

The master curves that resulted from the shifting process for S_{11} are shown in Fig. 5.6. To identify the true perspective and similarity between tests and stress levels, the full scale is shown in Fig. 5.7. The compliance in the axial direction is nearly linear in log time, even at long times, for all temperature levels which agrees with test results on single Kevlar fibers obtained by Horn, et al, [83] and by Ho, et al. [35].

The fiber/transverse coupling compliance, S_{12}, is obtained from loading a 0° unidirectional specimen and measuring the strain in the transverse direction as was explained in chapter 2. This allows the S_{11} and S_{12} compliance to be obtained from the same specimen during the same test by mounting strain gages transverse to the fibers while loading in the fiber direction. Therefore, the stress levels were the

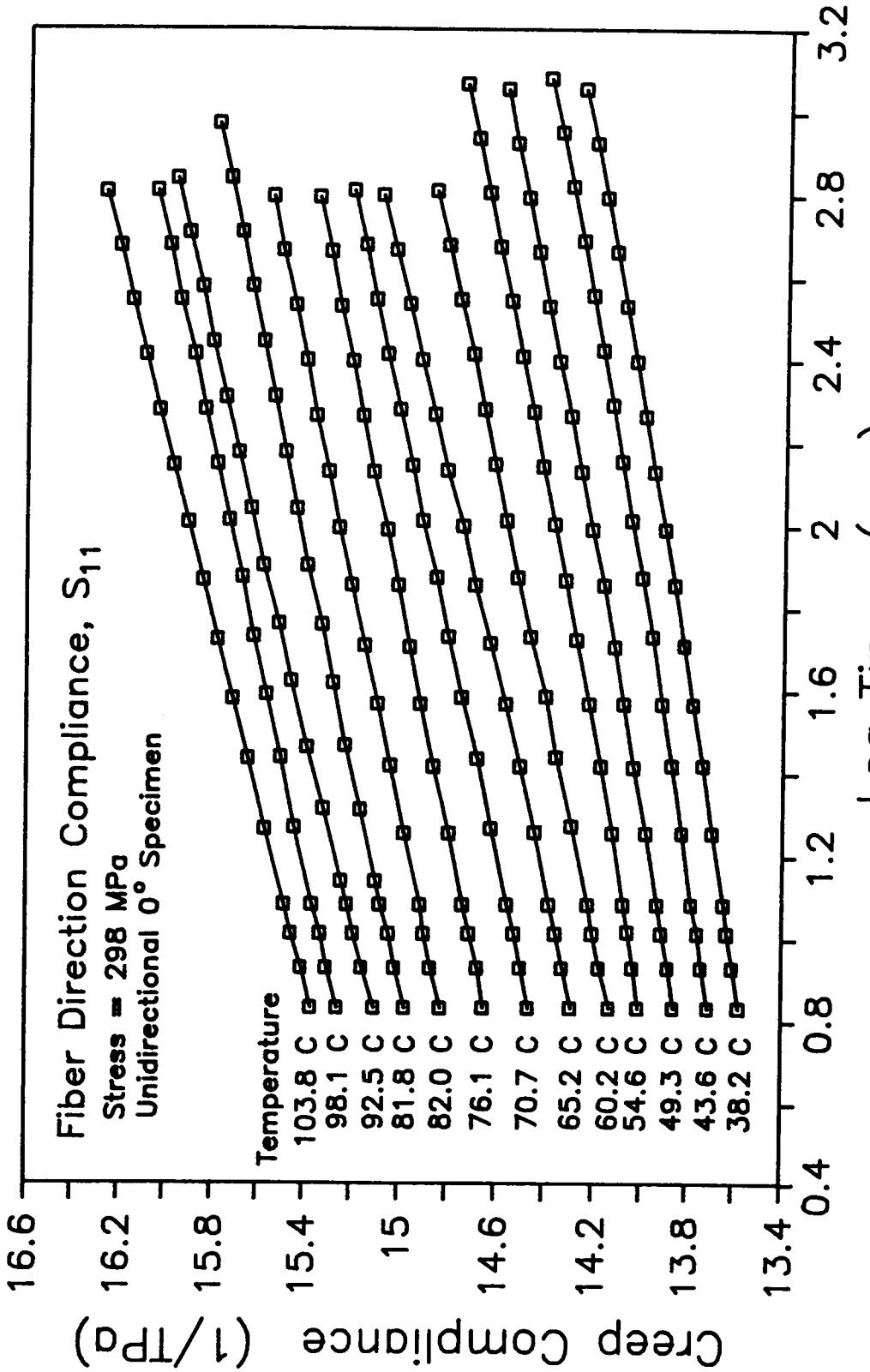

Fig. 5.2 Fiber Direction Compliance for Constant Stress (298 MPa) at Various Temperatures.

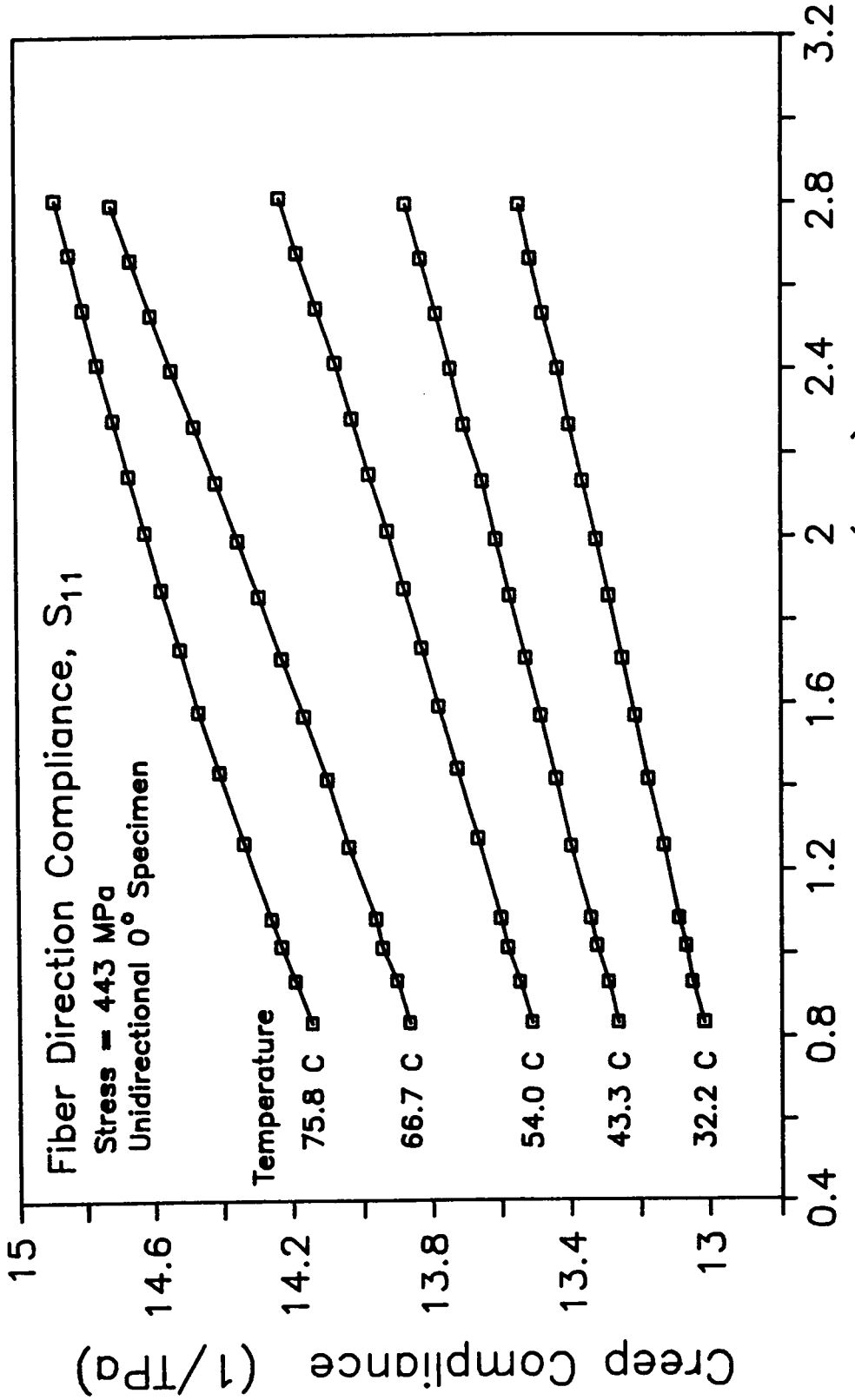

Fig. 5.3 Fiber Direction Compliance for Constant Stress (443 MPa) at Various Temperatures.

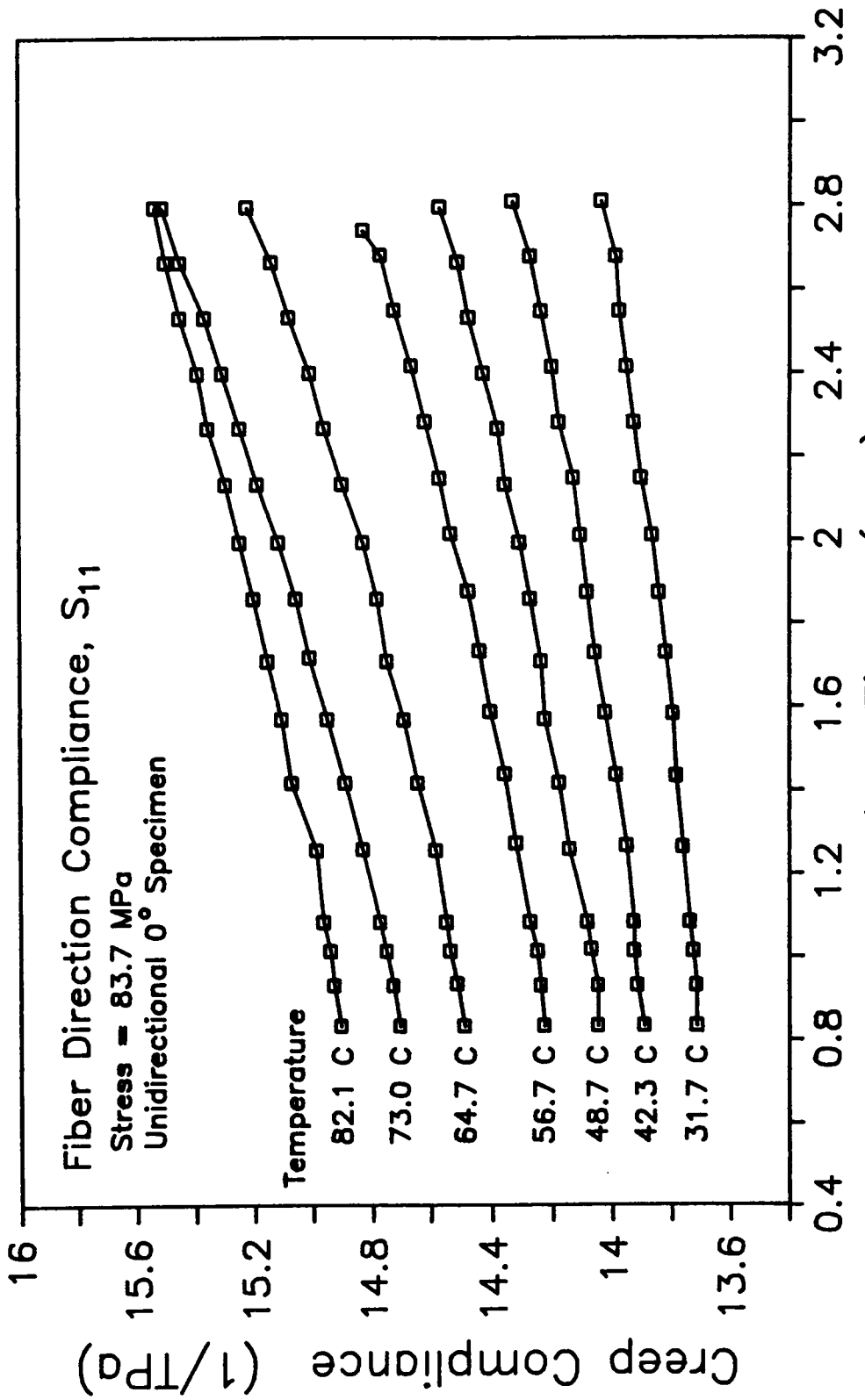

Fig. 5.4 Fiber Direction Compliance for Constant Stress (84 MPa) at Various Temperatures.

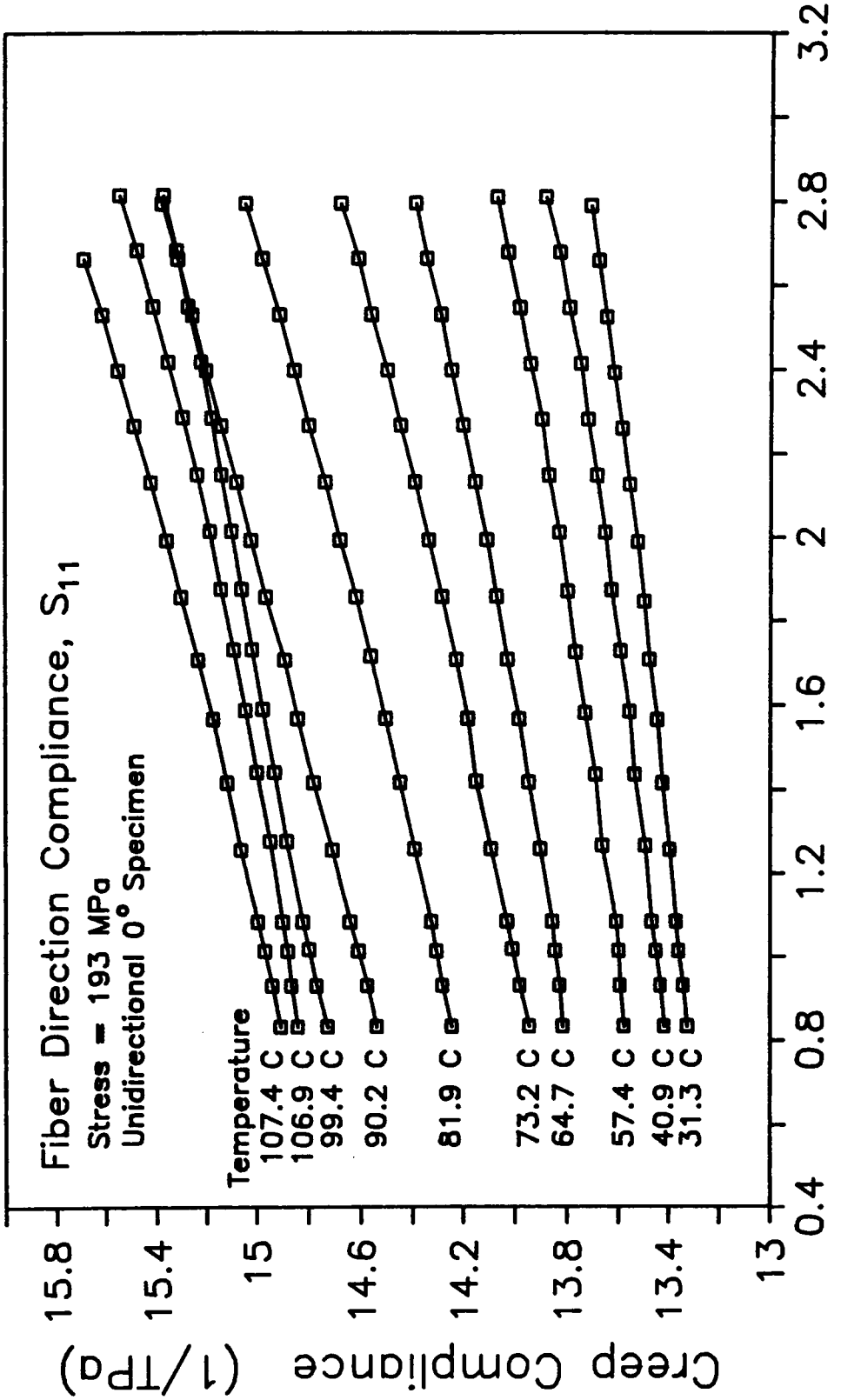

Fig. 5.5 Fiber Direction Compliance for Constant Stress (193 MPa) at Various Temperatures.

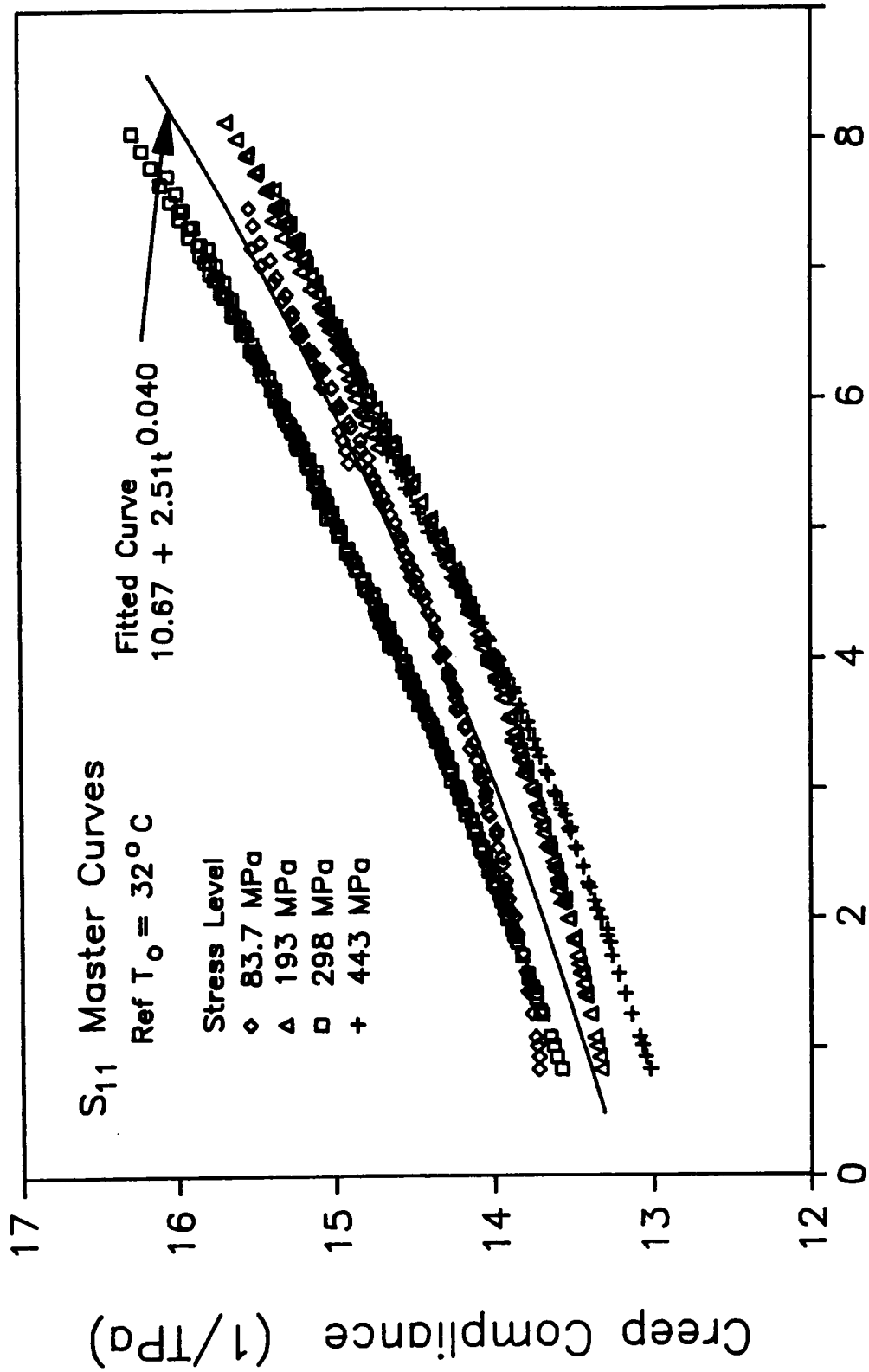

Fig. 5.6 Fiber Direction Compliance Master Curves.

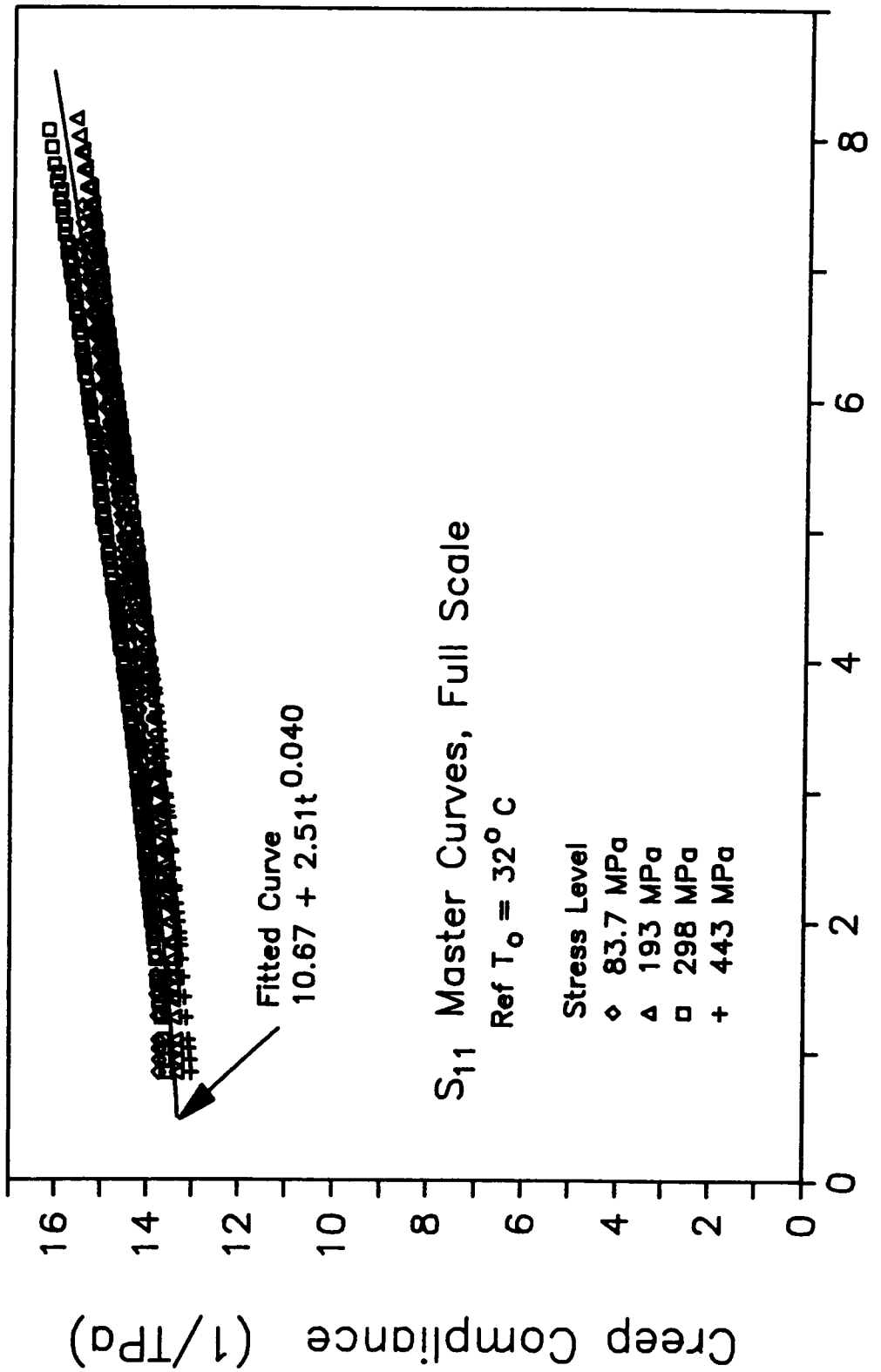

Fig. 5.7 Fiber Direction Compliance Master Curves (Full View).

same as for S_{11}, 83.7, 193, 298, and 443 MPa, as were the temperature increments. The individual creep curves are shown in Figs. 5.8-5.11 for each stress level.

Similar to the S_{11} compliance, the master curves were constructed by using 'ACS' which are shown in Figs. 5.12 and 5.13. The master curve, by definition, is negative and continues to decrease with increasing time. For the first six decades of time the master curve is smooth and continuous but then starts to vary slightly. Although the reason for this is not fully understood it could in part be due to the difficulty to obtaining the S_{12} compliance term. To calculate S_{12}, the strain in the transverse direction of a 0° unidirectional test specimen must be measured when loaded in the fiber direction. This requires a very high load in the fiber direction to detect any strain change in the transverse direction.

The individual creep test results for the transverse direction compliance, S_{22}, are shown in Figs. 5.14-5.17 for load levels of 1.43, 3.51, 5.30, and 7.47 MPa. These curves were shifted to construct the master curves shown in Fig. 5.18. The compliance in the transverse direction, S_{22}, for the master curves is more in the form of a power law than the previous two compliance terms. Only the two lower stress levels, 1.43 and 3.51 MPa, are distinctly visible through the entire spectrum of the viscoelastic response. The remaining two specimens, at higher stress levels, failed prior to reaching the tenth decade of time but they match the lower two stress levels up to the failure point. The compliance master curves at 1.43 and 3.51 MPa indicates a

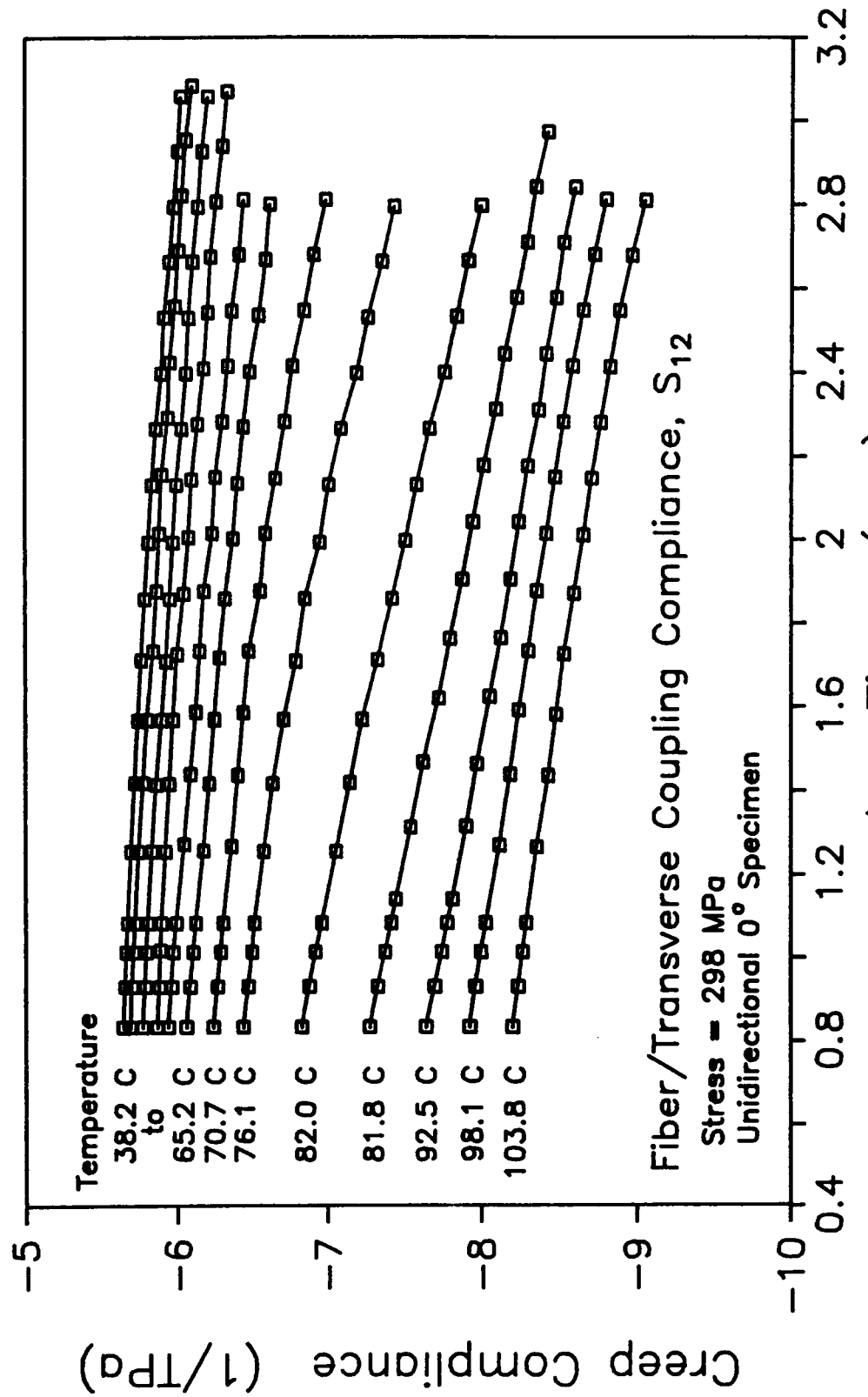

Fig. 5.8 Fiber/Transverse Coupling Compliance for Constant Stress (298 MPa) at Various Temperatures.

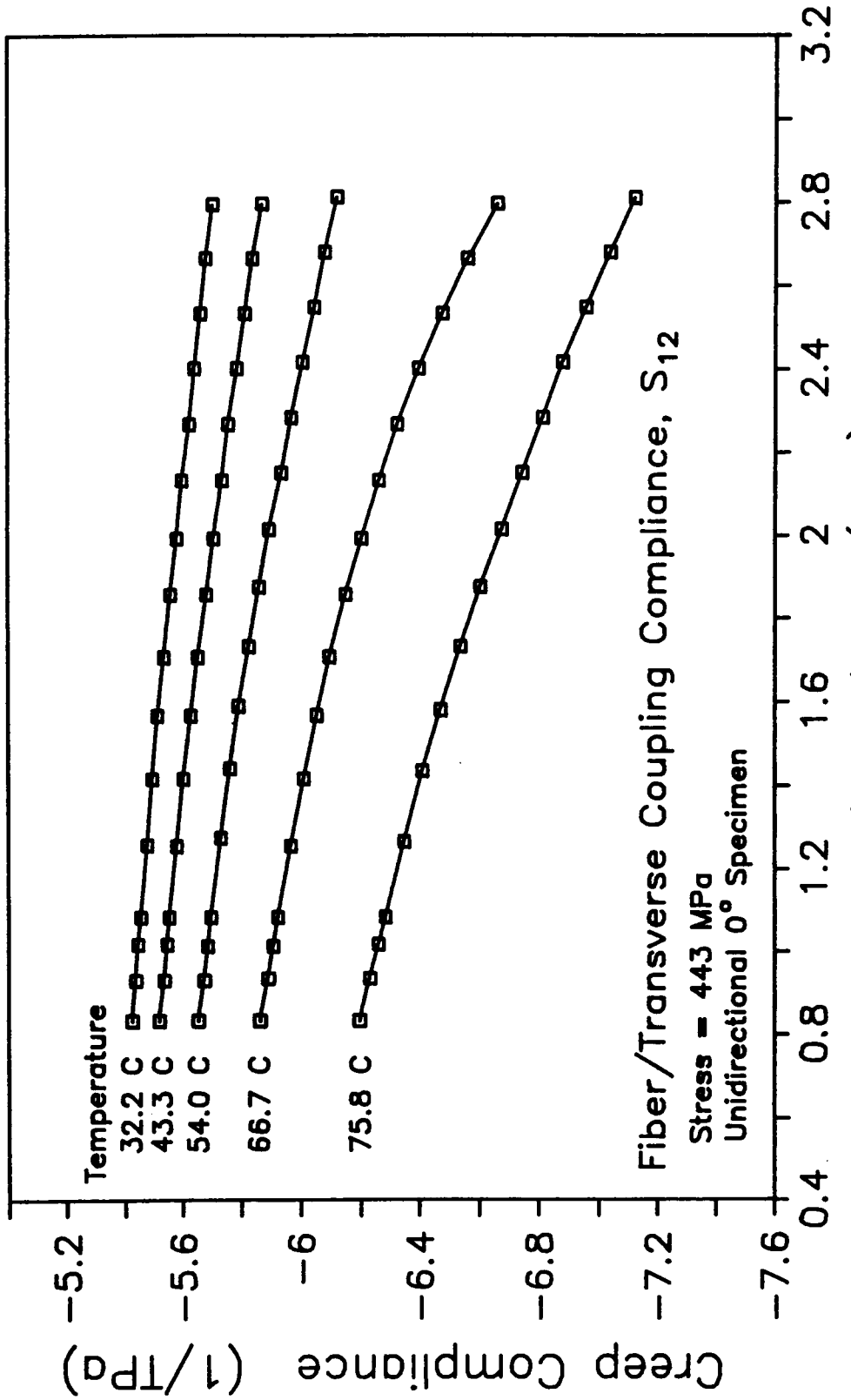

Fig. 5.9 Fiber/Transverse Coupling Compliance for Constant Stress (443 MPa) at Various Temperatures.

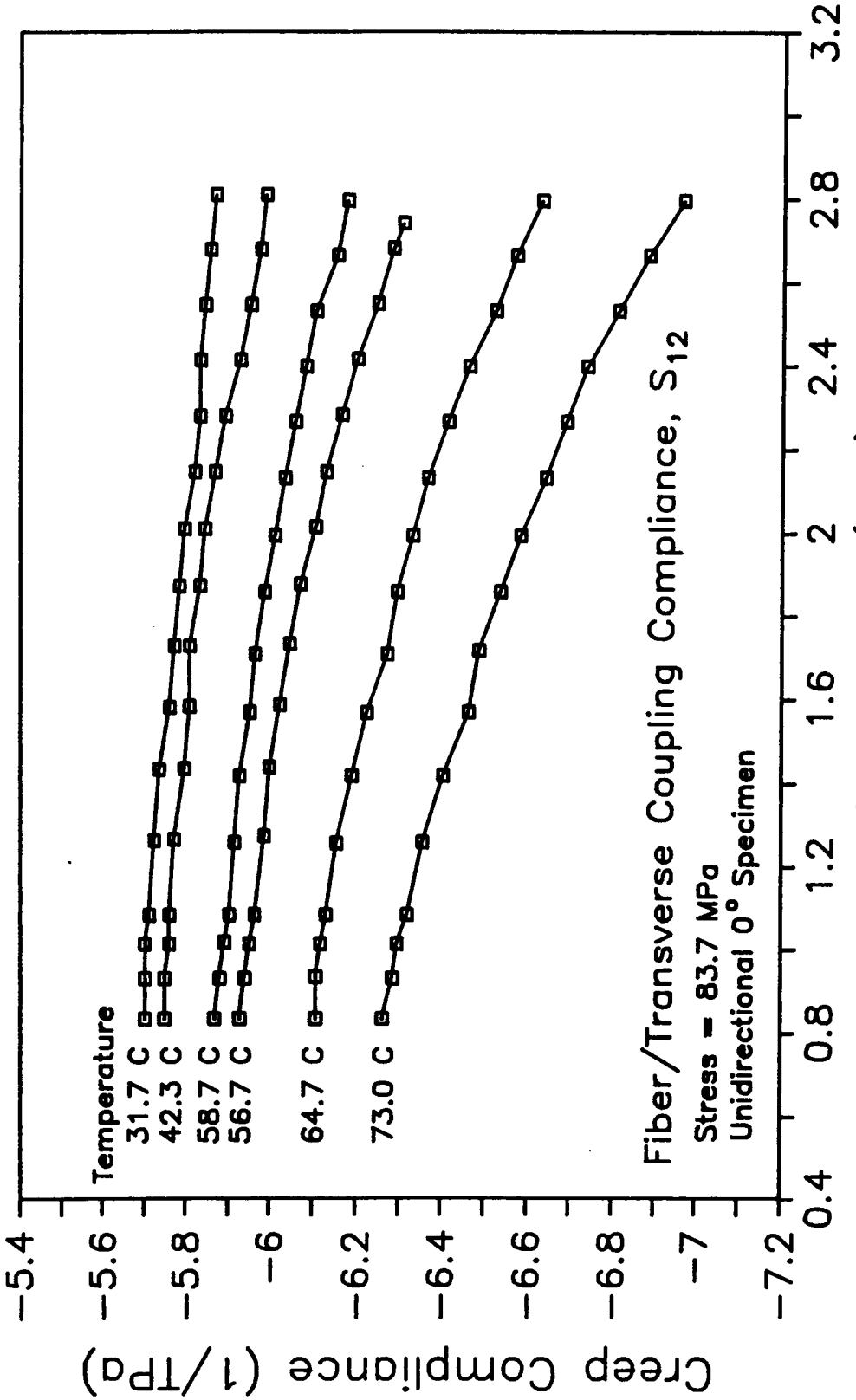

Fig. 5.10 Fiber/Transverse Coupling Compliance for Constant Stress (84 MPa) at Various Temperatures.

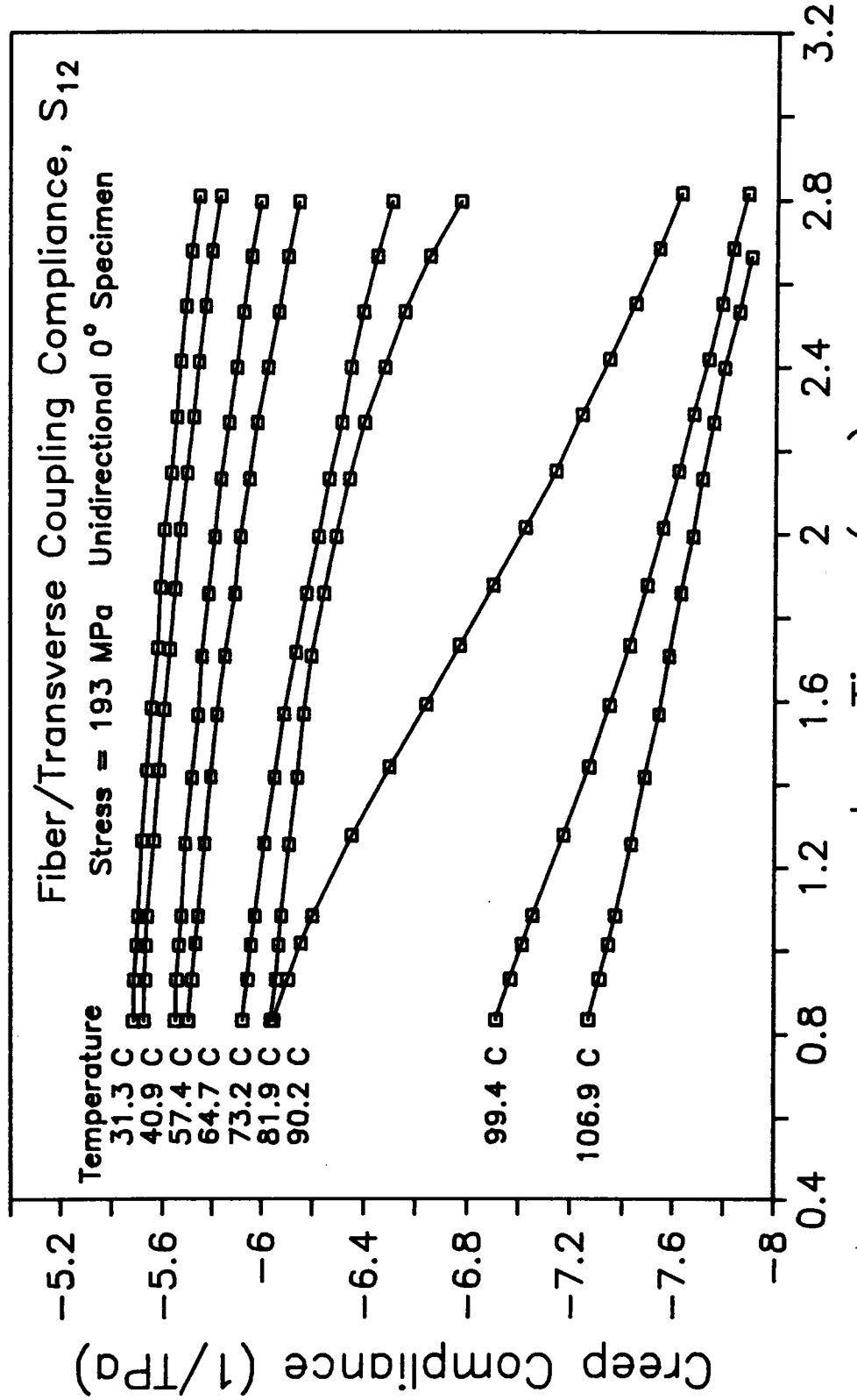

Fig. 5.11 Fiber/Transverse Coupling Compliance for Constant Stress (193 MPa) at Various Temperatures.

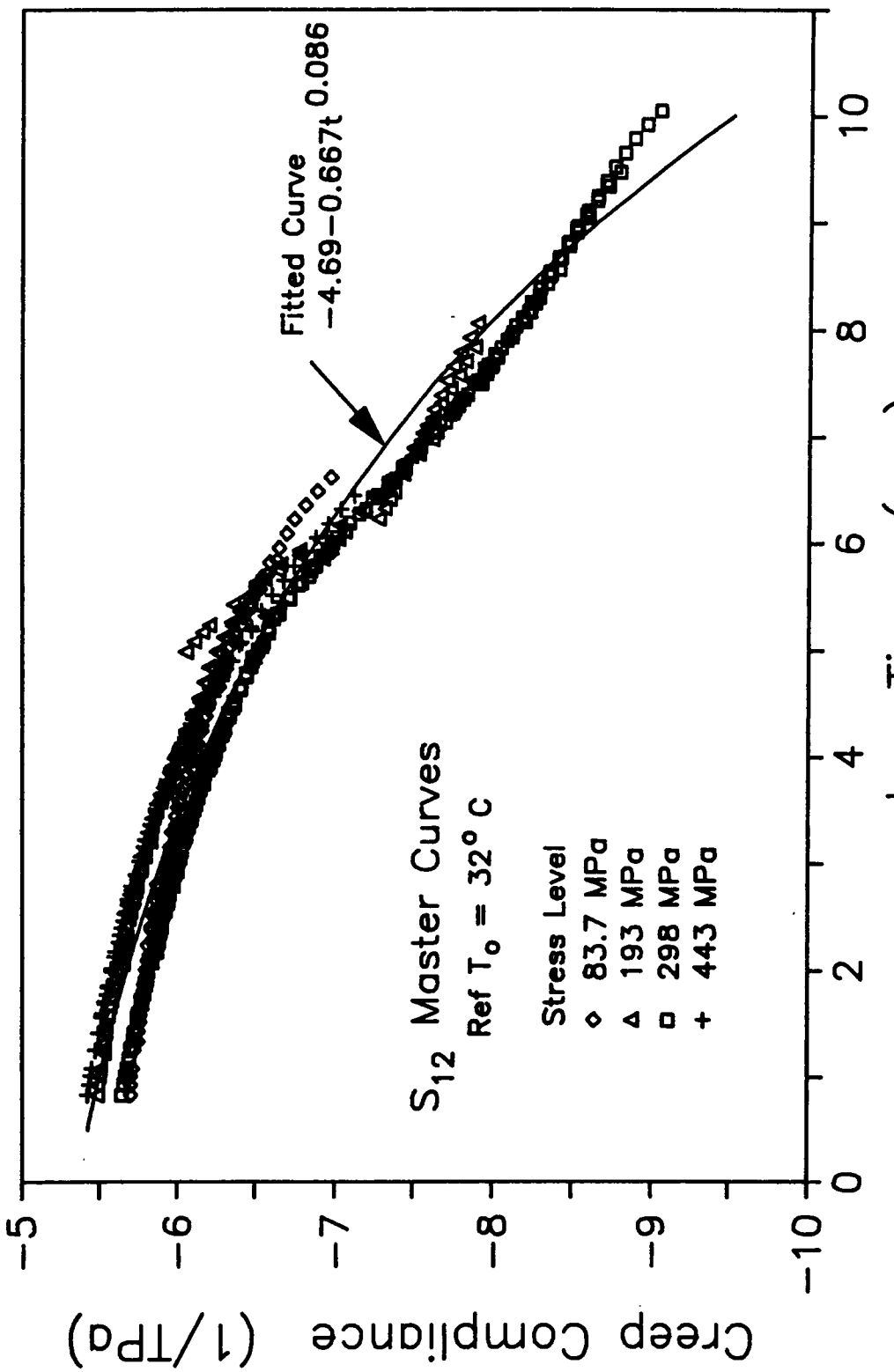

Fig. 5.12 Fiber/Transverse Coupling Compliance Master Curves.

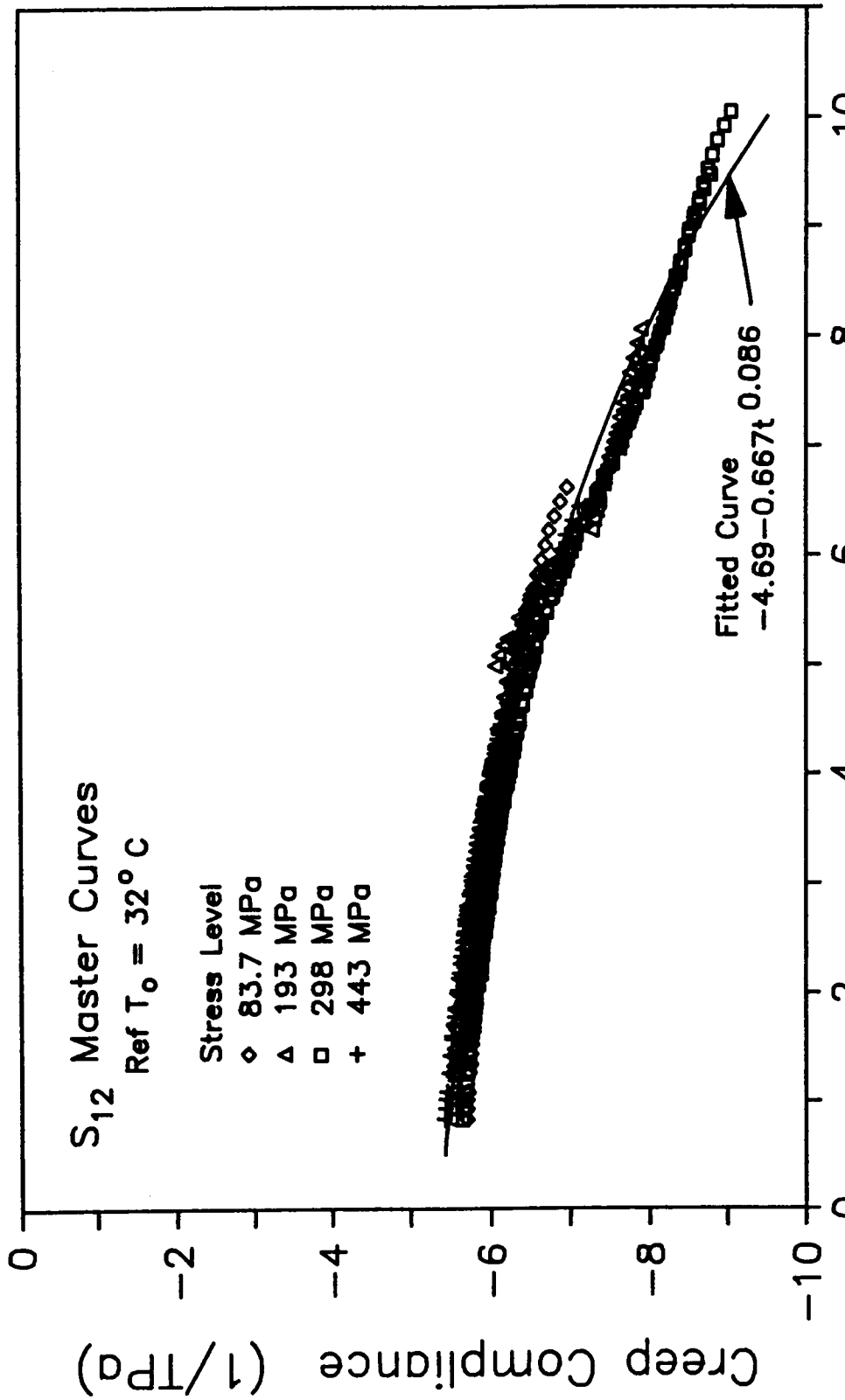

Fig. 5.13 Fiber/Transverse Coupling Compliance Master Curves (Full View).

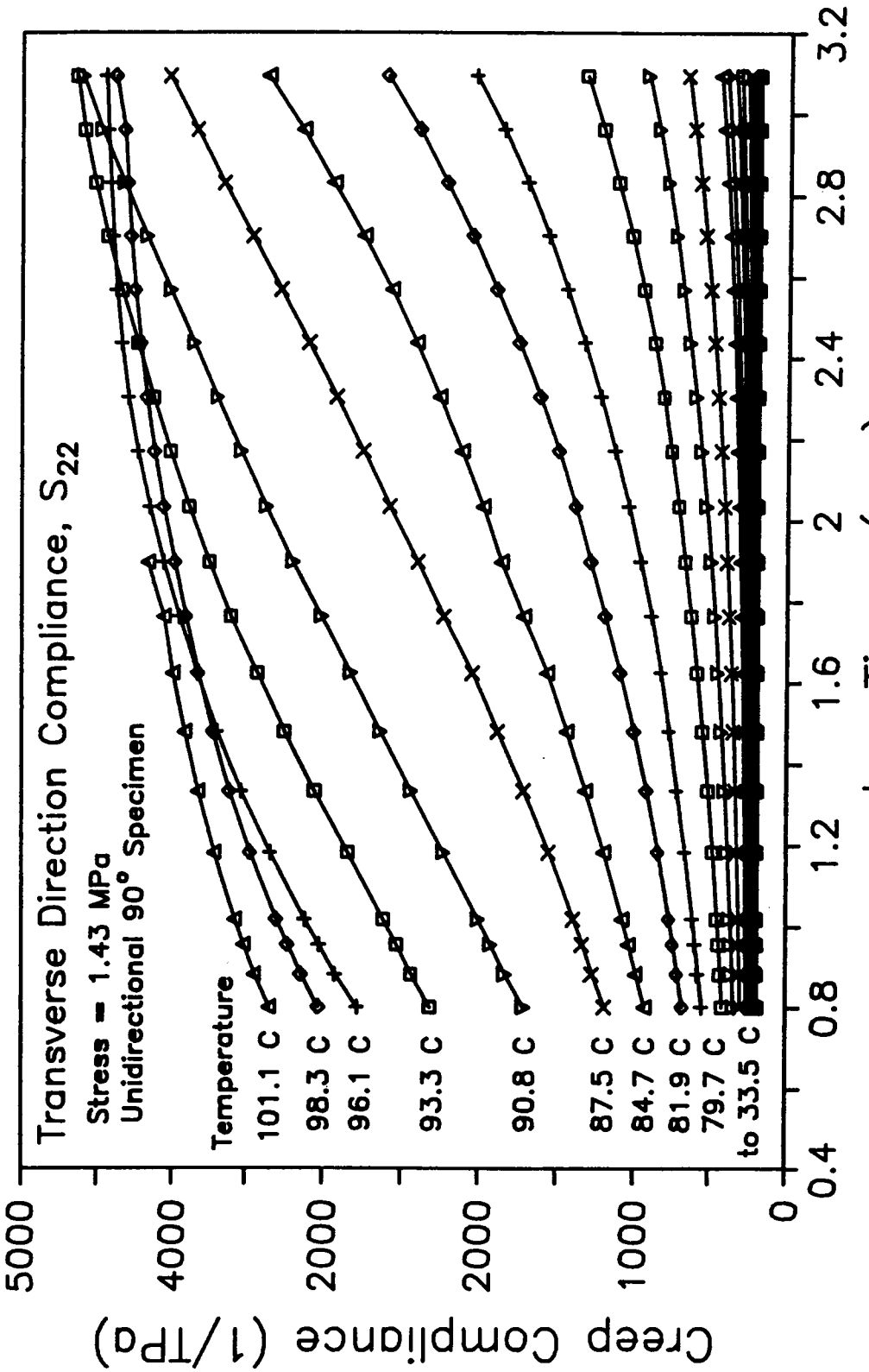

Fig. 5.14 Transverse Compliance for Constant Stress (1.43 MPa) at Various Temperatures.

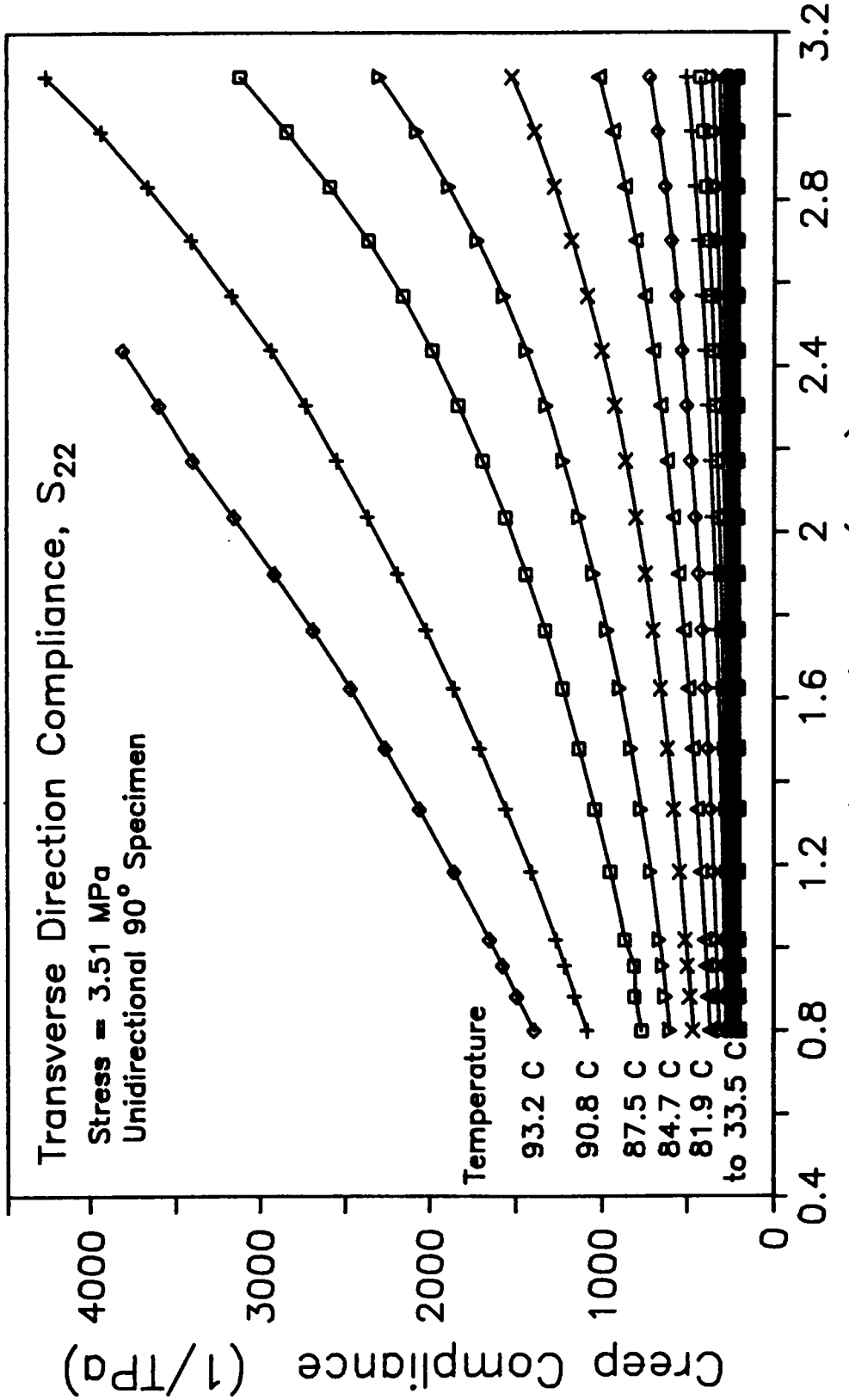

Fig. 5.15 Transverse Compliance for Constant Stress (3.51 MPa) at Various Temperatures.

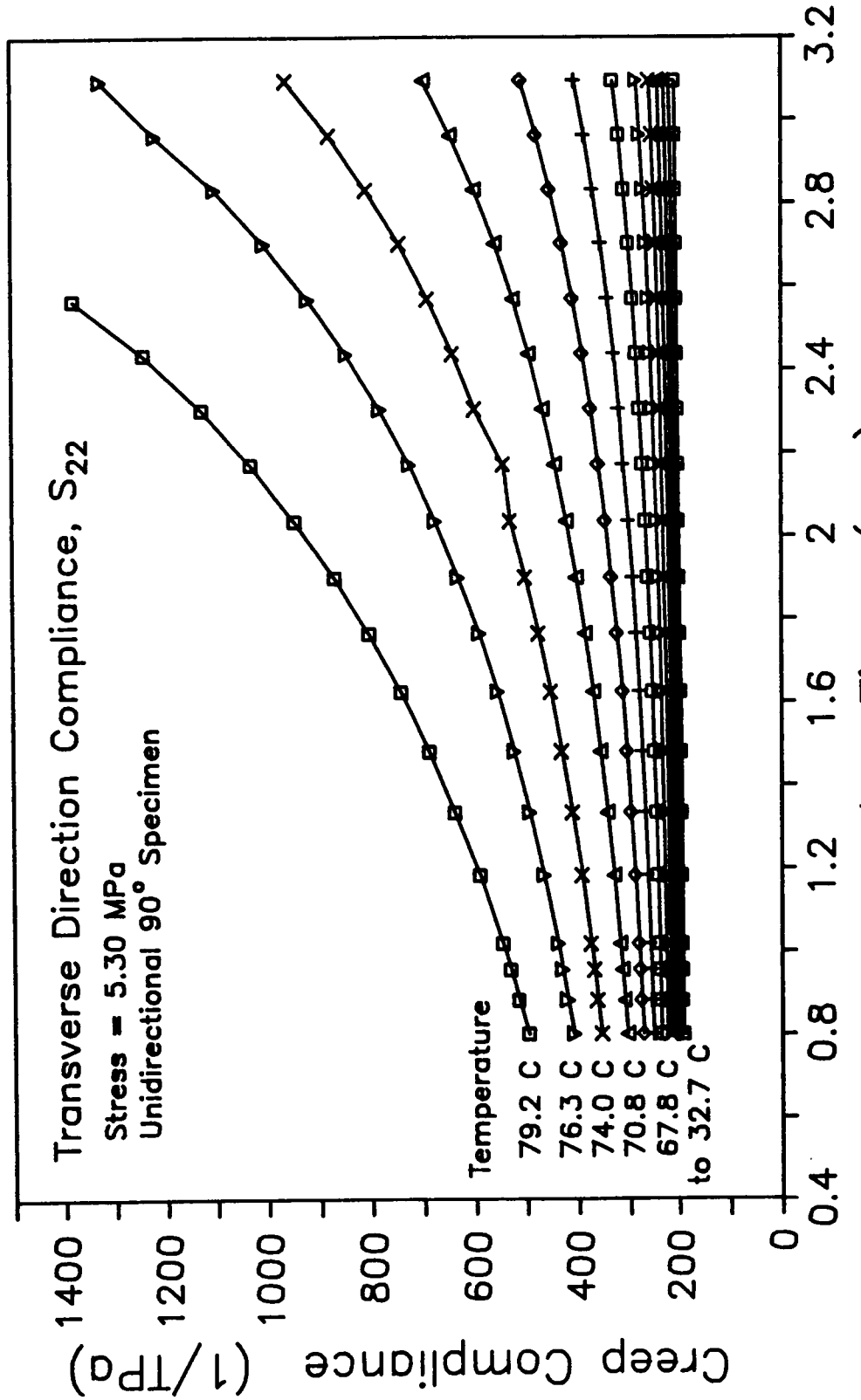

Fig. 5.16 Transverse Compliance for Constant Stress (5.30 MPa) at Various Temperatures.

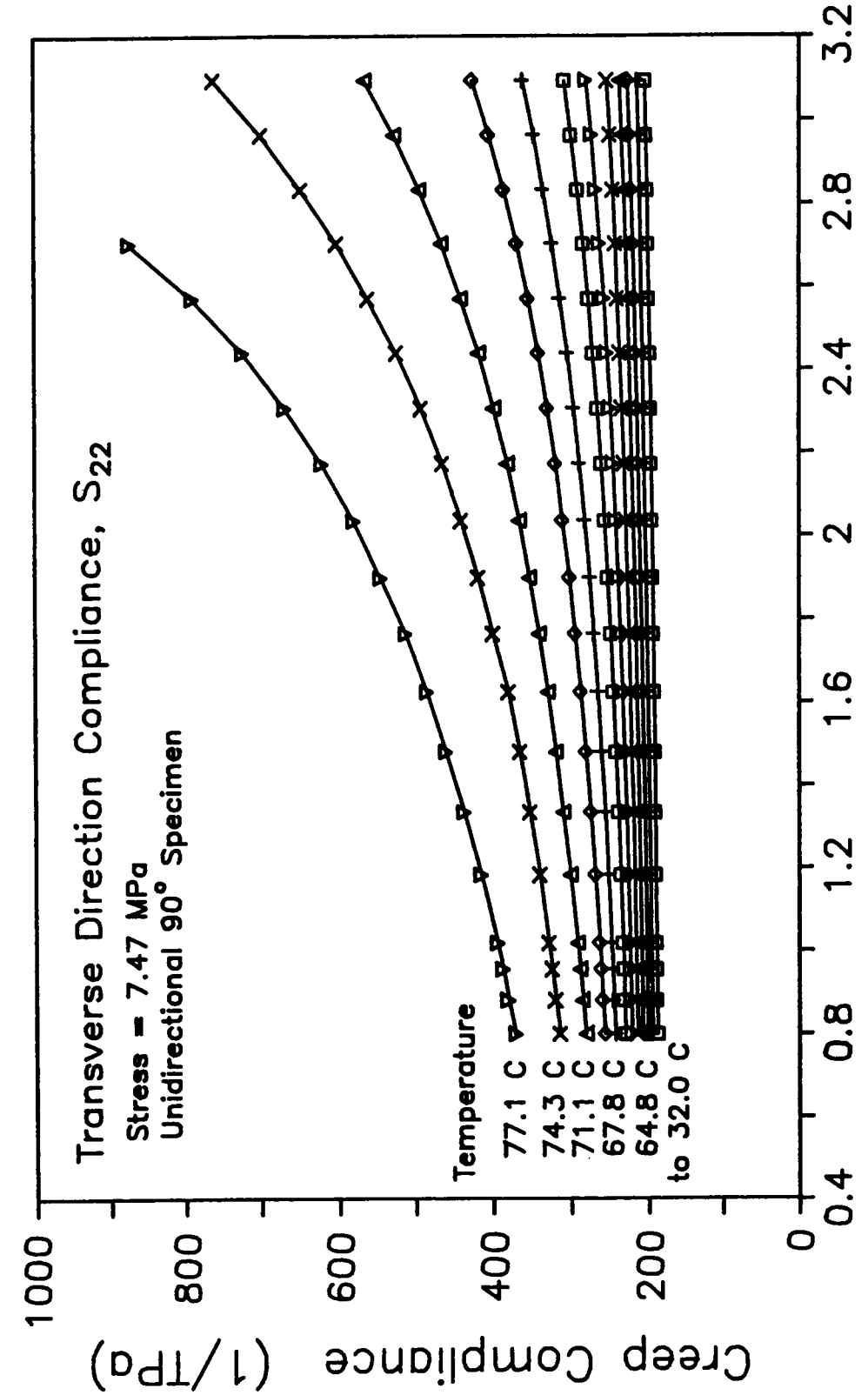

Fig. 5.17 Transverse Compliance for Constant Stress (7.47 MPa) at Various Temperatures.

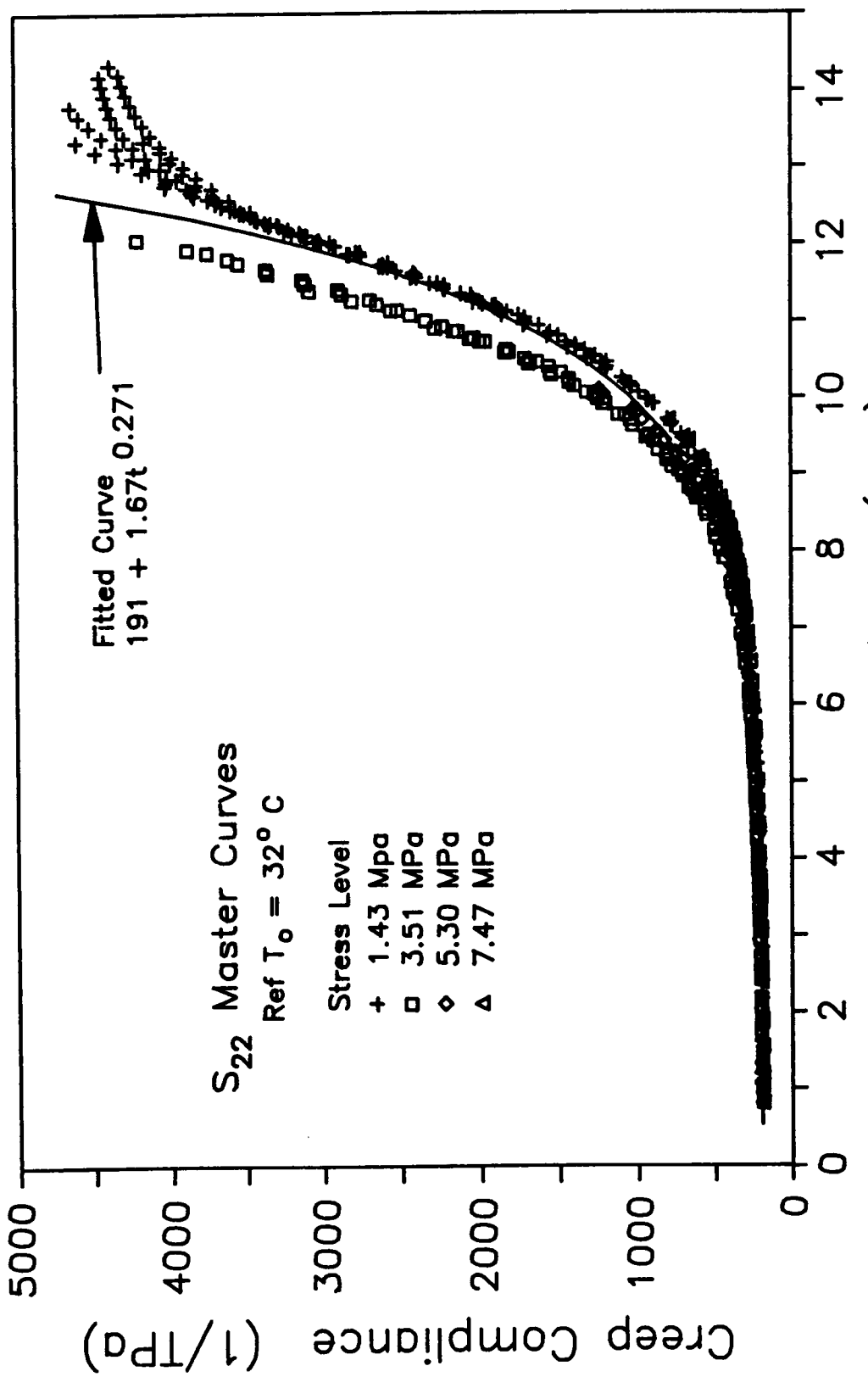

Fig. 5.18 Transverse Direction Compliance Master Curves.

nonlinear stress effect, but the 5.30 and 7.47 MPa stress levels do not continue the same trend. One possible reason for the difference between compliance curves is that different specimens were used for each stress level which can cause scatter. Later, a single specimen will be tested at different stress level with the temperature held constant, to identify the nonlinear stress effect.

A unique characteristic of the S_{22} term, not evident in the other compliance terms, is the leveling off of the compliance at long times. This conforms to the physical properties of most polymer based materials where they exhibit distinct glassy and rubbery plateaus where the compliance remains fairly constant over time. Since there was no vertical shifting done, the plateau effect seems to exhibit some scatter but the effect of entering into the rubbery region is evident. The characteristic in the rubbery region could not be investigated further due to specimens failing at the high temperatures ($\approx 100^{\circ}$ C). Another possible cause of the leveling off of the compliance is the adhesive used to adhere the strain gages could be creeping. The high temperature, 101.3° C, is the upper limit for the recommended temperature range.

The 10° unidirectional off-axis specimens used to calculate the shear compliance, S_{66}, were tested at three stress levels, 41.2, 112, and 148 MPa (global coordinate system). These short term tests are shown in Figs. 5.19-5.21. The associated master curves are shown in Fig. 5.22. The master curve is also of the power law shape and is continuous. The higher two stress level specimens failed at lower

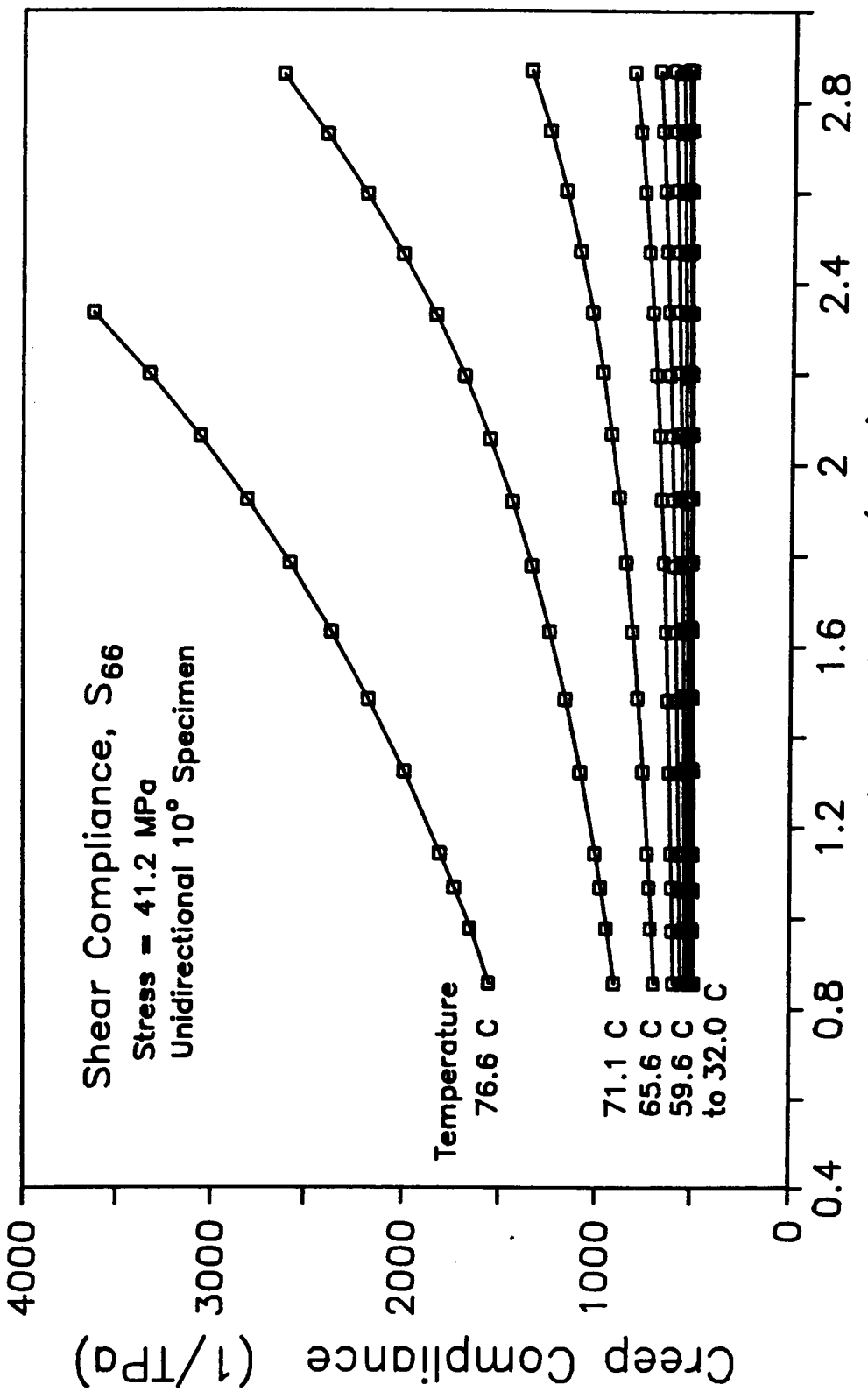

Fig. 5.19 Shear Compliance for Constant Stress (41.2 MPa) at Various Temperatures.

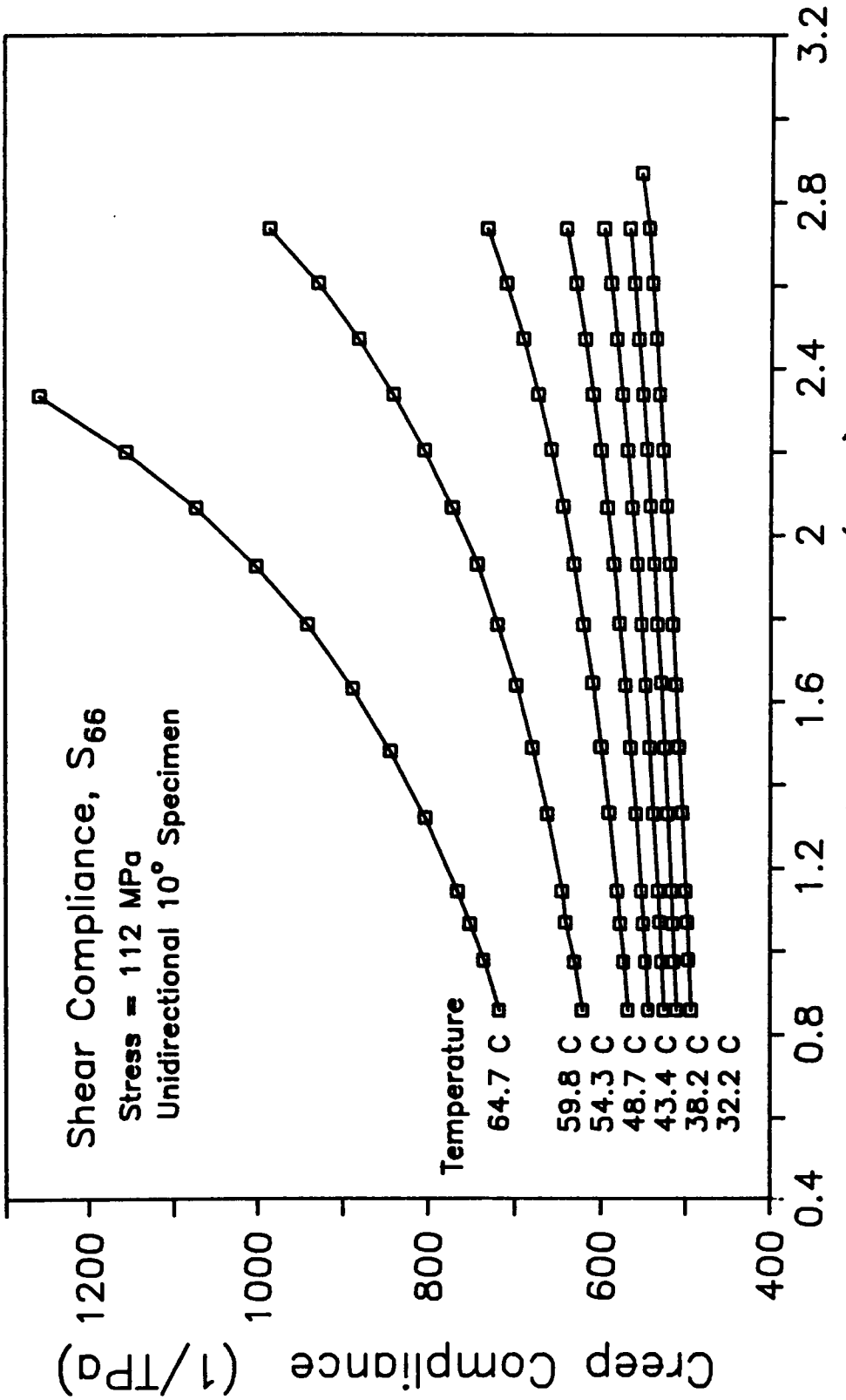

Fig. 5.20 Shear Compliance for Constant Stress (112 MPa) at Various Temperatures.

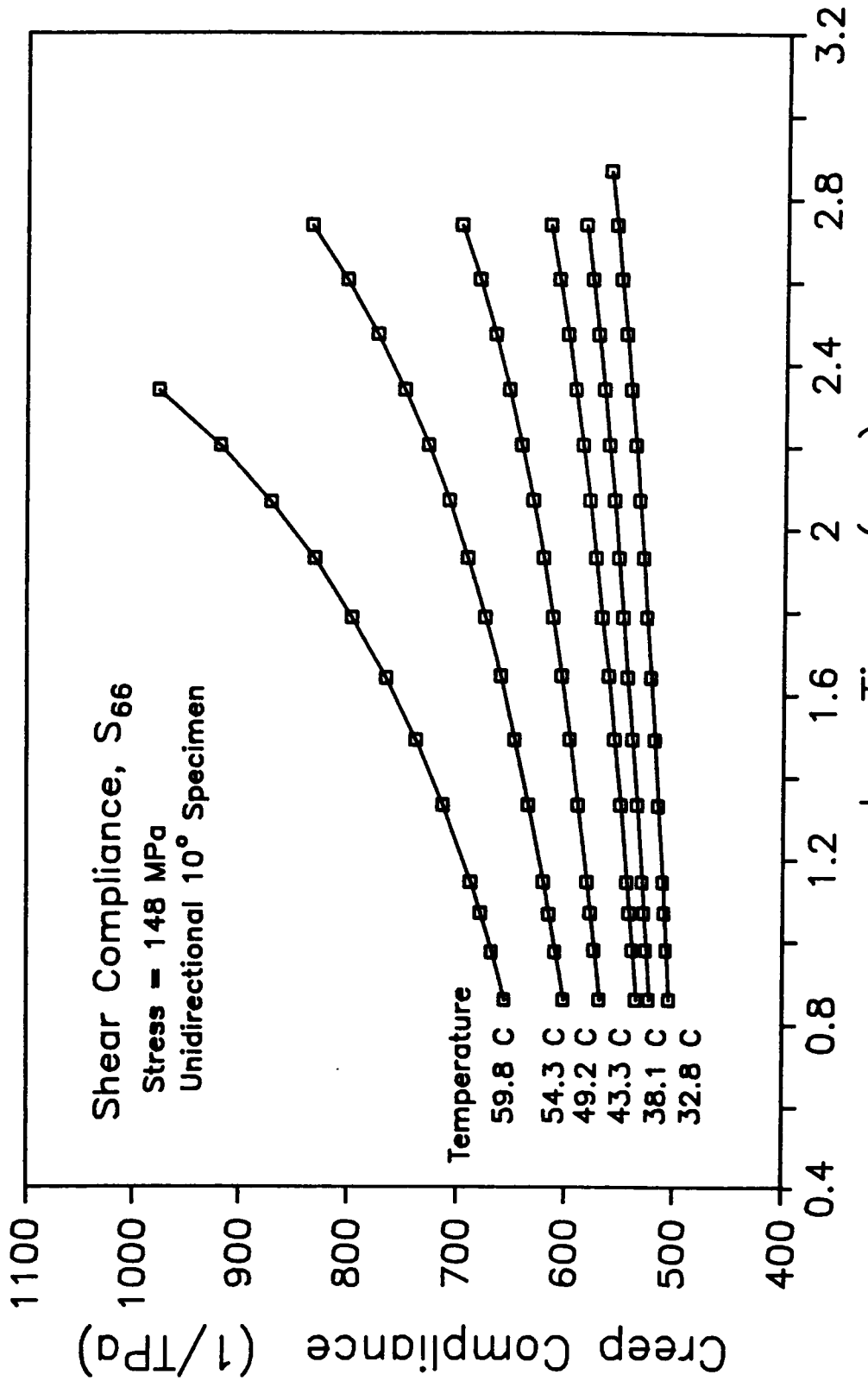

Fig. 5.21 Shear Compliance for Constant Stress (148 MPa) at Various Temperatures.

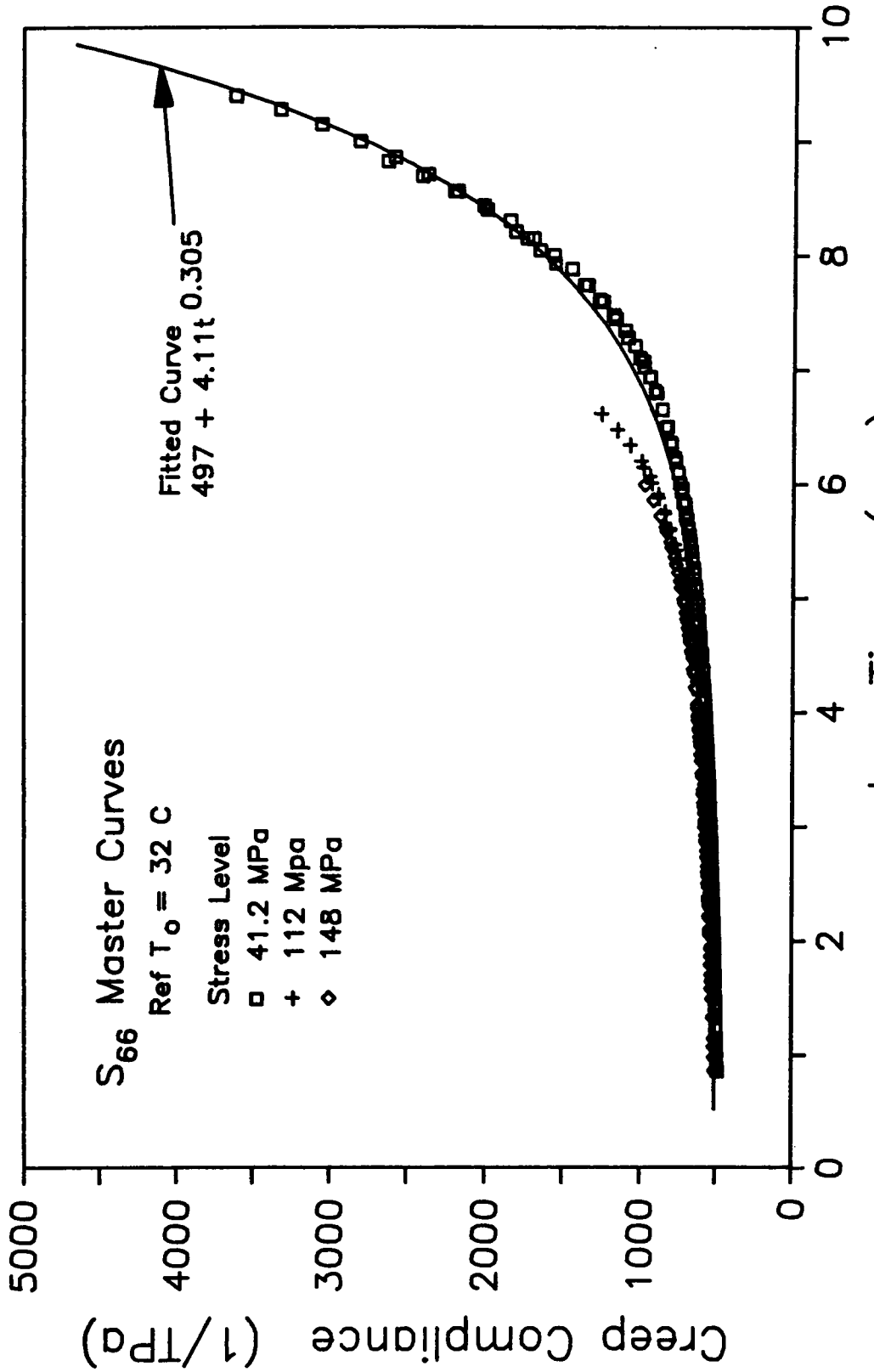

Fig. 5.22 Shear Compliance Master Curves.

compliances and do not show up well. These three master curves show the possibility of nonlinear stress effects, which up to this point has not been evident. The nonlinear stress effects will be discussed later.

Shift Factor Function

The temperature shift factors that were calculated by the 'ACS' program are plotted verses temperature in Figs. 5.23-5.26 for all tested stress levels. These factors tend to follow a linear relationship which is also drawn in the figures. Shift factor functions that are commonly used are the WLF (Williams-Landel-Ferry) equation for temperatures between Tg and 100° C above Tg and the Arrhenius equation for temperatures below Tg. While either the WLF or Arrhenius equation could have been used, the empirical linear equation seems to model the shift factor well and is easily used in a numerical procedure (see chapter 3).

The linear shift function for each of the directions, were calculated using a least-squares fit giving

$$\text{Log } a_{T_{11}} = 2.333 - 0.080\ T \qquad (5.2a)$$

$$\text{Log } a_{T_{12}} = 3.567 - 0.100\ T \qquad (5.2b)$$

$$\text{Log } a_{T_{22}} = 5.549 - 0.164\ T \qquad (5.2c)$$

$$\text{Log } a_{T_{66}} = 5.217 - 0.151\ T \qquad (5.2d)$$

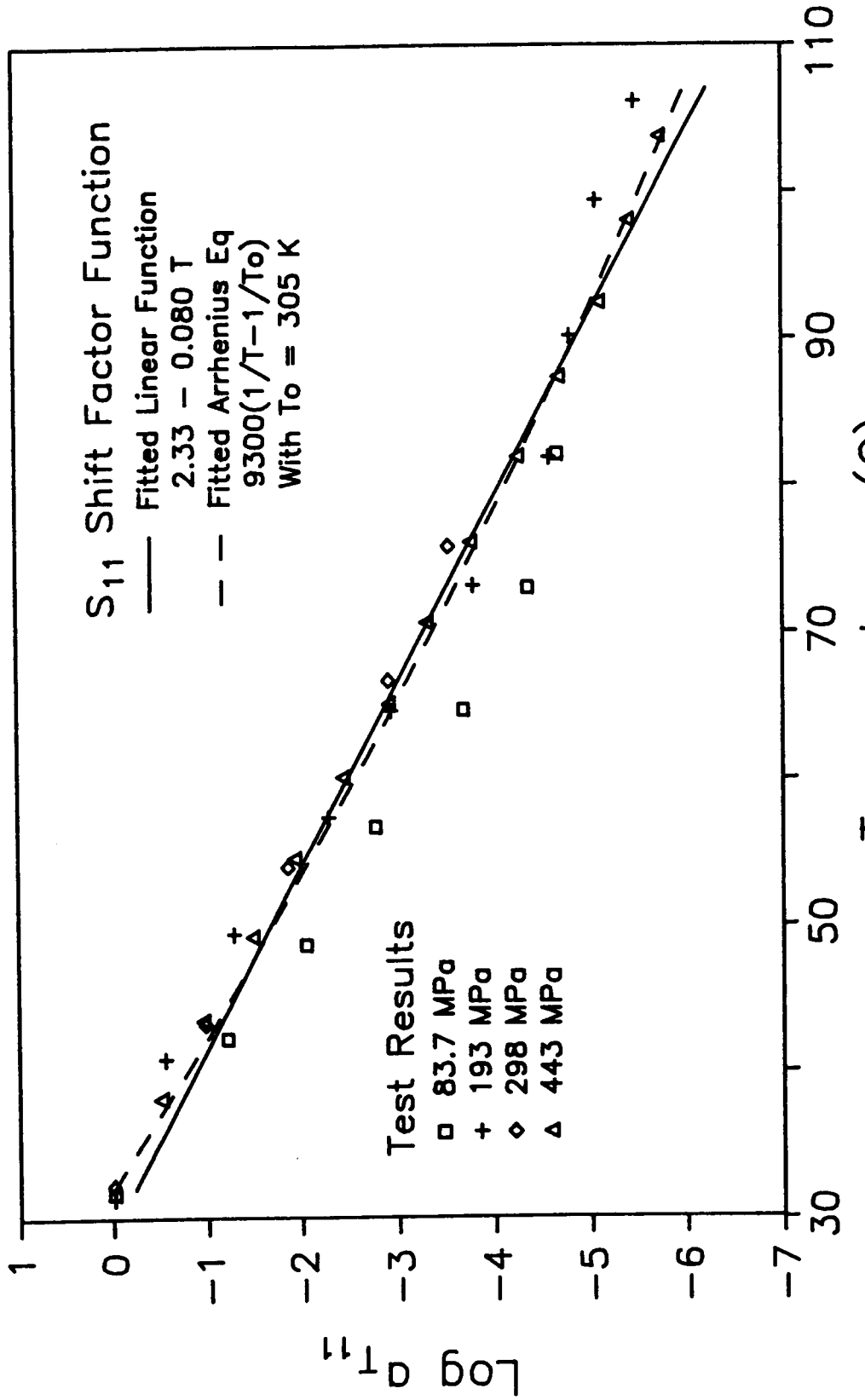

Fig. 5.23 Fiber Direction Shift Factor Function.

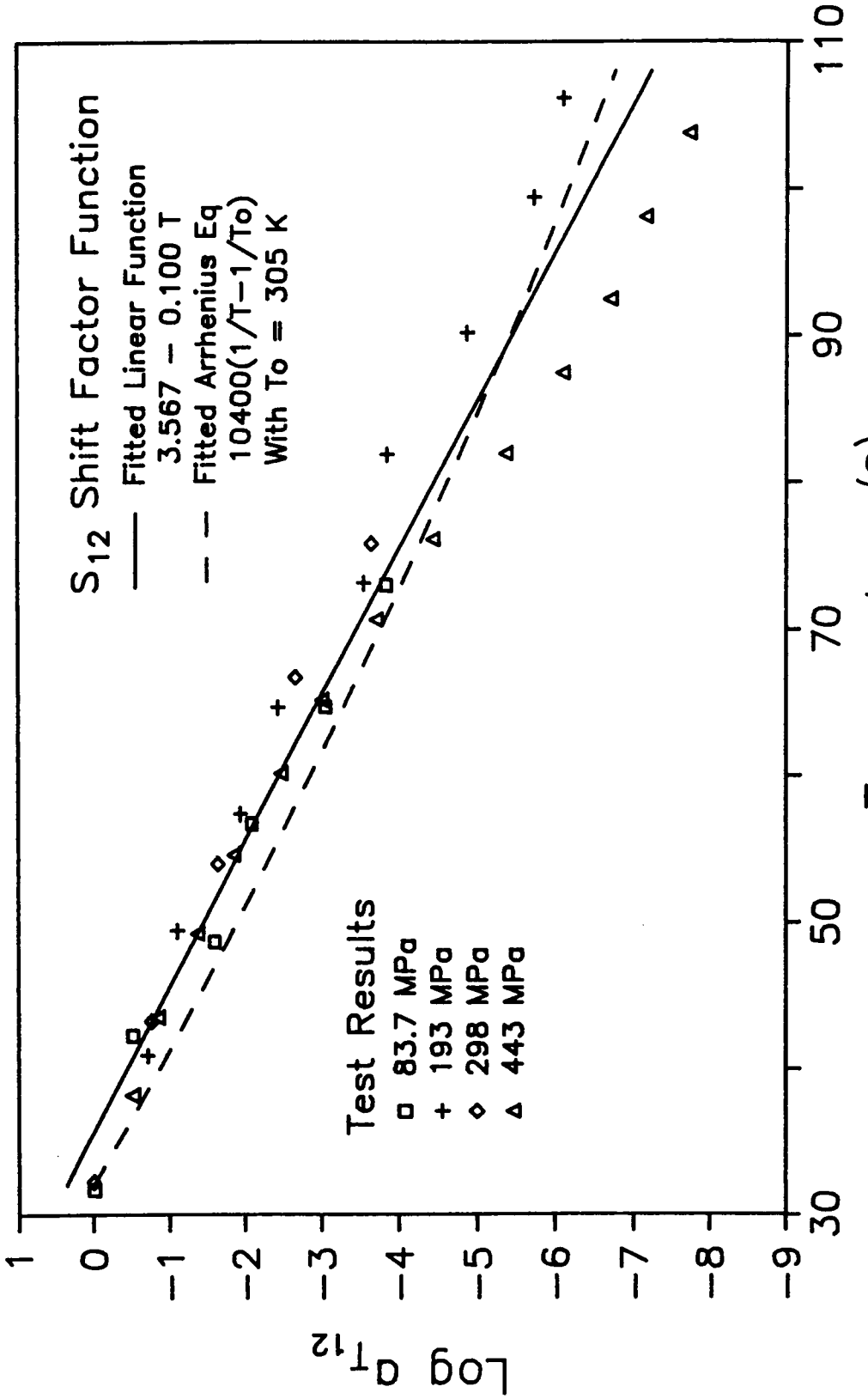

Fig. 5.24 Fiber/Transverse Coupling Shift Factor Function.

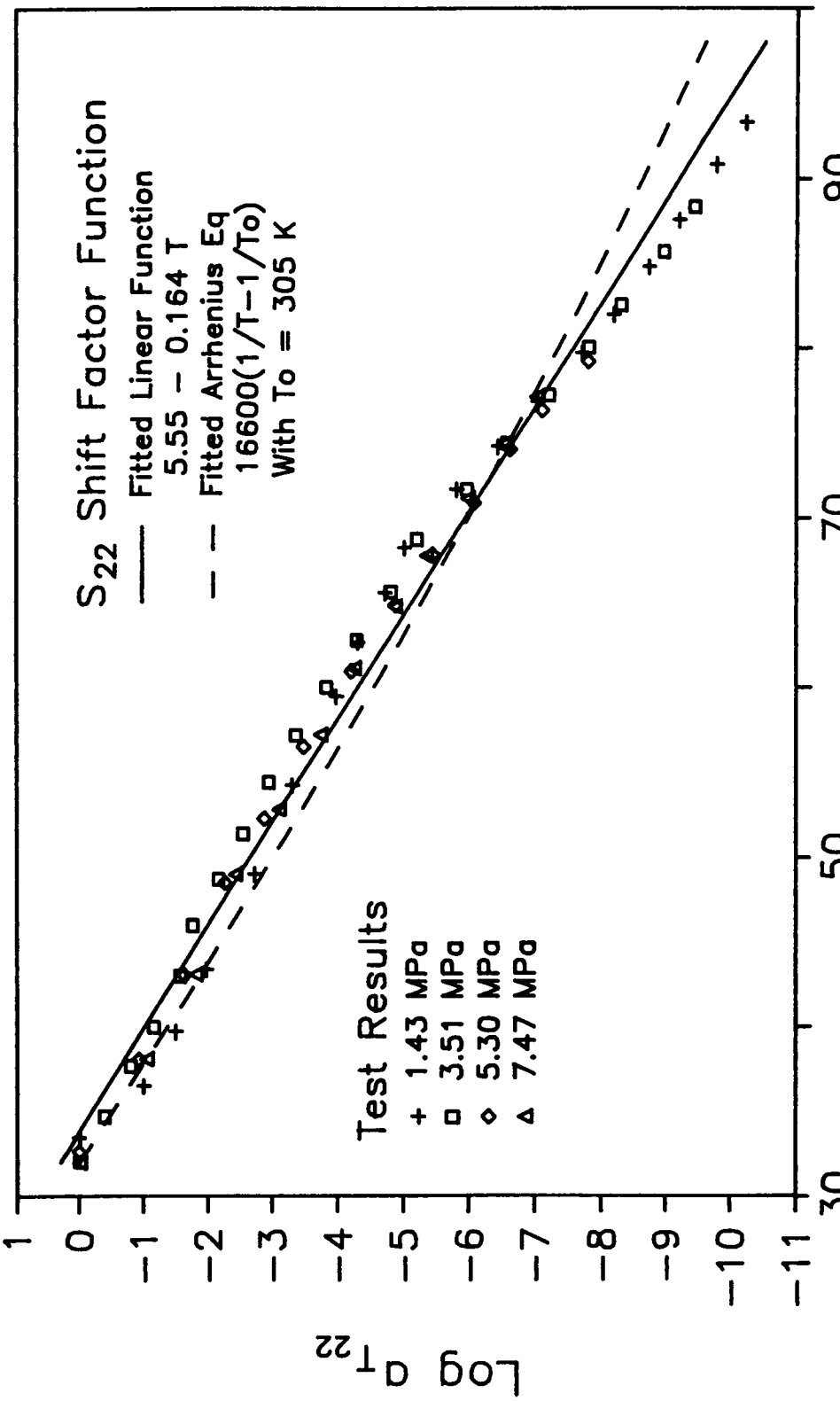

Fig. 5.25 Transverse Direction Shift Factor Function.

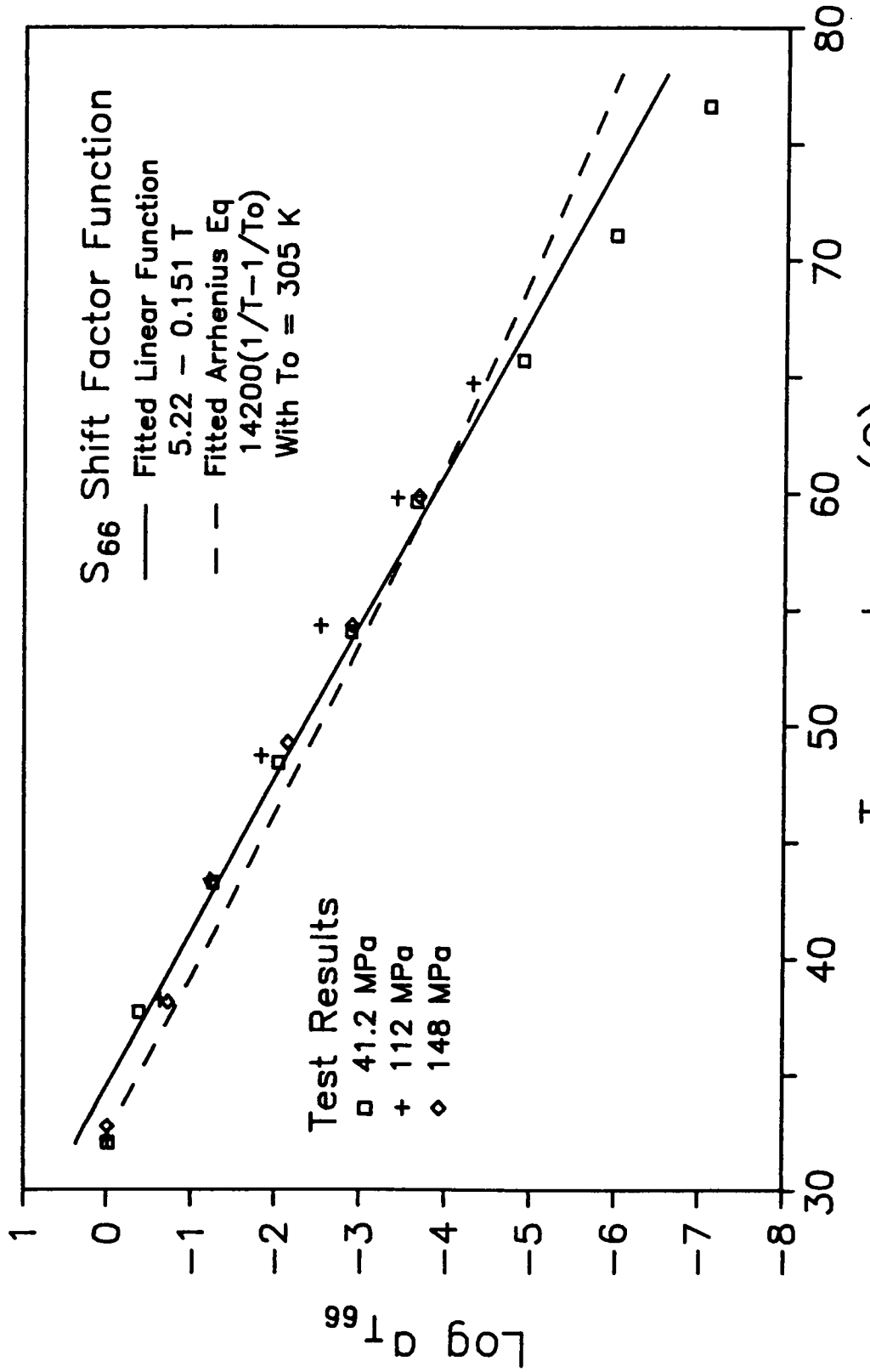

Fig. 5.26 Shear Shift Factor Function.

where T is temperature Celsius and $a_{T_{ij}}$ is the shift factor. The reference temperature, T_o, for all four compliance terms is 32° C. Ideally there should be two independent shift factor functions (SFF) for a FRP composite, one for the fiber material and one for the resin. The transverse direction and shear SFF, both resin dominated, are indeed similar and are within error limits of the experimental data. However, the fiber and coupling direction SFF are notably different which may be due to the difficulty in measuring the S_{12} compliance.

The Arrhenius equation was also calculated for each of the material properties and is shown in the respective figures (Figs. 5.23-5.26). The activation energy for each of the four material are 42.5, 47.4, 75.8, 64.9 kcal/mole-K for S_{11}, S_{12}, S_{22}, and S_{66}, respectively. Both the S_{11} and S_{12} shift factor functions are similar which is expected since they are both fiber dominated. The S_{22} and S_{66} are also similar which is expected since they are both resin dominated. The activation energy for the epoxy for reaction rate and curing is generally between 15 and 25 kcal/mole-K [116] which is significantly lower than the value obtained from applying the TTSP. One point to remember however, is that activation mechanism for curing and creep is different. The resin is more thermally sensitive than the fibers and thus the activation energy for creep is also higher than for the Kevlar fiber dominated compliances, S_{11} and S_{12}.

Modeling the Linear Viscoelastic Response

Each of the four master curves were modeled by a power law of the

form

$$S = S_o + mt^n \tag{5.3}$$

were m and n are the power law constants and S_o is the instantaneous compliance. This form was chosen for simplicity and ease of use in a numerical solution process. If nonlinear stress effects arise, S_o and m can be modeled as functions of stress. It is generally assumed that the exponent n is constant.

For linear viscoelastic compliance, the following curves were the best fit of the experimental master curves.

$$S_{11} = \left(10.677 + 2.515\ t^{0.040} \right) \text{TPa}^{-1} \tag{5.4a}$$

$$S_{12} = \left(-4.686 - 0.667\ t^{0.086} \right) \text{TPa}^{-1} \tag{5.4b}$$

$$S_{22} = \left(191.3 + 1.668\ t^{0.271} \right) \text{TPa}^{-1} \tag{5.4c}$$

$$S_{66} = \left(496.6 + 4.109\ t^{0.305} \right) \text{TPa}^{-1} \tag{5.4d}$$

where t is in seconds. These curves are plotted in Figs. 5.6, 5.7, 5.12, 5.13, 5.18, and 5.22 with the master curves to show the fit. For the S_{11}, S_{12} and S_{22} compliance terms, where the nonlinear stress effects are small, the modeled curve match well with the average of the master curves, where as the S_{66} compliance term, which has a stronger nonlinear stress effect, matches only the lowest stress

level. The nonlinear analysis will be presented in the next section to account for the nonlinear stress effects.

Nonlinear Viscoelastic Characterization

Although the master curves were constructed at three or four stress levels for each compliance term, they could not be used to determine the nonlinear stress effects since the scatter between each specimen was on the same order of magnitude as the nonlinear effects. The only exception to this was the shear compliance which had the high degree of stress nonlinearity. To reduce the scatter and better understand the nonlinear stress effects, additional tests become necessary where the temperature was held constant and the stress levels were varied on the same sample. It should be noted that a different specimen for each series of tests at each temperature level was used. These stress varied tests were done at two or three temperature levels for each material property. In the following paragraphs the results of these tests will be presented for each material property.

The model used for the nonlinear stress effects was a simple quadratic function for both the elastic and viscoelastic portion of the power law as explained more fully in chapter 2. The complete model follows the form

$$S = S_o(1+g\sigma^2) + m(1+f\sigma^2)t^n \qquad (5.5)$$

where S_o and m are constants determined from the linear viscoelastic

analysis, done in the previous section, and the g and f constants are determined from the nonlinear viscoelastic analysis. The nonlinear stress parameter, σ, is assumed to be the stress in the direction associated with the corresponding compliance. Thus, for the S_{11} and S_{12} terms, the nonlinear stress parameter would be the stress in the fiber direction, σ_{11}, for the particular ply that is of interest. Likewise, σ_{22} is used for S_{22} and σ_{12} is used for S_{66}. Another common nonlinear stress parameter is the matrix octahedral shear stress which accounts for stress interactions [30]. While this method works well for S_{22} and S_{66} it does not work for the S_{11} and S_{12} which are fiber dominated. Other models for nonlinear viscoelasticity, such as the Findley power law and Schapery Integral equation, have been used with success by others [26,30,77] however the simplicity and ease of use in a numerical procedure of the above quadratic model made it the one of choice for the slight nonlinearity observed with the current system. For a more complete explanation on stress nonlinear parameters refer to chapter 2 and 3.

The nonlinear stress analysis in the fiber direction revealed a slight elastic nonlinearity. Unlike most materials, Kevlar has been shown to have a small stiffening effect as the load is increased. This effect was also evident in this study when the stress levels were increased while the temperature remained the same. Figure 5.27 and 5.28 show the results of these tests at two temperatures. The slope creep rate is constant between tests but the creep progressively begin at a lower compliance level with increasing stress level. The lower

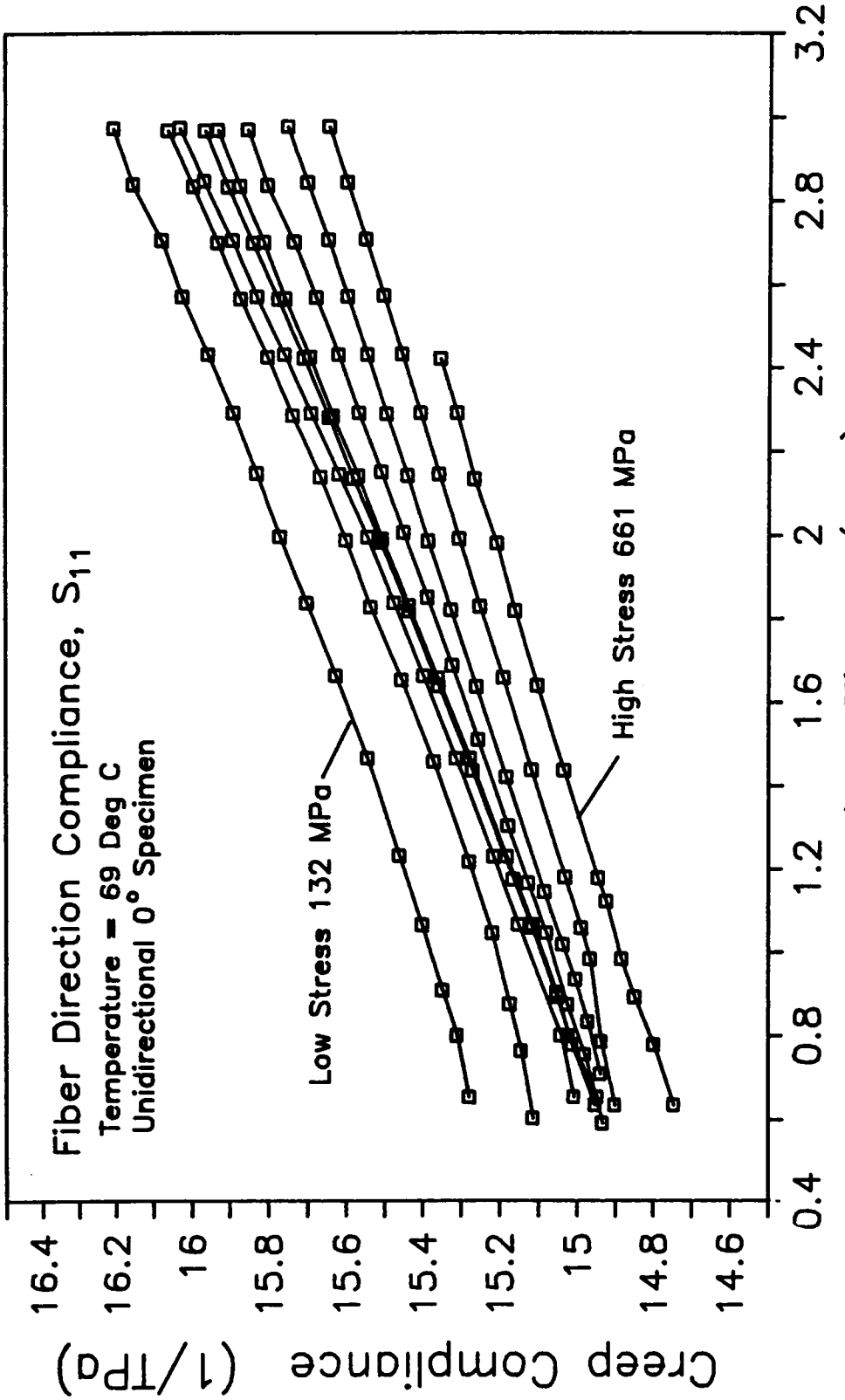

Fig. 5.27 Fiber Direction Compliance for Constant Temperature (69 C) at Various Stress Levels.

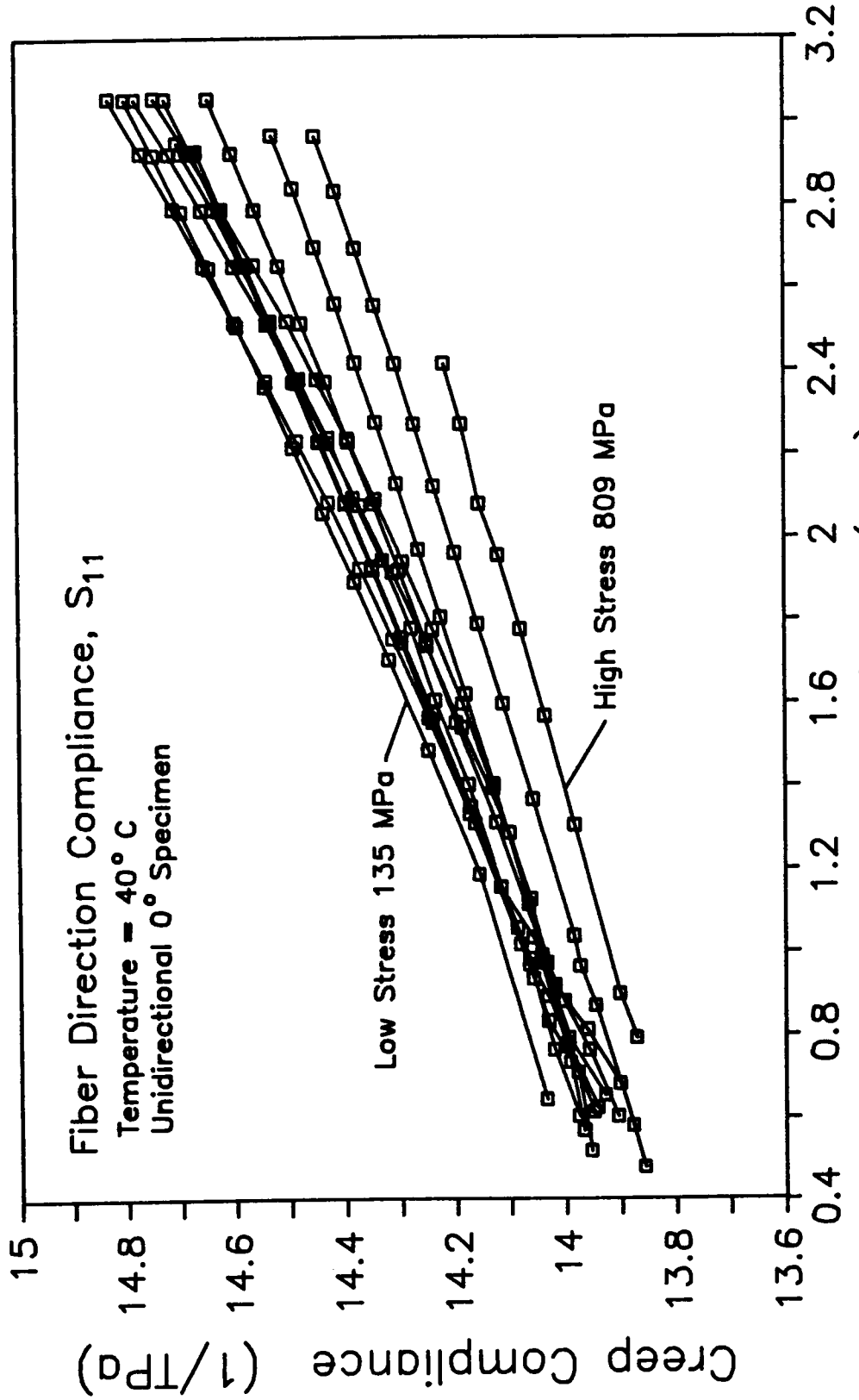

Fig. 5.28 Fiber Direction Compliance for Constant Temperature (40 C) at Various Stress Levels.

temperature tests, Fig. 5.28, does not exhibit as much nonlinear effect as the higher temperature tests, Fig. 5.27, which might be expected due to the accelerating effect of temperature. To understand and model the nonlinear stress effects, each of the individual tests at each temperature was modeled to a power law where n and m were fixed at the values established earlier for the linear model ($n = 0.040$, $m = 10.677$ at $T_o = 32^\circ$ C). This allowed only the S_o or the instantaneous compliance to vary and resulted in a series of decreasing values as the stress increased. These values, normalized to 1 are shown in Fig. 5.29. The higher temperature case decreased even at lower stress levels where as the lower temperature level case actually increased slightly before decreasing. The slight increase, less than 1%, is thought to be from experimental scatter. While there is evidences of temperature effect on the nonlinear stress effect, it was not modeled since there was only two test cases examined. Also, the nonlinear stress effect is less than 5% at the failure stress level. Therefore, the nonlinear stress effect was only modeled as a function of stress.

The model used was in the form of $(1 + g\sigma^2)$, as mentioned earlier, and was determined by a less squares fit of the data from both temperature levels. The nonlinear model is drawn in as a solid line in Fig. 5.29. To better understand the overall nonlinear effect, Fig. 5.29 was redrawn to full scale in Fig 5.30. One point to note is that the maximum stress level tested was only 800 MPa, approximately 66% of ultimate. Higher loads were not possible since the specimens

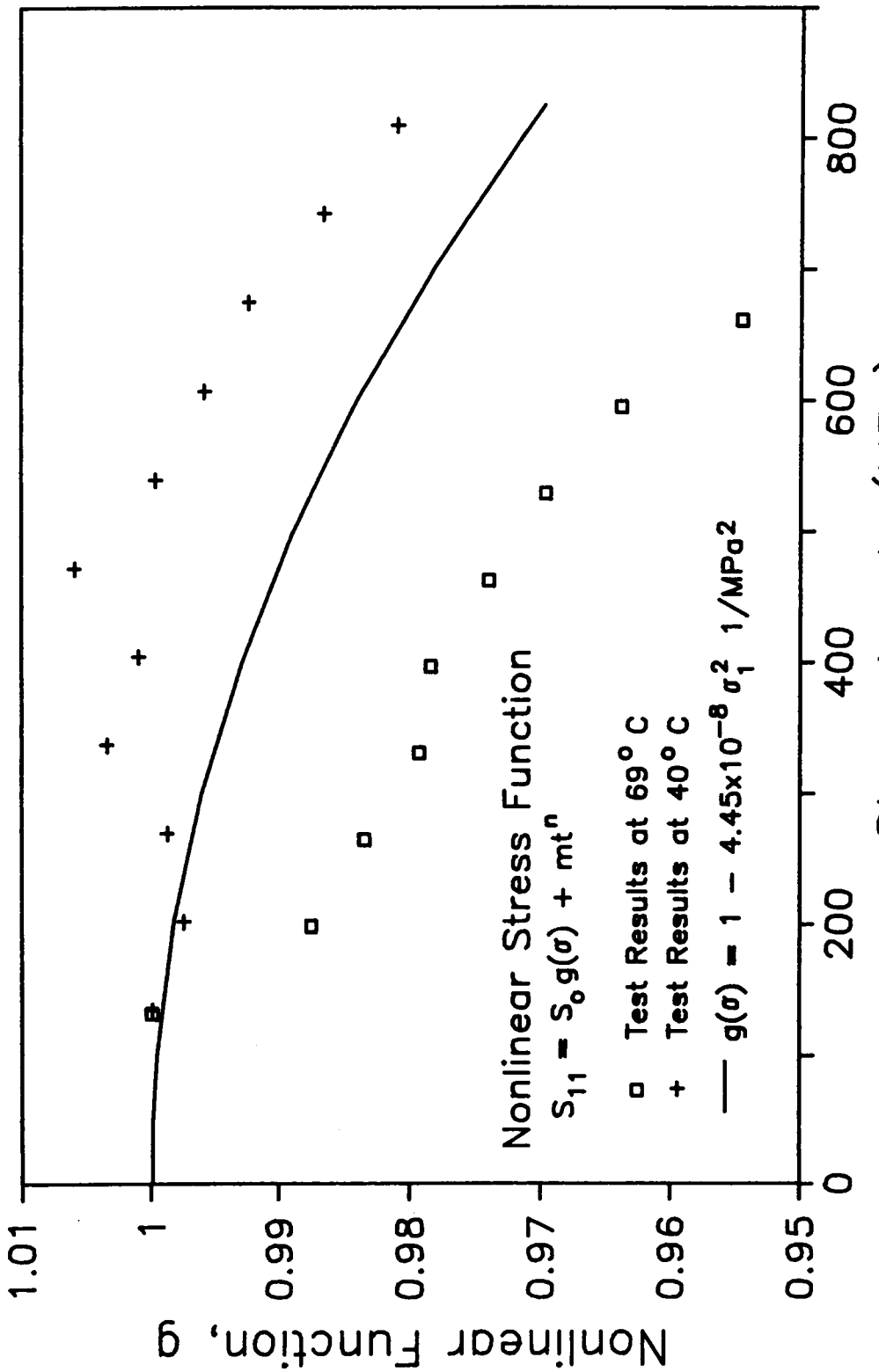

Fig. 5.29 Nonlinear Stress Function Model for the Instantaneous Response, g(σ), in the Fiber Direction Compliance.

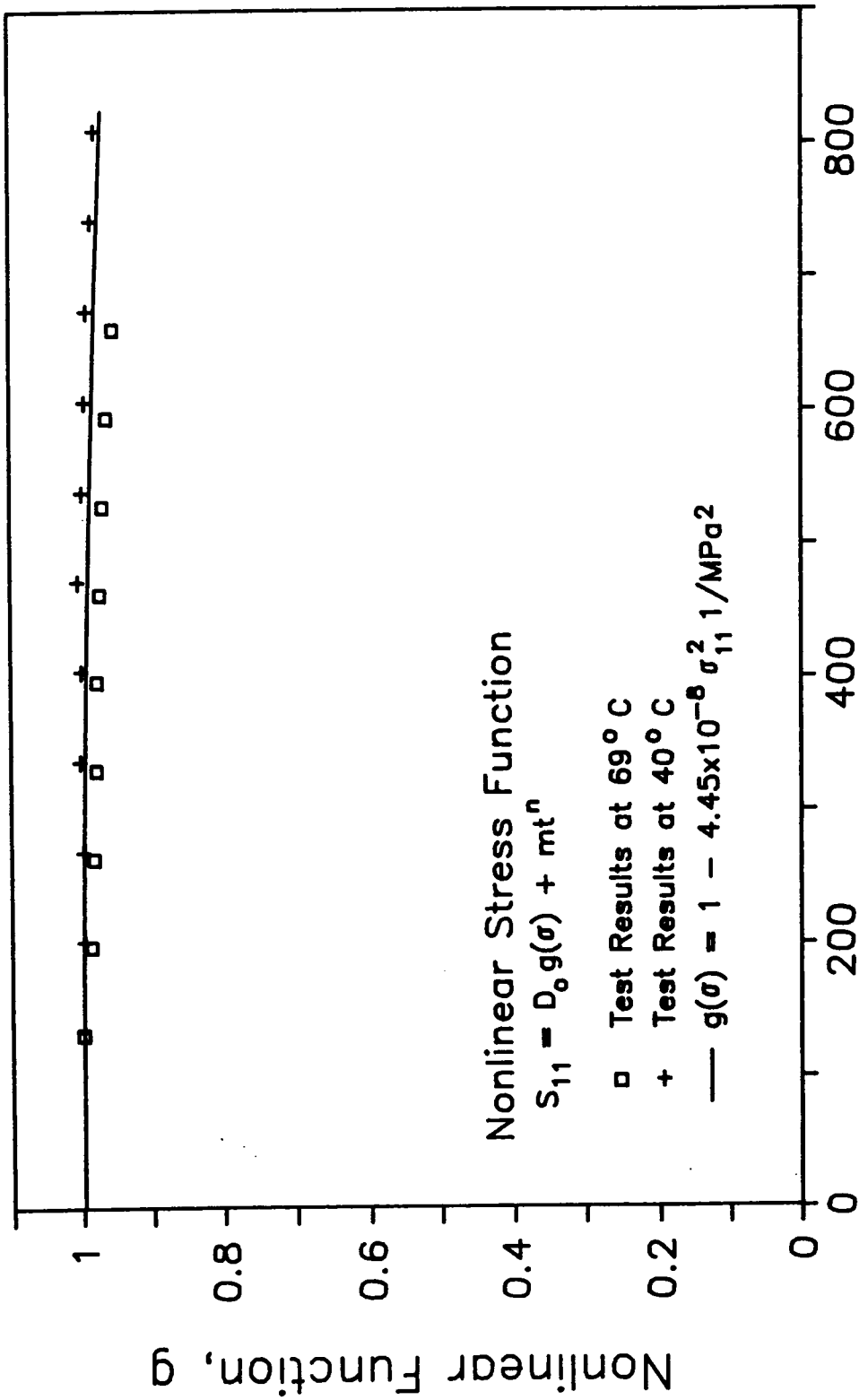

Fig. 5.30 Nonlinear Stress Function Model for the Instantaneous Response, g(σ), in the Fiber Direction Compliance (Full View).

would slid in the friction grips, particularly at the elevated temperature. The other material properties, except S_{12} did not have this problem since the ultimate stress, and subsequently the load carried by friction, was substantially lower. The final nonlinear viscoelastic model for the fiber direction is

$$S_{11} = \left[10.677 \ (1 - 4.448 \times 10^{-8} \ \sigma^2) + 2.515 \ t^{0.040} \right] \text{TPa}^{-1} \qquad (5.6)$$

The coupling compliance, S_{12} was similar to the S_{11} compliance in that only the instantaneous compliance was nonlinear. Figures 5.31 and 5.32 shows the effect of stress for two temperature levels. Like S_{11} the nonlinear stress effect has a stiffening effect which is expected since the S_{12} compliance is also fiber dominated. However the higher degree of nonlinearity, as much as 20% nonlinear effect at failure stress, was surprising (see Fig. 5.26) whereas S_{11} was only 5% nonlinear at failure stress. The model, $(1 + g\sigma^2)$, to model the nonlinear effects was fitted to the data and is drawn on Fig 5.33. The data for both temperature levels agreed surprising well which indicates no temperature dependence for nonlinear effects. For reference, the full scale is once again given in Fig. 5.34, which clearly shows the magnitude of nonlinear stress effects. The final nonlinear S_{12} model is

$$S_{12} = \left[-4.686 \ (1 - 1.764 \times 10^{-7} \ \sigma^2) - 0.667 \ t^{0.086} \right] \text{TPa}^{-1} \qquad (5.7)$$

The transverse compliance, S_{22}, also showed evidences of

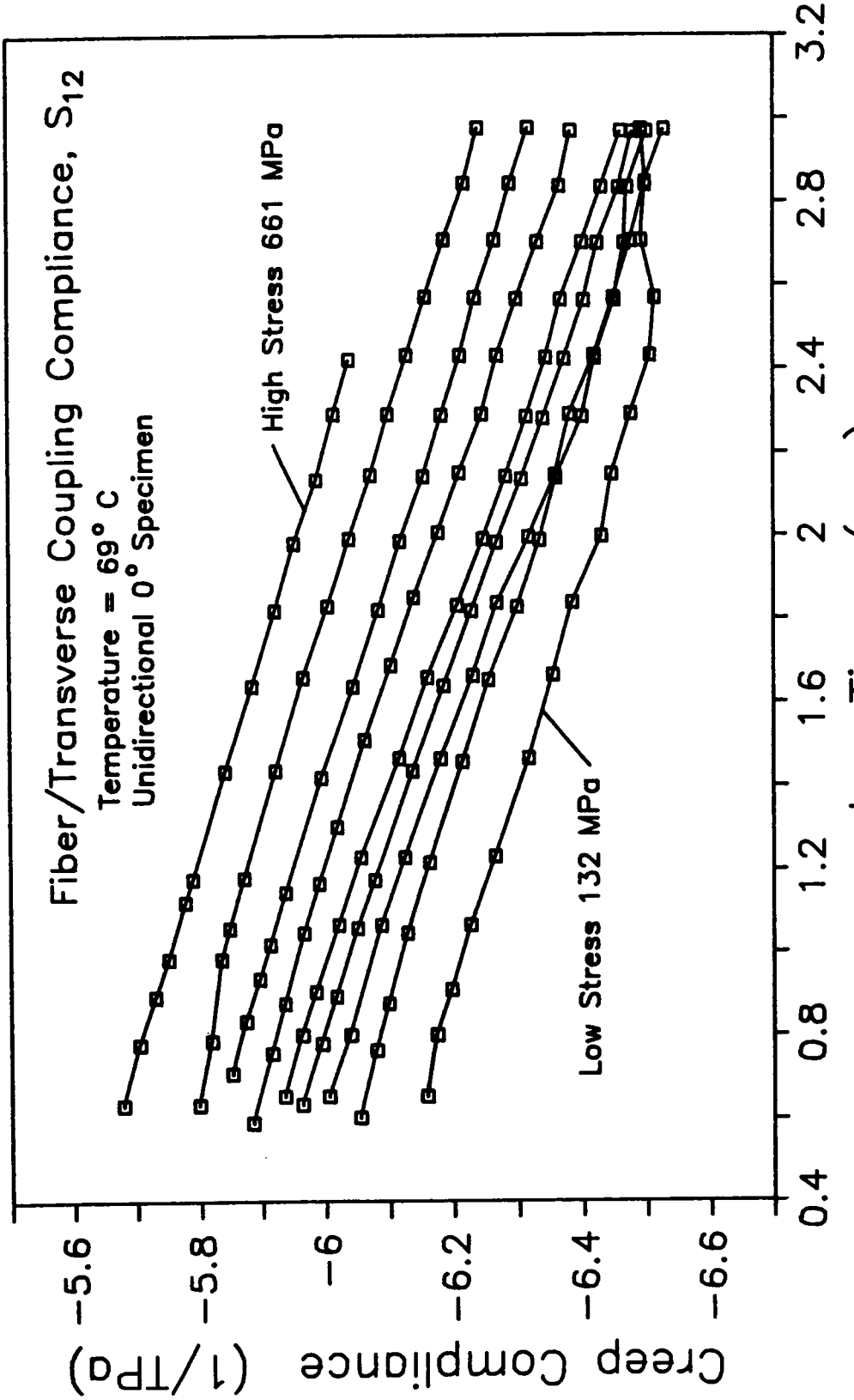

Fig. 5.31 Fiber/Transverse Coupling Compliance for Constant Temperature (69C) at Various Stress Levels.

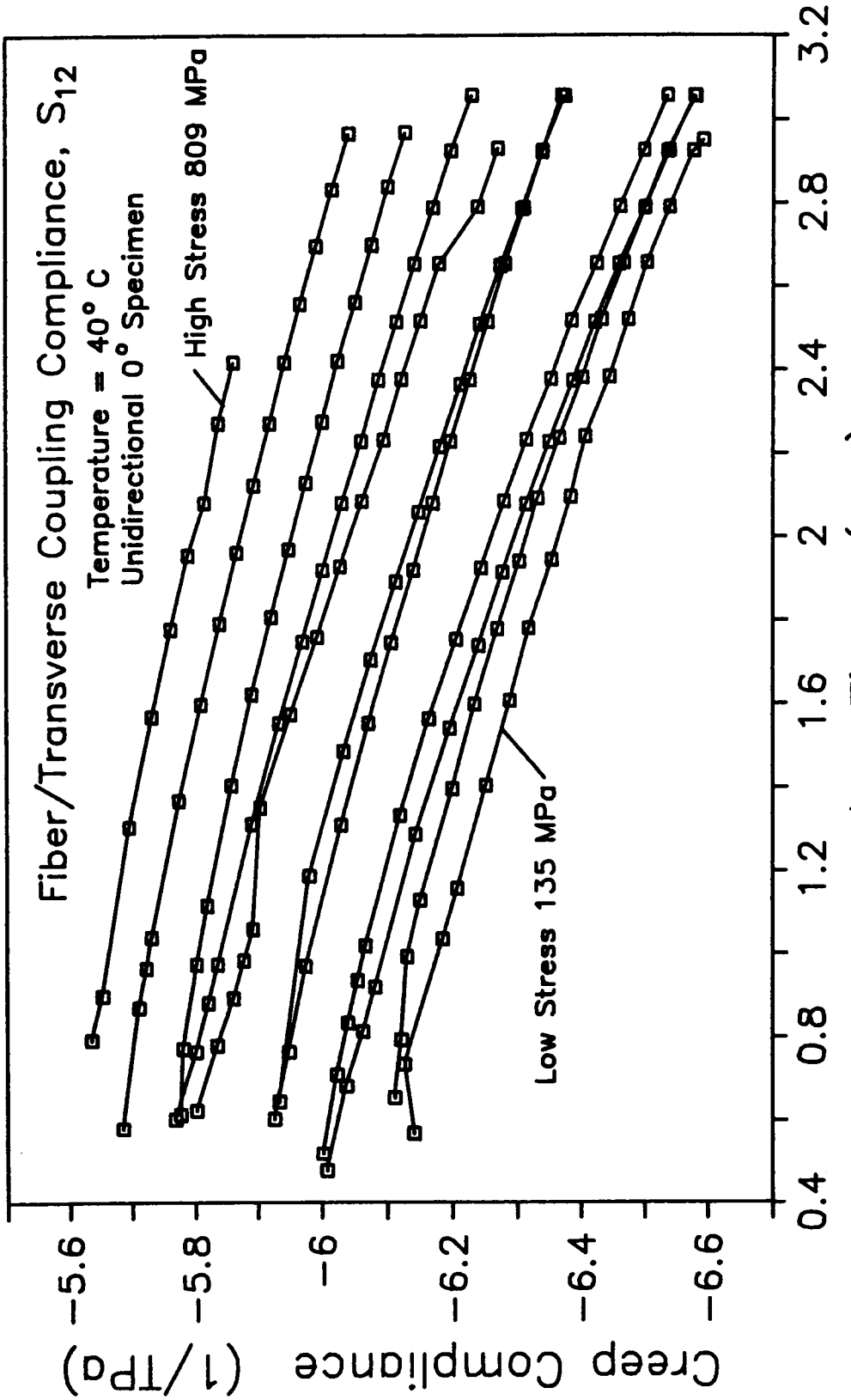

Fig. 5.32 Fiber/Transverse Coupling Compliance for Constant Temperature (40 C) at Various Stress Levels.

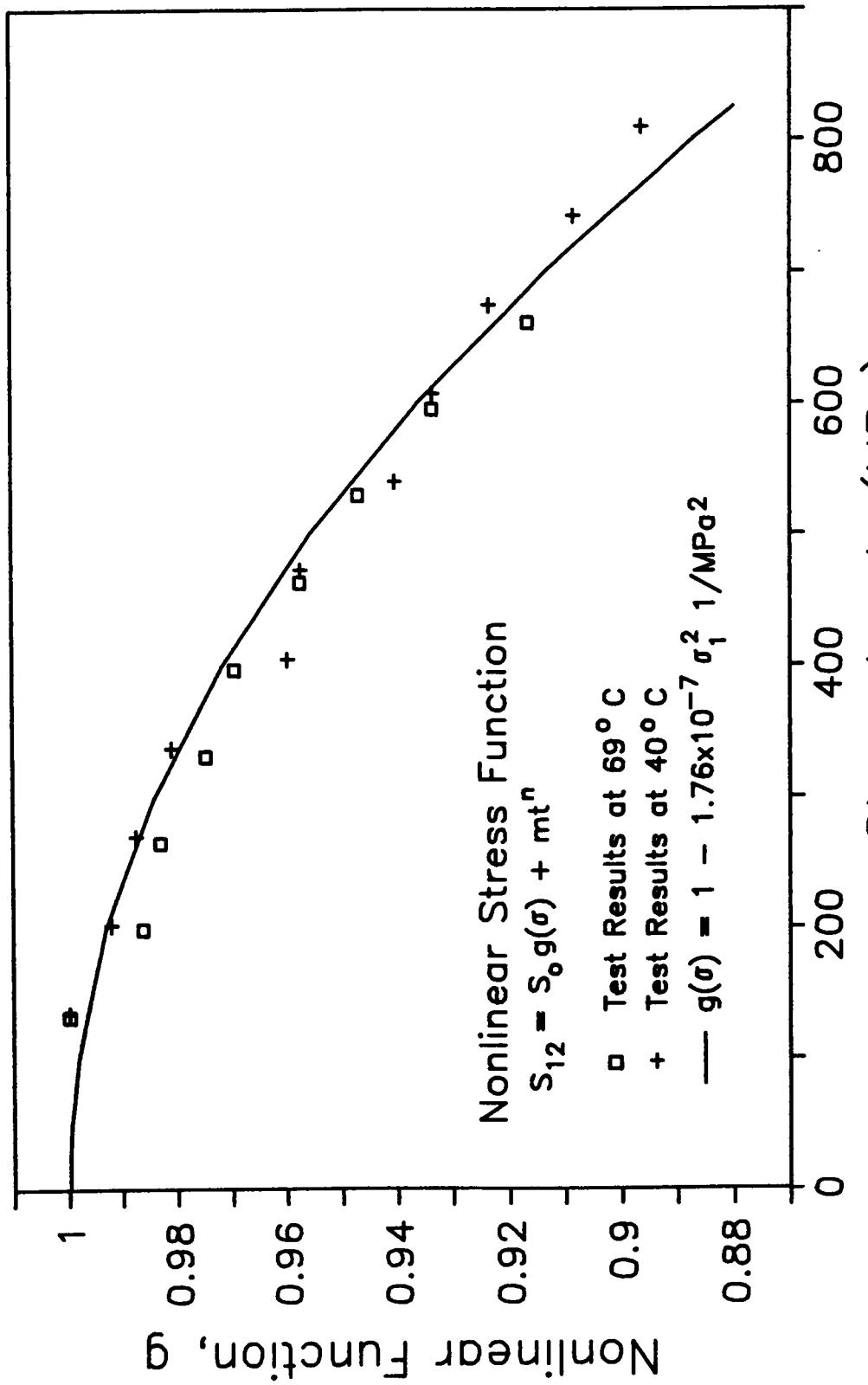

Fig. 5.33 Nonlinear Stress Function Model for the Instantaneous Response, g(σ), for the Fiber/Transverse Coupling Compliance.

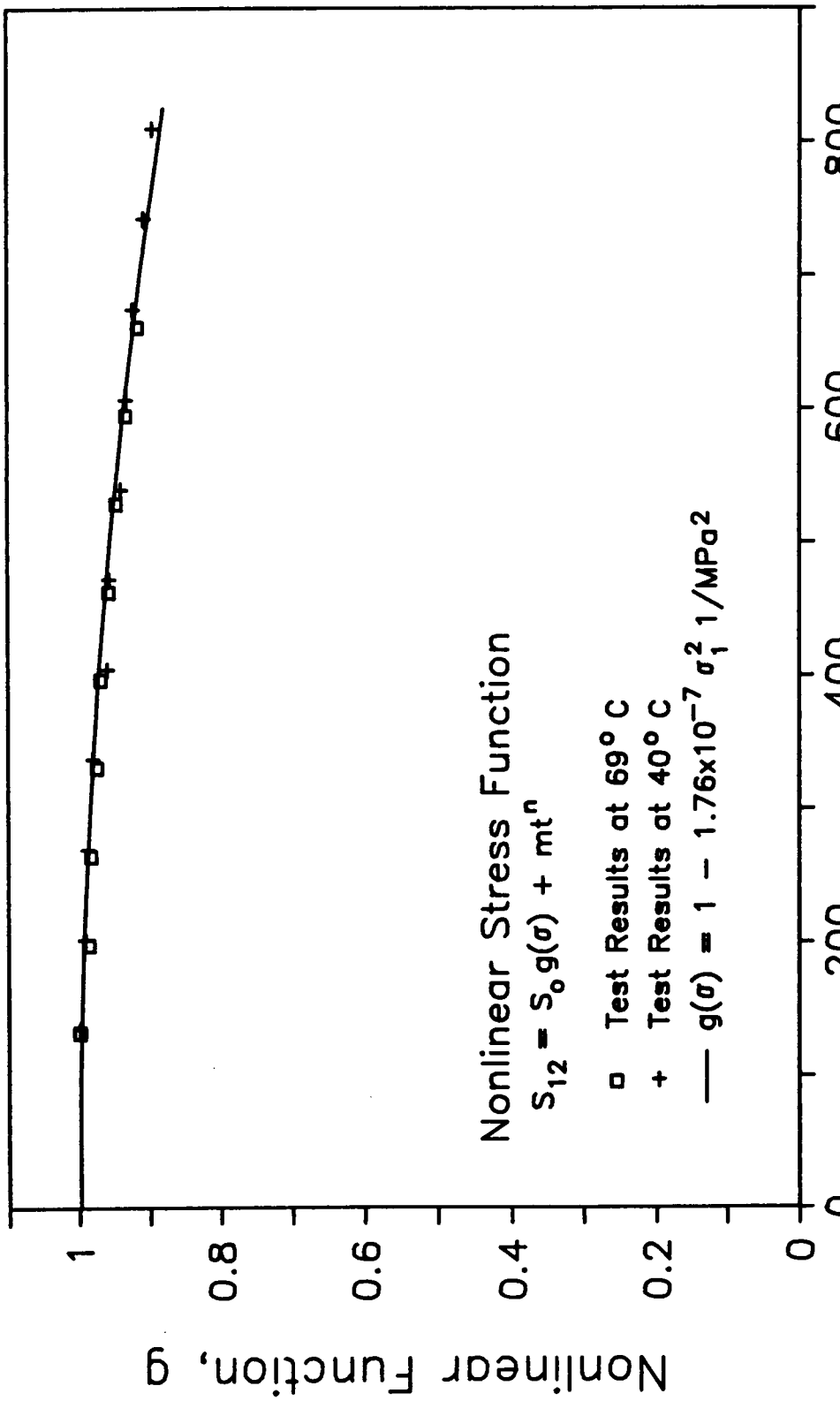

Fig. 5.34 Nonlinear Stress Function Model for the Instantaneous Response, g(σ), for the Fiber/Transverse Coupling Compliance (Full View).

nonlinear stress effects when the temperature was held constant and the stress level was increased on each individual test. The results of two such tests are shown in Figs. 5.35 and 5.36. Like the S_{11} and S_{12} tests, the rate of creep remained fairly constant between tests at different stress levels which indicates that only the instantaneous compliance is nonlinear. It should be noted that even the instantaneous nonlinear effects are small and thus the transverse compliance could be assumed a linear viscoelastic material property. This agrees with the conclusions reached by Heil [76] with T900/934 that the transverse direction is linear and only the shear compliance in nonlinear. Also, the transverse direction is more highly constrained then the shear in a physical sense, which would limit the nonlinear stress effects. However, for sake of completeness, the instantaneous nonlinear stress effect was modeled and the results are shown in Fig. 5.37 and 5.38. The scatter was large, partly due to the smallness on the nonlinear effect, but the general trend is evident. The complete S_{22} is modeled as

$$S_{22} = \left[191.3 \, (1 + 1.481 \times 10^{-2} \, \sigma^2) + 1.668 \, t^{0.271} \right] \text{TPa}^{-1} \qquad (5.8)$$

The shear compliance showed evidences of large nonlinear stress effects at high temperature (67° C) but none at low temperatures (40° C) as shown in Figs. 5.39 - 5.41. This dependence on temperature was not fully understood and needs more investigation. For this study it has been assumed that there is no temperature dependency in the

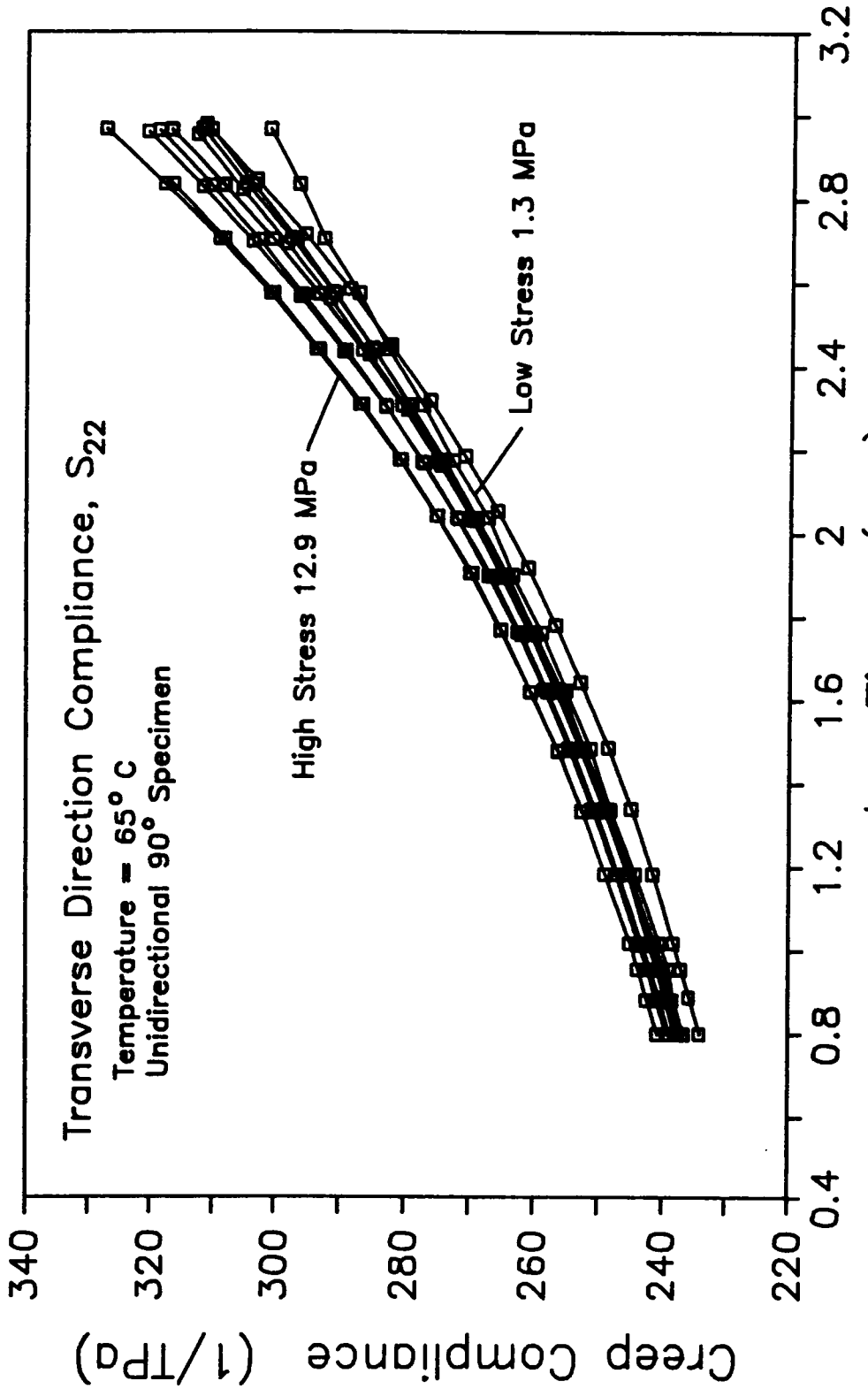

Fig. 5.35 Transverse Direction Compliance for Constant Temperature (65 C) at Various Stress Levels.

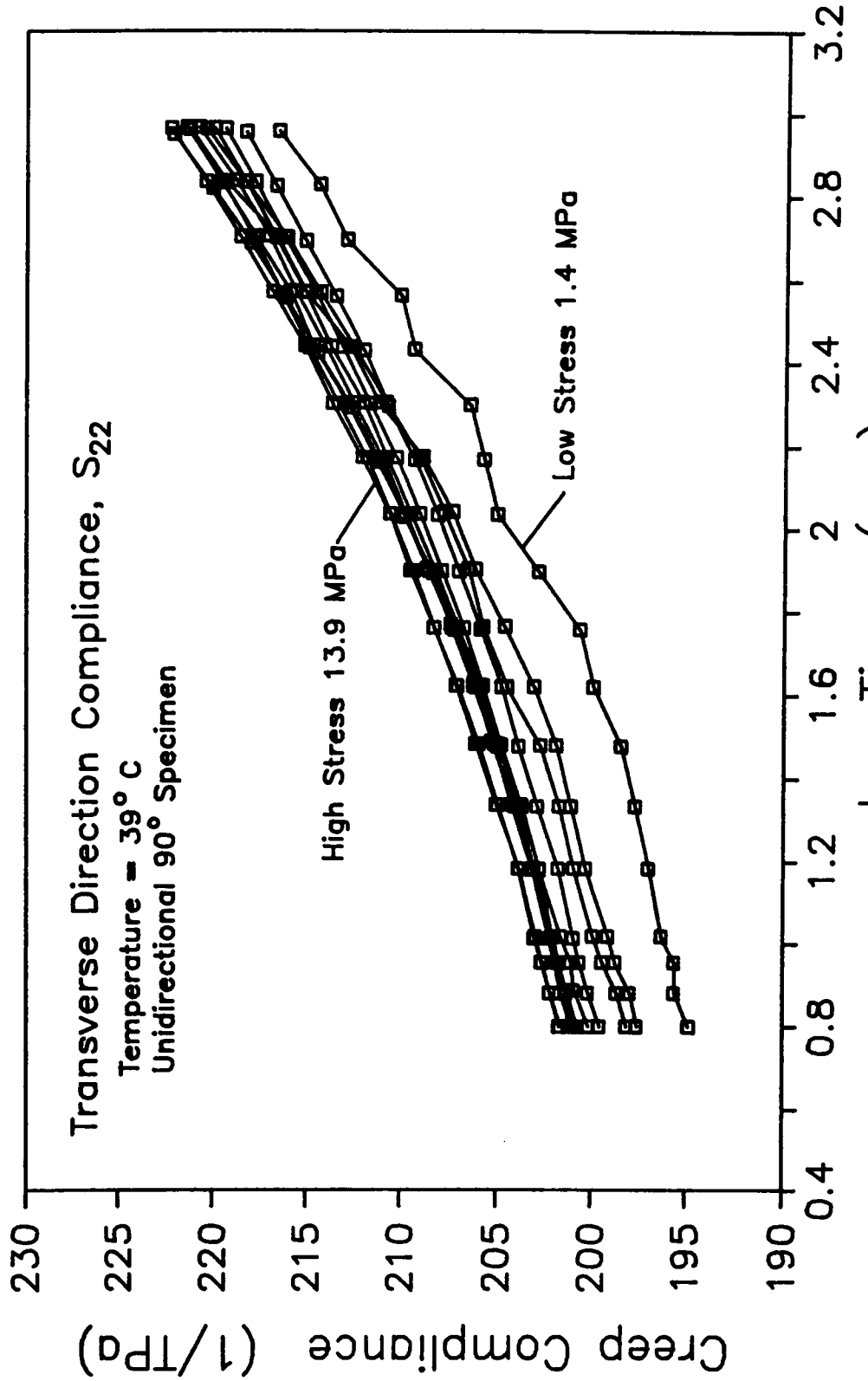

Fig. 5.36 Transverse Direction Compliance for Constant Temperature (39 C) at Various Stress Levels.

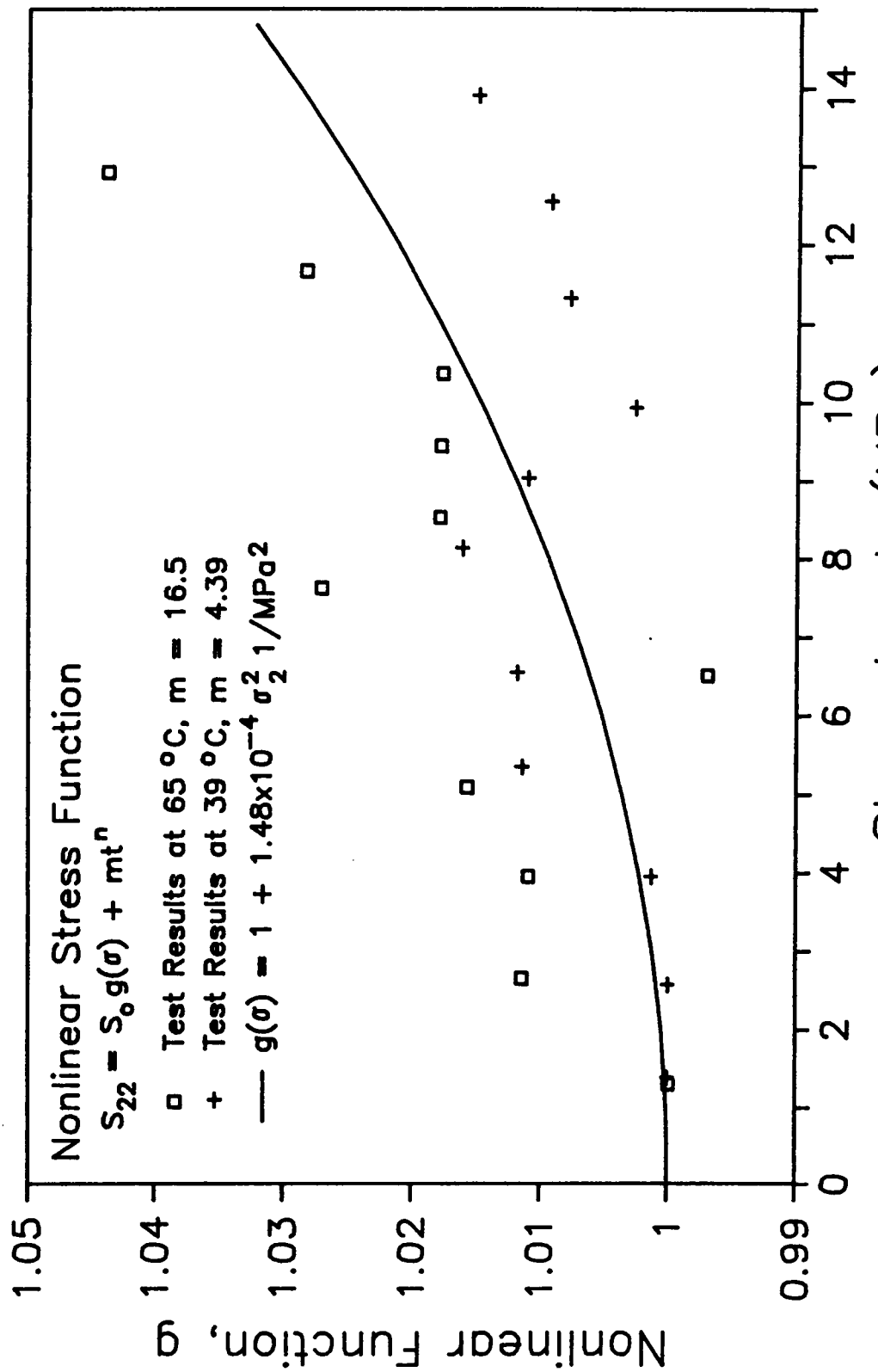

Fig. 5.37 Nonlinear Stress Function Model for the Instantaneous Response, g(σ), for the Transverse Direction Compliance.

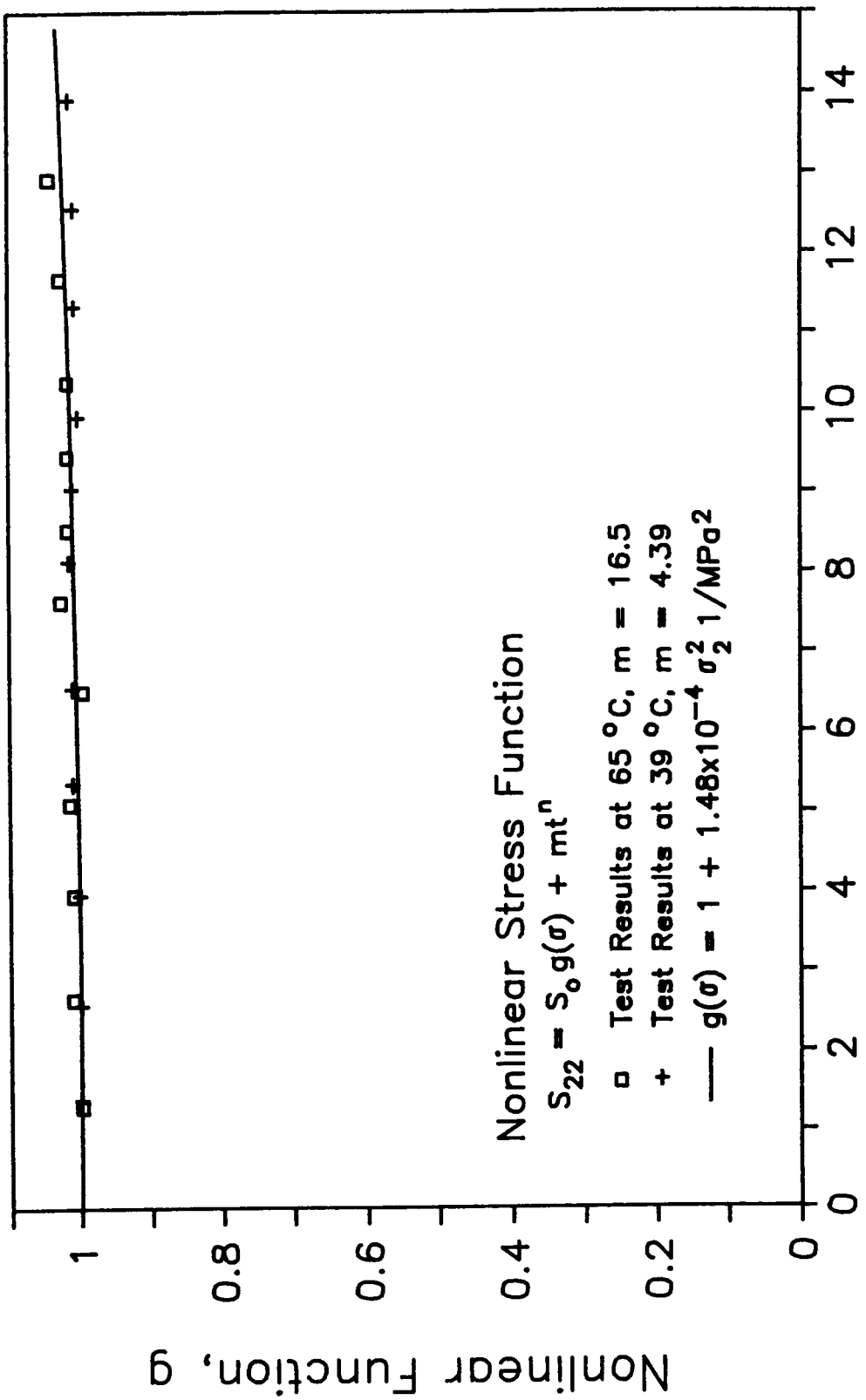

Fig. 5.38 Nonlinear Stress Function Model for the Instantaneous Response, g(σ), for the Transverse Direction Compliance (Full View).

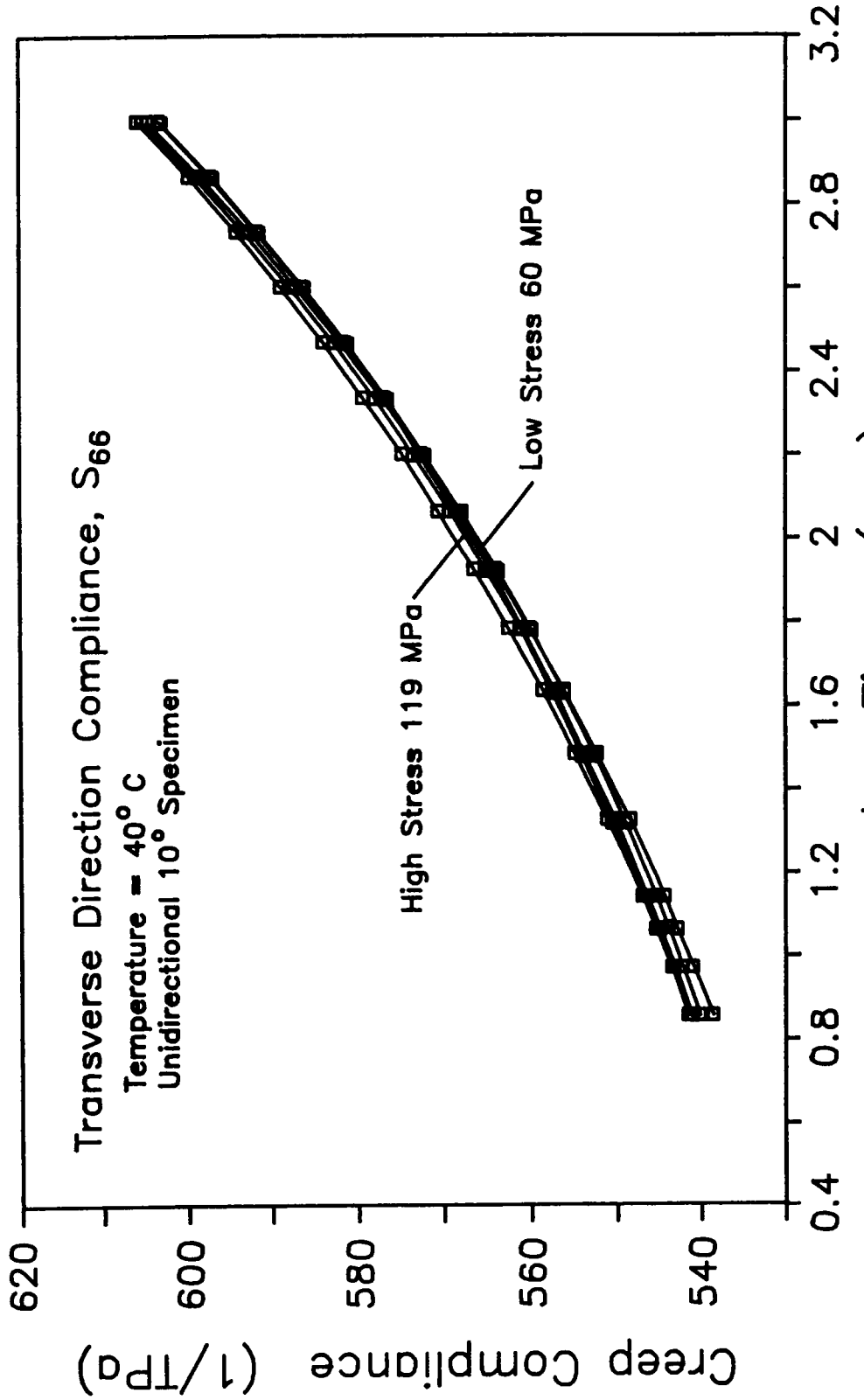

Fig. 5.39 Shear Compliance for Constant Temperature (40 C) at Various Stress Levels.

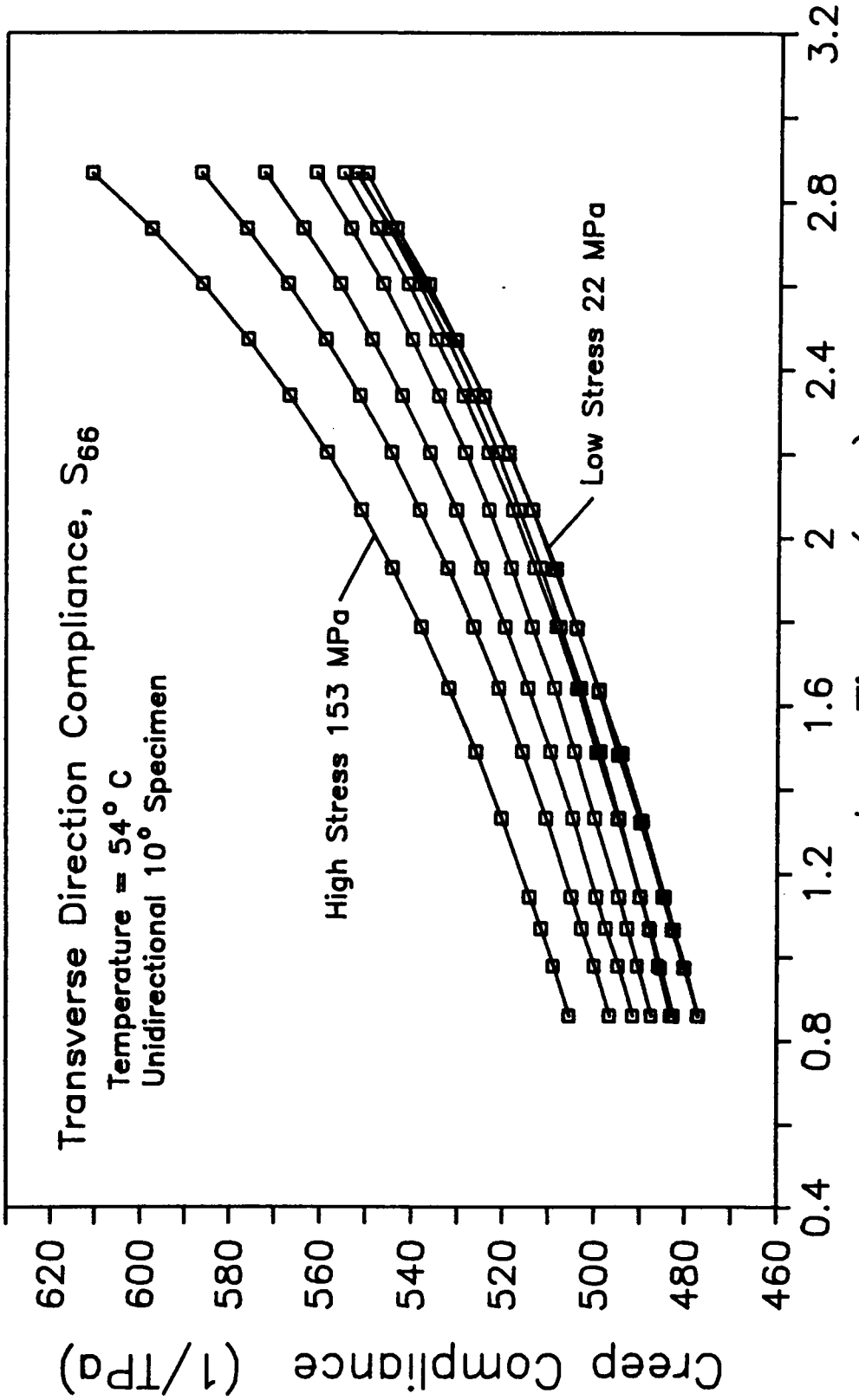

Fig. 5.40 Shear Compliance for Constant Temperature (54 C) at Various Stress Levels.

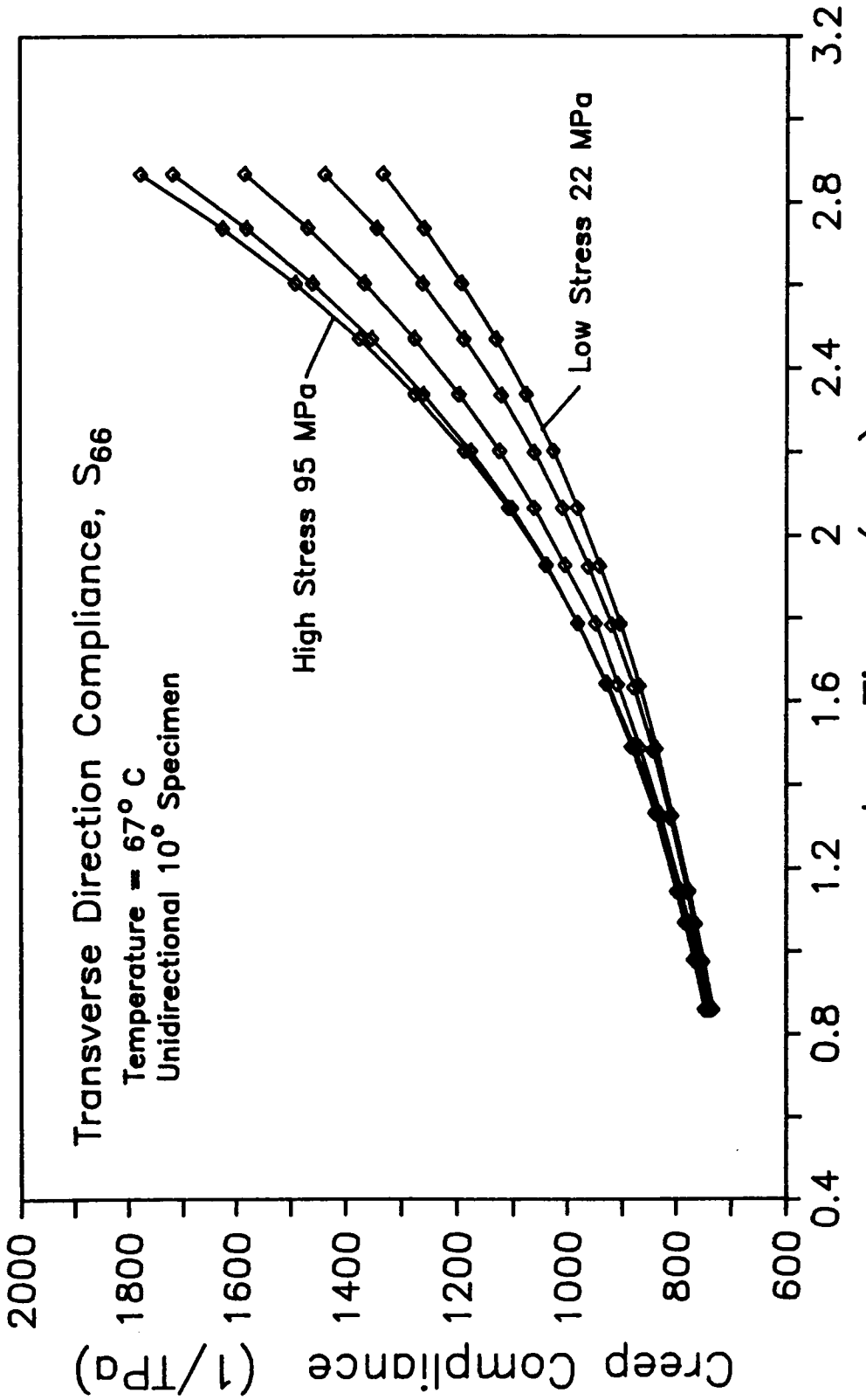

Fig. 5.41 Shear Compliance for Constant Temperature (67 C) at Various Stress Levels.

nonlinear stress effects, thus allowing the numerical procedures methods to work. To model the stress nonlinearities only the middle temperature results was used. Both the instantaneous and viscoelastic compliances were modeled using $(1 + g\sigma^2)$ and $(1 + f\sigma^2)$, respectively. The normalized results are shown in Figs. 5.42-5.45 along with the model. The complete viscoelastic model for the shear compliance is

$$S_{66} = \Big[\, 496.6\ (1 + 6.676 \times 10^{-5}\ \sigma^2) + 4.109\ (1 + 3.295 \times 10^{-4}\ \sigma^2)\ t^{0.305} \,\Big]\ \text{TPa}^{-1} \qquad (5.9)$$

The nonlinear viscoelastic constitutive model obtained experimentally will be used in the numerical procedure to predict the laminate viscoelastic response. Equations 5.4a-d describing the temperature effect as well as the viscoelastic models, Eqs. 5.6-5.9 are to be used in the numerical procedure. The following chapter will compare the numerical predictions and actual experimental tests on various laminates, including unidirectional, composites.

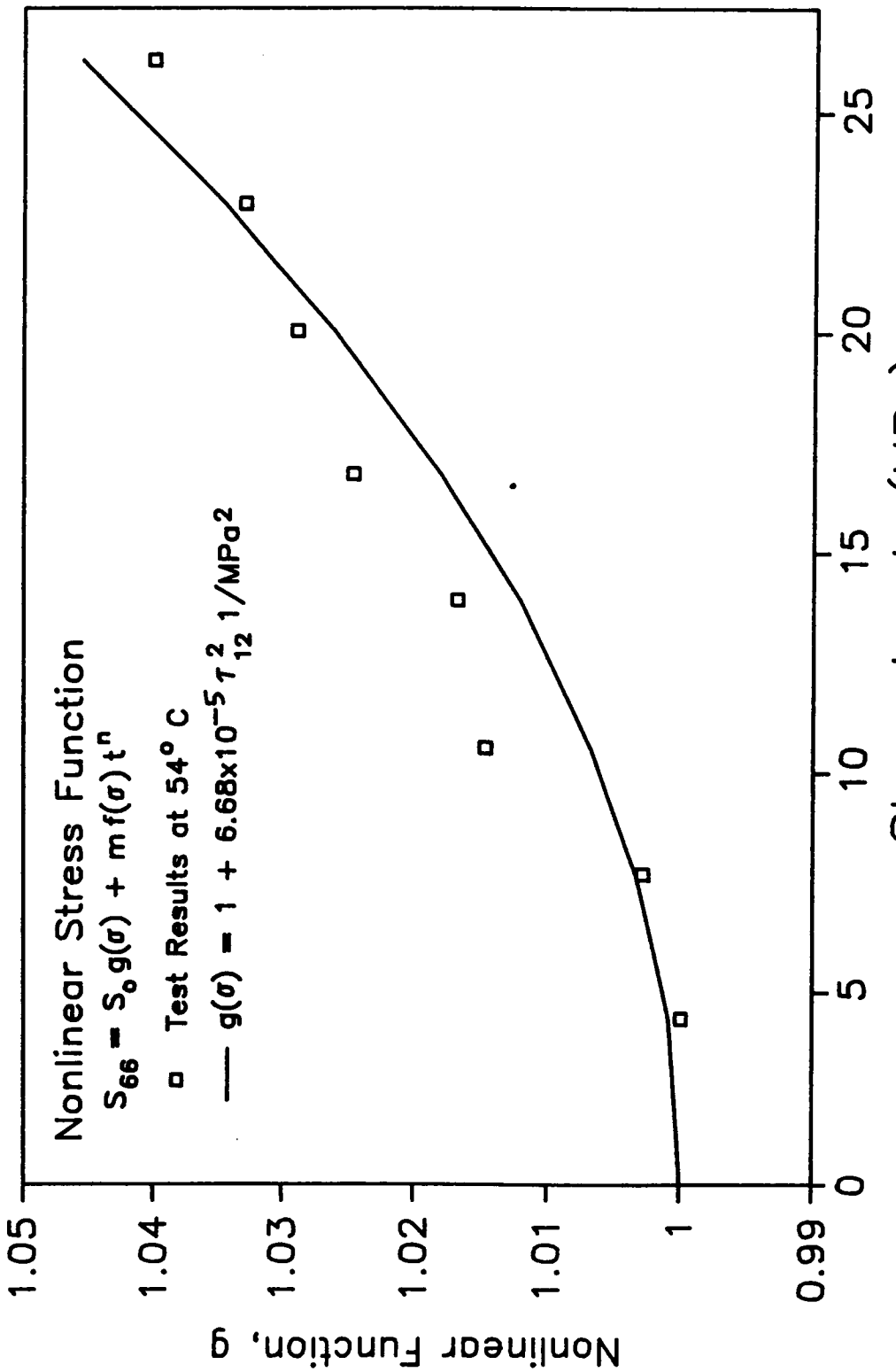

Fig. 5.42 Nonlinear Stress Function Model for the Instantaneous Response, g(σ), for Shear Compliance.

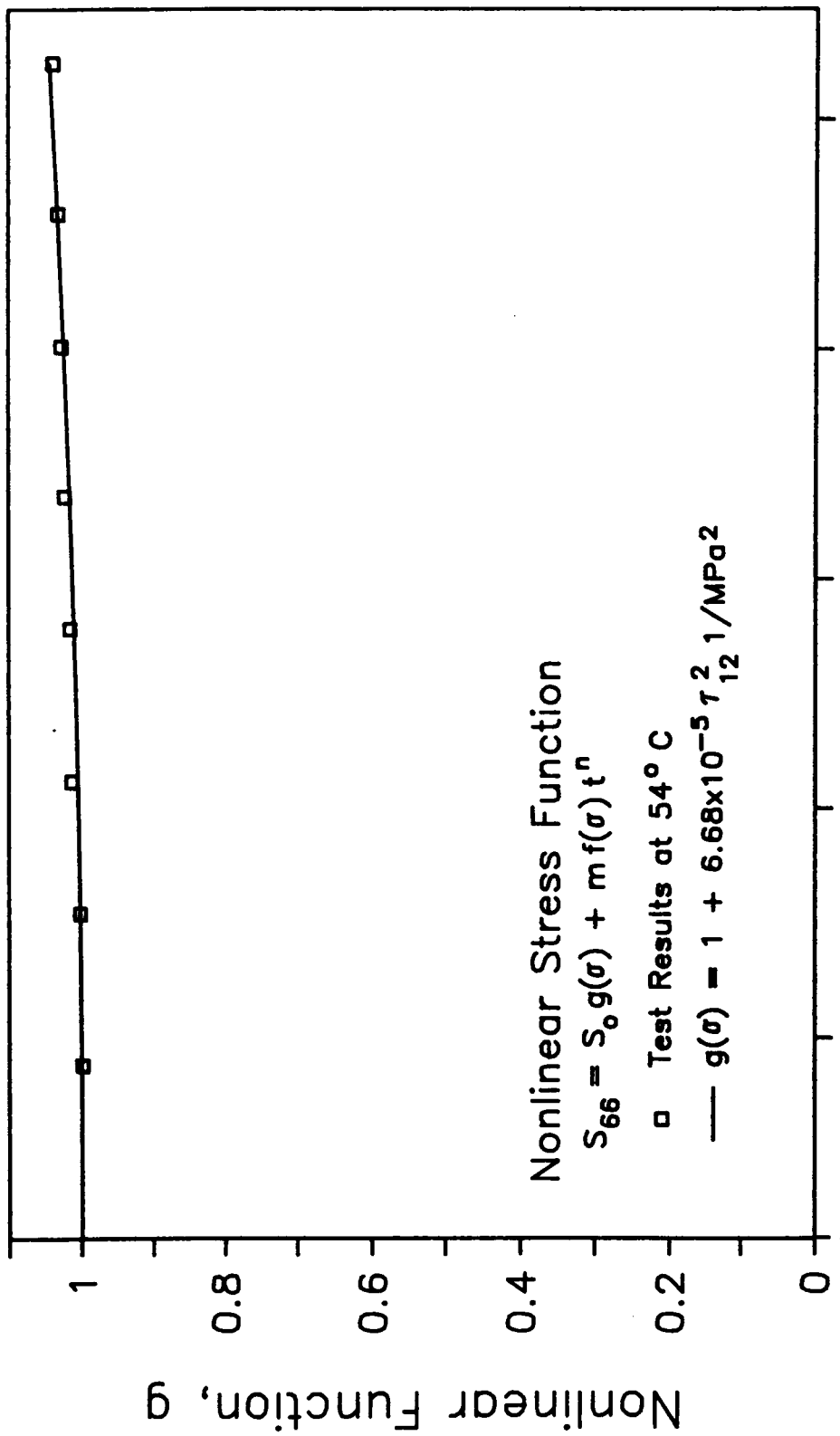

Fig. 5.43 Nonlinear Stress Function Model for the Instantaneous Response, g(σ), for Shear Compliance (Full View).

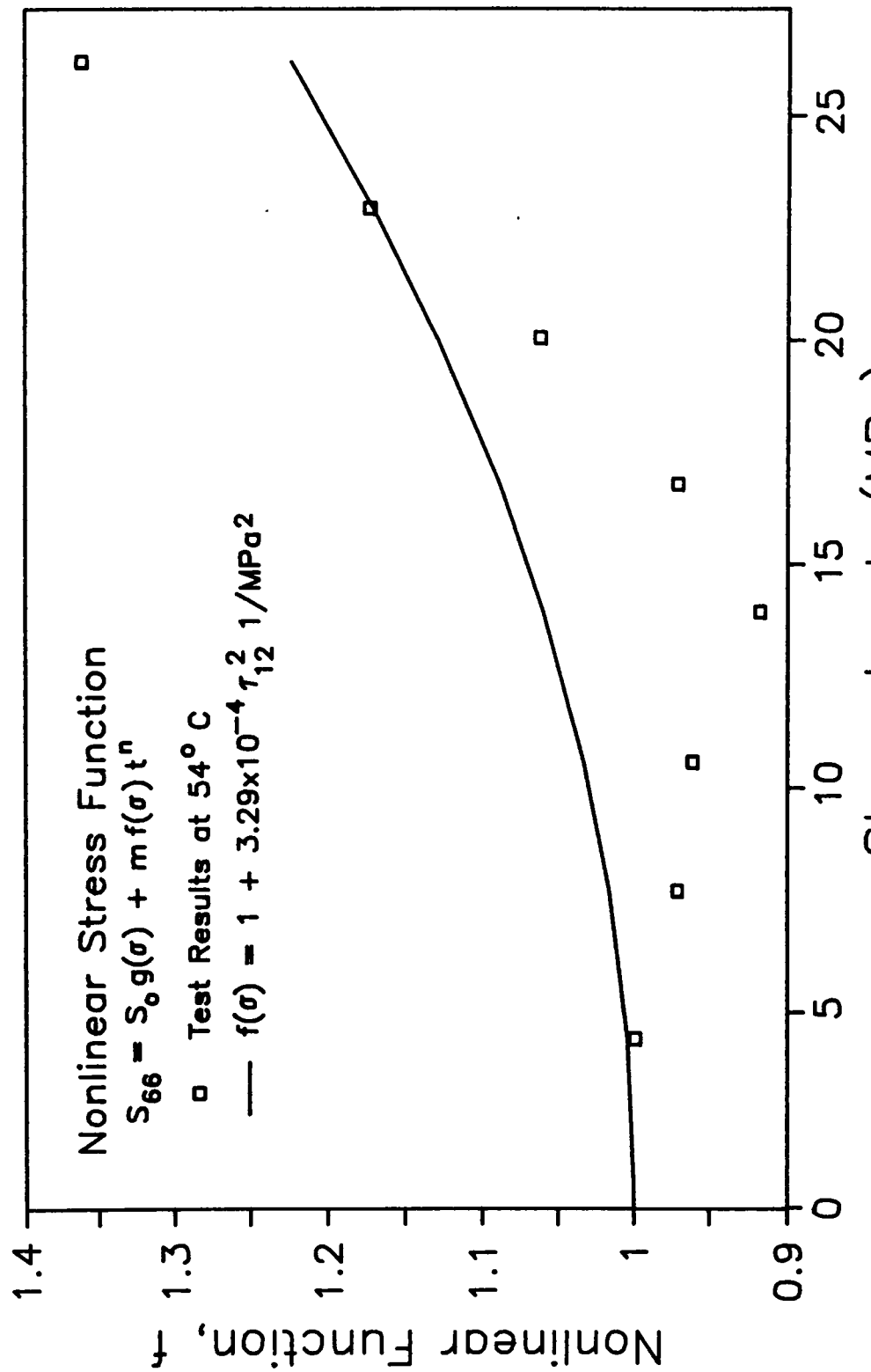

Fig. 5.44 Nonlinear Stress Function Model for the Viscoelastic Response, f(σ), for Shear Compliance.

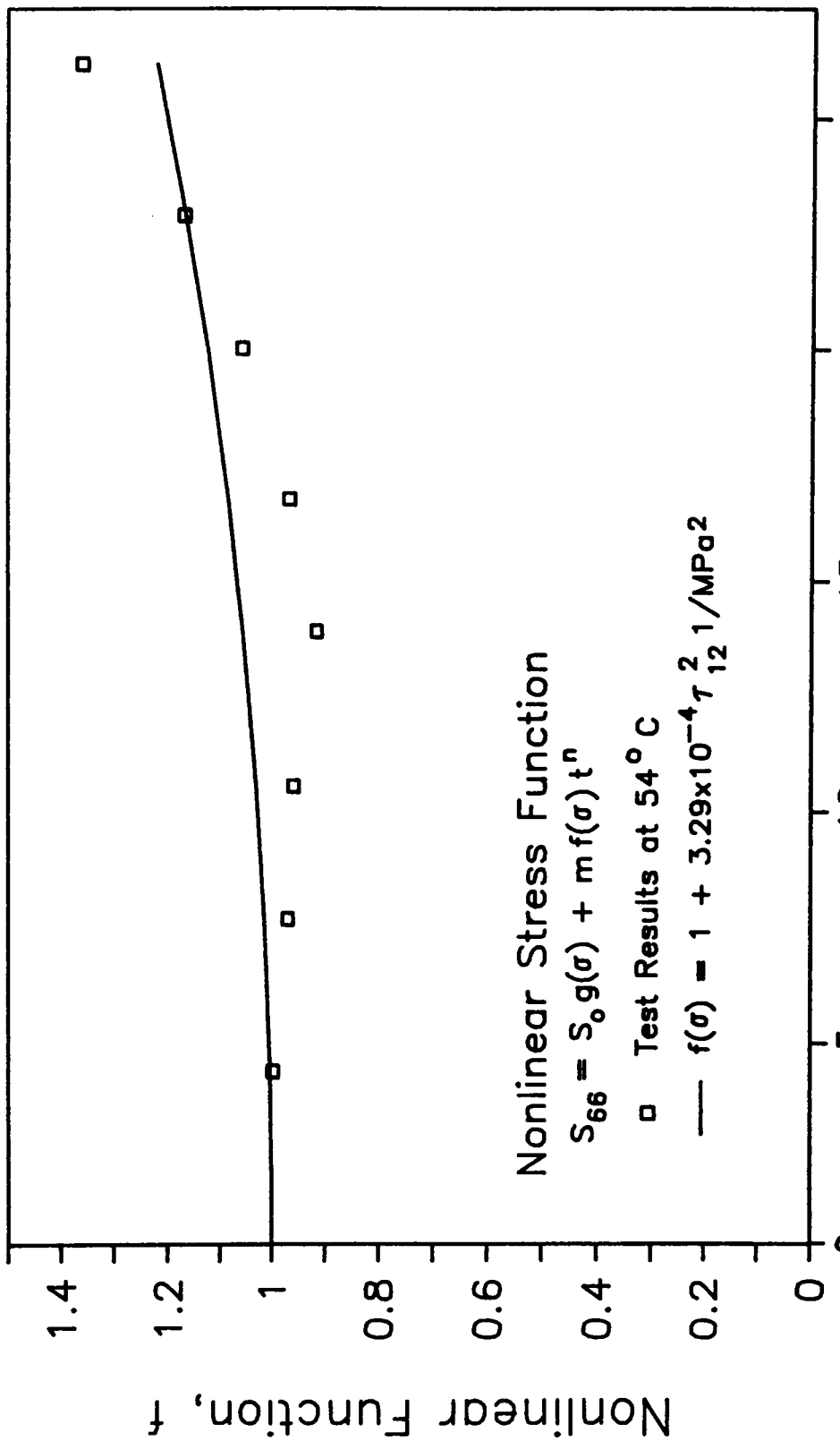

Fig. 5.45 Nonlinear Stress Function Model for the Viscoelastic Response, f(σ), for Shear Compliance (Full View).

Chapter 6

VERIFICATION OF TTSP CHARACTERIZATION

The Kevlar/epoxy lamina characterization and constitutive modeling in chapter 5 were based on using short term tests and then applying the TTSP. Master curves for all four compliance material properties were obtained in this manner for up to 15 decades of time. Even though actual creep tests cannot be performed for that length of time to verify that TTSP can be applied, shorter tests of two to four weeks are feasible. Through these shorter tests, but still much longer than the characterization tests (15-25 minutes), the general trend can be verified. Furthermore these medium length tests can be done at elevated temperature to insure the tests go through the glassy/rubbery transition region which was identified for the S_{22} and S_{66} terms. These medium lengths are designed to confirm the viscoelastic models developed in chapter 5.

A four week test was performed on an unidirectional 0° specimen made of eight plies. Testing was done on a creep testing machine at 320° C using strain gages similar to the short term tests. The creep compliance, shown in Fig. 6.1, initially is slightly less than the model predicts but matches the predictions after the first few minutes. More important is that the rate of creep (slope of the compliance curve in log time) is the same. This also agrees with the results obtained by Horn, et al [83], which are also shown in Fig 6.1.

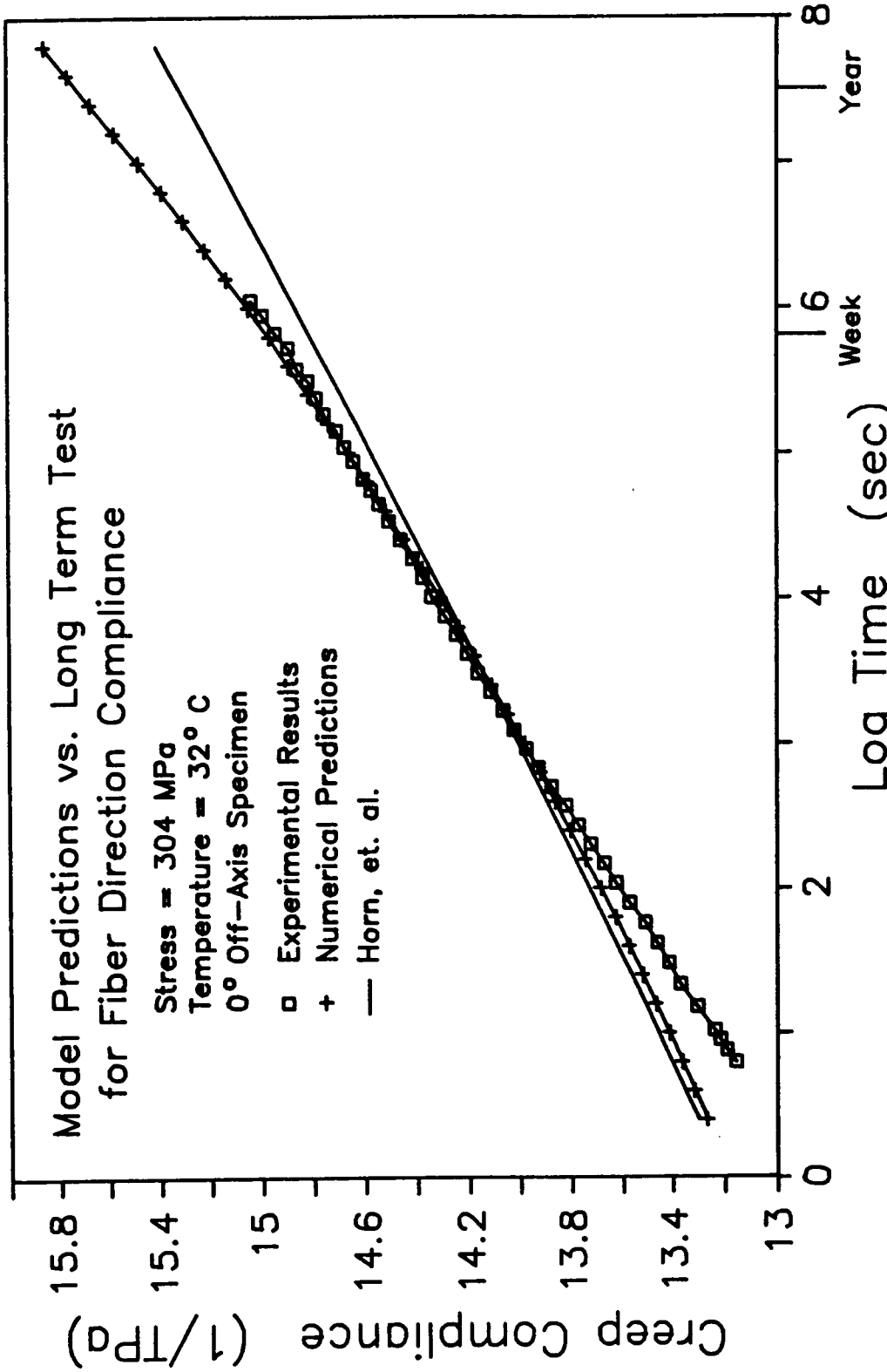

Fig. 6.1 Comparison of Numerical Predictions and Experimental Results for the Fiber Direction Compliance.

The trend or rate of creep is important if the prediction for longer time spans, such as years, are to be correct.

Unlike the S_{11} compliance which has a constant creep rate, the transverse compliance term, S_{22}, changes rapidly after the first 5 or 6 decades of time for 32° (see Figs. 5.18). In order to better verify the nonlinear model, medium length tests were done at temperatures higher than the reference temperature of 32° C so that the rapidly changing portion of the model would be detected. This amounts to shifting the basic compliance curves to the right so that the start of the transition region between the glassy and rubbery states will be evident in the 4 week time span of the actual tests. This does however, introduce further complications and possible experimental error due to the temperature and shift factor function dependency.

The two unidirectional, 90° specimens were tested at 49° C and 66° C in a similar fashion as other S_{22} tests done previously using strain gages. The results are shown in Figs. 6.2 and 6.3 along with the predictions. In both cases the actual test results are slightly lower than the predictions. For reference only, the predictions for 3° C lower temperatures are also shown, which match the actual test results. This indicates how sensitive the compliance is to small changes in temperature and how critical the shift factor function is to the predictions of creep. The agreement between the actual and predicted compliance for S_{22} is reasonable especially when considering the test were done at elevated temperatures and that the temperature accuracy of the ovens are is ±1° C.

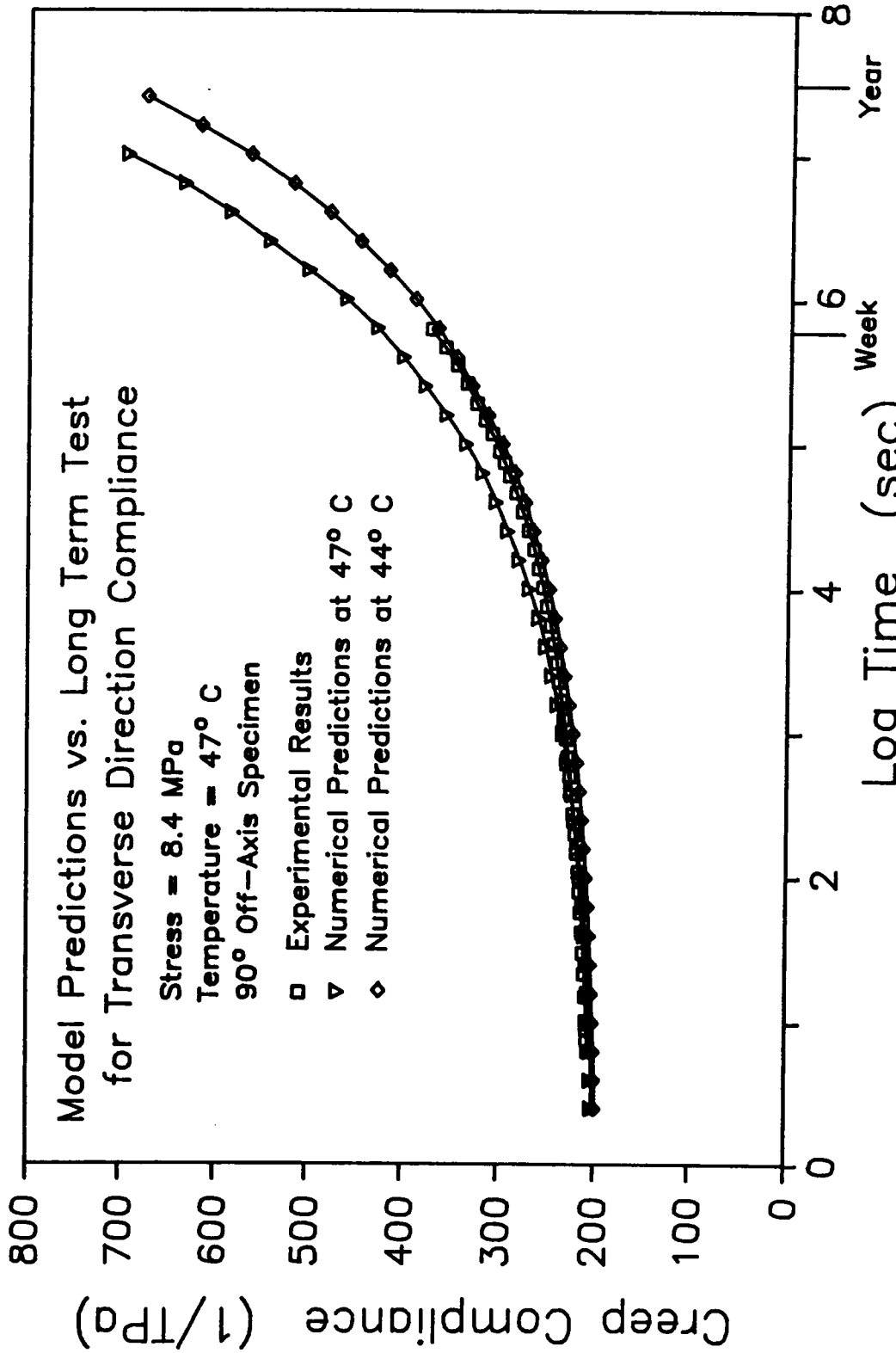

Fig. 6.2 Comparison of Numerical Predictions and Experimental Results for the Transverse Direction Compliance.

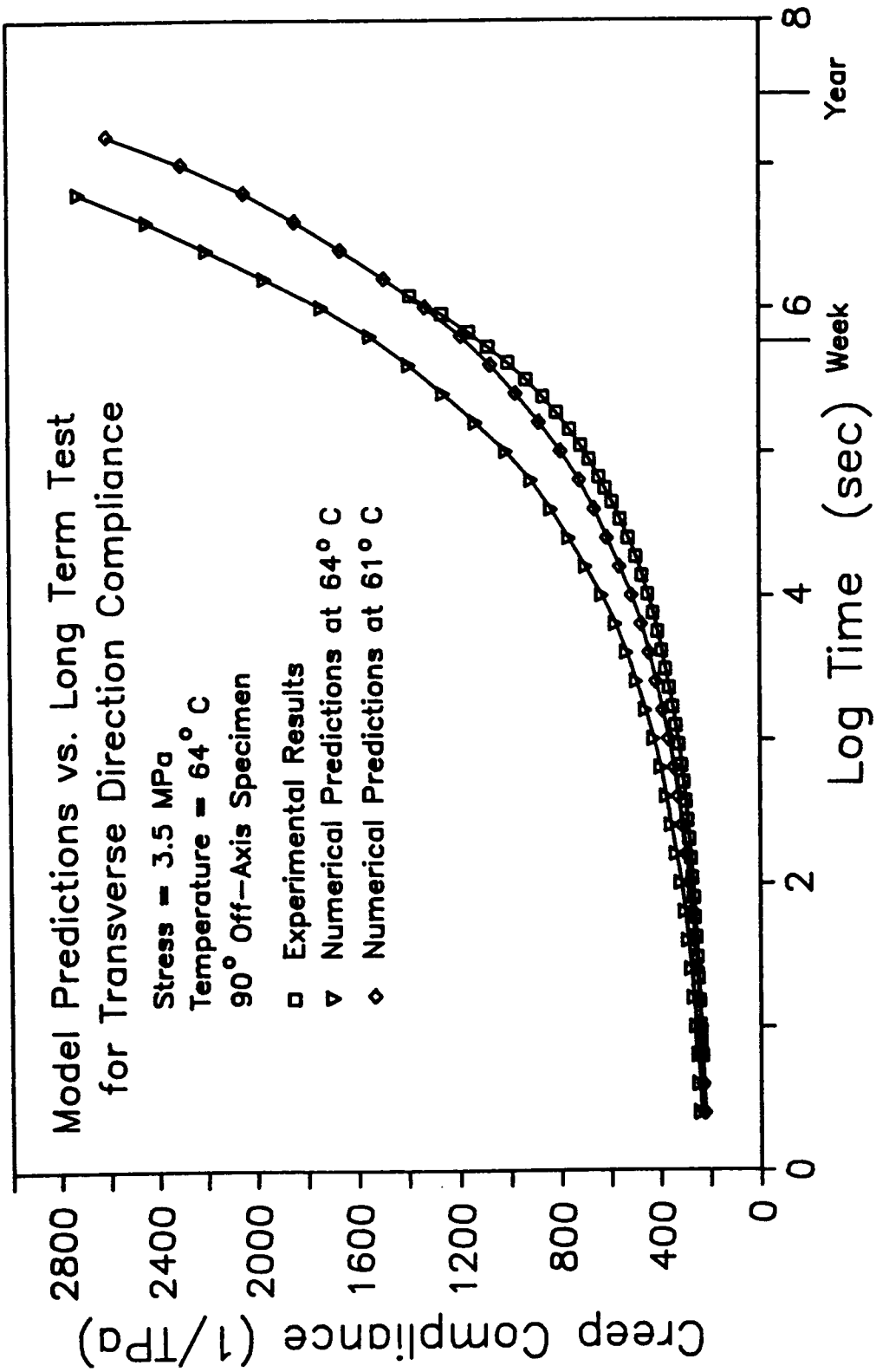

Fig. 6.3 Comparison of Numerical Predictions and Experimental Results for the Transverse Direction Compliance.

The last compliance term that was varied by medium term tests was the shear compliance, S_{66}. This test was on unidirectional 10° specimens at elevated temperature, 49° C, to verify the transition or the higher creep rate region. The results of the test, as shown in Fig 6.4, are slightly higher over the complete range of the test which could be attributed to a low shift factor at 49° C. However the trend is the same as the prediction.

The TTSP has been shown to be a reliable and accurate method to characterize long term properties of fiber reinforced composite materials. Medium length tests (2-4 weeks) for the creep compliance of S_{11}, S_{22}, and S_{66} agreed with the predicted compliance based on the master curve and models obtained from using the TTSP. Although long term tests have not been done to verify the complete master curve, the medium length tests confirm the trend for each material property.

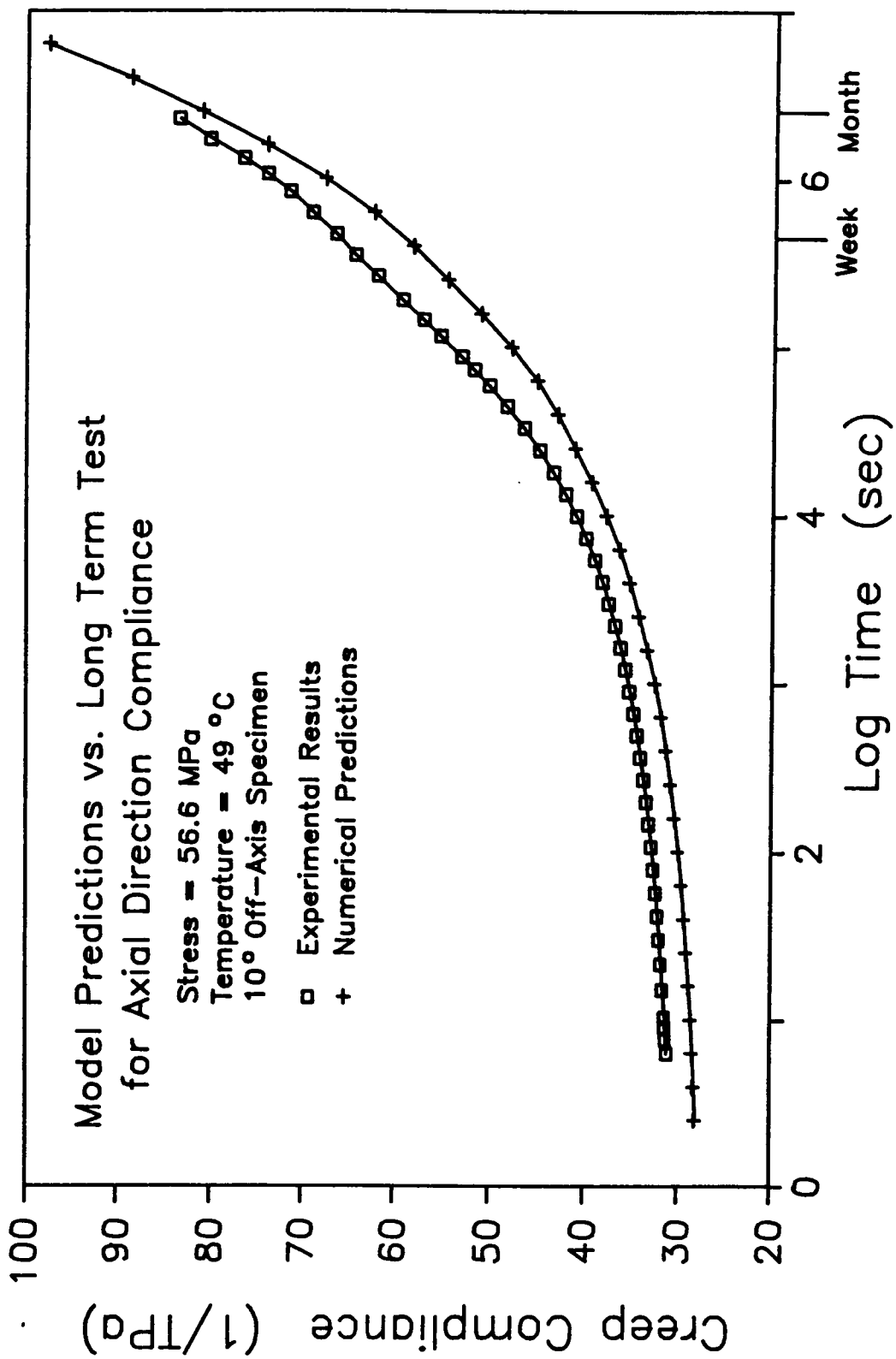

Fig. 6.4 Comparison of Numerical Predictions and Experimental Results for the Shear Compliance.

Chapter 7

ACTUAL LAMINATE CREEP RESPONSE VERSUS PREDICTION

The ultimate objective in characterizing and modeling a composite lamina is to predict the response of laminates constructed from the lamina. Chapter 3 outlined a numerical procedure to use the lamina models to predict the general response of any laminate. This chapter will present the creep test results conducted at various temperatures and stresses levels for two to four weeks on several laminates consisting of two, three, and four fiber directions. These results will be compared to the predicted values obtained from the computer program VCAP, which uses the numerical procedure presented in chapter 3 and described in Appendix C.

Two Fiber Direction Laminates

Three different types of two fiber direction laminates were tested, $[\pm 45]_{2s}$, $[30/-60]_{2s}$, and $[15/-75]_{2s}$. All three came from the same basic laminate cross-ply laminate, $[90/0]_{2s}$.

The first set of tests were done at elevated temperature, 49° C in order to rigorously check the prediction. By using a test temperature other than the reference temperature, the numerical prediction must use both the viscoelastic laminate model and shift factor function developed for each of the four compliance terms. The results for the $[30/-60]_{2s}$ and $[15/-75]_{2s}$ laminates, shown in

Fig. 7.1, agree well with the predictions but the results for the two $[\pm 45]_{2s}$ specimens were high at the start and low toward the end of the test. The beginning discrepancy could be the result of scatter between specimens, but the reason for the lower creep rate at the end of the test (2-3 weeks) is not known. Even though the two $[\pm 45]_{2s}$ specimens were tested at different stress levels, 10.7 and 13.0 MPa, nonlinear stress effects were not evident in the actual tests or the predictions. The strains are in the 0.5% range.

A second set of two tests were performed on the $[\pm 45]_{2s}$ type laminate to better understand the discrepancy between actual and predicted creep compliance. The tests were done at 32° C, the TTSP reference temperature, using different specimens at about 38 MPa for each. The results are shown in Fig. 7.2. The agreement between the actual results and predictions are better than the first set of $[\pm 45]_{2s}$ tests for both the elastic and viscoelastic portions. The two tests do show some scatter between themselves and the prediction but it is within expected bounds.

Three Fiber Direction Laminates

A total of six laminates constructed with three different fiber orientations were tested. The first set of three laminates included $[90_2/45/-45]_s$, $[45_2/0/90]_s$, and $[20_2/-25/65]_s$. The tests were performed at 70° C to again insure a rigorously check on the actual results and prediction comparison. The creep compliance for all three laminates are shown in Fig. 7.3. The experimental results for the

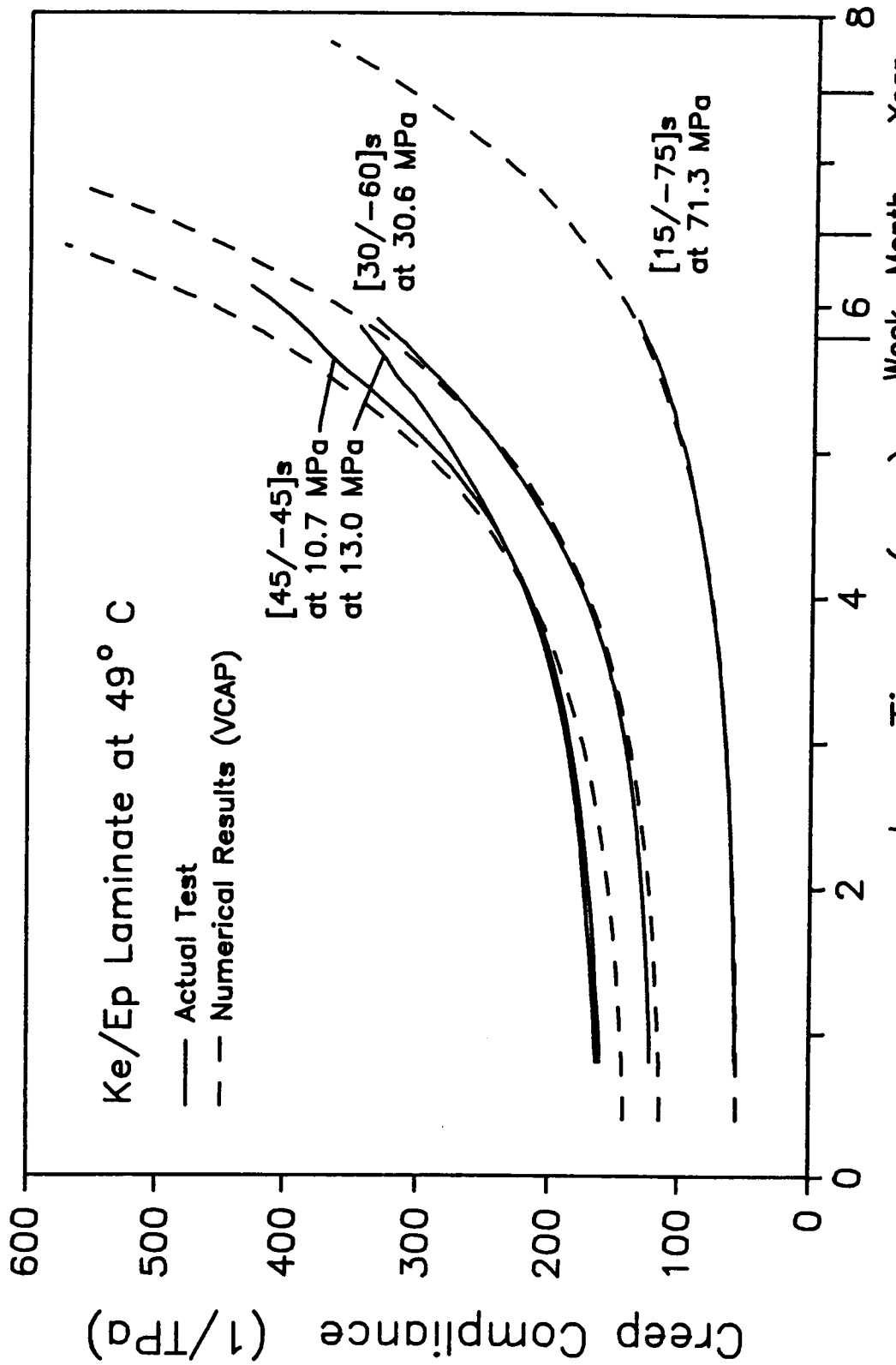

Fig. 7.1 Numerical Predictions and Actual Test Results for Cross Ply Laminates.

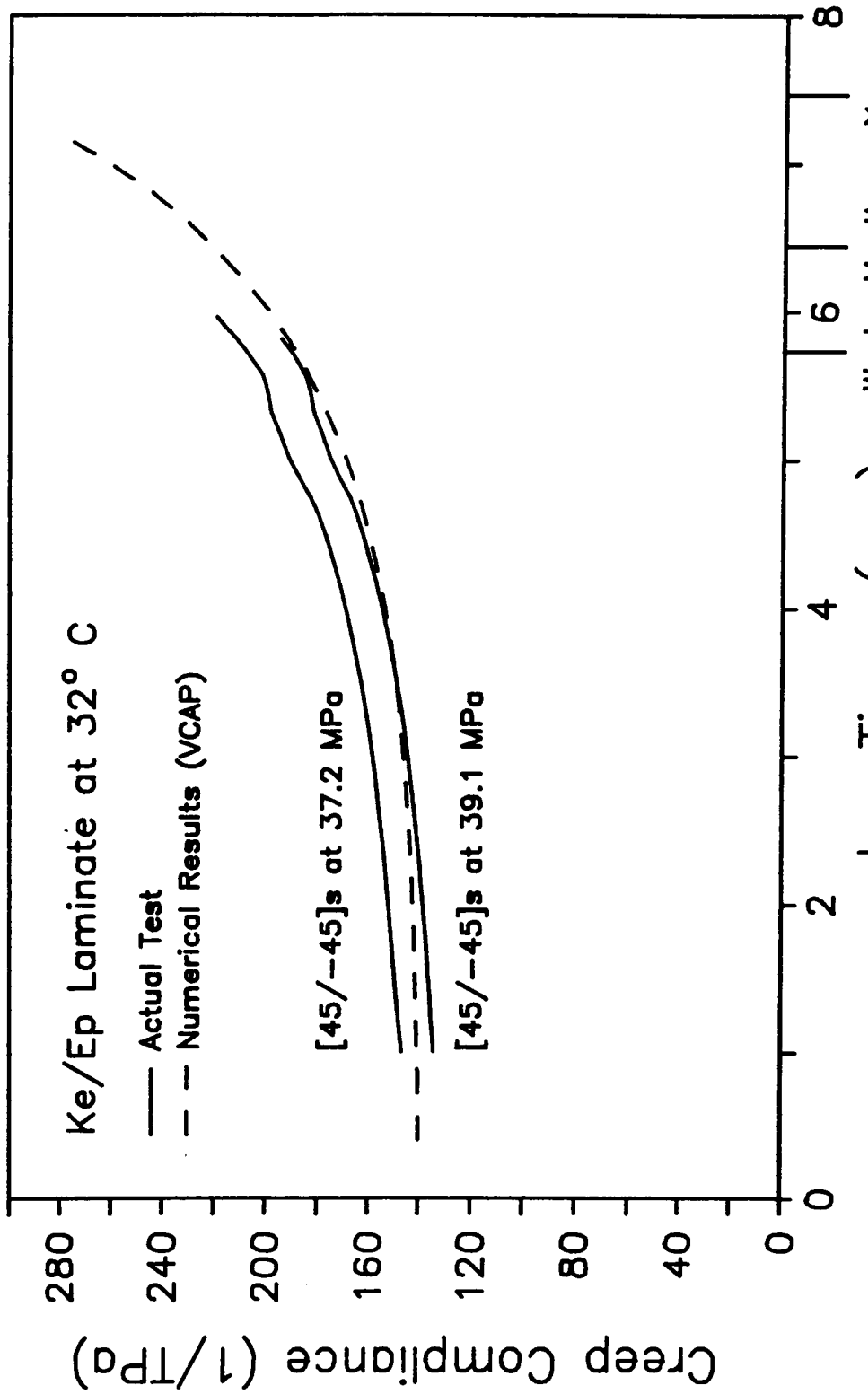

Fig. 7.2 Numerical Predictions and Actual Test Results for [45/−45]s Laminates.

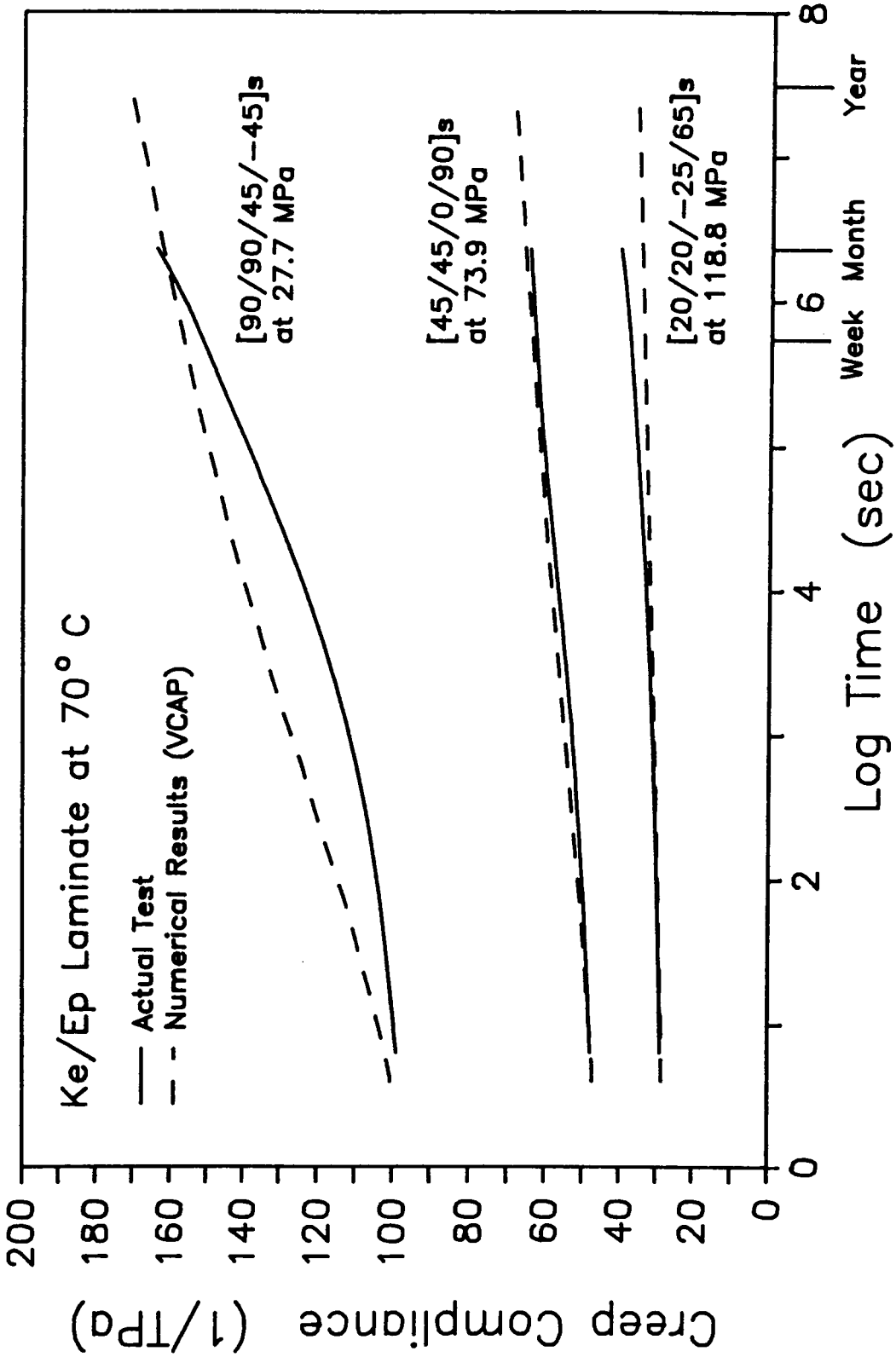

Fig. 7.3 Numerical Predictions and Actual Test Results for Three Fiber Direction Laminates.

$[45_2/0/90]_s$ and $[20_2/-25/65]_s$ laminates match well with the numerical predictions. However, the creep compliance for the $[90_2/45/-45]_s$ laminate increases slower than the prediction for the first few minutes of the test but then increases faster after a day. One possible explanation for the higher creep at long times is that the specimen has undergone damage and thus causes a higher creep rate. However, additional tests done on different $[90_2/45/-45]_s$ laminates at 49° C showed good agreement with predictions, Fig. 7.4, which suggests that some type of experimental error contributed to the actual and predicted compliance not matching. While damage certainly can contribute to creep, this study assumed that the load levels where low enough not to inflict damage to the test specimens, but in the future studies damage and its effect on creep should be examined. Another source of error is the fiber truss problem, (chapter 4) which theoretically restricts the total creep of a three or more fiber direction laminate of infinite width. Although 1 inch wide specimens were used to minimize the fiber truss effect, higher than predicted creep rate is possible. One final note, the stress level didn't effect the creep compliance, Fig. 7.4, as was predicted by the numerical procedure.

The second of three laminates, consisting of $[0_2/45/-45]_s$, $[-10_2/-55/-35]_s$, and $[-20_2/-65/25]_s$, were tested at 65° C. These laminates were tested to investigate the effect of off-axis loading on a typical laminate used in industry, which is analogous to loading a $[0_2/45/-45]_s$ laminate in the 0°, 10°, and 20° directions. The results

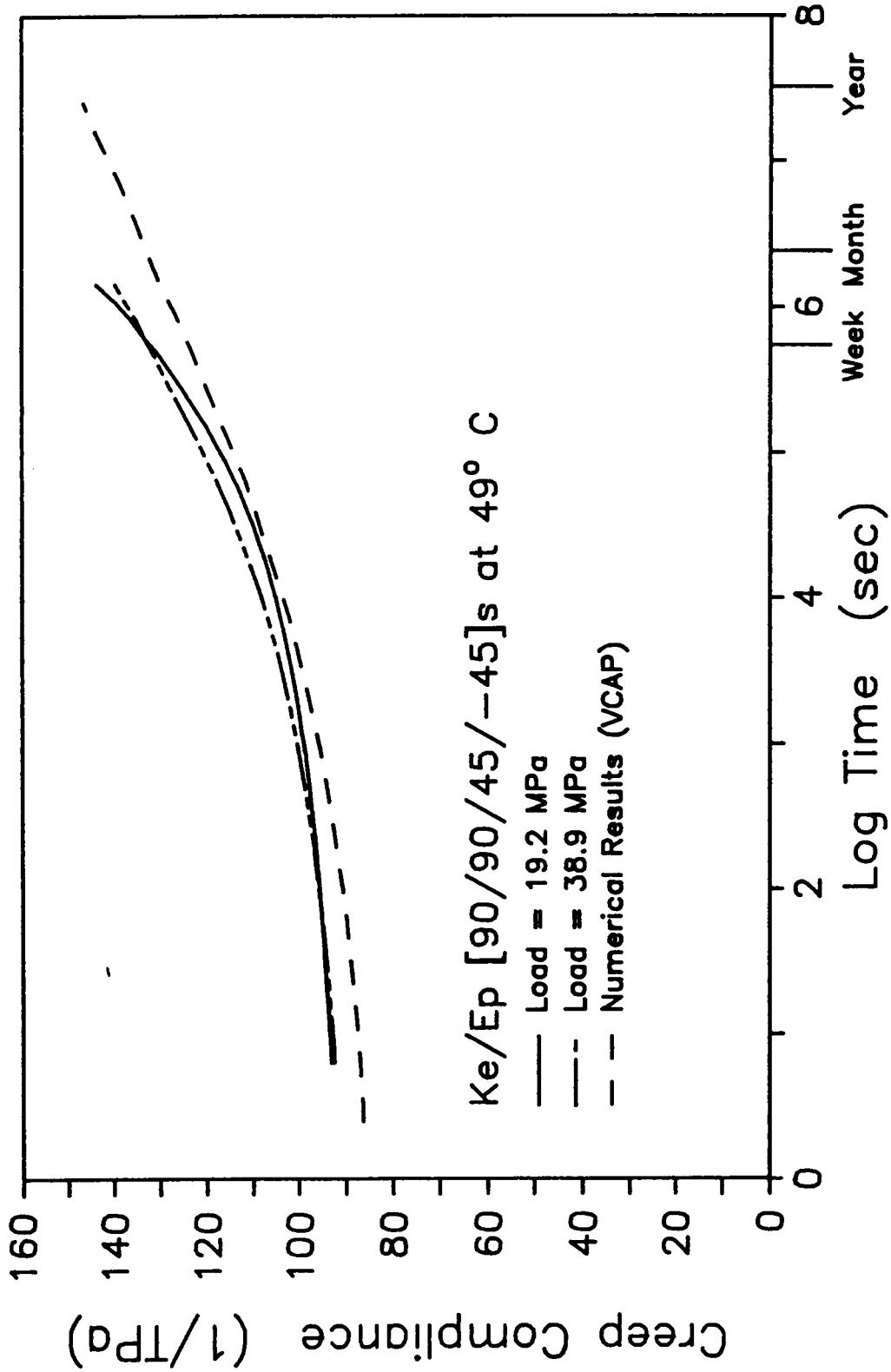

Fig. 7.4 Numerical Predictions and Actual Test Results for Three Fiber Direction Laminates.

are shown in Fig. 7.5 along with the numerical predictions. As would be expected, the further off-axis the laminate is loaded, the greater the creep compliance. However the actual tests show the difference much greater than the numerical procedure predicts. The numerical predictions indicate that the creep compliance for the $[0_2/45/-45]_s$ and $[-10_2/-55/-35]_s$ to be nearly equal, however the test results show them about 6% different. This could be due to both specimen differences and scatter, and from edge effects being greater in the off-axis specimens. More important, the creep rate is similar for all three laminates and predictions.

Four Fiber Direction Laminates

The last type of laminates tested were four direction laminates. The laminates tested were two $[90/-45/45/0]_s$, one $[10/55/-35/-80]_s$, and one $[20/65/-25/-70]_s$, which once again simulate off-axis loading effects. All four laminates are classified as quasi-isotropic which means that the material properties are the same in any direction, if the material is linear. Since the nonlinear viscoelastic response is minor for the fiber direction, which is dominant in this type of laminate, they should also be quasi-isotropic in terms of viscoelastic response. The test results, Fig. 7.6, show the creep compliance of all four laminates are indeed similar and the predictions are identical for all laminates. The experimental results do match the predictions fairly well, with the exception of same elastic strain scatter between specimens, and more importantly, the creep rate of all

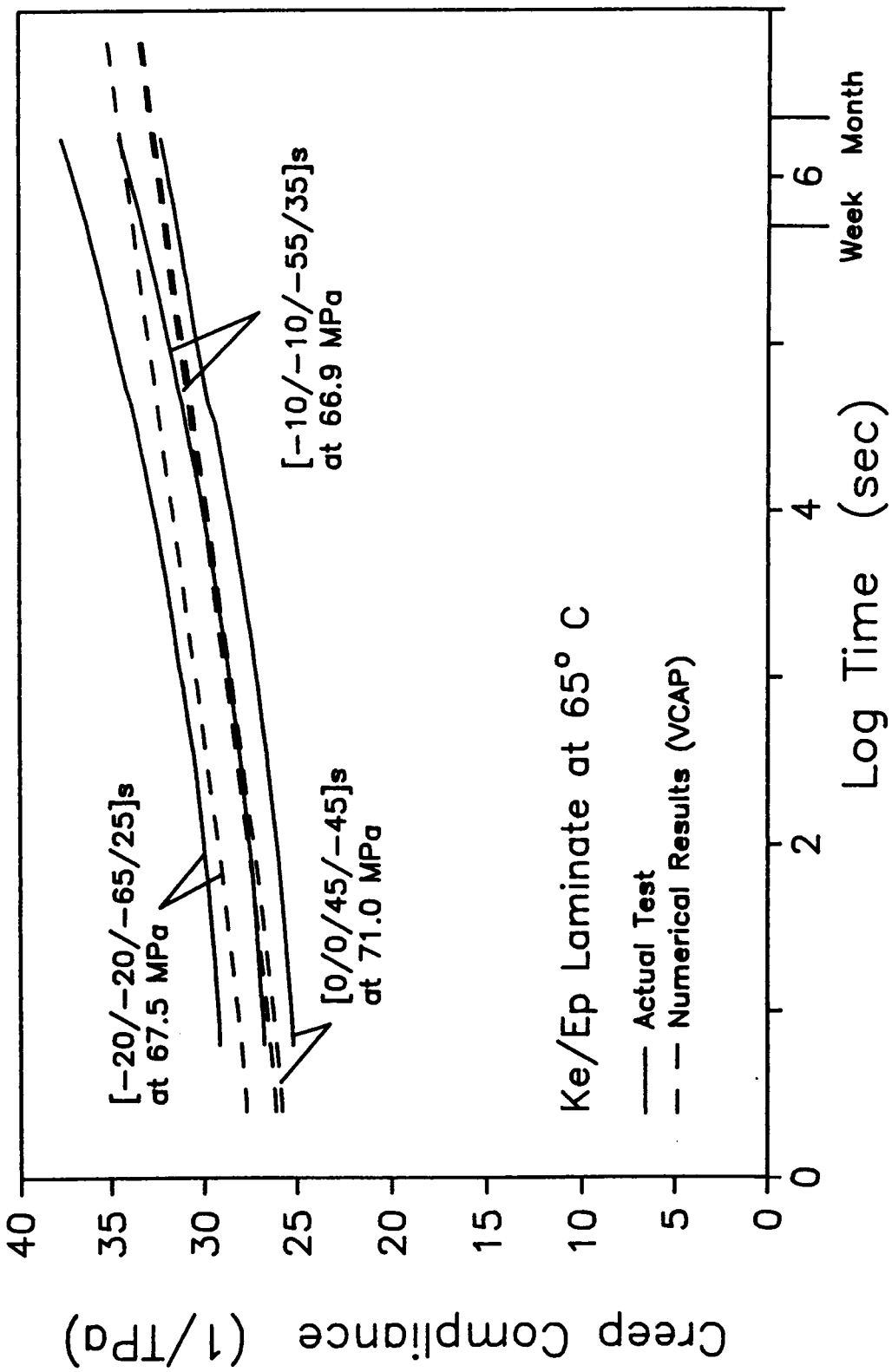

Fig. 7.5 Numerical Predictions and Actual Test Results for Three Fiber Direction Laminates.

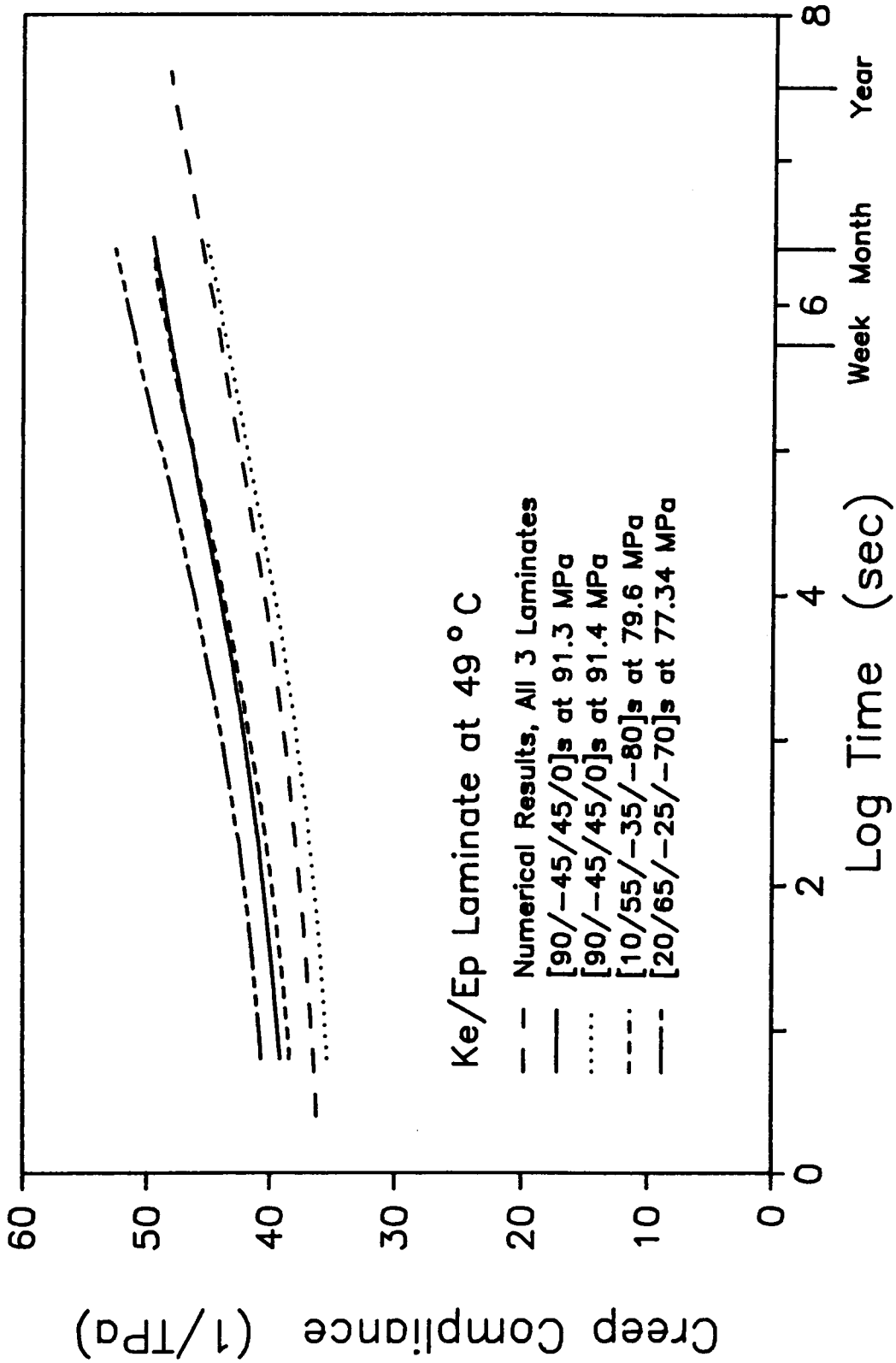

Fig. 7.6 Numerical Predictions and Actual Test Results for Four Fiber Direction Laminates.

laminates matches the prediction.

Nonlinear Stress Effects

Although nonlinear stress effects were modeled for all four compliance material properties, they were found to be insignificant except for the shear compliance, S_{66}. Even so, it was thought that the laminates of two or more fiber directions might exhibit some nonlinear stress effects. In order to identify these effects, laminates similar to those previously tested, were tested at a series of stress levels ranging from about 5-10% to 60-70% of ultimate which corresponds to roughly to 0.1-0.8% strain.. For each series of stress levels the same specimen was used and the temperature was held constant. If different specimens were used for each stress level, the scatter between specimens are enough to make identifying stress effects impossible since the nonlinear effects are so small. The length of each test was four to six hours which was longer than the characterization test but shorter than the long term confirmation tests discussed earlier in this chapter.

The first type of laminates tested were constructed with two fiber direction, $[30/-60]_{2s}$ and $[15/-75]_{2s}$. Since these laminates experience significant shear stresses between plies they should be sensitive to nonlinear stress effects. The results shown in Fig. 7.7 do show a slight stress effect in the actual tests but it is not dominant. The magnitude of the stress effect is predicted by the numerical procedure, VCAP, is also shown in Fig. 7.7. The $[15/-75]_{2s}$

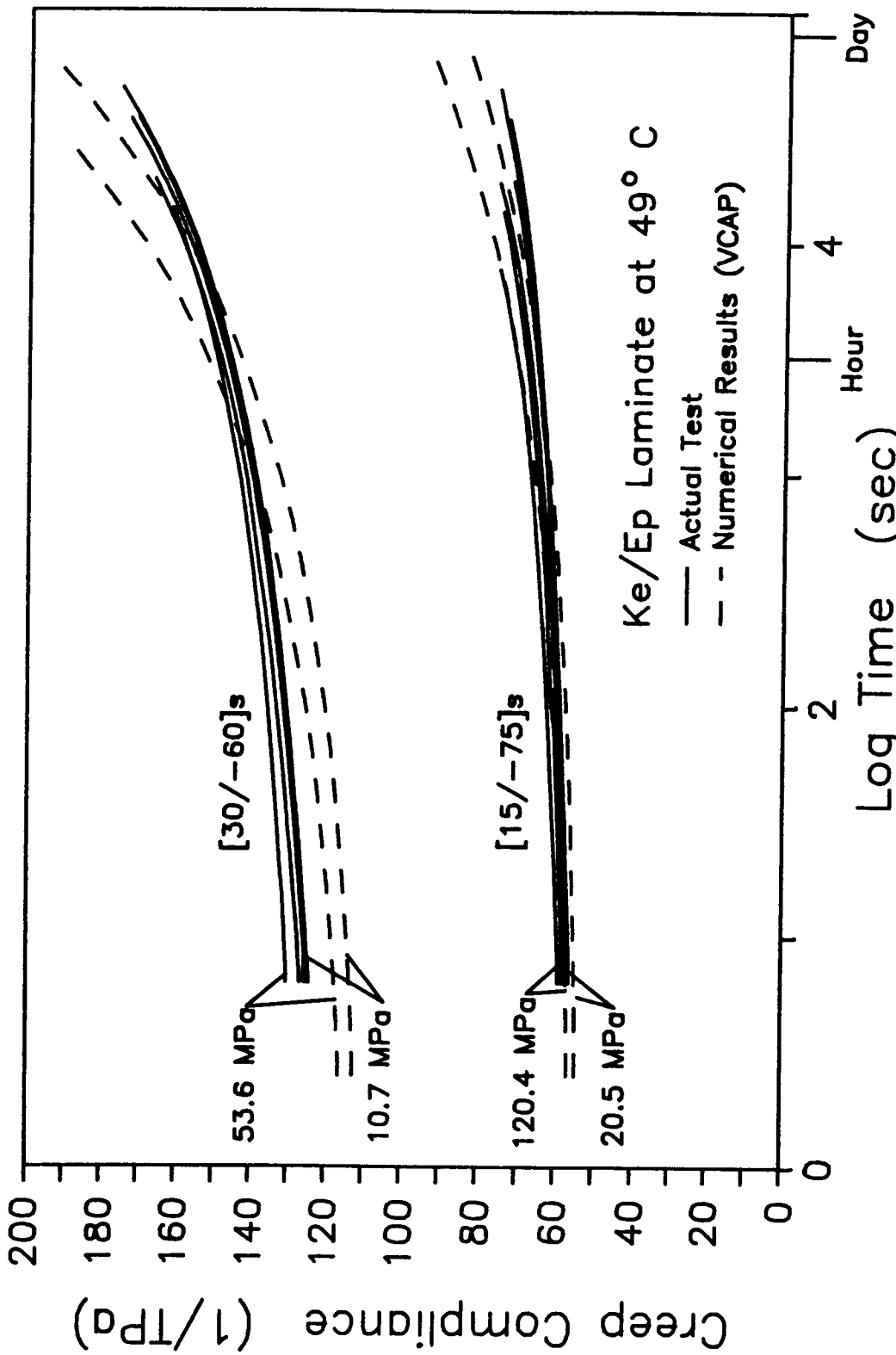

Fig. 7.7 Numerical Predictions and Actual Test Results for Two Fiber Direction Laminates at Various Stress Levels.

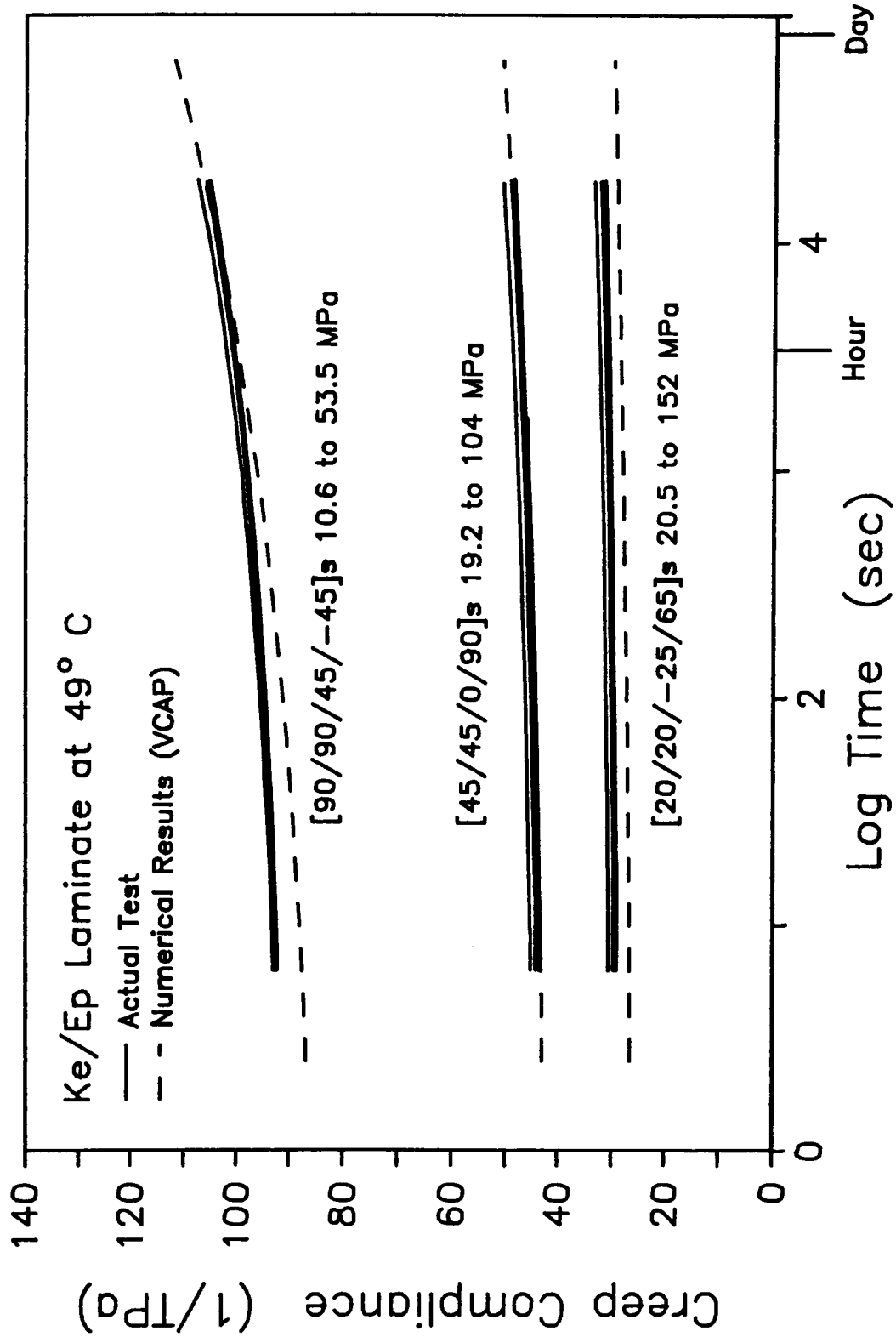

Fig. 7.8 Numerical Predictions and Actual Test Results for Three Fiber Direction Laminates at Various Stress Levels.

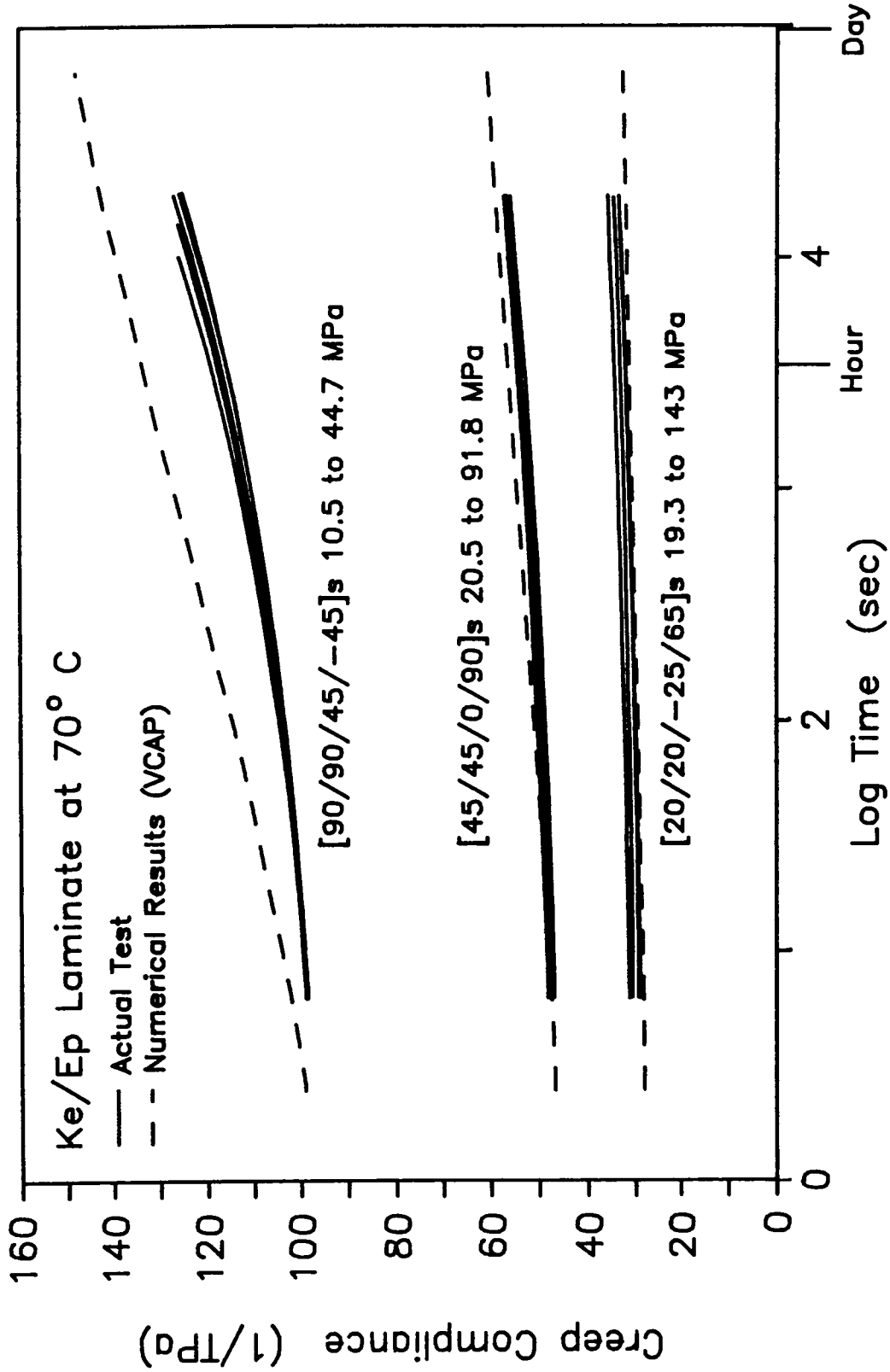

Fig. 7.9 Numerical Predictions and Actual Test Results for Three Fiber Direction Laminates at Various Stress Levels.

laminate agrees with the prediction well for both the compliance value and for the magnitude. However the compliance for $[30/-60]_{2s}$ laminate is higher than predicted and the rate of change is lower. The magnitude of the stress effects is however close to the predicted compliance.

The second type of laminates tested for stress effects had fibers running in three different fiber directions, $[20_2/-25/65]_s$, $[45_2/0/90]_s$, and $[90_2/45/-45]_s$. These laminates were tested at two different temperature levels to identify if temperature had an accelerating effect on the nonlinear stress effects. Different specimens were used at each of the two temperature levels. Again the strain levels ranged from 0.1% to about 0.8% which is the expected operating range for these composites in actual applications. The results for the 49° C and 70° C are shown in Figs. 7.8 and 7.9 respectively. The nonlinear stress for all laminates at both temperature levels is minor and what effect is shown could be considered within experimental error. The predicted nonlinear stress effect is less than 0.5% and is not identifiable in the figures. In conclusion, the nonlinear stress effects are slight or nonexistent in most laminates. Only the two fiber directions laminates, with their large shear stress, show any evidence of the nonlinear stress effect.

For both temperatures, the $[20_2/-25/65]_s$ and $[45_2/0/90]_s$ laminates did match well with the predictions for the compliance which is similar to the long term test presented in the previous sections. Again, the $[90_2/45/-45]_s$ laminate did not match as well at the high

temperature but did agree well at the lower temperature.

Chapter 8

SUMMARY, RECOMMENDATIONS, AND CONCLUSIONS

Summary of Work

This study investigated the thermoviscoelastic characterization and prediction of Kevlar/epoxy laminates. The work consisted of five basic areas; the thermoviscoelastic characterization of the four material properties of a orthotropic composite lamina, the development of a constitutive model describing the nonlinear viscoelastic properties, the development of a new numerical procedure to predict long term laminate properties without time constraints and numerical instabilities, the installation of the new numerical procedure into a microcomputer based program to facilitate ease of use, and the verification of the accelerated characterization process and numerical procedure by conducting long term creep tests. All five aspects were successfully accomplished in this study with the end result being a user friendly, microcomputer program that can be used by design engineers in industry to predict thermoviscoelastic properties of orthotropic composite materials.

A Kevlar/epoxy composite system was examined in this study since all four materials properties are viscoelastic which is unlike the previously studied graphite/epoxy composites with only two material properties viscoelastic. This allowed a more complete study of viscoelastic response of orthotropic materials and a rigorous check

for the numerical procedure to predict general laminate response.

The characterization process involved using three types of unidirectional composite laminates, [0°], [10°], and [90°] to determined the four independent material properties associated with FRP composites. An accelerated characterization technique developed and used previously at VPI&SU [72-82] for graphite/epoxy composite systems was employed. The technique involved using the Time-Temperature-Superposition-Principle to construct master curves for up to 14 decades of time from short term tests of only 15-20 minutes of length. This technique worked surprising well and the master curves were subsequently used to model the viscoelastic response of each of the four material properties. As an added benefit, the TTSP produced shift factor functions which enabled the model and numerical procedure to incorporate the effects of temperature. The characterization process also included nonlinear stress effects on long term compliance. However, only the shear compliance had any detectable nonlinear stress effect.

The experimentally developed master curves for creep compliance were used to develop the constitutive equations. Three types of models were examined, the Schapery integral, Findley power law and a newly proposed quadratic power law. While all three are basically empirical functions with equal chances of success, the quadratic power law was implemented because of its simpler form and for its easier numerical implementation. Only creep data was used to determine the 5 independent material properties for each compliance term even though

creep recovery data was available. This study showed that both creep and creep recovery data can be used equally well in determining the 'n' exponent value of the power law, but the creep recovery method has a significantly higher standard deviation and is more prone to error. The nonlinear stress parameter used to describe the stress effects on the compliance was also examined. While most nonlinear viscoelastic models use the matrix octahedral shear stress as the nonlinearizing parameter, this study used the actual stress in the direction of the desired compliance model since the fibers aer also viscoelastic and the matrix octahedral shear stress method cannot apply to the fiber direction compliance.

Originally, this study planned to use a previously developed numerical algorithm [77] to predict the viscoelastic response of general laminates. However, due to numerical instabilities and time limitations, a new procedure was developed. By using a nonlinear differential equation formulation based on a Kelvin element, a procedure was developed that is stable for all time step sizes and for non-positive definite stiffness matrices. In addition, the past stress and strain history does not need to be stored nor does the calculation time increase exponentially with each time step, as was previously the case. This allows very long time spans, i.e. 10^{20} seconds, to be accurately calculated within computer time restraints. The new numerical formulation also uses a 2^{nd} order solution technique which enables higher accuracy.

The most important benefit of the new procedure, with its reduced

need for computer time, was the ability to program the procedure on a microcomputer. There are many advantages of having the program run on an IBM PC type microcomputer, such as portability, ease of use, inexpensive operation, large installed base, etc. The program, called 'VCAP' (Viscoelastic Composite Analysis Program), incorporates help screens, graphics, menus, error analysis, and other features which allow the program to be easily used by industry.

The last part of this study involved verification of the TTSP acceleration technique and numerical predictions of general laminates constructed of Kevlar/epoxy. To check the validity of the TTSP, two to four week long term tests were conducted at various temperatures on different unidirectional specimens. The compliance curves from these longer term tests matched well with the results generated using the TTSP method. In some cases, however, the temperature was shown to greatly affect the creep compliance curve and thus cause some differences between TTSP results and actual results. Over a dozen different laminates, two, three, and four fiber direction types, were tested for up to four weeks. Overall, the agreement was very good between the numerical predictions and actual creep test results.

In summary, this study has successfully characterized a Kevlar/epoxy composite, modeled the thermoviscoelastic properties, developed a robust numerical procedure to predicting laminate viscoelastic response, and verified the above accomplishments with actual laminate creep tests.

Recommendations

While the objectives of this study were accomplished there are still a tremendous number of unanswered questions about the thermoviscoelastic characterization of composite laminates. The most noticeable deficiency of the this study is the limitations of the numerical procedure of only being able to predict point stresses and strains for in-plane loading cases. Work should be done to extend the procedure to include bending or moment loads and eventually out of plane loadings. Also, composite structures with non-uniform stress and strain fields need to be understood. To include these type of capabilities, the numerical procedure needs to be used in conjunction with a finite element procedure instead of the using the Classical Lamination Theory assumptions which currently being done. Although by using a finite element based procedure, the simple and easy to use program concept is no longer possible, and a microcomputer and its advantages can no longer be used.

Moisture, along with adsorption and desorption, needs to be included in the viscoelastic model since composite are affected by water in a similar manner as temperature. Along these same lines, the effect of temperature and stress variation or cycling on the viscoelastic properties needs to be better investigated since few composite structures experience only one temperature and stress level during its service life.

A large research effort is currently being devoted to understanding damage of composites. This effort needs to be extended

to the viscoelastic properties. Some of the laminates tested in creep did not match the predicted creep compliance which could have been associated with damage. This subject of damage is large and very complex and will require a long devoted effort.

In conjunction with damage, is the prediction of viscoelastic failure or time-to-rupture of composites. While this has been previously studied [76] for graphite/epoxy system with some success, there is still a tremendous amount of fundamental work to be done to fully understand when and how failure will occur at extended periods of time.

This study chose to characterize the unidirectional composite lamina and then predict any laminate constructed from lamina layers. Another and more fundamental approach would be to characterize the resin and fibers separately and then predict the lamina properties and eventually the laminate properties. While this approach has been used for elastic properties, it has not been accomplished for viscoelastic properties. There are many additional variables at the micro level that must be considered such as adhesion, debonding, chemical interdispersion between fibers and matrix, etc, which will make the task both difficult and challenging.

Conclusions

The composite industry has grown from being an infant who was unable to support himself, to a teenager, who has a tremendous amount of unrealized potential but still has a lot of learning to do. The

long term material properties of composites need to be better understood and methods to predict these properties, are vital to the continued use and growth of these new materials. This study has hoped to extend man's knowledge and understanding of composite materials so that they will be more fully utilized and their true potential can be reached.

REFERENCES

1. Ferry, J.D., Viscoelastic Properties of Polymers, Third Edition, Wiley, New York, 1980.

2. Biot, M.A., "Theory of Stress-Strain Relations in Anisotropic Viscoelasticity and Relaxation Phenomena," Journal of Applied Physics, Vol. 25, No. 11, 1954, pp. 1385-1391.

3. Krokosky, E., "Behavior of Time-Dependent Composite Materials," Modern Composite Materials, L.J. Broutman and Krock (Eds.), Chapter 4, Addison Wesley, 1967, pp. 120-145.

4. Williams, M.L., R.F. Landel and J.D. Ferry, "The Temperature Dependence of Relaxation Mechanisms in Amorphous Polymers and Other Glass-forming Liquids," Journal of the American Chemical Society, Vol. 77, 1955, pp. 3701-3706.

5. Wang, A.S.D., E.J. McQuillen and A.S. Ahmadi, "Analytical and Experimental Investigation of Time-Temperature Creep of Graphite-Epoxy Composite Laminates," unpublished paper, Drexel University.

6. Hopkins, I.L. and R.W. Hamming, "On Creep and Relaxation," Journal of Applied Physics, Vol. 28, No. 8, 1957, pp. 906-909.

7. Brody, H., "Stress-Time Superpositions as an Aid to Creep Evaluation," Plastics and Polymers, Feb. 1969.

8. Rosen, S.L., Fundamental Principles of Polymeric Materials, John Wiley, New York, 1982.

9. Christensen, R.M., Theory of Viscoelasticity - An Introduction, Second Edition, Academic Press, New York, 1982.

10. Flugge, W., Viscoelasticity, Second Edition, Springer-Verlag, New York, 1975.

11. Findley, W.N., J.S. Lai and K. Onaran, Creep and Relaxation of Nonlinear Viscoelastic Materials, North-Holland Publishing Company Amsterdam, New York, 1972.

12. Rabotnov, Y.N., Elements of Hereditary Solid Mechanics, MIR Publishers, Moscow, 1980, (English Translation).

13. Lockett, F.J., Nonlinear Viscoelastic Solids, Academic Press, London, 1972.

14. Halpin, J.C., "Introduction to Viscoelasticity," Composite Materials Workshop, Technomic, 1968, pp. 87-152.

15. Halpin, J.C. and N.J. Pagano, "Observations on Linear Anisotropic Viscoelasticity," Journal of Composite Materials, Vol. 2, No. 1, 1968, pp. 68-80.

16. Pagano, N.J. and J.C. Halpin, "Influence of End Constraint in the Testing of Anisotropic Bodies," Journal of Composite Materials, Vol. 2, No. 1, 1968, pp. 18-31.

17. Dillard, D.A. "Viscoelastic Behavior of Laminated Composite Materials," book chapter to be published 1988.

18. Sims, D.F. and J.C. Halpin, "Methods for Determining the Elastic and Viscoelastic Response of Composite Materials," Composite Materials, Testing and Design (Third Conference), ASTM STP 546, 1974.

19. Jones, R.M., Mechanics of Composite Materials, McGraw-Hill, New York, 1975.

20. Tsai, S.W. and H.T. Hahn, Introduction to Composite Materials, Technomic, Westport, Connecticut, 1980.

21. Halpin, J.C., Primer on Composite Materials, Revised, Technomic, Westport, Connecticut, 1984.

22. Lekhnitskii, S.G., Theory of Elasticity of an Anisotropic Body, MIR Publishers, Moscow, 1981, (English Translation).

23. Findley, W.N., and G. Khosla, "Application of the Superposition Principle and Theories of Mechanical Equation of State, Strain, and Time Hardening to Creep of Plastics Under Changing Loads," Journal of Applied Physics, Vol. 26, No. 7, 1955, pp. 821-831.

24. Findley, W.N. and J.S.Y. Lai, "A Modified Superposition Principle Applied to Creep of Nonlinear Viscoelastic Material Under Abrupt Changes in State of Combined Stress," Transaction of the Society of Rheology, Vol. 11, No. 3, 1967, pp. 361-381.

25. Lai, J.S. and W.N. Findley, "Creep of 2618 Aluminum Under Step Stress Changes Predicted by a Viscous-Viscoelastic Model," Journal of Applied Mechanics, Vol. 47, No. 21, Mar. 1980, pp. 21-26.

26. Findley, W.N., U.W. Cho and J.L. Ding, "Creep of Metals and Plastics Under Combined Stresses, A Review," Journal of Engineering Materials and Technology, Vol. 101, Oct. 1979, pp. 365-368.

27. Findley, W.N., C.H. Adams and W.J. Worley, "The Effect of Temperature on the Creep of Two Laminated Plastics as Interpreted by the Hyperbolic Sine Law and Activation Energy Theory," ASTM Proc., 48, 1948, pp. 1217-4239.

28. Findley, W.N. and D.B. Peterson, "Prediction of Long-Term Creep with Ten-Year Creep Data on Four Plastics Laminates," ASTM Proc., 58, 1958, pp. 841-855.

29. Schapery, R.A., "Stress Analysis of Viscoelastic Composite Materials," Journal of Composite Materials, Vol. 1, 1967, p. 228 (see also Composite Materials Workshop, Technomic, Stamford, 1968.

30. Lou, Y.C. and R.A. Schapery, "Viscoelastic Characterization of a Nonlinear Fiber-Reinforced Plastic," Journal of Composite Materials, Vol 5, 1971, pp. 208-234 (see also Tech. Report AFML-TR-70-113, Air Force Materials Laboratory, Wright-Patterson AFB, May 1970).

31. Schapery, R.A., "Viscoelastic Behavior and Analysis of Composite Materials," Composite Materials, G.P. Sendeckyj (Ed.), Chapter 4, Vol. 2, Academic Press, p. 85, 1974.

32. Schapery, R.A., "Effect of Cyclic Loading on the Temperature in Viscoelastic Media with Variable Properties," AIAA Journal, Vol. 2, No. 5, May 1964, pp. 827-835.

33. Schapery, R.A., "A Thermodynamic Constitutive Theory and Its Application to Various Nonlinear Materials," Int. J. Solids and Struct., Vol 2, No. 3, 1966, pp. 407-425.

34. Schapery, R.A., "Further Development of a Thermodynamic Constitutive Theory and Stress Formulation," A&ES Report No. 69-2, Purdue University, Feb 1969.

35. Ho, T., R.A. Schapery and B.C. Harbert, "The Viscoelastic Behavior of Kevlar/Epoxy Materials," LTV Aerospace Report, Contract No. DAAG46-83-C-0032, released thru U.S. Army Materials Technology Laboratory, Watertown, Mass., 1985.

36. Schapery, R.A., S.W. Beckwith and N. Conrad, "Studies on the Viscoelastic Behavior of Fiber-Reinforced Plastic," Air Force Technical Report AFML-TR-73-179, Texas A&M University, July 1973.

37. Koeller, R.C. "Applications of Fractional Calculus to the Theory of Viscoelasticity," Transactions of the ASME, Paper No. 84-APM-20, 1984.

38. Vautrin, A., "Generalization of the Thermorheologically Simple Behavior to Fiber Reinforced Behavior," Mechanics of Structured Media, A.P.S. Selvadurai (Ed.), Part B, Elsevier, 1981, pp. 57-69.

39. Brouwer, R., "Nonlinear Viscoelastic Characterization of Transversely Isotropic Fibrous Composites Under Biaxial Loading," Ph.D. Dissertation, University of Brussels, Belgain, 1986.

40. Knauss, W.G. and I.J. Emri, "Non-Linear Viscoelasticity Based on Free Volume Consideration," Computers and Structures, Vol. 13, Jan. 1981, pp. 123-128.

41. Knauss, W.G. and I.J. Emri, "Volume Change and the Non-Linearly Thermo-Viscoelastic Constitution of Polymers," Cal. Tech. SM Report 85-26, Oct. 1985.

42. Ferry, J.D. and R.A. Stratton, "The Free Volume Interpretation of the Dependence of Viscosities and Viscoelastic Relaxation Times and Concentration, Pressure, and Tensile Strain," Kolloid-Zeitschrift, Vol. 171 ,No. 2, 1960, pp.107-111.

43. Williams, M.L., "Free Volume Approach to Polystyrene Melt Viscosity," Journal of Applied Mechanics, Vol. 29, No. 10, Oct. 1958, pp. 1395-1398.

44. Schaffer, B.G. and D.F. Adams, "Nonlinear Viscoelastic Analysis of a Unidirectional Composite Materials," Journal of Applied Mechanics, Vol. 48, Dec. 1981, pp. 859-865.

45. Mohan, R. and Adams, D.F., "Nonlinear Creep-Recovery Response of a Polymer Matrix and its Composites," Experimental Mechanics, Vol. 25, No. 3, Sept. 1985, pp. 262-271.

46. Irion, M.N. and D.F. Adams, "Compression Creep Testing of Unidirectional Composite Materials," Composites, April, 1981, pp. 117-123.

47. Foye, R.L., "Creep Analysis of Laminates," Composite Reliability, ASTM STP 580, 1975, pp. 381-395.

48. Crossman, F.W. and D.L. Flaggs, "Dimensional Stability of Composite Laminates During Environmental Exposure," SAMPE Journal, Vol. 15, July/August 1979, pp. 15-20.

49. DeRuntz, Jr., J.A. and F.W. Crossman, "Time and Temperature Effects in Laminated Composites," Proc. of Conf. on Computer Simulation for Materials Applications, Gaithersburg, Md., Apr. 1976.

50. Min, B.K. and F.W. Crossman, "Analysis of Creep for Metal Matrix Composites," Journal of Composite Materials, Vol. 16, May 1982, pp. 188-203.

51. Crossman, F.W. and D.L. Flaggs, "Viscoelastic Analysis of Hygrothermally Altered Laminate Stresses and Dimensions," Lockheed Palo Alto Research Laboratory, Report No. LMSC-D633086, Nov. 1978.

52. Weitsman, Y., "On the Thermoviscoelastic Characterization of Adhesives and Composites," Progress in Science and Engineering of Composites, T. Hayashi, K. Kawata, and S. Umekawa (Eds.), ICCM-IV, Tokyo, 1982.

53. Jackson, S.P. and Y. Weitsman, "Moisture Effects and Moisture Induced Damage in Composites," Fifth International Conference on Composite Materials, ICCM-V, July 19 - Aug 1, W.C. Harrington Jr., J Strife and A.K. Dhingra (Eds.), The Metallurgical Society, Inc., 1985, pp. 1435-1452

54. Peretz, D and Y. Weitzman, "Nonlinear Viscoelastic Characterization of FM-73 Adhesives," Journal of Rheology, Vol. 26, No. 3, 1982, p. 245-261.

55. Peretz, D and Y. Weitzman, "The Nonlinear Thermoviscoelastic Characterization of FM-73 Adhesives," Journal of Rheology, Vol. 27, No. 2, 1983, pp. 97-114.

56. Weitsman, Y., "Residual Thermal Stresses Due to Cool-Down of Epoxy-Resin Composites," Journal of Applied Science, Vol. 46, Sept. 1979, pp. 563-567.

57. Charentanay, F.X. and M.A. Zaidi, "Creep Behaviour of Carbon-Epoxy [+45/-45o]2S Laminates," Progress in Science and Engineering of Composites, T. Hayashi, K. Kawata, and S. Umekawa (Eds.), ICCM-IV, Tokyo, 1982.

58. Vautrin, A., "Characterization of the Thermoviscoelastic Behavior of Kevlar 49/Epoxy Laminates," Proceedings of the European Colloquim 182, Mechanical Characterization of Load Bearing Composite Laminates, A.H. Cardon and G. Verchery (Eds.), Brussels, Aug 29-31, Elsevier Applied Science Publishers, New York, 1984, pp. 84-96.

60. Stratonova, M.M., "Calculation of One-Dimensional Polymer Creep Under Stepped Loading," Polymer Mechanics, Vol. 3, No. 4, 1967, pp. 671-675.

61. Gol'dam, A. Ya., "Nonlinear Viscoelastic Behavior of Polymer and Composite Materials with (Hydrostatic) Pressure-Dependent Properties," Fifth Annual All-Union Conference on the Mechanics of Polymer and Composite Materials, Riga, Oct. 1983, Pleum Publishing Corp. 1984, pp. 16-28.

62. Kovriga, V.V., et al., "Time-Temperature Superposition Applied to the Relaxation Properties of a Glass-Reinforced Plastic and Its Matrix," Polymer Mechanics, Vol. 8, No. 2, 1972, pp. 321-323.

63. Maksimov, R.D., V.P. Mochalov and Yu. S. Urzhumtsev, "Time-Moisture Superposition," Polymer Mechanics, Vol. 8, No. 5, 1972, pp. 685-689.

64. Maksimov, R.D., C.L. Daugste and E.A. Sokolov, "Characteristics of the Observance of Temperature-Time Analogy in Physically Nonlinear Creep of a Polymeric Material," Polymer Mechanics, Vol. 10, No. 3, 1974, pp. 350-358.

65. Maksimov, R.D., E.A. Sokholov and V.P. Mochalov, "Effect of Temperature and Moisture on the Creep of Polymeric Materials," Polymer Mechanics, Vol. 11, No. 3, 1975, pp. 334-339.

66. Maksimov, R.D., V.P. Mochalov and E.A. Sokholov, "Influence of Temperature and Humidity on the Creep of Polymeric Materials," Polymer Mechanics, Vol. 12, No. 6, 1976, pp. 859-864.

67. Urzhumtsev, Yu. S., "Time-Temperature Superposition for Thermorheological Complex Materials," Polymer Mechanics, Vol. 10, No. 2, 1974, pp. 180-185.

68. Stratonova, M.M., "Calculation of One-Dimensional Polymer Creep Under Stepped Loading," Polymer Mechanics, Vol. 3, No. 4, 1967, pp. 445-447.

69. Urzhumtsev, Yu. S., "Time-Temperature Superposition. Review," Polymer Mechanics, Vol. 11, No. 1, 1975, pp. 57-72.

70. Urzhumtsev, Yu. S. and R.D. Maksimov, "Multiparametric Prediction of the Creep of Polymer Materials," Polymer Mechanics, No. 3, 1970, pp. 357-364.

71. Skudra, A.M. and F. Ya Bulavs, "Strength and Creep Micromechanics of Composites," Mechanics of Composites, I.F. Obraztsov and V.V. Vasil'ev (Eds.), MIR Publishers, Moscow, 1982, (English Translation), pp. 80-109.

72. Morris, D.H., Y.T. Yeow and H.F. Brinson, "The Viscoelastic Behavior of the Principle Compliance Matrix of a Unidirectional Graphite/Epoxy Composite," Virginia Polytechnic Institute and State University, VPI-E-79-9, Blacksburg, Va, February 1979.

73. Griffith, W.I., D.H. Morris and H.F. Brinson, "The Accelerated Characterization of Viscoelastic Composite Materials," Virginia Polytechnic Institute and State University, VPI-E-80-15, Blacksburg, Va, April, 1980.

74. Dillard, D.A., D.H. Morris and H.F. Brinson, "Creep and Creep Rupture of Laminated Graphite/Epoxy Composites," Virginia Polytechnic Institute and State University, VPI-E-81-3, Blacksburg, Va, February 1981.

75. Tuttle, M.E. and H.F. Brinson, "Accelerated Viscoelastic Characterization of T300/5208 Graphite/Epoxy Laminates," Virginia Polytechnic Institute and State University, VPI-E-84-9, Blacksburg, Va, March 1984.

76. Hiel, C., A.H. Cardon and H.F.Brinson, "The Nonlinear Viscoelastic Response of Resin Matrix Composite Laminates," Virginia Polytechnic Institute and State University, VPI-E-83-6, Blacksburg, Va, March 1983.

77. Dillard, D.A. and H.F. Brinson, "A Numerical Procedure for Predicting Creep and Delayed Failures in Laminated Composites," Long Term Behavior of Composites, ASTM 813, T.K. O'Brain (Ed.), 1983, pp. 23-37.

78. Dillard, D.A., D.A. Morris and H.F. Brinson, "Predicting Viscoelastic Response and Delayed Failures in General Laminated Composites," Composite Materials: Testing and Design (Sixth Conf.), ASTM STP 787, I.M. Daniel(Ed.), 1982, pp. 357-370.

79. Tuttle, M.E., and H.F. Brinson, "Resistance Foil Strain Gage Technology as Applied to Orthotropic Composite Materials," Experimental Mechanics, Vol. 24, No. 1, Mar. 1984, pp. 54-65.

80. Brinson, H.F., "Viscoelastic Behavior and Lifetime (Durability) Predictions," Proceedings of the European Colloquim 182, Mechanical Characterization of Load Bearing Composite Laminates, A.H. Cardon and G. Verchery (Eds.), Brussels, Aug 29-31, Elsevier Applied Science Publishers, New York, 1984, pp. 3-20.

81. Dillard, D.A., M.R. Straight and H.F. Brinson, "The Nonlinear Viscoelastic Characterization of Graphite/Epoxy Composites," Polymer Engineering and Science, Vol. 27, No. 2, Jan. 1987, pp. 116-123.

82. Yen, S.C., C. Hiel and D.H. Morris, "Viscoelastic Response of SMC-R50 Under Different Thermomechanical Conditions," High Modulus Fiber Composites in Ground Transportation and High Volume Applications, ASTM STP 873, D.W. Wilson (Ed.), American Society for Testing and Materials, Philadelphia, 1985, pp. 131-143.

83. Horn, M.H., P.G. Riewald and C.H. Zweben, "Strength and Durability Characteristics of Ropes and Cables from Kevlar Aramid Fibers," Oceans '77 Conference, Los Angles, Calf., Oct 17-19, 1977.

84. Miner, L.H., R.A. Wolffe and C.H. Zweben, "Fatigue, Creep, and Impact Resistance of Aramid Fiber Reinforced Composites," Composite Reliability, ASTM STP 580, 1975, pp. 549-559.

85. Conway, J.B., Numerical Methods for Creep and Rupture Analyses, Gordon and Breach, Science Publishers, New York, 1977.

86. Donea, J., "The Application of Computer Methods to Creep Analysis," Creep of Engineering Materials and Structures, Chap. 12, G. Bernasconi and G. Piatti (Eds.), Applied Science Publication, London 1978, pp. 341-359.

87. Zienkiewicz, O.C., M. Watson and I.P. King, "A Numerical Method of Viscoelastic Stress Analysis," Int. J. Mech. Sci., Vol. 10, 1986, pp. 807-827.

88. Booker, J.R. and J.C. Small, "An Investigation of the Stability of Numerical Solutions of the Equations of Viscoelasticity," International Journal for Numerical Methods in Engineering, Vol. 11, 1977, pp. 1819-1830.

89. Henriksen, M., "Nonlinear Viscoelastic Stress Analysis - A Finite Element Approach," Computers and Structures, Vol. 18, No. 1, 1984, pp. 133-139.

90. Laws, N. and R. McLaughlin, "Self-Consistent Estimates for the Viscoelastic Creep Compliances of Composite Materials," Proc R Soc London A, Vol. 359, No. 1697, Feb 1978, pp. 251-273.

91. Calabrese, S.J. and P. Smith, "Method of Determining Creep Characteristics of Composite Materials," Proc. Intersoc Energy Convers Eng Conf 16th, Vol 1., Atlanta, Ga., 1981, pp. 871-874.

92. Pipes, R.B. and B.W. Cole, "On the Off-Axis Strength Test for Anisotropic Materials," Journal of Composite Materials, Vol 7., April 1973, pp. 246-257.

93. Pindera, M.J. and C.T. Herakovich, "An Endochronic Model for the Response of Unidirectional Composite under Off-Axis Tensile Load," Mechanics of Composite Materials, Recent Advances, Proc. IUTAM, Z. Hashin and C.T. Herakovich (Ed.) 1982, pp. 367-381.

94. Chamis, C.C. and J.H. Sinclair, "10° Off-Axis Test for Shear Properties in Fiber Composites," Experimental Mechanics, Vol. 17, No. 9, Sept. 1977, pp. 339-346.

95. Green, A.E. and R.S. Rivlin, "The Mechanics of Nonlinear Materials with Memory," Arch. Ration. Mech. and Anal., Vol. 1, No. 1, 1957, pp. 1-21.

96. Leaderman, H. "Elastic and Creep Properties of Filamentous Materials and Other High Polymers," The Textile Foundation, Washington, 1943, p. 175.

97. Carnahan, B., H.A. Luther, and J.O. Wilkes, Applied Numerical Methods, John Wiley, New York, 1969.

98. Boyce, W. and R.C. DiPrima, Elementary Differential Equations and Boundary Value Problems, John Wiley, Third Edition, New York, 1977.

99. Delves, L.M. and J.L. Mohamed, J.L., Computational Methods for Integral Equations, Cambridge University Press, Cambridge, 1985.

100. Hochstadt, H., Integral Equations, John Wiley, New York, 1973.

101. Day, J.T., "A Starting Method for solving Nonlinear Volterra Integral Equations," Math. of Computation, Vol. 21, No. 98, 1967, pp. 179-188.

102. Day, J.T., "Numerical Solution of the Convolution Integral Equation," BIT, Vol. 9, 1969, pp. 81-82.

103. Cameron, R.F., and S. McKee, "The Direct Numerical Solution of a Volterra Integral Equation Arising out of Viscoelastic Stress in Materials," Computer Methods in Applied Mechanics and Engineering, Vol. 29, 1981, pp. 219-232.

104. Jones, J.G., "On the Numerical Solution of Convolution Integral Equations and Systems of such Equations," Math. of Computation, Vol. 15, 1961, pp. 131-142.

105. Zienkiewicz, O.C., The Finite Element Method, McGraw-Hill, London, 1977.

106. Synder, M.D. and K.J. Bathe, "A Solution Procedure for Thermo-Elastic-Plastic and Creep Problems," Nuclear Eng and Design, Vol. 64, 1981, pp. 49-80.

107. Perry, C.C., "The Resistance Strain Gage Revisited," Experimental Mechanics, Vol. 24, No. 4, Dec 1984, pp. 286-299.

108. Perry, C.C., "Strain-Gage Reinforcement Effects on Orthotropic Materials," Experimental Techniques, Feb 1986, pp. 20-24.

109. Smith, R., Personal Communication, Technical Support, Micro-Measurements, May 1986.

110. Jerina, K.L., R.A. Schapery, R.W. Tung, and B.A. Sanders, "Viscoelastic Characterization of a Random Fiber Composite Material Employing Micro-Mechanics," MM3979-80-5, Texas A&M University, College Station, Texas, 1980.

111. Struik, L.C.E., Physical Aging in Amorphous Polymers and Other Materials, Elsevier, Amsterdam, 1978.

112. DuPont Data Manual for Kevlar 49 Aramid, E.I. DuPont de Nemours & Co., Inc., May 1986.

113. Dupont Bulletin K-5, E.I. DuPont de Nemours & Co., Inc., Sept. 1981, pp. 3-12.

114. Tsai, S.W., Composites Design 1986, Think Composites, Dayton, 1986.

115. Kibler, K.G., "Time-Dependent Environmental Behavior of Graphite/Epoxy Composites," Air Force Technical Report AFWAL-TR-80-4052, General Dynamics, May 1980.

116. Bear, S. and S. Matsuoka, Personal Communication, Bell Laboratory, New Jersey, Feb 1988.

Appendix A

USER'S GUIDE AND REFERENCE MANUAL TO THE CURVE FITTING (CFIT) PROGRAM FOR VISCOELASTIC ANALYSIS.

This guide is to be used in conjunction with the CFIT (Curve Fitting) program that fits various models or curves to experimental data in an easy and convenient fashion. The program was specifically designed for fitting experimental data to various nonlinear viscoelastic models such as the Findley power law and the Schapery integral models. There are however other general curves that can also be used, such as exponential, logarithmic, polynomial.

The user can input the data through the keyboard or from a file on disk. After choosing a particular curve or model the program will calculate and display the best curve for the data by means of a least-squared routine for linear curve fits. Nonlinear curve fits are accomplished by minimizing the error between the calculated curve and data points. Both the data and calculated curve can be viewed in graphical form on the screen for visual inspection.

The program was designed to be user friendly and self explanatory which minimizes the need of a reference manual. The basic structure of the program is a menu system with three levels; the main, edit and calculate menus. The program can detect most types of wrong or illegal data and informs the operator what should be done. The input choices and options of the program should be easily understood.

System Requirements and Program Start Up

The program currently will only run on a IBM PC or compatible computer. The machine must have a Color Graphics Adapter (CGA), at least 256 K memory and an 8087 math co-processor chip.

The distribution disk includes three files, CFIT.EXE, CGA.BGI, and LITT.CHR. The CFIT.EXE is the executable program code and the other two files CGA.BGI and LITT.CHR are used by the graphics routines in the program. Both CGA.BGI and LITT.CHR need to be on the default drive of the computer system in order for the graphics to work properly. The default drive (where the graphics programs are found) can be changed within the program.

To run the program, insert the distribution disk into drive A. Then type 'A:' and hit the return key (this causes drive A to be the default drive). Next type the program name 'CFIT' and hit the turn. The program will carry it from there.

Operations

The program is split into three basic menus; the main, edit, and calculation menus, which are detailed in Fig. A.1. When the program is started, an introductory screen will appear, and then the main menu will be displayed. The main menu is where the user input data is entered. The menu selection is made by simply hitting the key that is highlighted in blue on the screen. It can be upper or lower case if a letter character is needed. Once a selection is made, the program will prompt the user for input if needed. When prompted for input,

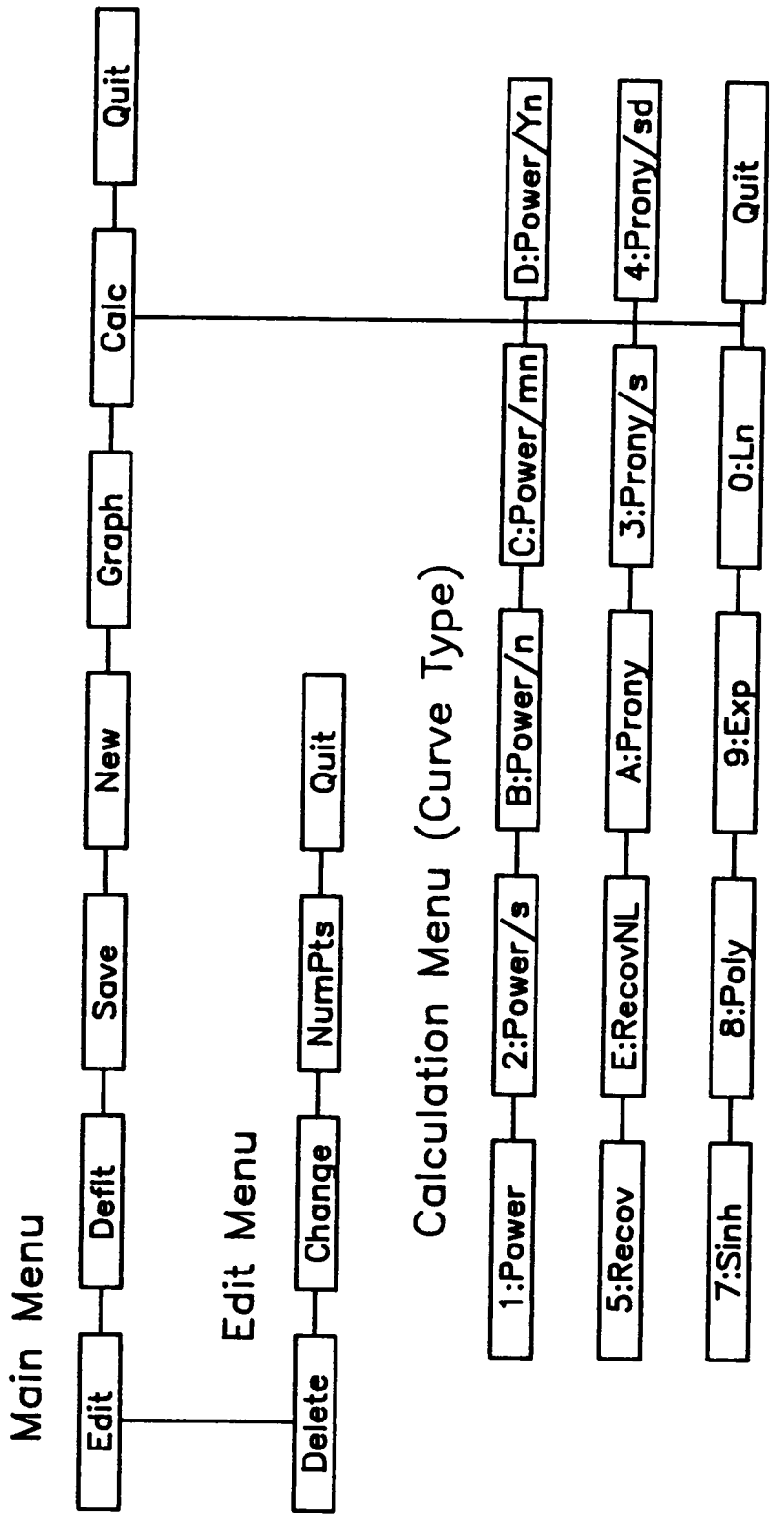

Fig. A.1 Menu Structure for 'CFIT' Program.

type in the desired value and hit the return. If just the return is hit, the current or default value will remain. The input value can be modified by using the backspace key before the return key is hit.

Main Menu

The main menu selections include Edit, Deflt, Save, New, Graph, Calc, Quit, and BeepN. 'E' will invoke the edit menu which is discussed in the following section. 'D' allows the default values for the x-axis scale, x or y-axis in log form, curve coefficients, and the graphic or default drive to be changed through a series of questions will appear on the screen. The x-axis scale pertains to how much of the fitted curve and data will be shown on the screen during graphing. The default is 1.2 which means 20% more of the curve past the last data point in the x-axis direction will be shown. The value must always be greater than 1. The y-axis scale is automatically scaled and can't be changed. Both the x-axis and y-axis are displayed in normal or log form depending on if 'y' or 'n' is specified to the questions 'X Log (Y/N)' and 'Y Log (Y/N)'. The default value is 'n', which means all graphing is done in normal scale. The curve or model variables can be changed by the user, which overrides the calculated variables, just before graphing if the 'Change Coef' is answered 'y'. This allows the operator to adjust manually the fitted curve. The 'Graphic Drive', which tells the program where the graphic routines are located, is assumed to be the current default drive of the system. It can changed to any valid drive but both graphic routines, CGA.BGI

and LITT.CHR, must be present on the new drive.

Returning to the main menu selection, the 'S' command will save the current data on disk. Similarly the, 'N' command will retrieve data from disk. Both commands will request the user to specify the drive and file name to store or retrieve the data. The current directory of all files will be listed for the drive specified.

The command 'G' will graph the curve fitting results on the screen for inspection, however the curve must have been previously calculated. Both the data and calculated curve will appear on the curve. The calculation is performed by using the command 'C' which is more fully detailed in calculation section. The last commands 'Q' and 'B' allow the user to exit the program and to turn the beeper on (BepY) or off (BepN), respectively. The beeper is used to notify the user when a calculation is done or if there is an error.

Edit Menu

The edit menu, accessed by pressing 'E' at the main menu, lets the user change, add, and delete data points that are used in curve fitting process. The menu has four choices, Delete, Change, NumPts, and Quit. The 'D' command allows a complete data set, both x and y value, to be deleted. The user will specify the data set by its location, in ascending order, which is shown on the screen. If '0' is inputted, then nothing will be deleted. After deletions, the remaining data sets are resorted in ascending order for x values.

The 'C' command will step through all data points in ascending

order, and allows the user to modify one or all of the data points, both x and y values. In order to add more data points the 'N' command is used, which asks for the total number of data point sets with a maximum of 500 and a minimum of 3. If the number is less than the current number of points, then only those points up to the new number are used. If the inputted number is more than the current number then extra points are added. In either case all points are resorted. After the number of data points are increased, the 'C' command can be used to modify the added points. The 'Q' command will return the user to the main menu.

Calculation Menu

The calculation menu is the heart of the program where the user chooses which curve is to be fitted to the data. There are currently 14 curve types to chose from which are briefly listed in Table A.1, along with the command key used to access them. By hitting the key indicated, the program will request information needed, if any, and then calculate the best curve by the least-squares method. For the nonlinear curve fits, the error between calculated curve and data points is minimized in addition to using the least-squares method for the linear portion. The results are displayed in the form of an equation, along with the y mean value, standard deviation, and coefficient of variation.

The first five curves listed in Table B.1 are derived from the power law of the form

Table A.1. Curve Types Available in CFIT.

Key	Name	Description
'1'	Power	- Power Law with Spring Specified
'2'	Power/s	- Power Law with Free Spring
'B'	Power/n	- Power Law with Exponent Specified
'C'	Power/mn	- Power Law with Exponent and Coefficient Specified
'D'	Power/Yn	- Power Law with Exponent and Spring Specified
'5'	Recov	- Creep Recovery Curve
'E'	RecovNL	- Nonlinear Creep Recovery Curve
'A'	Prony	- Prony Series
'3'	Prony/s	- Prony Series with Free Spring
'4'	Prony/sd	- Prony Series with Free Spring and Dashpot
'7'	Sinh	- Hyperbolic Sine Curve
'8'	Poly	- Polynomial Curve
'9'	Exp	- Exponential Curve
'0'	Ln	- Natural Logarithm Curve

$$y = y_o + mx^n \tag{A.1}$$

where y_o, m and n are the curve fit constants that can be calculated by the program and x and y are the data variables. The command '1' allows the user to specify y_o and then the program will give m and n for the best fit. '2' will calculate all three parameters, y_o, m and n for the given data. 'B' allows the user to specify the exponent n, 'C' lets m and n to be specified, and 'D' allows y_o and n to be specified with the other parameters calculated by the program.

The '5' and 'E' commands will fit the data to the following two similar curves that are used in describing creep recovery and nonlinear creep recovery data, respectively.

$$y = a\,[(1+\lambda)^n - \lambda^n] \tag{A.2}$$

$$y = a\,[(1+b\lambda)^n - (b\lambda)^n] \tag{A.3}$$

where $\lambda = (x-x_1)/x_1$ and x_1 is the starting point for the curve. For '5', Eq. A.2, the user must specify x_1 and a range of expect n values, and then the program will calculate a and n values. For 'E', Eq. A.3, x_1 and n must be given, and a range of expected b values and then the a and b will be calculated for the best fit.

Commands 'A', '3', '4', will fit the data to a Prony Series type curve of the form

$$y = y_o + \sum_{i=1}^{n} D_i\left[1 - e^{-t/\lambda_i}\right] + ct \qquad i = 1,2,3..n \qquad (A.4)$$

where λ is called the relaxation time and n is the total number of Kelvin elements to be used in the curve fit model, which is specified by the user. The λ_i are given by the user by specifying the first relaxation time, λ_1, and then specifying the interval multiple for each of the following λ's. For example, if the user specifies n = 4, λ_1 = 10, and relaxation interval equal to 10, then $\lambda_2 = \lambda_1 \cdot 10 = 10 \cdot 10 = 100$, $\lambda_3 = \lambda_2 \cdot 10 = 1{,}000$, and $\lambda_4 = 10{,}000$. For 'A', the program will calculate only the D_i with $y_o = c = 0$. For '3' D_i and y_o are calculated with c = 0. For '4' all parameters, D_i, y_o and c, are calculated by the program.

The '7' command will fit the data to a hyperbolic sine curve of the form

$$y = a \cdot \sinh(x/b) \qquad (A.5)$$

where a and b are the calculated parameters. The '8' will calculate any degree of polynomial equation desired to the data. The equation form is

$$y = C_o + C_1x + C_2x^2 + \ldots\ldots + C_nx^n \qquad (A.6)$$

where n is called 'the number of terms' in the program and must be specified by the user and C_i are the coefficients that are calculated.

The remaining two curves, Exp and Ln, ('9' and '0' respectively)

are of the form

$$y = a \cdot e^{bx} \tag{A.7}$$

$$y = a + b \cdot \mathrm{Ln}(x) \tag{A.8}$$

with a and b the curve parameters determined by the program. The last option is 'Q' which allows the user to exit and return to the main menu.

Appendix B

BACKWARD TRAPEZOIDAL METHOD

In chapter 3 the Backward Euler Method was used in solving the nonlinear viscoelastic problem of orthotropic composite laminates and a detail derivation was given. The Backward Trapezoidal Method (BTM) will be briefly developed in this appendix.

Recall the basic differential equation, Eq. 5.8, of a single Kelvin element

$$ {}_{kl}\dot{\varepsilon}_{ij} = \sum_{q=1}^{4} \left[\frac{{}_{kl}D_{qij}}{\lambda_l} \right] {}_{kl}\sigma_{ij} - \frac{{}_{kl}\varepsilon_{ij}}{\lambda_l} \qquad (B.1) $$

where ${}_{kl}\dot{\varepsilon}_{ij}$ and ${}_{kl}\varepsilon_{ij}$ are the strain rate and strain, respectively, ${}_{kl}\sigma_{ij}$ is the stress in each Kelvin element, l, ply, k, compliance direction, q, and rotated position, (i,j). Using the BTM the numerical approximation becomes

$$ \frac{{}_{kl}\varepsilon_{ij}^{t+1} - {}_{kl}\varepsilon_{ij}^{t}}{\Delta t} = \frac{1}{2} \left\{ \sum_{q=1}^{4} \left[\frac{{}_{kl}D_{qij}}{\lambda_l} \right] {}_{kl}\sigma_{ij}^{t+1} - \frac{{}_{kl}\varepsilon_{ij}^{t+1}}{\lambda_l} + \sum_{q=1}^{4} \left[\frac{{}_{kl}D_{qij}}{\lambda_l} \right] {}_{kl}\sigma_{ij}^{t} - \frac{{}_{kl}\varepsilon_{ij}^{t}}{\lambda_l} \right\} \qquad (B.2) $$

where Δt is the time step size, t+1 is the new time and t is the old

time. This can be rewritten as

$$ {}_{kl}\varepsilon_{ij}^{t+1} = \frac{h}{2\lambda_1+h}\sum_{q=1}^{4} {}_{kl}D_{qij}\cdot {}_{kl}\sigma_{ij}^{t+1} + \frac{h}{2\lambda_1+h}\sum_{q=1}^{4} {}_{kl}D_{qij}\cdot {}_{kl}\sigma_{ij}^{t} $$

$$ + \frac{2\lambda_1-h}{2\lambda_1+h}\cdot {}_{kl}\varepsilon_{ij}^{t} \qquad \text{(B.3)} $$

where $h = \Delta t$. When the nonlinear stress function is included (Eq. 5.10) Eq A.3 becomes

$$ {}_{kl}\varepsilon_{ij}^{t+1} = \frac{h}{2\lambda_1+h}\sum_{q=1}^{4} {}_{kl}D_{qij}\cdot {}_{kl}\sigma_{ij}^{t+1}\cdot f_q({}_k\sigma^{t+1}) + $$

$$ + \frac{h}{2\lambda_1+h}\sum_{q=1}^{4} {}_{kl}D_{qij}\cdot {}_{kl}\sigma_{ij}^{t}\cdot f_q({}_k\sigma^{t}) + \frac{2\lambda_1-h}{2\lambda+h}\cdot {}_{kl}\varepsilon_{ij}^{t} \qquad \text{(B.4)} $$

This can be further simplified as

$$ {}_{kl}\varepsilon_{i}^{t+1} = \sum_{q=1}^{4}\left[{}_{kl}C_{qij}\cdot f_q({}_k\sigma^{t+1})\right]\cdot {}_k\sigma_j^{t+1} + {}_{kl}E_{ij}^{t} \qquad \text{(B.5)} $$

where $$ {}_{kl}E_{ij}^{t} = \sum_{q=1}^{4}\left[{}_{kl}C_{qij}\cdot f_q({}_k\sigma^{t})\right]{}_k\sigma_j^{t} + \frac{2\lambda_1-h}{2\lambda+h}\cdot {}_{kl}\varepsilon_{ij}^{t} $$

$$ {}_{kl}C_{qij} = \frac{h}{(2\lambda_1+h)}\cdot {}_{kl}D_{qij} $$

$$ {}_k\sigma_j^{t+1} = {}_{kl}\sigma_{ij}^{t+1} $$

Summing all the creep strains together for each element in the series of Kelvin element will give, similar to BEM,

$$ {}^{c}_{k}\varepsilon_{i}^{t+1} = \sum_{j=1}^{3} \sum_{l=1}^{n} \left\{ \sum_{q=1}^{4} \left[{}_{kl}C_{qij} \cdot f_q({}_{k}\sigma^{t+1}) \right] \cdot {}_{k}\sigma_{j}^{t+1} + {}_{kl}E_{ij}^{t} \right\} \qquad (B.6) $$

From this point the derivation is the same as the BEM. As with the BEM, the BTM is unconditionally stable for all time steps. It is a second order method which will be more accurate than the BEM.

Appendix C

USER'S GUIDE AND REFERENCE MANUAL TO THE VISCOELASTIC COMPOSITE ANALYSIS PROGRAM (VCAP)

This manual is to be used in conjunction with 'VCAP' (Viscoelastic Composite Analysis Program) which was written to help design engineers predict viscoelastic response of any general laminate. The program allows the user to specify the laminate layup, in-plane loads or stresses, and the time span of the analysis. The program requires the user to supply the lamina material properties that make up the laminate. However, there are three materials (graphite/epoxy T300/934 and T300/5280, and Kevlar/epoxy Ke 49/Fiberite 7714A) that have been characterized at Virginia Polytechnic Institute and State University and are included as default materials properties in the program.

The output will be the in-plane stresses and strains in the global or local ply coordinate system as well as the compliance in the load direction. This information can be viewed immediately in table or graph form, or saved to disk for later viewing and editing.

The program was designed to be user friendly and self explanatory which minimizes the need of a reference manual. The basic structure of the program is a menu system with three levels, the main, edit and output menus. The program can detect most types of wrong or illegal data and informs the operator what should be done. The input choices

and options of the program should be understood to someone involved with viscoelastic composite analysis with only minimal need of this reference.

System Requirements and Program Start Up

The program currently will only run on a IBM PC or compatible computer. The machine must have a Color Graphics Adapter (CGA), at least 512 K memory and an 8087 math co-processor chip.

The distribution disk includes three files, VCAP.EXE, CGA.BGI, and LITT.CHR. The VCAP.EXE is the executable program code and the other two files CGA.BGI and LITT.CHR are used by the graphics routines in the VCAP program. Both CGA.BGI and LITT.CHR need to be on the default drive of the computer system in order for the graphics to work properly. The default drive can be changed within the program.

To run the program, insert the distribution disk into drive A. Then type 'A:' and hit the return (this causes drive A to be the default drive). Next type the program name 'VCAP' and hit the return. The program will carry it from there.

Operations

The program is split into three basic menus; the main, edit, and output menus, which are detailed in Fig. C.1. When the program is started, two introductory screens will appear, and then the main menu will be displayed. A menu selection is made by simply hitting the key that is highlighted in blue on the screen. It can be upper or lower

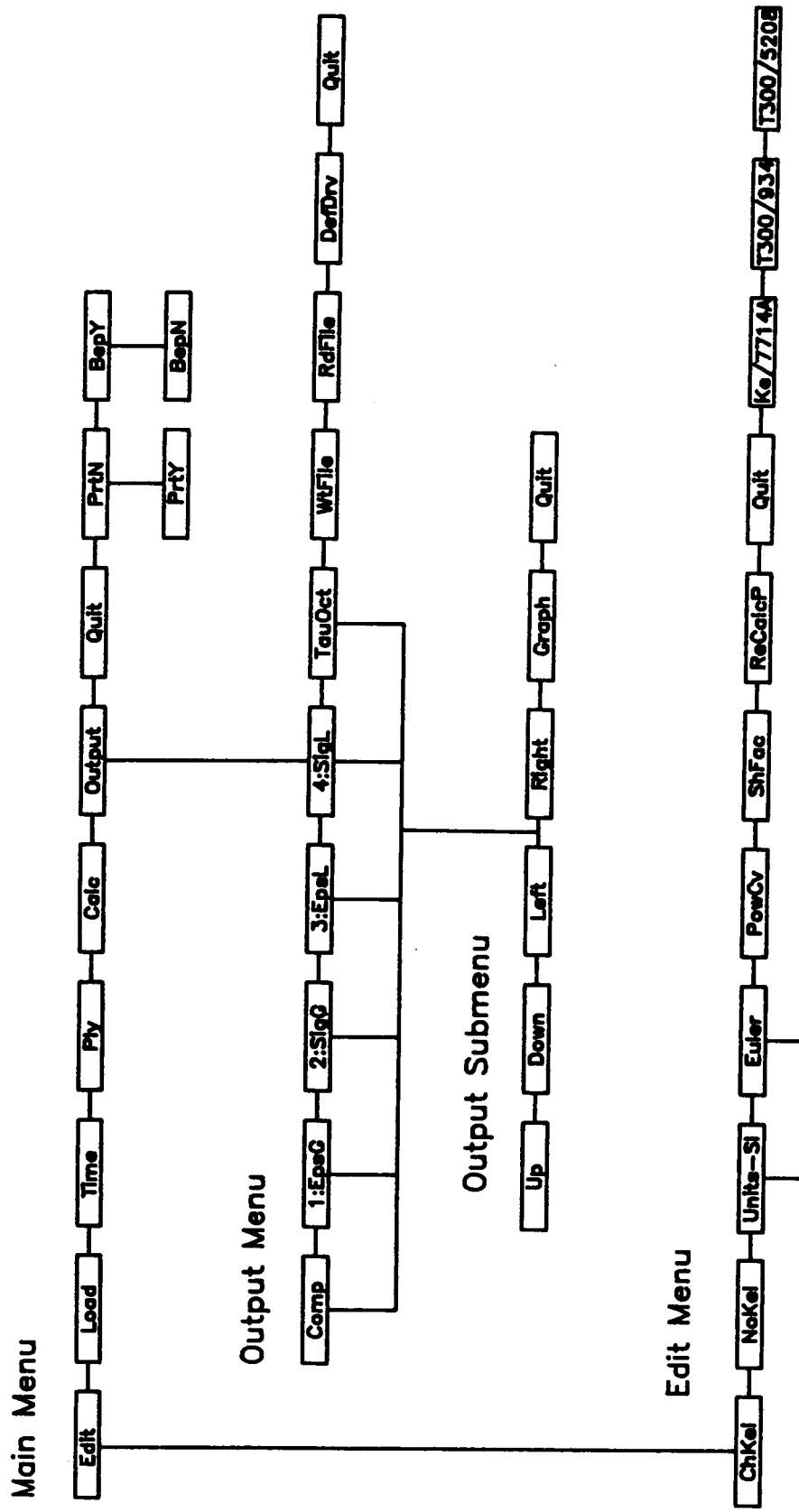

Fig. C.1 Menu Structure for 'VCAP' Program.

case if a letter character is needed. Once a selection is made, the program will prompt the user for input if needed. When prompted for input, type in the desired value and hit the return. If just the return is hit, the current or default value will remain. The input value can be modified by using the backspace key before the return key is hit.

Main Menu

The main menu selections include Edit, Load, Time, Ply, Calc, Output, Quit, PrtN, and BepY. 'E' will invoke the edit menu which is discussed in the following section. 'L' allows the in-plane stresses to be modified. 'T' allows the start time, the number of steps per decade, and the total number of decades to be specified. The minimum and maximum for the steps per decade is 5 and 10 respectively. The maximum total decades is 22. 'P' allows the laminate layup to be changed. The number of plies can range from 1 to 6. The angle is restricted to >= -90° and <= 90° and the thickness must be <= 999.9. 'C' Begins the actual calculation process. The time required for an analysis depends of the number of plies and the total number of decades desired. An analysis of a 2 ply laminate for 6 decades takes about one minute and for a 6 ply laminate for 22 decades it takes about one hour. 'O' allows the results to be viewed or saved to disk as explained in the output section. 'Q' quits the program and takes the user back to the DOS level. 'R' activates the printer (PrtY) to receive intermediate results as the program does the calculations.

'B' turns the beeper on (BepY) or off (BepN). The beeper is used to notify the user when a calculation is done or if there is an error.

Edit Menu

The edit menu lets the user change the material properties of the basic lamina. The user can enter the Prony series coefficients and relaxation times directly or use a power law based model such as the Schapery or Findley model. If a power law model is input, then the program will generate the Prony series which is needed to perform the analysis.

The selections for the edit menu include ChKel, NoKel, Units-SI or Units-Eng, Euler or EulMod, PowCv, ShFac, ReCalcP, Quit, 1:Ke/7714A, 2:T300/934, and 3:T300/5208. 'C' allows the user to directly input the Prony series coefficients and relaxation times directly for each of the four material properties. The relaxation times will be the same for each of the basic four directions or material properties as dictated by the program algorithm. 'N' lets the user change the total number of Kelvin elements or Prony series terms to be included. This only applies for the Prony series input by the user and not for the power law generated Prony series. 'U' will switch between SI and English which specifies the units and format on input and output screens. 'E' allows the user to switch between two solution techniques, Euler and EulMod. The Euler stands for the Backward or Implicit Euler method and EulMod stands for the Modified Backward Euler Method. The Euler is a first order solution technique

and EulMod is a second order. The EulMod takes slightly more time but is also slightly more accurate.

'P' allows the user to specify the type of viscoelastic model to be used and its coefficient parameters. Currently there are three choices for models, the Schapery, Findley, and quadratic. The Schapery model used is in the form of

$$S = g_o S_o + \frac{g_1 g_2 C t^n}{a_\sigma^n} \qquad (C.1)$$

which requires S_o, m, n, g_o, g_1, g_2, and a_σ parameters to be specified. S_o, m and n are constants and g_o, g_1, g_2, and a_σ are nonlinear stress functions. The g_o, g_1, and g_2 functions are assumed to be a bilinear functions of the form

$$g_i = 1 \qquad \text{for } 0 \le \sigma \le b \qquad (C.2a)$$

$$g_i = 1 + a(\sigma - b) \qquad \text{for } b < \sigma \qquad (C.2b)$$

where a and b are user input constants. The bilinear function is graphically shown in Fig. C.2. The constant b and a represent the stress level at which nonlinear effects begin and its rate, respectively. The a_σ functions has a exponential form

$$a_T = 1 \qquad \text{for } 0 \le \sigma \le b \qquad (C.3a)$$

$$a_T = e^{a(\sigma - b)} \qquad \text{for } b < \sigma \qquad (C.3b)$$

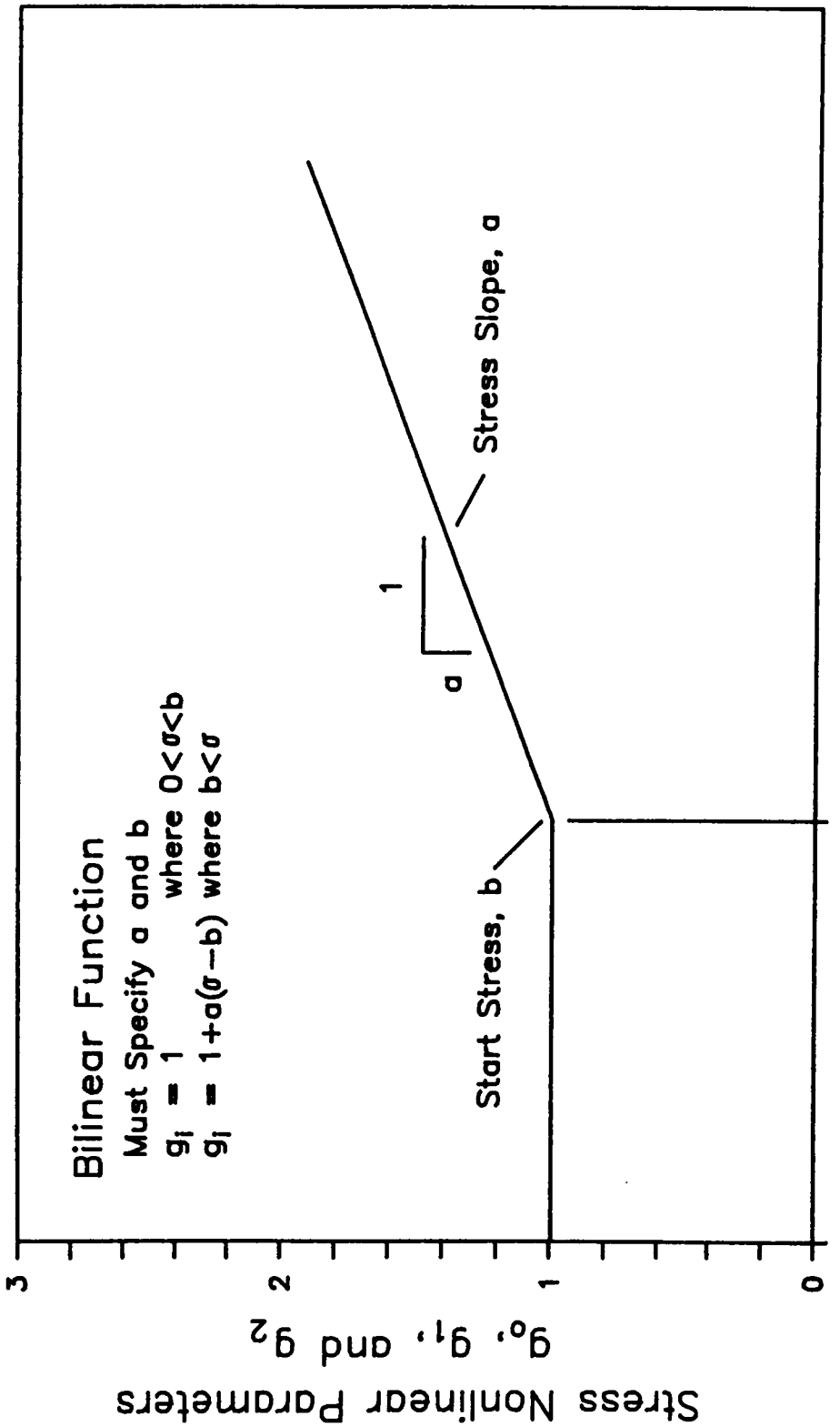

Fig. C.2 Bilinear Function Approximation for the g_o, g_1, and g_2 Nonlinear Stress Parameter for the Schapery Model.

where again b is the stress level at which the nonlinear stress effects begin and a is a type of rate constant for the nonlinear effects. The exponential form restricts a_T from becoming negative or zero. Figure C.3 shows an example of a typical a_T nonlinear stress function.

For the Findley model,

$$S = \frac{S_o}{\sigma} \sinh\left[\frac{\sigma}{g}\right] + \frac{m}{\sigma} \sinh\left[\frac{\sigma}{f}\right] t^n \qquad (C.4)$$

there are five parameters, S_o, m, n, g, and f, all constants, that the user must specify for each of the four material properties. The parameters f and g are the nonlinearizing terms in the hyperbolic sine function. The term σ is the current nonlinear stress parameter.

The simplest model is the quadratic model of the form

$$S = S_o\left[1+g\cdot\sigma^2\right] + m\left[1+f\cdot\sigma^2\right]t^n \qquad (C.5)$$

Like the Findley model there are five parameters that need to be specified, S_o, m, n, g, and f, where σ is the current nonlinear stress parameter.

In addition to basic models, the user must specify the current nonlinear stress parameter, σ, for calculating the nonlinear compliance. There are two options, the matrix octahedral shear stress parameter, and actual stress. The matrix octahedral stress is a combination of stresses in the matrix, both transverse and shear

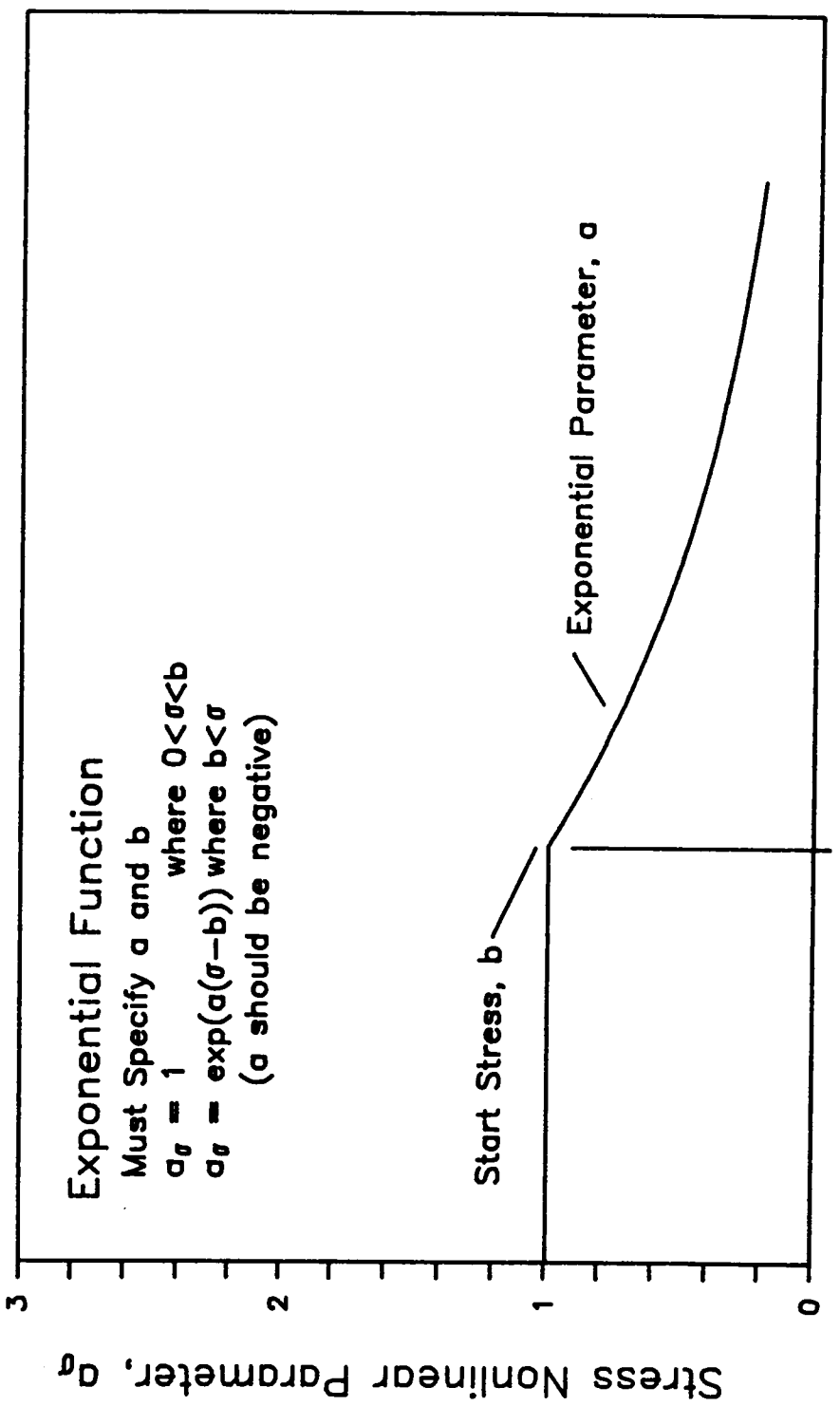

Fig. C.3 Exponential Function Approximation for the a_σ Nonlinear Stress Parameter for the Schapery Model.

directions which is used to calculate the S_{22} and S_{66} compliance terms. For the S_{11} and S_{12} terms, the actual stress in the fiber direction is used. If the octahedral option is chosen, then the matrix Poisson's ratio must also be specified. For the second option, actual stress, the stress in a particular direction is used to calculate that direction compliance, i.e., the fiber direction stress, σ_1, is used for the S_{11} and S_{12} terms, transverse fiber stress, σ_2, is used for the S_{22} term, and the shear stress, σ_{12} is used to the S_{66} term.

'S' allows the user to specify the temperature and the temperature shift factor functions. The temperature is assumed to be in degree celsius. There are three shift factor functions currently available: a linear equation, the Williams-Landel-Ferry equation, and the Arrhenius equation. The user needs to input the constants that correspond to a particular model. If the shift factor function is unknown then the user can input zeros for all constants and no shifting will take place.

There are currently three composite materials and their properties, stored in the program. These materials have been tested and modeled at Virginia Polytechnic Institute and State University and can be accessed by the user by hitting the '1', '2', or '3' number key. The first material, tested and characterized by Gramoll,[1]

---

[1]Gramoll, K.C., D.A. Dillard and H.F. Brinson, "Thermoviscoelastic Characterization and Prediction of Kevlar/Epoxy Composite Laminates," Conf Proc 9th Symposium on Composite Materials: Testing and Design, Reno, Nevada, April, 1988.

(accessed by key '1'), is made from Kevlar 49 and 7714A Fiberite epoxy. The Kevlar/epoxy data has shift factor functions, used for temperature effects, which are automatically loaded with the material properties. The second material, key '2', is graphite T300/934 epoxy composite system that was tested and analyzed by Griffith and Dillard[2]. The last material system available is graphite T300/5208 epoxy that was characterized by Tuttle[3]. There are no shift factor function available for either graphite/epoxy material system.

'R' will recalculate the Prony series from the user entered model. The Prony series should be recalculated after all changes to the model and shift factor function parameters have been completed. The program uses the Prony series and not the power law models in its analysis. The number of terms in the series that are calculated depends on the number of decades the analysis is to be performed, which is specified in the main menu under 'Time'. 'Q' will return the user back to the main menu.

Output Menu

The output menu is accessed through the main menu. The user can view the analysis results in table form or in graph form. The options in the menu are Comp, EpsG, SigG, EpsL, SigL, TauOct, WtFile, RdFile,

---

[2]Dillard, D.A., D.H. Morris and H.F. Brinson, "Creep and Creep Rupture of Laminated Graphite/Epoxy Composites", VPI&SU Report VPI-E-81-3, March 1981.

[3]Tuttle, M.E. and H.F. Brinson, "Accelerated Viscoelastic Characterization of T300/5208 Graphite-Epoxy Laminates", VPI&SU Report VPI-E-84-9, March 1984.

and Quit. The following gives a brief description of each command

'C' Compliance in the load direction only
'1' Strain in the global coordinate system (laminate)
'2' Stress in the global coordinate system (laminate)
'3' Strain in the local coordinate system (lamina or ply)
'4' Stress in the local coordinate system (lamina or ply)
'T' Matrix octahedral shear stress in each ply

For each of the above choices, the results will be shown in table form. The information can be scrolled up and down, and if there is multiple plies, it can be scrolled sideways between plies, by using the arrow keys. The data can be graphed by hitting 'G'. After the graphing the table form reappear. There are two possible options in the graphing, material property direction (1 to 4) and if all plies will be graphed together or separately. To return to the basic output menu just hit 'E' for Exit.

The other options on the output menu are WtFile and RdFile. These commands allow the user to write the results to disk or to read a previously saved result back into the program for viewing and graphing. The file is written in ASCII format which allows it to be accessed by almost all other work processing, spread sheet, and graphing program packages. A third command on this menu is DefDrv which allows the user to change the default drive where the graph drivers are located.

Appendix D

USER'S GUIDE AND TECHNICAL REPORT FOR THE AUTOMATED CURVE SHIFTING (ACS) PROGRAM

The computer program, Automated Curve Shifting (ACS), was developed for automating the curve shifting process that is used in many engineering applications. The basic concept is the shifting of multiple curves horizontally to form a single curve. Figure D.1a shows this concept for a horizontal shifting process and how a new master curve can be formed. Curve shifting by hand is a time consuming and tedious job, which requires curves to be shifted by trial and error. One area of engineering that curve shifting is used extensively is polymer science, which uses the Time-Temperature-Superposition-Principle (TTSP) relating temperature and time. This allows long-term mechanical response of polymer materials to be deduced from short-term test results through the curve shifting of different temperature level tests.

The program described in this report has the ability to shift up to 30 curves of 54 data points each to construct a single master curve. The user can override the automatic shifting and manually input the shift factors for each curve. In both cases the results can be viewed and graphed on the computer screen. The program has the ability to read data from a disk file or let the user enter the data through the program's editor. The data can be viewed and edited at

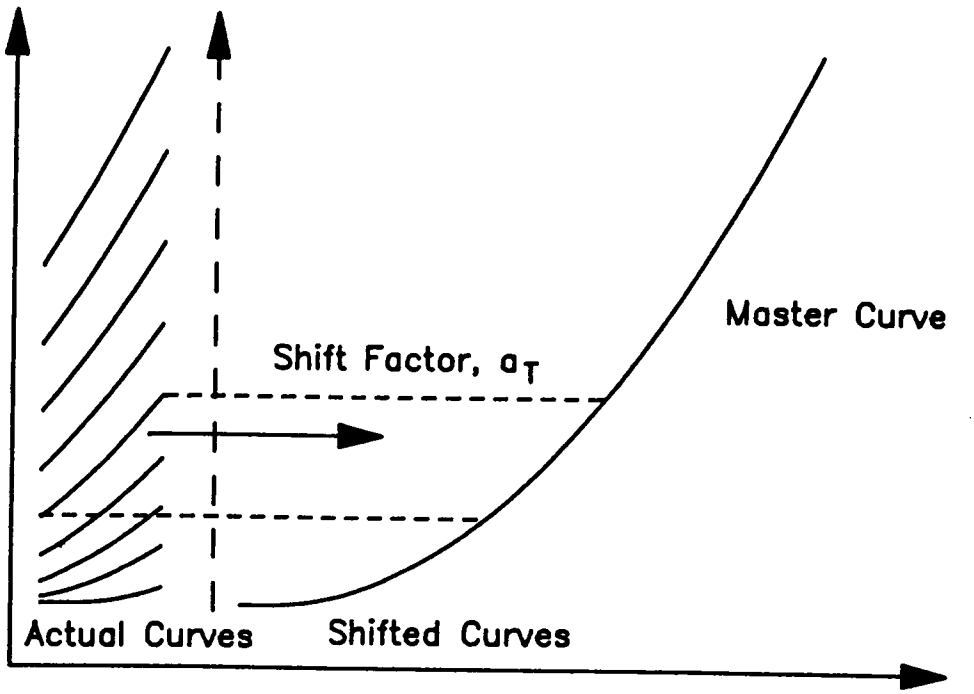

Fig. D.1a Horizontal Curve Shifting to Form Master Curve.

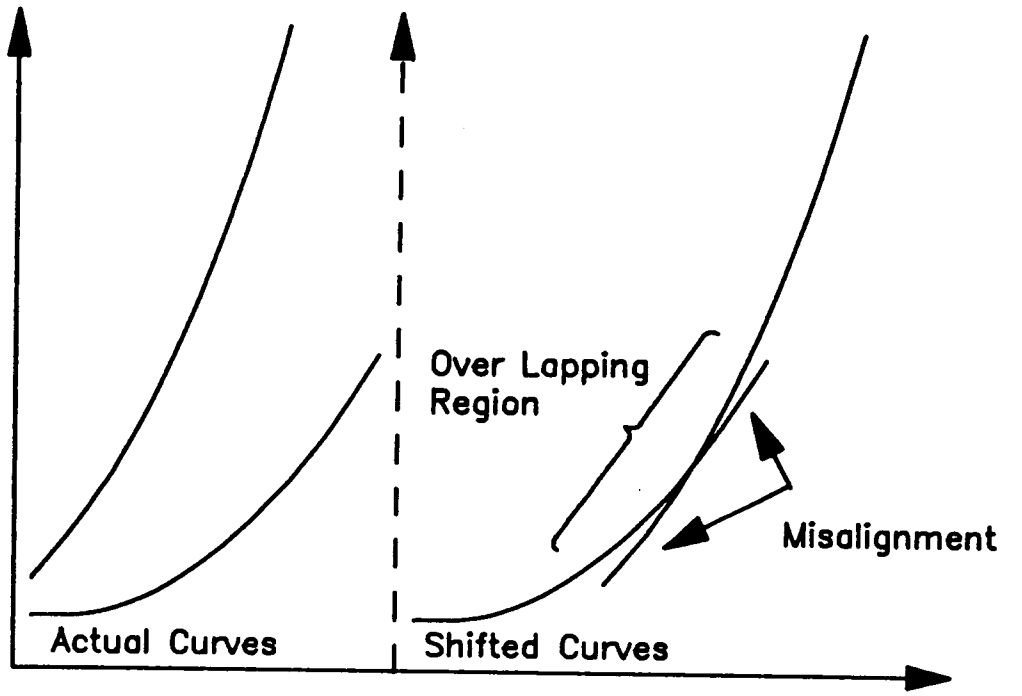

Fig. D.1b Observed Misalignment from Experimental Data when Curve Shifting.

any time while the program is running. The data can be saved to disk for later use and reference. The overall design of the program was for user-friendliness and ease of use. The program is self explanatory and menu driven. There is error checking and reporting to help the user understand any mistakes.

The sections that follow are mainly for reference only and are not necessary to operate the program. The first section describes the method of solution and the algorithm used to automate the curve shifting process and the second section explains the overall operation and use of the program ACS along with its limitations.

Shifting Method and Algorithm

The basic idea of curve shifting is to match a series of curves, one on top of another, to form a new curve called a master curve. Although the master curve is actually made up of many shorter, over-lapping curves it should resemble a single curve with a minimum of projections from the individual curves. The objective of curve shifting is to find the best shift factor, a_T, between any two overlapping curves that allows the two curves to lay on top of one another with a minimum misalignment (Fig. D.1b). A human is able to discern any misalignment quickly through visual inspections but a numerical method is necessary in order for a computer to perform this same task. Thus, in order to automate this curve shifting process, an algorithm must first be developed.

One method to minimize any misalignment between curves is based

on minimizing the area between the two respective curves. Figures D.2 and D.3 show two methods to calculate the area between any two over lapping curves which can be easily implemented on a computer. The first method, called x-axis method, is to find the area between the overlapping section of each curve and the x-axis as shown in Fig. D.2 and then take the absolute difference between each area. If A_1^x and A_2^x are the respective areas, then the basic objective function to be minimized would be

$$\text{Minimize } | A_1^x - A_2^x | \qquad (D.1)$$

Similarly, the second method, called the y-axis method, finds the area between two curves by taking the absolute difference between the respective curves and the y-axis (Fig. D.3). The objective function becomes

$$\text{Minimize } | A_1^y - A_2^y | \qquad (D.2)$$

Although the x-axis and y-axis methods are similar in implementation for any two overlapping curves, the y-axis method is unconditionally stable whereas the x-axis method is not. The unstable condition for x-axis method is due to having two minimums for equation (D.1). The first minimum, and the one desired, occurs when the two curves are closely aligned. However a second minimum occurs when curve 2 is shifted past the last point on curve 1 causing Eq. D.1 to become 0. Although this over-shifting of the second curve past the first curve happens rarely, the possibility still exists and has

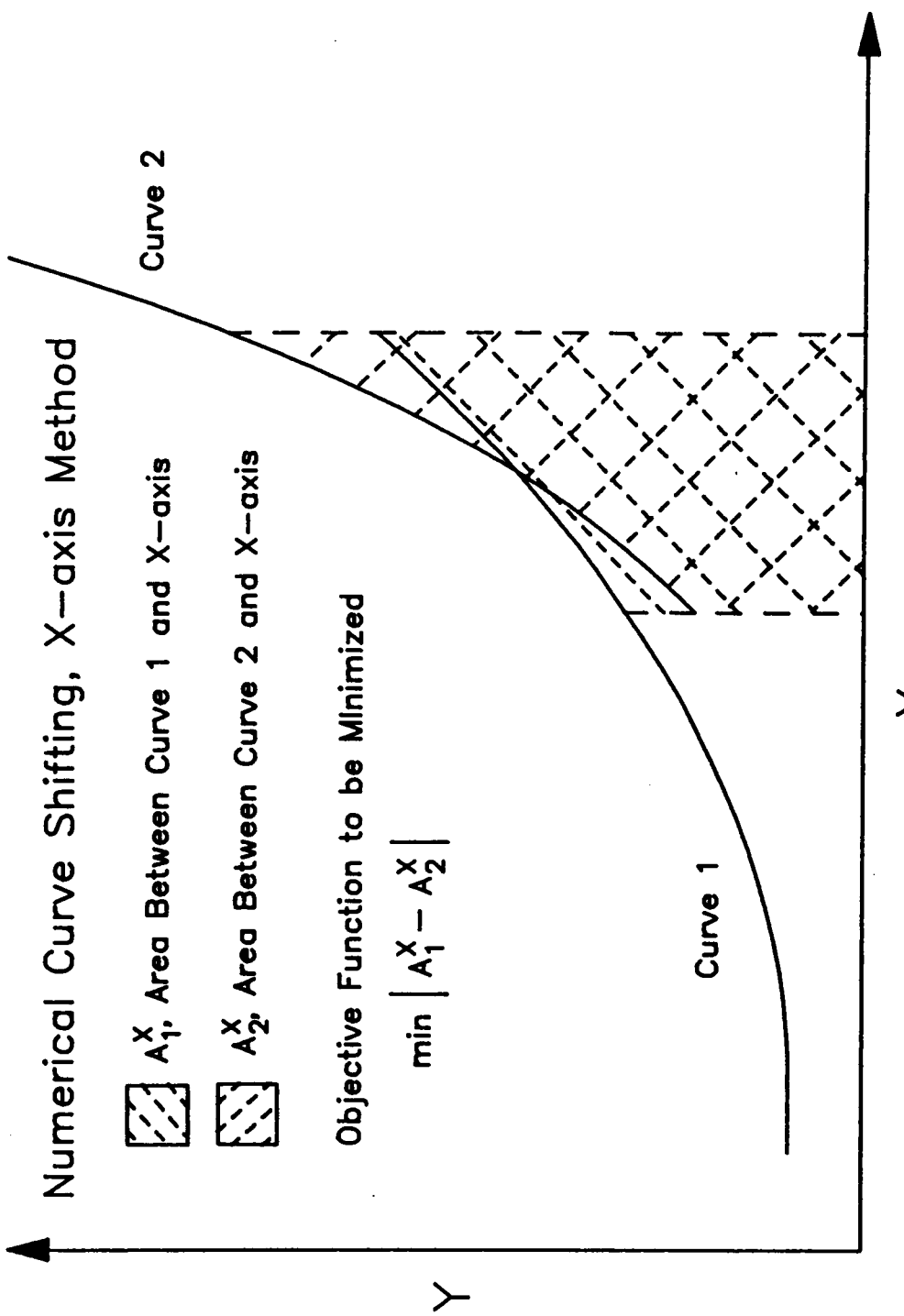

Fig. D.2 X–axis Method for Curve Shifting.

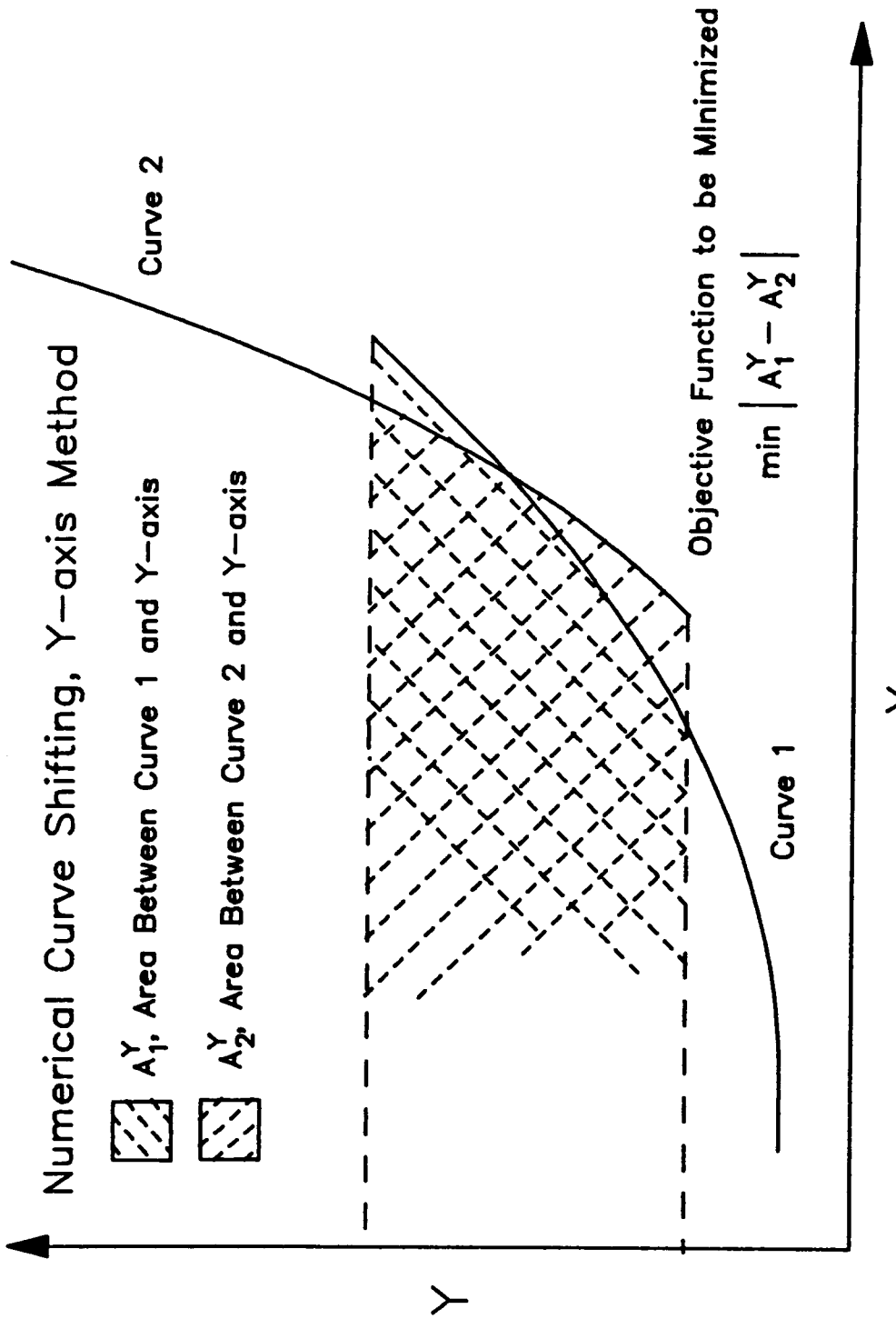

Fig. D.3 Y-axis Method for Curve Shifting.

happened on test cases. The y-axis method does not suffer from this double minimum problem regardless of how far the curves are shifted.

It should be noted that both methods do not give the same exact shift value for the same curves. The x-axis method will always give a higher value than the y-axis method. However the difference between the two values is less than 1% for actual TTSP curves and if the difference is greater than 2-3% then the shiftability of the curves is in question.

Because of the stability problem of the x-axis method, the y-axis method was chosen to be used in the 'ACS' program. In all test cases the y-axis method gave excellent shift factors and matched those obtained by other graphical methods.

The trapezoidal rule was used in calculating the areas between the overlapping curves and the y-axis. The curves are not continuous functions but a collection of data points and when the word 'curve' is used it refers to the data points. In all calculations the data points are used in calculating and minimizing areas. When an end point of one curve does not coincide with a data point in the over-lapping curve, then linear interpolation is used to obtain a new data point. This new point is needed at each end of the over-lapping curves in order to use the trapezoidal rule at the end points.

The Bracketing and Golden Section methods[1] were used together to find the minimum area difference between the curves to be shifted.

---

[1]Haftka, R.T. and Kamat, M.P., Elements of Structural Optimization, Martinus Nijhoff Publ., Boston, 1985, pp 84.

The Bracketing method starts with the shift factor, a_T, at zero and then marches in a geometric manner in the positive direction until the minimum is bracketed. After the minimum is bracketed then the Golden Section search method is used to approach the minimum. When any two successive a_T values are less than 10^{-6} apart, then the search is terminated. The Golden Search method is very similar to the Bisection method but converges more rapidly. A flow chart showing this procedure is given in Fig. D.4.

One limitation of the algorithm used is its restriction to positive shift factors, i.e. curves can only be shifted right. Another limitation is only positive data points can be used. This is due to the x-axis being converted to log scale which then prohibits any negative numbers. Also note that the algorithm assumes the objective function being minimized is unimodal, or that is has only one minimum. Although a well behaved set of shiftable curves are unimodal, there might be more than one minimum if there is scatter in the data. However, even with uneven data the multiple minimums that might be present would be very closely spaced and the value for a_T for each of these minimums would be nearly the same.

Program 'ACS' Program Description and Use

The Automated Curve Shifting (ACS) computer program was designed to aid the engineer or scientist in shifting multiple curves to obtain a master curve without using the time consuming and tedious graphical method. Since curve shifting is empirical in nature and that there is

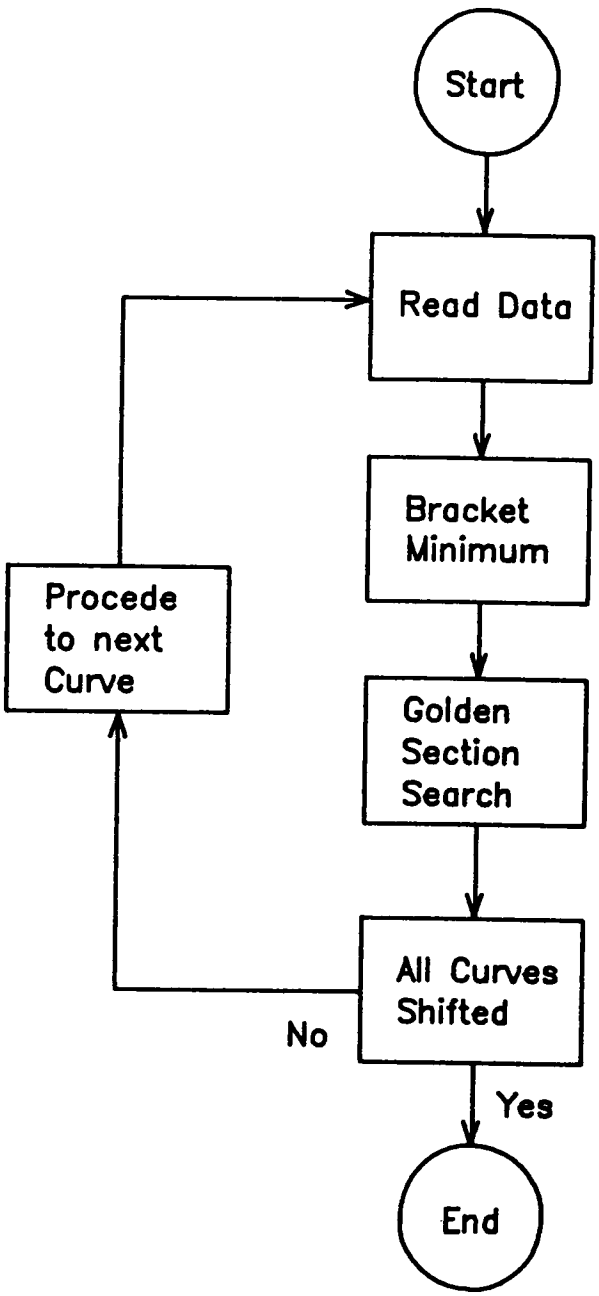

Fig. D.4 Basic Flow Shart for 'ACS' Program.

more than one possible curve shifting method, any values obtained from ACS should be only as a starting point in deriving a shift factor function. The program itself is designed to be self explanatory and user friendly so that anybody could use it with a minimum knowledge of computers. ACS uses menus to guide the user through all aspects of the program. The data can be read from disk or input directly through the keyboard. The automated shifting capabilities can be overridden by the user and all results can be viewed in graphical form.

The basic procedure to use the program is input data, calculate the shift factors for each curve and then visually view the results. However, to help the user to accomplish those basic three tasks, there are other options available. Figure D.5 shows the main menu and submenu selections that are possible. The following paragraphs will explain each option and menu selections along with their limitations. Each command is chosen by hitting the letter of the command or the blue highlighted letter.

The 'Retrieve' function allows the user to import a data file on disk that is written in ASCII format. The program will first ask for the disk drive letter were the data file is stored and will then display all current files on that disk to aid the user in choosing the proper data file. The user will then type the desired file name and hit return. If no name is entered then the default file, called 'MAT.DAT', will be retrieved. Data files can be constructed from the 'Edit' and 'Save' commands in this program or from any word processor or editor. However, the data must be in the format shown in Table

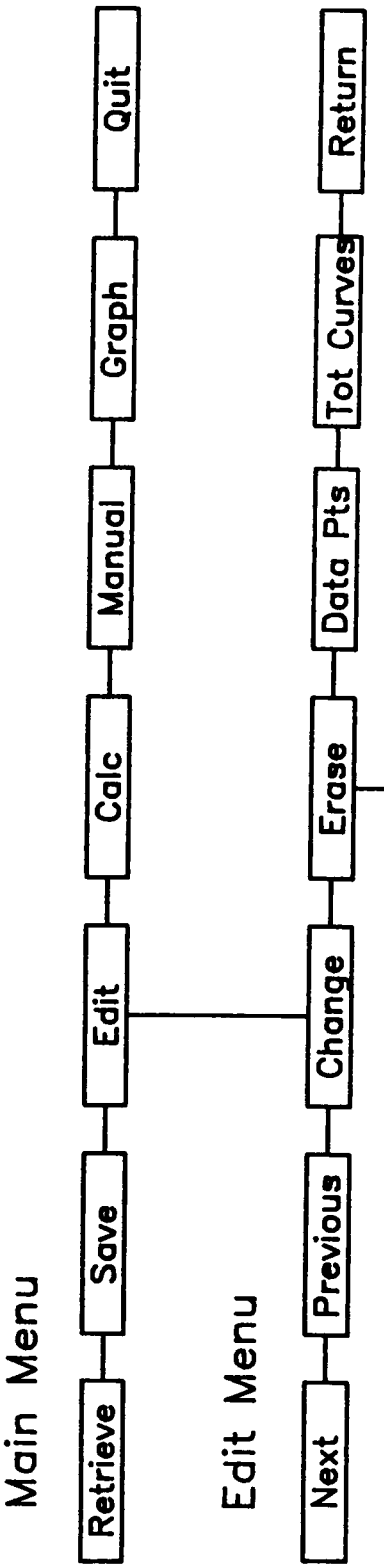

Fig. D.5 Menu Structure for 'ACS' Program.

D.1, however the column positions are not critical. The maximum number of curves that can be fitted at one time is 30 and the maximum number of data points permitted per curve is 54.

Table D.1 Sample Data File Format (Column Not Critical).

Actual File		Comments
3		← number curves (30 max)
4		← number of data points in 1st curve (54 max)
10	20	← 1st data point in 1st curve
100	30	← 2nd data point in 1st curve
200	40	← 3rd data point in 1st curve
500	50	← 4th data point in 1st curve
3		← number of data points in 2nd curve
10	25	← 1st data point in 2nd curve
100	38	← 2nd data point in 2nd curve
200	50	← 3rd data point in 2nd curve
3		← number of data points in 3rd curve
10	28	← 1st data point in 3rd curve
100	40	← 2nd data point in 3rd curve
200	65	← 3rd data point in 3rd curve

The 'Save' command is the opposite of the 'Retrieve' command. All data that is currently being used in the program will be saved on disk in ASCII format. The program will ask what disk drive will to be used and the name of the data file. If no name is given, then the default name of 'MAT.DAT' will be used.

The user can enter new data or change existing data with the 'Edit' command. A submenu of editor commands will appear at the bottom of the screen. At the top of the screen the current curve number and the total number of curves is shown. In the submenu, the 'Next' and 'Previous' commands allow the user to page through the

individual curves, until the desired curve appears. Each time these two commands are used the screen is rewritten with the new curve data. All editing will be done only on the current curve. To change the value of any data point, use the 'Change' command. The program will highlight each data point in sequence and allows the user to change the value. However, only positive values can be used. To get out of the change mode, simply go through all data points and after the last point, the program will automatically exit. The data will be automatically sorted by the x data value so that the lowest value will be first the largest will be last.

The 'Erase' command in the 'Edit' submenu allows the user to delete any particular data point in the current curve data file or to delete complete curves. Upon using this command, a second submenu will appear with three entries, 'Point', 'Curve', and 'Return'. If 'Point' is used, the program will ask which data point of the current curve should be deleted. If there is no point to be erased then enter 0, which allows the user to escape. The number of the data point to be deleted must be greater or equal to 0 and not more than the total number of data points. If there are only two data points then the program will not permit any data points to be deleted. The 'Curve' command asks the user which curve should be deleted. Again 0 means delete no curves and the curve number must be a positive integer and not more than the total number of curves. Also if there are only two curve files, then no curve can be deleted. 'Return' simply returns the user to the 'Edit' submenu.

The remainder of the commands in the 'Edit' submenu are 'Data Points', 'Total Curves', and 'Return'. To change the total number of data points in the current curve use 'Data Points' command and to change the total number of curves use 'Total Curves'. In both cases the program will display the old number and request the new number. The program does not actually erase any data if the number of data points or curves are reduced but just ignores the data. Thus, the user can change back to the original number of data points or curves and retrieve any data. The 'Return' will place the user back to the main menu.

Back to the main menu, the 'Calc' command will begin the automatic curve shifting routine for all curves. This procedure will take about 15 seconds for each curve to be shifted, assuming that the 8087 co-processor chip is installed. The results will be displayed as the calculation precedes. The program only shifts curves right or in the positive direction. In other words there is no negative shift values allowed in the calculation process. If the minimization process takes more than 100 iterations then an error message will be displayed and the automatic shifting process will be stopped. The 'Manual' command allows the user to change the shift factors or input new ones. It will accept negative values but care needs to be used since the graphing is in log time.

The 'Graph' command is used to graph the results of the program and to visually examine the results. The user will specify the first curve and the last curve of any group of sequential curves to be

graphed. The default will graph curve 1 through the total number of curves. The user can request a hard copy to be printed on any Epson RX, FX or IBM Graphics printer. The current programs supports only the Color Graphics Adapter (CGA) type of color monitor. The last command 'Quit' will exit the program.

Comments and Conclusions

This program was designed as a tool to aid the engineer and scientist in curve shifting and developing master curves by automating the process. The program automatically shifts curves by minimizing the area difference between the two curves. The program is written to be user friendly and easy to use. The data can be input by the user through the program's editor or can be read in directly from disk. In both cases the data can be changed and edited within the program. The results can be graphed immediately on the screen for inspections and adjustment by the user. The maximum number of curves that can be shifted at one time is 30 and each curve can have up to 54 data points.

The shifting algorithm used minimizes the area difference between the over lapping portions of any two curves. The minimum is located first by the Bracketing method and the refined by using the Golden Section Search method. Each curve is shifted to the right of the previous curve. This method is empirically based and thus care should be taken with the results and should be checked graphically.

The vita has been removed from the scanned document